

For Reference

NOT TO BE TAKEN FROM THIS ROOM

Ex libris
UNIVERSITATIS
ALBERTAENSIS



BRUCE PEEL SPECIAL COLLECTIONS LIBRARY
UNIVERSITY OF ALBERTA LIBRARY

REQUEST FOR DUPLICATION

I wish a photocopy of the thesis by

_____ (author)

entitled _____

The copy is for the sole purpose of private scholarly or scientific study and research. I will not reproduce, sell or distribute the copy I request, and I will not copy any substantial part of it in my own work without permission of the copyright owner. I understand that the Library performs the service of copying at my request, and I assume all copyright responsibility for the item requested.

THE UNIVERSITY OF ALBERTA

RELEASE FORM

NAME OF AUTHOR PETER KONRAD KAISER
TITLE OF THESIS TIME-DEPENDENT BEHAVIOUR OF TUNNELS IN
 JOINTED ROCK MASSES
DEGREE FOR WHICH THESIS WAS PRESENTED DOCTOR OF PHILOSOPHY
YEAR THIS DEGREE GRANTED FALL, 1979

Permission is hereby granted to THE UNIVERSITY OF ALBERTA LIBRARY to reproduce single copies of this thesis and to lend or sell such copies for private, scholarly or scientific research purposes only.

The author reserves other publication rights, and neither the thesis nor extensive extracts from it may be printed or otherwise reproduced without the author's

THE UNIVERSITY OF ALBERTA

TIME-DEPENDENT BEHAVIOUR OF TUNNELS IN JOINTED ROCK MASSES

by



PETER KONRAD KAISER

A THESIS

SUBMITTED TO THE FACULTY OF GRADUATE STUDIES AND RESEARCH
IN PARTIAL FULFILMENT OF THE REQUIREMENTS FOR THE DEGREE
OF DOCTOR OF PHILOSOPHY

IN

CIVIL ENGINEERING

DEPARTMENT OF CIVIL ENGINEERING

EDMONTON, ALBERTA

FALL, 1979

THE UNIVERSITY OF ALBERTA
FACULTY OF GRADUATE STUDIES AND RESEARCH

The undersigned certify that they have read, and recommend to the Faculty of Graduate Studies and Research, for acceptance, a thesis entitled TIME-DEPENDENT BEHAVIOUR OF TUNNELS IN JOINTED ROCK MASSES submitted by PETER KONRAD KAISER in partial fulfilment of the requirements for the degree of DOCTOR OF PHILOSOPHY in CIVIL ENGINEERING.

IN MEMORY OF MY DEAR FATHER

ABSTRACTS

The results of an investigation of the time-dependent behaviour of jointed, strain-weakening rock during fracture and the response of rock masses, with time-dependent strength and deformation properties, to tunneling, are reported in this thesis. Modell tests with regularly, but discontinuously, jointed coal as a model material have been undertaken under plane strain condition. The testing apparatus, which allows variations in the stress ratio from hydrostatic to uniaxial loading, with a maximum capacity of 15 MPa field stress is described.

In the first part of this thesis the time-dependent fracture behaviour of rock has been investigated by multiple-stage repeated relaxation tests during triaxial compression tests on jointed coal at low confinement pressure. This brittle material can be described as a visco-elastic, visco-plastic strain-weakening material. The stress-strain behaviour can be separated into a stable zone, where time-dependent deformations terminate within an engineering time-scale, and an unstable zone, within which the rate of deformation is a function of the stress level relative to the current available strength. This current available strength is the resistance which can be mobilized if the rock is loaded instantaneously. It is stress-history and rock structure-dependent. Depending on the loading history, different rock structures are created and therefore different current available strengths are mobilized. The

time-dependent behaviour of rock and rock masses is a direct response to the rock structure at a particular instant.

A phenomenological model has been developed which simulates the evolution of the rock structure and predicts the time-dependent behaviour of brittle rock subjected to many different loading histories. This model has been verified qualitatively on test results available in the literature and it describes successfully all investigated loading histories. The model shows that both a time-dependent and a time-independent resistance can be mobilized in rock but that the relative proportion of these resistances is history-dependent and a function of the accumulated strain.

The model test results reported cover mainly the behaviour of tunnels in the stress range before collapse is initiated by rupture or local instability. It has been found that stress - redistribution due to non-linear stress-dependent creep properties, anisotropic creep properties and local yielding are much more important than generally accepted. Global yielding is only one of many stress-redistribution mechanisms. The stress-redistribution due to tunnel excavation causes tunnel closures which are identical to the displacement pattern created around an equivalent opening in an elastic or visco-elastic material. This approach of comparing measured displacements to displacements around an "equivalent opening" has been used to describe the test results and it indicates that

deformations in excess of purely elastic deformations do not have to be caused by yielding or the creation of a plastic zone exclusively.

The "equivalent opening approach" can be used to evaluate effects of influence parameters such as initial stress field, rock mass properties, excavation procedures, and initial support systems on the tunnel behaviour. Implications related to design procedures, construction procedures and support measures are discussed in detail.

RESUME

Cette thèse explore le comportement différé d'une roche jointive et fragile lors de sa rupture et l'influence du percement d'un tunnel sur une roche dont la résistance et les déformations dépendent du temps. A ces fins, l'auteur a entrepris des essais sur modèles réduits de tunnel, en déformation plane, dans un charbon dont le jointolement est régulier mais discontinu. L'appareillage utilisé pour ces tests permet une grande flexibilité dans les conditions de chargement, qui peuvent varier d'hydrostatiques à uniaxiales. Il transmet à l'échantillon une pression maximale de 15 MPa et il est décrit dans le présent ouvrage.

La première partie de cette thèse concerne l'étude de la fracture différée des roches. Des essais de relaxation répétés, conduits dans des conditions triaxiales, à des niveaux de contrainte successifs et à faible étreinte, ont permis de caractériser ce charbon comme étant visco-élastique et visco-plastique, et comme présentant un affaiblissement des contraintes après rupture. Le chargement d'un échantillon comporte deux phases successives : Dans la phase stable les déformations s'arrêtent après un certain temps, et dans la zone instable, la vitesse des déformations différées est fonction du niveau de contrainte, relativement à la "résistance momentanément disponible". L'expression: "Résistance momentanément disponible" est utilisée pour qualifier la résistance que pourrait développer une roche à une certaine étape de son chargement, si elle était au même

instant chargée instantanément jusqu'à la rupture. Cette variable dépend de l'historique du chargement et de la structure du rocher. Suivant les étapes de cet historique, le chargement génère différentes structures dans le rocher et on observe ainsi différentes "résistances momentanément disponibles". Le comportement différé des roches et des massifs rocheux reflète fidèlement la structure de ce rocher à un instant donné.

Un modèle phénoménologique a été développé pour simuler l'évolution de la structure du rocher et prédire le comportement différé d'une roche fragile soumise à de nombreux types de chargements différents. Des résultats expérimentaux, issus de la littérature, ont servi à confirmer la validité de ce modèle, qui décrit avec succès les différents chargements étudiés. Il montre aussi que le rocher présente, confondues, une résistance dépendante du temps, et une qui n'en dépend pas, dans des proportions qui sont fonction de l'historique du chargement et du niveau de déformations cumulées.

Les résultats des essais sur modèles réduits concernent essentiellement le comportement des tunnels dans la zone de chargement précédant la ruine (amorcée par la rupture ou l'instabilité locale de la paroi). On a montré que les phénomènes de redistribution des contraintes jouent un rôle beaucoup plus important qu'on le pense en général. Ces phénomènes ont plusieurs causes: propriétés de fluage non linéaires et dépendantes du niveau de contrainte, fluage

anisotrope ou local, plastification locale du matériau, le développement d'une zone plastique uniforme n'étant qu'une raison parmi beaucoup d'autres. La redistribution des contraintes autour d'un tunnel après son percement fait que les mesures de convergence sont identiques à celles d'un tunnel équivalent, percé dans un milieu élastique ou visco-élastique. Cette méthode, consistant à comparer les déplacements observés dans la réalité à ceux observés autour d'un tunnel équivalent, a été utilisée pour décrire les résultats expérimentaux obtenus sur modèles. Elle montre que les déformations qui semblent sortir du domaine élastique ne sont pas nécessairement dues au développement d'une zone plastique.

La "méthode de la cavité équivalente" peut servir à évaluer les effets sur le comportement des tunnels de facteurs tels : le champ initial de contraintes, les propriétés de la masse rocheuse, la méthode de percement et le soutènement initial. La méthode et ce qu'elle implique pour le calcul, la construction et le soutènement des tunnels sont largement décrits.

Zusammenfassung

Das zeitabhaenige Deformationsverhalten von geklueftetem Fels, mit dehnungsabhaengiger Festigkeit waehrend des Bruches und dessen Einfluss auf das Verhalten von Untertagebauten, wurde im Zusammenhang mit dieser Doktorarbeit untersucht. Modell Versuche wurden mit gleichmaessig und undurchgehend gekluefteter Kohle als Modell Material unternommen. Mit der speziell angefertigten Versuchseinrichtung kann das Spannungsverhaeltnis vom einachsigen zum hydro-statischen Spannungszustand, unter Beibehaltung des ebenen Dehnungszustandes, variiert werden und diese Spannungen koennen ueber laengere Zeitspannen konstant gehalten werden.

Im ersten Teil dieser Arbeit wird das zeitabhaengige Bruchverhalten von Fels, in mehrstufigen Relaxations Versuchen mit wiederholter Relaxation von konstanter Ausgangsspannung, untersucht. Die geklueftete Kohle wurde auch fuer diese Versuche benuetzt, die unter dreiachsialem Spannungszustand mit niederem Zelldruck ausgefuehrt wurden. Dieses sproede Material kann kurz als visco-elastisch, visco-plastisch mit dehnungsabhaengiger Festigkeit umschrieben werden. Das Spannungs- und Dehnungsverhalten wird in zwei Zonen unterteilt: In eine stabile Zone, in der zeitabhaengige Verschiebungen begrenzt sind, und in eine unstabile Zone, in der die Deformationsgeschwindigkeit von der Groesse der Spannung relative zur gegenwaertig vorraetigen Festigkeit abhaengt. Diese gegenwaertig

vorraetige Festigkeit ist die unter maximaler Belastungsgeschwindigkeit verfuegbare Festigkeit. Sie ist vom Spannungsweg und von der augenblicklich vorhandenen Felsstruktur abhaengig. Je nach Belastungsgeschichte werden verschiedene Felsstrukturen erzeugt und die gegenwaertig vorraetige Festigkeit aendert sich entsprechend. Das zeitabhaenige Verhalten von Gestein und Fels ist eine direkte Folge des gegenwaertigen Zustandes des Gesteines und deren Verhalten waehrend einer Spannungsaenderung haengt vom Strukturentwicklungsprozess ab.

Ein phenomenologisches Modell wurde auf Grund dieser Erkenntnisse entwickelt. Es simuliert die Entwicklung der Felsstruktur und sagt das zeitabhaenige Verhalten von sproedem Fels vorher. Dieses Modell wurde qualitativ an veroeffentlichten Versuchsergebnissen verschiedener Versuchstypen erfolgreich verifiziert. Dabei wurde gezeigt, dass zeitunabhaenige und zeitabhaengige Widerstaende im Fels mobilisiert werden koennen. Diese Widerstaende, sowie deren relativer Anteil an der Gesamtfestigkeit, sind eine Funktion der Belastungsgeschichte und der akkumulierten Dehnung.

Die Resultate der Modelversuche beschreiben vor allem das Verhalten von Tunnels vor dem Einsturz. Es wurde gezeigt, dass Spannungsumlagerungen, die durch nicht lineare, spannungsabhaenige Kriecheigenschaften, anisotrope Kriecheigenschaften und lokales, plastisches Verhalten erzeugt werden, oft viel wichtiger sind als generell

angenommen wird. Globales, plastisches Verhalten, das sehr oft in Betracht gezogen wird, umfasst nur eine von vier moeglichen Ursachen, die fuer die Spannungsumlagerung verantwortlich sind. Die durch Spannungsumlagerung erzeugten Verschiebungen der Tunnelwand koennen mit berechneten Verschiebungen von einer equivalenten Oeffnung in einem elastischen oder visco-elastischen Material verglichen werden. Diese neue Betrachtungsweise und Annaeherung wurde zur Erklaerung der Versuchsergebnisse benuetzt. Daraus geht hervor, dass Verschiebungen, die groesser sind als die von der Elastizitaetstheorie vorhergesagten, nicht unbedingt durch plastische Deformationen hervorgerufen werden.

Diese Betrachtungsweise, die "equivalent opening approach" genannt wird, kann dazu benuetzt werden um die folgenden Einfluesse zu beurteilen: Groesse des Spannungsfeldes, Eigenschaften der Felsmassen, Ausbruch Verhalten und Ausbausystem. Schlussfolgerungen, sowie deren Auswirkungen auf den Entwurf von Tunnels, die Bauvorgaenge und Ausbautypen, wurden ausfuehrlich diskutiert.

ACKNOWLEDGEMENTS

The author of this thesis would like to thank his thesis supervisor Dr. N.R. Morgenstern for his guidance, encouragement and enthusiastic support during the past four years. His continuous effort to seek funding for this project made it possible to study one of the most important and most difficult areas of rock engineering with special equipment.

My wife, Kathi, deserves special recognition for her patience, love, and understanding. Without her steady encouragement and her assistance the completion of this thesis would not have been possible.

I also wish to thank my dear mother, who continuously encouraged me to continue my education up to the University level, for her moral and financial support through the last twenty years.

The writer wishes to express his sincere appreciation for technical advice and moral support by many professors in the Department of Civil Engineering. I would particularly like to thank Professors Z. Eisenstein for his encouragement to enter the Ph.D. program, D.Cruden for his technical support, and M.Dusseault for his most useful and critical advice in many areas and for his special effort in proof-reading this thesis.

Technical expertise provided by Al Muir during the design and construction of the model test apparatus, by Woody (O.Wood) throughout this project for the work in the

laboratory and during the sampling program in the field, and by Roy Gitzel and Ray Howells in the areas of electronics and computing, have been greatly appreciated. Furthermore, I would like to thank Don Fushtey, Steve Gamble, Scotty Rogers, and the administrative staff of the Department of Civil Engineering for their help, and particularly Julie Loach for typing this thesis.

The work presented in this thesis has benefited greatly from discussions with many colleagues at the University of Alberta. The close working relationship with Alain Guenot has been very fruitful. The assistance by Oldrich Hungr and Paul Weerdenburg, and discussions with Sergio da Fontoura and other fellow graduate students, notably Jeff Weaver, John Simmons, Luciano Medeiros, Wayne Savigny and Dave Sego, have been appreciated.

Financial support has been provided by Canada Council and the Swiss Government through scholarships, and bursaries and partial teaching assistantships by the University of Alberta and the Department of Civil Engineering. I would like to thank Walter Steiner for bringing the Canada Council Scholarship to my attention since this was actually the initial cause for my study leave to Canada.

The National Research Council and the University of Alberta are responsible for the major funding of this research project, and both Calgary Power Ltd. and Manalta Coal Ltd. at Sundance (Alberta) have supported the sampling program. Particularly Bob Kirby, the mining engineer of

Calgary Power Ltd., was very helpful.

The writer wishes to express his sincere appreciation for all the help received from many people, whose names have not been mentioned, throughout his work at the University of Alberta.

TABLE OF ABBREVIATIONS

Special symbols used in Chapter 3 are explained in Section 3.3 and the remaining symbols are defined throughout the text whenever they are first encountered.

A dot below a letter means that this letter is a subscript. The following subscripts are commonly used:

rradial or residual
 ttangential or tensile
 vvertical
 hhorizontal
 llongitudinal
 nnormal
 ult ...ultimate
 ppeak
 iinternal
 max ...maximum
 min ...minimum

Some of the more frequently used symbols are:

σsigma, normal stress
 τtau, shear stress
 Ddeviatoric stress = $\sigma_1 - \sigma_3$
 Nstress ratio; σ_h/σ_y , or the ratio between minimum and maximum principal field stress

Estiffness, Young's Modulus
 νPoisson's Ratio
 KBulk Modulus
 GShear Modulus
 N_{12}, N_{22}coefficient of viscosity

σ_cunconfined compressive strength
 ϕfriction angle

ϵ orstrain
 $\dot{\epsilon}$ orstrainrate
 u or \dot{u}tunnel wall displacement or closure; and corresponding closure rate
 θangle generally measured from a vertical axis
 Xdegree of separation = area of open joint / total crosssectional area

δsmall increment or derivative.

Table of Contents

Chapter		Page
CHAPTER 1		
	INTRODUCTION.....	1
1.1	<u>General</u>	1
1.2	<u>Time-dependent Response of a Rock Mass to Excavation of a Tunnel</u>	5
1.3	<u>Scope and Organization of this Thesis</u>	9
CHAPTER 2		
	GEOLOGY AND MECHANICAL PROPERTIES OF COAL.....	13
2.1	<u>Introduction</u>	13
2.2	<u>Geology</u>	14
2.2.1	Site Location.....	14
2.2.2	General Geology.....	14
2.2.3	Structure of Coal.....	15
2.2.4	Composition of Coal.....	17
2.3	<u>Strength of Coal</u>	18
2.3.1	Information from Previous Testing.....	18
2.3.2	Sampling and Sample Preparation for Laboratory Testing.....	20
2.3.2.1	Method of Sampling.....	20
2.3.2.2	Trimming.....	22
2.3.2.3	Casting.....	22
2.3.3	Direct Shear Tests.....	22
2.3.3.1	Testing Procedure.....	23
2.3.3.2	Sample Orientation and Description...	24
2.3.3.3	Direct Shear Test Results.....	25
2.3.4	Triaxial Compression Tests.....	30
2.3.4.1	Testing Procedure.....	30

2.3.4.2	Sample Orientation and Description...	33
2.3.4.3	Triaxial Compression Test Results....	38
CHAPTER 3		
	MULTIPLE-STAGE REPEATED RELAXATION TESTS (MSRRT).....	49
3.1	<u>Introduction and Background</u>	49
3.2	<u>Test Procedure and Factors Affecting the Results</u> ...	61
3.2.1	Test Procedure.....	61
3.2.2	Testing Environment.....	66
3.2.3	Relaxation of the Testing Machine.....	69
3.3	<u>Behaviour of Ideal Materials During Multiple-Stage Repeated Relaxation Tests</u>	76
3.4	<u>Results from Multiple-Stage Repeated Relaxation Tests</u>	93
3.5	<u>Interpretation of Results</u>	129
3.5.1	Introduction.....	129
3.5.2	Schematic Stress-Strain Diagram for Rock....	133
3.5.2.1	Behaviour in Zone A (below peak long-term strength).....	136
3.5.2.2	Behaviour in Zone B (near ultimate strength).....	139
3.5.2.3	Behavior in the Transition Zone C...	150
3.6	<u>Conclusions</u>	154
CHAPTER 4		
	PHENOMENOLOGICAL MODEL FOR ROCK WITH TIME-DEPENDENT STRENGTH.....	163
4.1	<u>Introduction</u>	163
4.2	<u>Required Properties of Model</u>	166
4.3	<u>Proposed Model and its Element Properties</u>	167
4.4	<u>Comparison of Model with Published Test Data</u>	174
4.4.1	Special Case of Model.....	174
4.4.2	Constant Strain Rate Test.....	176

4.4.3 Tests with Varying Strain Rate.....	183
4.4.4 Multiple-Stage Single Relaxation Tests.....	186
4.4.5 Multiple-Stage Repeated Relaxation Test.....	191
4.4.6 Single-Stage Creep Tests.....	194
4.4.7 Multiple-Stage Creep Tests.....	199
4.4.8 Static and Dynamic Fatigue.....	204
4.5 <u>Recommended Approach to Develop the Phenomenological Model to a Mathematical Model</u>	207
4.6 <u>Summary and Conclusions</u>	214
CHAPTER 5	
DEVELOPMENT OF GEOMECHANICAL MODELING TECHNIQUE.....	220
5.1 <u>Introduction</u>	220
5.1.1 Reasons for Geomechanical Model Studies.....	220
5.1.2 Scope of Study.....	223
5.2 <u>Rock Modeling Materials</u>	224
5.2.1 Sampling Procedure.....	227
5.3 <u>Model Test Apparatus</u>	231
5.3.1 Introduction.....	231
5.3.2 Description of the Model Loading System.....	235
5.3.3 Instrumentation, Preparation and Installation of Model Blocks.....	244
5.3.4 General Loading History.....	251
5.3.5 Data Processing.....	255
5.3.6 Preliminary Tests.....	261
CHAPTER 6	
INTERPRETATION OF MODEL TEST DATA.....	265
6.1 <u>Introduction</u>	265
6.2 <u>Description of Test MC-2</u>	266
6.2.1 Sample Description.....	266

6.2.2	Loading History.....	270
6.2.3	Presentation of Measurements.....	272
6.2.3.1	Stress-Strain Relationship.....	272
6.2.3.2	Strain - Time Relationship.....	273
6.3	<u>Interpretation of Data by Linear Elastic Model</u>	280
6.3.1	The "Equivalent Opening Approach".....	288
6.3.1.1	Tunnel Closure and External Displacement.....	290
6.3.1.2	Internal Radial Strains.....	299
6.3.1.3	Extension of "Equivalent Opening Approach" Beyond Yielding.....	306
6.3.1.4	Implications Resulting from Stress - Strain Observations.....	311
6.4	<u>Interpretation of Time - Dependent Data</u>	312
6.4.1	Interpretation of Time - Dependent Results by Equivalent Opening Approach.....	313
6.4.2	Interpretation of Data by Linear Visco - Elasticity.....	321
6.4.2.1	Effect of Time - Independent, Non - Linear Modulus of Compressibility...	324
6.4.2.2	Effect of Hydrostatic Creep.....	329
6.4.3	Conclusion.....	337
CHAPTER 7		
CONCLUSIONS, IMPLICATIONS AND RECOMMENDATIONS.....		338
7.1	<u>Time-Dependent Properties of Rock Masses</u>	338
7.2	<u>Underground Openings in Rock Masses with Time-Dependent Properties</u>	340
7.2.1	Model Testing.....	340
7.2.2	Application to Underground Openings.....	343
APPENDIX A5		
WORKING DRAWINGS OF MODEL TEST APPARATUS.....		361

APPENDIX A6

A6.1 DERIVATIONS AND EQUATIONS

A6.2 SELECTED MODEL TEST DATA.....370

List of Figures

Figure	Page
1.1 Rail Tunnel (1880) and Road Tunnel (1978) through the Arlberg, Austria.....	2
2.1 Mohr Diagram of Direct Shear Test Data (Test No.1,2,3 and 5A to 5F).....	26
2.2 Mohr Diagram for Triaxial Compression Test Data ($\bar{\sigma}_3 < 1$ Mpa).....	39
2.3 Mohr Diagram for Triaxial Compression Test Data ($\bar{\sigma}_3 = 3.5$ to 10.0 Mpa).....	40
2.4 Summary Plot of Stress-Strain and Volume Change Data from Triaxial Compression Tests.....	41
2.5 Stress-Strain and Volume Change Data of Test No. TR-1A.....	44
2.6 Stress-Strain and Volume Change Data of Test No. TR-1B.....	45
2.7 Stress-Strain and Volume Change Data of Test No. TR-1C.....	47
3.1 Uniaxial Compression Test on a Sandstone; Data from Bieniawski(1970).....	54
3.2 Interpretation of Uniaxial Compression Test on Sandstone (Data from Bieniawski,1970) by Mueller and Goetz (1973).....	56
3.3 Normalized Deviatoric Stress and Total Vertical Strain Versus Time of Test No. CTR-2A, Stage 6.....	63
3.4 Normalized Deviatoric Stress and Total Vertical Strain versus Time of Test No. CTR-2D, Stage 1.....	65
3.5 Test Assembly for Relaxation Test and Load - Displacement Diagrams for Test on Steel Block.....	71
3.6 Load Change versus Logarithm of Time for Relaxation Tests on Steel.....	73
3.7 Linearized Data from Relaxation Test on Steel (corresponding to data in Figure 3.6).....	74
3.8 Schematic Stress - Strain - Time Diagrams for Ideal Materials.....	80

3.9	Schematic Diagram: Normalized Stress Drop versus Stress Level and Inelastic Strain for Ideal Materials	83
3.10	Schematic Diagram: Stress Ratio versus Normalized Stress Drop for Ideal Materials.....	88
3.11	Stress Ratio versus Normalized Stress Drop for Linear Viscous Models.....	90
3.12	Stress-Strain Diagram of Test No. CTR-2B.....	94
3.13	Stress-Strain Diagram of Test No. CTR-2C.....	97
3.14	Stress-Strain Diagram of Test No. CTR-2A.....	100
3.15	Normalized Deviatoric Stress and Total Vertical Strain versus Time of Test No. CTR-2A (Stages 13 to 15).....	102
3.16	Normalized Deviatoric Stress and Vertical Strain Difference versus Logarithm of Time during Relaxation of Sample No. CTR-2A.....	103
3.17	Accumulated Strain versus Logarithm of Number of Cycles, Test No. CTR-2A.....	105
3.18	Normalized Deviatoric Stress Drop versus Deviatoric Stress and Inelastic Strain ϵ^* , Test No. CTR-2A, Stages 1 to 6.....	110
3.19	Normalized Deviatoric Stress Drop versus Inelastic Strain ϵ^* , Test No. CTR-2A, Stages 7 to 9.....	111
3.20	Normalized Deviatoric Stress Drop versus Inelastic Strain ϵ^* , Test No. CTR-2A, Stage 10....	112
3.21	Stress Ratio versus Normalized Stress Drop, Test No. CTR-2A, Stages 7 to 9.....	113
3.22	Stress Ratio versus Normalized Stress Drop, Test No. CTR-2A, Stage 10.....	114
3.23	Stress Ratio versus Normalized Stress Drop, Test No. CTR-2A, Stages 11 to 24.....	115
3.24	Stress-Strain Diagram of Test No. CTR-2D.....	116
3.25	Normalized Deviatoric Stress and Total Vertical Strain versus Time of Test No. CTR-2D, Stages 8 to 10.....	117
3.26	Normalized Deviatoric Stress and Vertical Strain	

	Difference versus Logarithm of Time during Relaxation of Sample No. CTR-2D.....	118
3.27	Normalized Deviatoric Stress versus Logarithm of Time, Test No. CTR-2D.....	119
3.28	Normalized Deviatoric Stress Drop versus Deviatoric Stress and Inelastic Strain ϵ^* , Test No. CTR-2D, Stages 1 to 11.....	120
3.29	Normalized Deviatoric Stress Drop versus Deviatoric Stress and Inelastic Strain ϵ^* , Test No. CTR-2D, Stages 12 to 16.....	121
3.30	Stress-Strain Diagram of Test No. CTR-2F.....	122
3.31	Normalized Deviatoric Stress versus Logarithm of Time, Test No. CTR-2F, Stage 8.....	123
3.32	Normalized Deviatoric Stress versus Logarithm of Time, Test No. CTR-2F, Stage 9.....	124
3.33	Normalized Deviatoric Stress Drop versus Inelastic Strain ϵ^* , Test No. CTR-2F, Stages 1 to 4.....	125
3.34	Stress Ratio versus Normalized Stress Drop, Test No. CTR-2F, Stages 4 to 8.....	126
3.35	Stress Ratio versus Normalized Stress Drop, Test No. CTR-2F, Stage 8.....	127
3.36	Stress Ratio versus Normalized Stress Drop, Test No. CTR-2F, Stages 9 to 13.....	128
3.37	Schematic Stress-Strain Diagram of Rock.....	134
4.1	a) Schematic Diagram of Model b) Simple Version of Model with Mechanical Elements.....	168
4.2	Schematic Stress-Strain Curves for Minimum and Maximum Loading Rate on Model (Figure 4.1, $m = 1$, $n = 2$).....	170
4.3	Special Case of Phenomenological Model.....	175
4.4	Stress-Strain Diagram from Uniaxial Compression Tests reported by a) Bieniawski (1970), b) Ruesch (1960) and c) Peng and Podnieks (1972).....	179
4.5	Special Case of Model for Rock with Time - Independent Stiffness below the Yield Strength....	180

4.6	Stress-Strain Diagrams from Tests on Solenhofen Limestone (Rutter, 1972).....	182
4.7	Special Case of Model for Rock in Variable Strain Rate Tests.....	185
4.8	Special Case of Model for Rock in Multiple-Stage Single Relaxation Test.....	188
4.9	Special Case of Model during Relaxation for Comparison with Test Data (Peng, 1973).....	189
4.10	Axial Strain versus Time Curves of i) Shale and ii) Marble (Singh, 1975).....	196
4.11	Special Case of Model for Rock in Single-Stage Creep Tests.....	198
4.12	Stress-Strain Diagram of Multiple-Stage Creep Tests, Lama (1974).....	200
4.13	Special Case of Model for Rock in Multiple-Stage Creep Tests.....	203
4.14	Continuous Parameter Distribution Functions (a,b,c after Kovari, 1977).....	208
4.15	Creep Test on Model with Continuous, Linear Parameter Distribution Function; $\dot{\epsilon} = \dot{\epsilon}_1$	210
4.16	Creep Test on Model with Continuous, Linear Parameter Distribution Function; II) $\dot{\epsilon} = \dot{\epsilon}_1$, III) $\dot{\epsilon} = \dot{\epsilon}_2$	212
4.17	Schematic Stress-Strain Diagrams Predicted by Proposed Model.....	215
5.1	Typical Stress versus Strain and Strain versus Time Plot.....	256
5.2	Typical Log Strain Rate versus Log Time and Normalized Stress versus Log Time Plot.....	257
5.3	Processed Artificial Data and Effect of Recording Error.....	262
6.1	Crack Pattern Inside and Near Tunnel after Unloading during Test MC-2.9.....	268
6.2	Typical Tunnel Closure Rate Diagrams from Tests MC-2.6 and MC-2.9 at 13 MPa.....	274
6.3	Summary Sketch of Tunnel Closure Rates for all Increments During Test MC-2.6.....	275

6.4	Summary Sketch of Tunnel Closure Rates for all Increments During Test MC-2.9.....	276
6.5	Stress versus Creep Strain Diagrams for Tests MC-2.6 and MC-2.9; Strain after 20 Hours and 100 Hours.....	277
6.6	Schematic Diagram Illustrating Stress Redistribution around an Opening.....	287
6.7	Equivalent Opening Approach for an Axisymmetric Case..	291
6.8	Equivalent Opening Approach for a Case with Non-Symmetric Stress Redistribution.....	293
6.9	Closure Ratio as a Function of (A) Stress Ratio N , (B) Equivalent Opening Shape b/a , and (C) Anisotropy Ratio.....	296
6.10	Schematic Diagram to Illustrate Radial Strain Development.....	301
6.11	Test MC-2.9: Stress versus Radial Strain Measurements at $N=0.2$	303
6.12	Crack Pattern near Tunnel and Location of Internal Sample Instrumentation.....	305
6.13	Stress-Strain Diagrams of Internal Gauges; Test MC-2.8.....	308
6.14	Stress-Strain Diagrams of Test MC-2.8.....	309
6.15	Schematic Diagram to Illustrate the Time - Dependent Radial Strain Development.....	314
6.16	Schematic Log Strain Rate versus Log Time Diagrams in Comparison with Measurements.....	316
6.17	Summary of Strain - Time Diagrams from Test MC-2 for one Specific Instrument; $N=1, 0.75, 0.33$ and 0.2	318
6.18	Schematic Diagram to Illustrate Effect of Non-Linear Bulk Modulus.....	326
6.19	Time-Dependent Behaviour of a Linear Visco-Elastic Material; Bulk Modulus $K=1000, 500, 100$ MPa.....	327
6.20	Linear Visco-Elasticity with Deviatoric and Hydrostatic Creep; $N=1$	331

6.21	Strain-Time Diagrams: Linear Visco-Elasticity with Deviatoric and Hydrostatic Creep; $N=1/3$	332
6.22	Log Strain Rate - Log Time Diagrams: Linear Visco-Elasticity with Deviatoric and Hydrostatic Creep; $N=1/3$	333
6.23	Summary Plots in Log Strain Rate - Log Time Diagrams: Linear Visco-Elasticity with Hydrostatic and Deviatoric Creep, $N=1$, $N=1/3$	334
7.1	Process and Factors Controlling the Development of a Stable Equilibrium Condition around an Opening in a Rock Mass with Time-Dependent Properties	347
7.2	Development of the Equivalent Opening during two Excavation Layouts.....	350
A5.1	Test Frame, Side View.....	362
A5.2	Bottom Reaction Head.....	363
A5.3	Loading Head.....	364
A5.4	Top Reaction Head.....	365
A5.5	Lateral Reaction Head 1.....	366
A5.6	Lateral Reaction Head 2.....	367
A5.7	Assembly of Lateral Loading Elements.....	368
A5.8	Schematic of Hydraulic System.....	369
A6.1	Stress-Strain Diagram: Test MC-2.0; no record of internal gauges due to technical problems.....	383
A6.2	Stress-Strain Diagram: Test MC-2.4; no record of internal gauges due to technical problems.....	384
A6.3	Stress-Strain Diagram and Loading History: Test MC-2.6.....	385
A6.4	Stress-Strain Diagram and Loading History: Test MC-2.7.....	386
A6.5	Stress-Strain Diagram and Loading History: Test MC-2.9.....	387
A6.6	Strain-Time Diagram: Test MC-2.6, Gauges 1 to 16..	388
A6.7	Log Strain Rate - Log Time Diagram: Test MC-2.6, Gauges 1 to 4.....	389

A6.8	Log Strain Rate - Log Time Diagram: Test MC-2.6, Gauges 5 to 8.....	390
A6.9	Log Strain Rate - Log Time Diagram: Test MC-2.6, Gauges 9 to 12.....	391
A6.10	Log Strain Rate - Log Time Diagram: Test MC-2.6, Gauges 13 to 16.....	392
A6.11	Strain-Time and Normalized Stress - Time Diagram: Test MC-2.6, Gauges 17 to 22.....	393
A6.12	Log Strain Rate - Log Time Diagram: Test MC-2.6, Gauges 17 to 20.....	394
A6.13	Log Strain Rate - Log Time Diagram: Test MC-2.6, Gauges 21 to 22.....	395

List of Plates

Plate	Page
2.1	Drilling of Samples Perpendicular to Bedding of Coal.21
2.2	Sample No.TR-1B after Testing.....42
3.1	Sample CTR-2A after Testing.....99
3.2	Sample CTR-2F after Testing.....108
5.1	Drilling of Holes along Sample Boundaries and Breakage of Rock Bridges.....228
5.2	Excavation around Samples, Breaking off and Loading of Samples.....229
5.3	Loading Apparatus.....237
5.4	Lateral Load Distribution by Triangle System.....239
5.5	Pressure Control Systems and Data Acquisition System.241
5.6	Instrumentation for Tunnel Closure Measurements...246
5.7	Old Extensometer to Measure Internal Strain.....248
5.8	New Extensometer to Measure Internal Strain.....250
5.9	Coal Sample in Mould Ready for Casting.....252
5.10	Drilling of Tunnel through a Coal Sample.....254
6.1	Crack Pattern on Top Face of Sample MC-2 and Details near and inside Tunnel.....269

Table 1: Summary of Data					1000
Category A					100
Category B					100
Category C					100
Category D					100
Category E					100
Category F					100
Category G					100
Category H					100
Category I					100
Category J					100
Category K					100
Category L					100
Category M					100
Category N					100
Category O					100
Category P					100
Category Q					100
Category R					100
Category S					100
Category T					100
Category U					100
Category V					100
Category W					100
Category X					100
Category Y					100
Category Z					100

List of Tables

Table		Page
2.1	Properties of Triaxial Test Samples TR-1A, TR-1B and TR-1C.....	34
2.2	Properties of Triaxial Test Samples CTR-2A/2F.....	36
2.3	Properties of Samples from High Pressure Triaxial Test.....	37
3.1	Relaxation Test on Steel Block.....	70

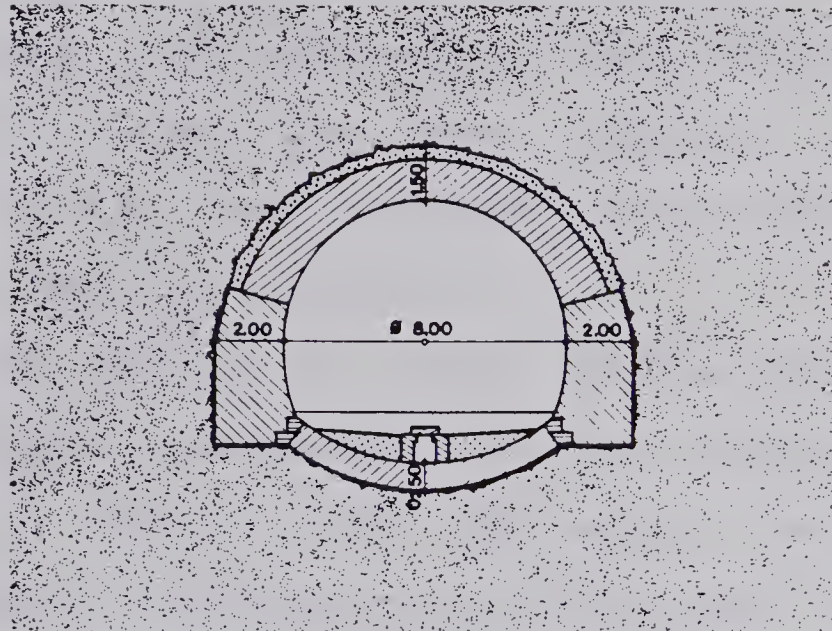
CHAPTER 1

INTRODUCTION

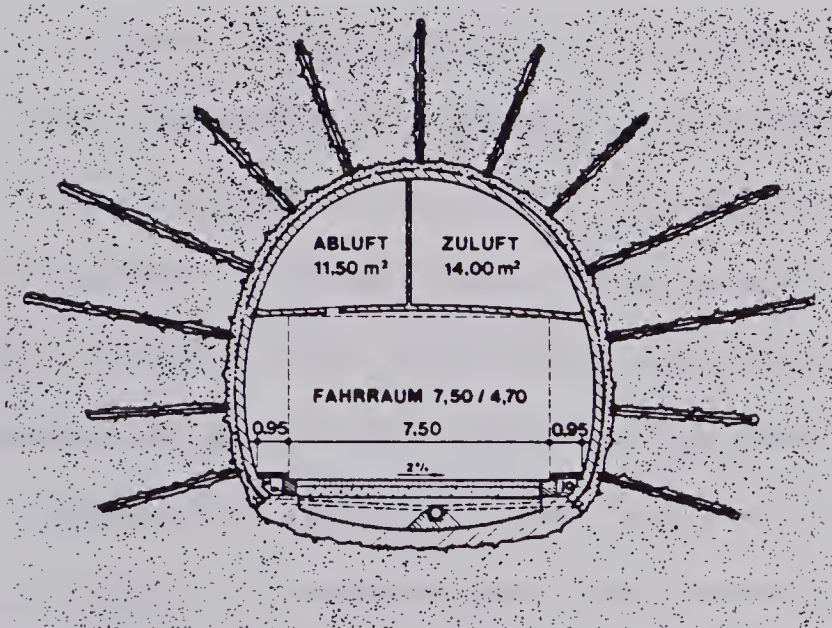
1.1 General

Tunneling is an old art. Many different tunneling methods have been developed over the last century and considerable improvements have been made in investigation, design and construction techniques. For example, at the Arlberg Tunnel, Austria (John(1976) or Posch(1978)), two almost parallel tunnels have been driven; one has been completed in 1880 and the other in 1978. With an area of excavation of 95 m^2 a free opening of 50 m^2 with a support volume of 45 m^3 was achieved in 1880 while in 1978 an excavated opening of 95 m^2 resulted in a free opening of 80 m^2 with a support volume of only 15 m^3 (Figure 1.1). This tremendous improvement has been reached through the application of new technologies (shotcrete, rate of excavation, rock bolting), new design and construction procedures (flexible initial and stiff final support) and field instrumentation (extensometers, closure measurement devices, anchor load observations).

Today, the rock is incorporated into the support system by anchors or rockbolts and observations are used to evaluate the opening stability, to modify design, and to optimize the lining cost and its installation time. All these factors are circumscribed by the general terms: "Observational Tunneling Method" or "New Austrian Tunneling



Crossection of Railway Tunnel (1880)



Crossection of Road Tunnel (1978)
(Posch, 1978)

Figure 1.1 Rail Tunnel (1880) and Road Tunnel (1978) through the Arlberg, Austria.

Method (NATM)". Many authors treat these methods separately on the basis of minor differences but this is not really justified since both are an application of the present understanding of the behaviour of underground openings. They both employ the two most important principles of "mobilization of rock strength" and "monitoring to guide both design and construction".

Current methods of tunnel design have evolved from three different approaches to this engineering problem: experience, based on qualitative or quantitative observations; development of theoretical or analytical methods; and model testing for specific prototypes or general investigations. Each area has its proper application and only a blend of information gained from all three approaches may increase our present understanding of tunnel behaviour. Application of analytical methods, particularly numerical methods, has dominated the research in this area over the last decade. Many important contributions have been made by consideration of the post-failure behaviour of rock, of the discontinuities in rock masses, the three-dimensional state of stress near the tunnel face, and both the active and passive time-dependent processes such as tunnel advance rate and time-dependent rock properties. But it seems that these techniques have often been misused by curve fitting without proper consideration of the physical processes involved. For example, the elastic, strain-weakening, plastic model with complete loss of

cohesion has been used in cases where observed strains were not sufficient to cause complete strength loss. Linear visco-elastic models have been used to fit, apparently successfully, field observations in materials which have not been proven to be linearly visco-elastic. On the other hand, enormous amounts of field observations have been collected (e.g. Tauern or Arlberg Tunnel) and this information has been applied empirically to control tunnel construction but has not been adequately analysed from the research point of view. There has been some interaction between observation and design; nevertheless, major deficiencies still exist in the understanding of the processes causing deformations and instabilities. The most promising approach which has, because of obvious reasons, not been applied enough, particularly to investigate the time-dependent processes, is physical modeling. Modell tests have many disadvantages but they allow better control of boundary conditions (e.g. stress field) and material properties than in the field, and it is not necessary to fix certain, poorly understood, mechanisms as input parameters. The latter is a major deficiency of most analytic, conceptual, and numerical models.

Larger and deeper tunnels under less favorable conditions are being built today resulting in the need for an even better understanding of the rock mass response to an excavation of an underground opening. In the last few years it has been generally accepted that field observations are

essential for the success of a tunneling project and that these initial investments result in significant financial savings if applied correctly. The feedback from observation to design and extrapolation beyond the time of the last measurement are the most difficult tasks for the tunneling engineer and this problem constitutes the weakest point in the tunnel design procedure. The author concluded that the most important areas in rock tunneling are related to the time-dependent response of a rock mass to a change in stress field, and the problem of extrapolation from field measurements to a particular time after tunnel completion. To make any extrapolation in time it is essential to understand the processes involved, and it follows that the initial investigation should delineate the processes relevant for the time-dependent behaviour of strain - weakening rock masses.

This view is supported by Muir Wood(1979) who, in a detailed exposition on the ground behaviour during tunneling, concluded that unification in the field of time - dependent deformation is required.

1.2 Time-dependent Response of a Rock Mass to Excavation of a Tunnel

Many time-dependent processes may cause time-dependent straining within the rock mass and consequent deformation of a tunnel. Some of the processes which will not be discussed deal with viscous rock (rock salt) and swelling rocks

(shale). Time-dependent weakening and the influence of time-dependent post-failure behaviour are two mechanisms which may influence the stability of an opening and may control the time-dependent deformations around an underground opening. Egger(1973) and Daemen(1975) showed the importance of the post-failure relationship between stress and strain for tunnel stability. From their work it follows directly that time-dependent failure processes and time-dependent post-peak stress-strain relationships must play a dominant role in the behaviour of strain-weakening materials with a time-dependent peak strength.

Most rocks have been deformed and fractured during this long geological history through the action of tectonic and other stresses. The rock mass is therefore weakened and excavation of an opening in this material causes overstressing due to stress concentrations created near the opening. The following time-dependent process has been developed as a working hypothesis for this thesis.

As soon as an opening is excavated tangential stress concentrations are created near the opening wall, where the radial or confining stresses are smallest. The stress level, relative to the rock mass peak strength is highest near the opening. Most rock materials show a stress-dependent creep rate and this results in a rapid stress relaxation near the opening and in a stress redistribution due to differential creep rates to a zone of higher confinement (This is illustrated in Chapter 6, Figure 6.6.a). At great depth or

in weak rock the stress concentrations are too high and the rock yields. A plastic zone is created in which elements closest to the tunnel are strained beyond their peak strength, elements farther inside the rock mass, in an intermediate zone, are strained to near-peak stress levels, and elements even farther inside the rock mass are strained within the elastic range. The process of stress redistribution due to differential creep rates still applies but other processes are superimposed. In the intermediate zone, an element loses strength since most rocks have a long-term strength which is lower than the short-term strength. This loss in strength has to be balanced by a stress redistribution to stronger elements or elements in higher confinement areas. Any stress transfer results in additional strains and displacements which in turn cause an additional strength loss in the plastic zone closer to the tunnel wall. An element in this zone will gradually approach its ultimate strength and if it possesses a time-dependent or rate-dependent strength, like a visco-plastic material, it loses some of its resistance with time and contributes to a further stress redistribution. (This is illustrated in Chapter 6, Figure 6.6.b). Furthermore, an element which was initially in the elastic zone, but close to its peak strength, will be loaded and overstressed as a consequence of this stress transfer. It will lose strength as a function of time and cause propagation of the plastic zone as well as additional stress redistribution. In summary,

stress-dependent creep properties, time-dependent strength loss and strain - weakening are three major causes of time-dependent stress redistribution which have to be considered in the evaluation of tunnel closure and extensometer measurements. The major aim of this thesis is to investigate the relevance of the two latter points , strength loss and weakening. The work presented by Guenot (1979) is a continuation of this objective and the thesis by da Fontoura(1980) is closely related to this topic.

The time-dependent propagation of the plastic zone terminates eventually for several reasons. The stress level to which rock elements outside the plastic zone are stressed decreases with increasing distance from the tunnel wall and yielding as well as stress redistribution becomes less likely and less dominant during the expansion of the plastic zone. The rock mass becomes more ductile as the confinement pressure increases and this causes a further slow-down of the fracture propagation resulting in a decelerating stress transfer. The effective size and shape of the opening changes towards the most stable configuration during stress redistribution or yields unless overall instability (fracture propagation to the surface) is initiated.

In the case of non-symmetric propagation of a plastic zone, strength and ductility may change due to a change in rock element size and shape at the fracture point. Local weaknesses become less important and local instabilities less likely. This process normally reaches a stable

equilibrium which does not preclude fractured rock penetrating the opening. It indicates rather that there is only a limited zone of rock which has failed and needs support. This point is supported by observations discussed by Professor Tincelin at the AFTES-meeting in Paris (1978) who observed that support pressures in practice seldom exceed 0.1 to 0.2 MPa, pressures significantly lower than theoretically predicted by various methods.

1.3 Scope and Organization of this Thesis

The objective of this thesis, very broadly formulated, is to study the influence of time-dependent rock mass properties and the time-dependent fracture process on the behaviour of tunnels in a strain-weakening rock mass. Because of the special emphasis put on the study of rock mass rather than on intact rock behaviour, only two possible approaches appeared practical: a study of case histories or model testing. The first possibility was eliminated for two reasons: (a) loading history (face advance), boundary conditions, and rock structure cannot be controlled to eliminate complex interaction, and observations can normally be started only after excavation; (b) ideal case histories where time-dependent fracture processes dominate are rare and were not accessible. Even though model testing has many drawbacks, it was found to be the only alternative. The fact that a natural, jointed material (coal) with most of the required properties was available and could be used as a

model material convinced the author of the usefulness of model studies. Some of the most important characteristics of the selected model material are:

- discontinuous jointing at a regular spacing of 1 to 3 cm;
- brittleness, even at high confining pressures (>1.0 MPa);
- time-dependent strength; and
- high frictional resistance.

This material had been studied by Noonan (1972) in direct shear tests but additional information, especially on the time-dependent fracture behaviour, was needed.

Chapter 2 summarizes the origin and the geology as well as the mechanical properties of the coal. Data from direct shear tests and triaxial compression tests at confining pressures up to 1 MPa conducted by the author and Guenot (1979) are shown.

In Chapter 3 results from multiple-stage repeated relaxation tests are discussed to describe the time - dependent fracture behaviour of the coal at low confining pressure. Only one mode of failure, the development of a shear plane parallel to existing joints but through rock bridges, is investigated. A schematic stress - strain diagram for a brittle rock is developed and used to describe the time - dependent fracture process. A summary of this chapter has been published by Kaiser and Morgenstern (1979).

As a result of these investigations, a phenomenological

model which describes (and explains to some extent) the time - dependent fracture behaviour of strain-weakening rock has been developed. The response of this model to various loading histories has been illustrated by a simplified model and compared with test data, reported in the literature, from tests on rock subjected to corresponding loading histories. The results of this investigation are reported in Chapter 4.

The second part of this thesis deals with model tests. Reasons for the model testing, the scope of the program, and the model test apparatus are discussed in Chapter 5. The method of sample preparation, the general loading history, the data processing procedures and an explanation of the various ways of data presentation are presented in the same chapter.

An interpretation of the test results from tests on one coal sample are given in Chapter 6. Reloading cycles and stage creep tests have been undertaken with stress ratios N varying between 1.0 and 0.2. The stress ratio N is defined as the ratio between minimum (or horizontal) principal field stress and maximum (or vertical) principal field stress. Linear elastic and linear visco-elastic material models have been used to interpret the test results, and a new approach, called "equivalent opening approach", has been developed to explain observations made during these model tests.

In the final Chapter 7 conclusions are summarized and implications as well as recommendations for further research

are discussed.

CHAPTER 2

GEOLOGY AND MECHANICAL PROPERTIES OF COAL

2.1 Introduction

The coal investigated was selected as a model material because of two major factors. First, as a jointed, brittle material with time-dependent strength and deformation characteristics, coal is an ideal material for the investigation of the effects of the time-dependent failure mechanisms. Second, the regular joint pattern, with a spacing of less than a few centimeters, and the strength of the coal are ideal for the modeling of a rock mass surrounding an opening. The use of a natural material overcomes many deficiencies of an artificial model material. The brittleness allows the study of the effects of strength loss at low confinement whereas the time-dependent strength enables the investigation of these processes as a function of time. The nearly linear elastic properties within a limited stress range make it possible to check the instrumentation, to estimate the stress distribution and to predict performance under changing stress conditions.

The purpose of this chapter is to describe the coal used as a model material, to establish its mechanical properties, and to investigate the time-dependent failure mechanisms of a jointed rock mass near failure. The term "failure" is used in this context with a somewhat wider definition than usual to describe the entire range where

excessive yielding occurs with or without simultaneous strength loss. Initial failure occurs at peak strength and subsequent failures are possible after reloading at strains exceeding peak failure strain at stresses below peak but at, or above, ultimate strength.

2.2 Geology

2.2.1 Site Location

All samples tested in direct shear, triaxial compression or model tests were obtained from the Highvale Mine of the Sundance Power Plant on the south shore of Wabamun Lake approximately 75 km west of Edmonton in Tp 52, R4, W. 5th Mer. The Highvale Mine is operated by Alberta Coal Ltd. and produces the coal for the power plant owned by Calgary Power Ltd. The Wabamun Lake district is an area of low relief at elevations between 700 and 800 meters within the plains area of central and eastern Alberta.

2.2.2 General Geology

The geology of the Wabamun district is described in a report by Pearson(1959) and a brief summary is given here. Sandstones, shales and coal seams of late Cretaceous and early Tertiary ages deposited in a fresh-water environment constitute the bedrocks of the Wabamun Lake district. The upper Cretaceous is represented by the upper part of the Edmonton Formation composed of bentonitic clay-shales, with minor sandstones and coal seams of varying thickness up to 5

meters. The lower Tertiary is represented by the Paskapoo Formation, a massive sandstone with a few thin shale bands. A thick coal-bearing zone has been found near the top of the Edmonton Formation at numerous points throughout the Wabamun district from Pembina River 6.5 km north of Entwistle to the North Saskatchewan River at Coal Arch. This coal unit is laterally discontinuous and can be subdivided into several seams separated by shale or sandstone. In the vicinity of Wabamun Lake it is approximately 10 m thick. The coal at Sundance is less fractured than on the north side of the lake. This can be attributed most likely to ice thrust action during Pleistocene times.

A mantle of glacial tills, sands and gravels of generally less than 15 m thickness overlies most of the Edmonton and Paskapoo strata in the Wabamun Lake district except for a belt a few miles wide along the south shore of Wabamun Lake. The tills are largely clayey to sandy in texture.

The Cretaceous and Tertiary strata in the Wabamun Lake district dip between 4 and 10 meters per kilometer to the southwest. The dip is modified by near-surface features produced by ice movement. The distance between these small "anticlines" and "synclines" ("rolls") is in general less than 100 m.

2.2.3 Structure of Coal

All samples were obtained from the west pit at the Highvale Mine (Sundance). Two major seams are mined at this location after removing about 10 m of till by dragline. The seams have to be blasted with light explosive charges to loosen them for loading.

The samples were taken from the upper of the two main seams. A detailed structural survey was conducted by Noonan(1972) and is summarized briefly. The coal seam is horizontally bedded with a major set of joints oriented N45°E perpendicular to the bedding. The spacing of these essentially planar but discontinuous joints is in general between 1 cm and 3 cm with an average of approximately 2 cm. They do not continue across major bedding planes that consist of thin bands of clay-rich coal or shale interbedded within the coal. Fractures normal to the joint planes are non-planar and do not continue across joint planes. The bedding planes and the joints constitute major planes of weakness.

Coal is a product of plant material sedimented in water together with pockets or layers of sand, silt or clay and it is an extremely heterogeneous rock containing remnants of tree trunks and branches. These inclusions cause variations in stiffness that lead to differential straining during stress release. As a result, fan-shaped or circular fracture patterns can be observed which dominate the structure locally. These patterns were often observed on the blocks used for model testing and must be considered in the

interpretation of test results.

2.2.4 Composition of Coal

Standfield and Lang(1944) classified the coal in the Wabamun district as subbituminous B according to the Canadian classification. Approximate analyses of three samples showed the following composition in percent weight (Pearson(1959)):

Moisture	21.4	21.8	18.4
Ash	8.0	14.9	11.9
Volatile Matter	28.3	24.4	27.4
Fixed Carbon	42.3	38.9	42.3
Fuel Ratio	1.50	1.59	1.54
Gross B.t.u. per lb.	8920	8000	8720

The last two columns are the results from an analyses made by the Research Council of Alberta on samples from the Upper Main Seam and the Lower Main Seam south of Wabamun Lake, respectively (Pearson(1959)).

Pearson(1959) describes the composition of the coal using the petrographic classification system suggested by Hacquebard(1951) (Vitrain with 100-96% Vitrinite; Clarain with 95-51%, Claro-Durain with 50-21% and Durain with 20-0% Vitrinite) as follows:

"All seams in the Wabamun Lake district are thinly layered, and the four rock types (vitrain, clarain, claro-durain, and durain) are intimately mixed in the heterogeneous coal mass. Clarain generally predominates, but vitrain is present in lenses up to 5 mm thick in some samples; the coals are essentially bright, with lenses and layers of dull coal. Examination of samples from drill holes south of Wabamun Lake indicate that the major parts of the two main seams are bright coals consisting largely of vitrain and clarain."

This description applies accurately to the coal tested in this research program.

2.3 Strength of Coal

A number of direct shear and triaxial compression tests were undertaken to evaluate the strength parameters and the stress-strain relationship of the coal, particularly in the direction of the joints. At the outset, only soil triaxial compression test cells with a maximum confinement pressure of 1 MPa and one rock shear test machine were available. In the final stage of this study a few high pressure triaxial compression tests (up to 10 MPa) were conducted on small diameter samples.

2.3.1 Information from Previous Testing

Strength testing on this coal was conducted by Noonan(1972) in direct shear tests on precut and "intact" samples. The results of this study were summarized by Morgenstern and Noonan(1974) .

A series of classification tests yielded average values for moisture content, specific gravity and bulk density of

24%, 1.58 and 1.38 g/cm³ with no significant deviation from these average values. Saturation ranged from 79 to 100%. A constant residual angle of friction of $\phi_r = 30^\circ$ was obtained on pre-cut samples (5.1 by 5.1 cm) with the shear plane parallel to the bedding plane, the joint planes perpendicular to it and a maximum normal stress of 7 MPa. Young's Modulus E was estimated and varied depending on sample orientation and normal stress (less than 0.7 MPa) between 140 and 550 MPa. The Young's Modulus tends to increase with increasing normal stress due to fracture and joint closure. The peak strength parameters c and ϕ for low normal stresses of less than 0.55 MPa were determined for several sample orientations. Along the bedding plane $\phi = 41^\circ$, c = 0.39 to 0.52 MPa and perpendicular to it with varying joint plane orientation $\phi = 66^\circ$, c = 0.12 to 0.35 MPa was calculated. Shear displacement at peak failure was several orders of magnitude greater than the measured dilation. It was concluded that the peak friction angle for discontinuous shear planes is a function of material strength rather than the geometry of the discontinuities.

For continuous shear surfaces after the peak strength was overcome the shear resistance could be related to $\tan(\phi_r + i)$ where ϕ_r is the residual friction angle and i the inclination of the shear surface with respect to the direction of the applied shear load.

These results are supported in general by the direct shear test data presented later.

2.3.2 Sampling and Sample Preparation for Laboratory Testing

2.3.2.1 Method of Sampling

First an attempt was made to drill 25 cm diameter undisturbed samples perpendicular to the bedding plane with the drill equipment shown in Plate 2.1. This machine was built at the University of Alberta and an earlier version was first used and described by Krahn(1974) . Due to rotation of the core and shearing along the bedding plane it was not possible to recover samples longer than approximately 20 cm. Many of the bedding planes were separated during the blasting operation needed to assist loading of the coal. These cores were large enough to trim samples for the direct shear tests but not sufficient for the triaxial compression tests. From this and Noonan's experience it was concluded that the only way to get good and consistent samples was to collect large blocks of coal (60 by 60 by 30 cm) and to drill samples from them in the laboratory with special coring equipment. By this method it was possible to recover about ten samples per block with a success rate of 50 to 70% and to ensure reasonable consistency. The digit in the sample number indicates the block number from which the sample was cored (e.g. TR-1B, stands for triaxial compression test sample - Block 1, Core B). Blocks and samples were wrapped with plastic and stored in a moist room at 10⁰ C and 100% relative humidity after transportation to the laboratory, after coring or trimming and after casting before testing. Only samples which were



Plate 2.1 Drilling of Samples Perpendicular to Bedding of Coal

kept for a few years showed signs of dessication.

2.3.2.2 Trimming

The blocks for the direct shear tests were cut to about one half centimeter under shear box size on all sides using a Northland concrete saw (Noonan(1972)) and stored for casting. The ends of the cores for the compression tests were trimmed to the proper length by a specimen saw which allowed more accurate alignment. Water was used as a cutting fluid. The cut-off ends were used to determine the pre-test moisture content. After trimming, the ends were ground with decreasing grades of sandpaper to parallel surfaces within about a tenth of a millimeter. It was difficult to prevent chipping of the edges of the sample and extreme care was necessary to obtain acceptable samples.

2.3.2.3 Casting

The samples for the direct shear test were cast in Devcon B plastic steel epoxy to ensure snug fit in the shear box and flat surfaces for seating and loading. A one centimeter gap was left open in the middle of the sample to accommodate the shear plane. If any portion of a joint was visible it was positioned at this elevation to cause failure through the joint.

2.3.3 Direct Shear Tests

2.3.3.1 Testing Procedure

A series of 9 tests were run on 6 cm thick coal samples in the modified direct shear machine described by Noonan (1972). The design of the machine allowed the use of two different sizes of shear boxes, a 9 by 12 cm and a 5.08 by 5.08 cm box. Tests 1 to 3 were conducted in the larger box and tests 5A to 5F in the smaller box. All samples were tested in their natural state at a constant deformation rate of 0.0488 mm/min up to the first peak and 0.244 mm/min after peak and on displacement reversals. The normal load was applied one day before shearing was started. A maximum shear displacement of one centimeter in each direction and at least one reversal of the displacement direction were imposed on the samples. A maximum of five reversals were applied to sample 5E. Horizontal displacement of the shear box and vertical movement of the normal load frame were measured using linear voltage displacement transducers (LVDTs). The shear force was measured by a load cell with 45 kN capacity. A shear load versus displacement graph was plotted on a X-Y-recorder and the output of the three measuring devices was printed at selected intervals.

All shear stress displacement graphs showed a sharp drop of shear stress after peak strength was reached, as a result of the release of strain energy stored in the relatively soft loading system.

2.3.3.2 Sample Orientation and Description

The moisture content of the samples was determined indirectly on the portions cut off during trimming of the samples. The average moisture content was 23.8% with little variation. Drying at temperatures between 75⁰ and 125⁰C for an additional period of up to 5 days did not produce any significant changes in the moisture content.

Sample 1 was the only sample tested with the shear plane parallel to the bedding plane and the shear force acting parallel to the vertical joint plane. This configuration corresponds to type A (Morgenstern and Noonan(1974)) and the observed peak strength is close to the failure envelope reported by these authors. The sample area was 84 cm² and the joint spacing was approximately 6 mm.

Samples 2 and 3, with an area of 103.6 cm² and 100.4 cm², were sheared parallel to the joint plane with the bedding plane vertical and parallel to the shear force. This configuration corresponds to type F (Morgenstern and Noonan(1974)) and again good agreement with the peak strength envelope reported by them was observed. The degree of separation \bar{X} , the ratio between open joint area and total cross-sectional area, was estimated by eye to be 20% and 30%, respectively. Open joints could be distinguished easily from the dull, crushed rock bridges because of the bright appearance (vitrain and clairain) of the joint surfaces. This method of estimating the degree of separation was used for all direct shear and triaxial compression tests. Even

though \bar{X} is not measured accurately it gives a good indication of the sample's intrinsic strength since the peak strength is directly related to the percentage of intact rock.

Samples 5A to 5E were also of the type F configuration with joint planes parallel to the shear plane and bedding planes parallel to the direction of the shear force. These samples with cross-sectional areas of 14.7 to 15.8 cm² were tested in the smaller shear box. The estimated degrees of separation were approximately 20, 50, 55, 75, 25 and 65% for samples 5A to 5F respectively, and are indicated in Figure 2.1 in brackets beside the peak strength.

2.3.3.3 Direct Shear Test Results

The strength data are summarized in a shear stress versus normal stress plot in Figure 2.1. The shear and normal stresses were corrected as a function of shear displacement to compensate for the reduction in the cross-sectional area. Test numbers are circled and the maximum and minimum shear resistances for each shear displacement reversal are numbered consecutively (1 for first shear, 2 for reversed shear, etc.). The results from Noonan (1972) for type A and F are indicated on Figure 2.1 by two lines for the peak strength (normal stress range 0 to 1 MPa) and the ultimate resistance for shear along the bedding plane (normal stress range 0 to 7 MPa). Reasonable agreement with these data can be observed. The ultimate resistance

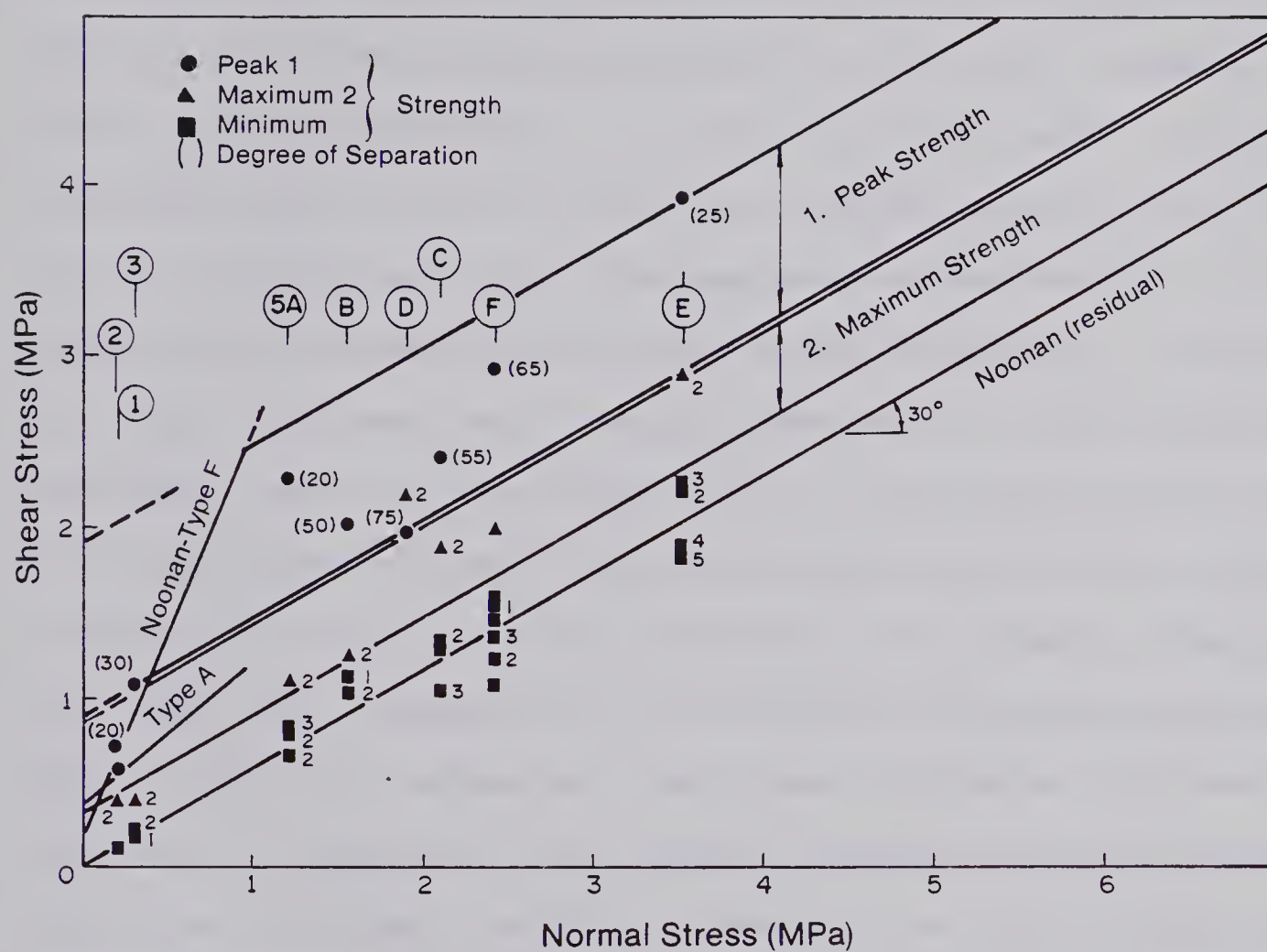


Figure 2.1 Mohr Diagram of Direct Shear Test Data (Test No.1,2,3 and 5A to 5F)

corrected for dilation, and indicated by the squares, was calculated in the following manner (or measured at a point where no dilation was observed). The inclination i of the shear plane was determined from the measured shear and vertical displacement and the resistance was then calculated under the assumption that the cohesion was small enough to be neglected. Patton's (1966) shear strength equation $\tau = (5p) \tan(\phi_r + i)$ was assumed applicable. From this equation it follows that $\tan(\phi_r + i)$ is equal to the ratio between measured shear stress and normal stress. If i is known ϕ_r can be calculated. The corresponding resistance $\tau_r = (5p) \tan(\phi_r)$ was then calculated and plotted as squares in Figure 2.1. The various data points correspond to the different reversals and to values determined at the beginning and end of a particular reversal. The figure shows that these points lay on both sides of Noonan's envelope for ultimate strength and that the assumption of an ultimate friction angle of $\phi_{ult} = 30^\circ$ is adequate. The term ultimate instead of residual is used by the author because of the fact that there is no true residual strength of rock (Krahn and Morgenstern(1979)).

During initial loading the sample is deformed until stresses locally exceed the strength of the material. Depending on the original structure of a sample, failure may start from the stress concentrations near the point of load application, from internal stress concentrations at the end of existing fractures, joints or cracks, or from areas where

tensile stresses exceed the tensile strength of the material. During this failure process the sample dilates and a shear surface is created. Peak dilation angles in the order of $20-30^{\circ}$ were observed. The displacement at peak shear strength was 2.96, 4.0 and 5.18 mm for the sample No. 1 to 3 and between 2.16 and 3.7 mm for the samples No. 5A to 5F. The geometry of these shear surfaces depends on the failure process. In most samples a shear plane with a step-like appearance with fewer steep steps in the direction of initial shear was observed. This non-symmetric shear surface is the reason for a second, but reduced, peak strength (called Maximum in Figure 2.1) when the shear direction is reversed. This second peak is reached as soon as the sample passes the shear box mid point. If the inclination of these steps is too high, less force is needed to shear them off than to dilate, and an apparent cohesion or fundamental shear strength is observed. This additional resistance disappears during later reversals if these steps are sheared off. The ultimate strength was reached after large deformations of several millimeters. It is evident that the shear strength is a function of the size and the number of rock bridges (or steps) as well as the normal stress acting on the shear plane. The failure envelope is most likely non-linear with respect to normal stress, but there is not sufficient data to justify drawing it in this manner. A bi-linear relationship seemed appropriate. Lajtai(1969) suggested the following form for the total

shear strength S_f :

$$S_f = S_0 + (1 - \%) \delta \tan \phi_i + \% \delta \tan \phi_p$$

where:

S_0 = fundamental shear strength

$\%$ = degree of separation (area of open joint per total area)

ϕ_i = angle of internal friction

ϕ_p = angle of joint friction

If it is assumed that $\phi_i = \phi_p = \phi_{ult}$ the above equation reduces to Coulomb's failure criteria $S_f = S_0 + \delta \tan \phi_{ult}$. The fundamental shear strength would have to be a function of the degree of separation. The term "fundamental shear strength" is therefore used in this thesis to describe the resistance mobilized in jointed rock in excess of purely frictional resistance. It is a function of rock structure and confining pressure. The fact that both components may not be mobilized simultaneously should be considered during application of these strength parameters. The validity of the assumption $\phi_i = \phi_p = \phi_{ult}$ was not investigated and it seems that ϕ_p is less than ϕ_i because of the fact that preexisting joint surfaces are extremely smooth. In the framework of this rather limited investigation such a simplification seems reasonable, and it follows, for a normal stress range between 1 and 4 Mpa, that $\phi_{ult} = 30^\circ$ and S_0 (peak) = 0.87 to 1.90 MPa for degrees of separation between approximately 75% and 20%. For reversed shear and the same stress range the fundamental strength S_0 (called Maximum Strength in Figure

2.1) increases from 0.30 MPa to 0.85 MPa as the normal stress, which restricts dilation increases. It vanishes during subsequent reversals. For the low normal stress range between 0 and 1 MPa the failure envelope determined by Noonan (1972) should be applied. A similar approach was used later to analyse the results from the triaxial compression tests and a peak fundamental shear strength of $S_0 = 0.70$ to 2.05 MPa for confining pressures below 1 MPa and $S_0 = 2.0$ to 3.3 MPa for confining pressures up to 10 MPa was calculated. It should be pointed out that a direct comparison is not justified because of differences in stress fields before and during failure.

2.3.4 Triaxial Compression Tests

2.3.4.1 Testing Procedure

A series of triaxial compression tests at low confining pressure have been conducted in a universal triaxial cell for samples up to 100 mm in diameter (maximum cell pressure 1.5 MPa). Triaxial compression tests at high confining pressures up to 10 MPa have been undertaken in a Wykeham Farrance high pressure triaxial cell for rock samples up to 50 mm in diameter. These cells are conventional testing equipment and described in the manufacturers' manuals. The compression test machines used were both built by Wykeham Farrance Engineering Ltd; WF 10,071 compression test machine with 100 kN capacity and a 42 speed gearbox with a range from 4.1 mm to 0.00008 mm per minute, WF 10,081 compression

test machine with 250 kN capacity and a variable speed range between 6.35 mm and 0.0004 mm per minute. The vertical ram displacement and the load were measured electronically and recorded on a digital data logger with a recording accuracy of 0.01 mV. The volume change in the cell was measured by a volume change indicator with an accuracy of $\pm 0.05 \text{ cm}^3$ and corrected for ram displacement. Small leaks inhibited long-term volume change measurements. Gas was emitted from the coal during long-term testing which would have made volume change measurements at the back pressure inlet inaccurate. It was not possible to use high enough back pressures to prevent or significantly reduce the effect of gas generation because of the low confining pressure limit.

Samples with a diameter of 6.95 cm and 3.55 cm and a length of approximately 20 cm and 7.1 cm, for low and high pressure tests, respectively, were used. A length to width ratio of 2 to 3 was selected in order to have as many joints as possible crossing the samples without intersecting the load caps.

The samples were installed in the triaxial cells with porous stones at both ends and filter cloth around the sample to allow free drainage. Water was used as cell fluid. For the low pressure tests the sample was sealed with a thin (0.332 mm) latex membrane with double O-ring seals at the load caps. This membrane was not strong enough for long-term testing and was punctured by sharp corners of the coal sample after sustained pressure. For long-term testing a

latex sleeve of 3 cm width at each sample end and a second membrane was added. To reduce the possibility of puncture of the outer membrane a thin plastic sheet was imbedded in Dow Corning Vacuum grease between the two membranes. This plastic sheet was folded and allowed to stretch to prevent additional confinement at large strains. The O-rings were pressured by screw-clamps to improve the seal between membrane and load cap. In this way it was possible to seal the sample for long-term tests up to more than 4 months. Only one membrane broke after about one month where the membrane was installed without the plastic sheet. The high pressure samples were sealed with a specially shaped and manufactured high strength neoprene membrane (1.59 mm thick). This membrane was used for short-term tests and small leaks at pressures of 10 MPa were difficult to prevent.

All samples were consolidated for at least one day under the confining pressure selected for the test before the sample was axially loaded at a constant rate of 1.52 mm per hour. According to the volume change recorded during consolidation, no pore pressures should build up at this fixed strain rate, and the tests can be considered to be drained triaxial compression tests. Permeability tests by Patching(1965) on coal from Canmore and Star-Key showed permeabilities in the order of 10^{-5} to 10^{-8} cm/sec at confining pressures between 70 and 700 kPa and less than $k=10^{-7}$ to 10^{-10} cm/sec for confining pressures near 7 MPa.

Nevertheless it is felt that the selected strain rate is low enough to cause full drainage because of the fact that failure was anticipated and achieved along joint planes where drainage conditions are favourable and the local permeability is significantly higher than the overall permeability as measured by Patching (1965).

2.3.4.2 Sample Orientation and Description

It was the intention of this testing program to investigate failure processes in a rock mass. Shear along planes of weakness is known to dominate rock mass deformation and failure at least at low confining pressures. It is therefore of prime interest to orient samples with their joints as planes of weakness in such a manner that failure occurs along these planes. For an angle of friction of 30° a joint plane inclined at 30° to the sample axis will theoretically be a plane of maximum obliquity. This sample orientation was selected for the low confining pressure tests and the corresponding test results therefore constitute a lower bound strength envelope. Inclinations of joint planes of 30° , 45° , and 60° were selected for the high pressure triaxial test. Since all samples failed more or less along a joint plane no upper bound strength was measured. The bedding plane was always parallel to the sample axis.

The properties of sample 1A, 1B and 1C are listed in Table 2.1 and the corresponding data for the samples tested

Table 2.1 Properties of Triaxial Test Samples TR-1A, TR-1B and TR-1C

SAMPLE NUMBER	TR-1A	TR-1B	TR-1C
σ_3 , kPa	800	400	1000
Backpressure	---	---	---
σ_3' , kPa	800	400	1000
$(\sigma_1 - \sigma_3)_f$, kPa	7621	3171	5347
$(\sigma_1 - \sigma_3)_{e=2\%}$, kPa	4900	1370	3400(±)
$(\sigma_1 - \sigma_3)_{e=3\%}$, kPa	4300	1270	<u>2900</u>
E, MPa	1103.4	869.6	1100.9
e_g , %	0.14	0.29	0.17
e_f , %	0.835	0.715	0.93(±)
e^*f , %	0.05	0.06	0.27(±)
\dot{e} , %/hr	0.75/3.75	0.74/3.70	0.75/3.75
G_s	1.51	(1.51)	1.53
γ , g/cm ³	1.38	---	1.40
γ_d , g/cm ³	1.11	---	1.12
w(sample), %	24.5	23.5	24.3
w(ends), %	24.2	24.8	24.3
S_r , %	90.1	---	102.6?
Void ratio, %	42.9	---	36.1
$\bar{\alpha}$ (estimated), %	50	85	70
β , (°)angle between Joint and sample axis	27	30	26

(±)...approximately

xxx...extrapolated

(xxx)...assumed value

?...questionable data

for definition of strain terms see Chapter 3.

in multiple stage repeated relaxation tests are summarized in Table 2.2 . The condition of eight samples tested under high confining pressure are described by Guenot(1979) and their properties are summarized in Table 2.3 .

Sample TR-1A: The failure plane inclined at 27.5° intersected the sample wall 36 mm below the load cap. Approximately 50% of the shear plane was clearly a joint plane, the rest was crushed coal with a small portion sheared along a vertical bedding plane resulting in a degree of separation of less than 50%. There was some indication of vertical tensile fracture parallel to the bedding plane, most likely caused by differential shearing after one half of the sample sheared along a joint and a bedding plane.

Sample TR-1B: The slightly curved joint and failure plane was inclined at 32° to 26° intersecting the sample wall 10 mm below the load cap. Another slightly open joint intersected the sample end surface but was not sheared. Approximately 85% of the shear plane was a joint and no shear along bedding was observed.

Sample TR-1C: The failure plane inclined at 26° was step-like across the sample and one joint intersected the load cap whereas the other joint as a portion of the failure plane intersected the sides of the sample 20 mm below the load cap. The coal on one corner was overstressed and fractured during straining and this resulted in a stress-strain curve displaying ductile behaviour. The degree of separation was approximately 70%.

Table 2.2 Properties of Triaxial Test Samples CTR-2A/2F

SAMPLE NUMBER	CTR-2A	CTR-2B	CTR-2C	CTR-2D	CTR-2F
$\bar{\sigma}_3$, kPa	400	588	600	900	800
Backpressure	---	---	---	100	---
$\bar{\sigma}_3'$, kPa	400	588	600	800	800
$(\bar{\sigma}_1 - \bar{\sigma}_3)_f$, kPa	4150R (4500)	4950±	5940R (6200)	7810F (8700)	8080R (8300)
$(\bar{\sigma}_1 - \bar{\sigma}_3)_{e=2\%}$, kPa	2250	2500(±)	<u>3500</u>	6800	<u>4750</u>
$(\bar{\sigma}_1 - \bar{\sigma}_3)_{e=3\%}$, kPa	2130	2400	---	<u>4500</u>	<u>4200</u>
F, MPa	892.9	1315.8	1067.6	947.4	1185.2
e_g , %	0.14	0.03	0.07	0.15	0.18
e_f , %	0.76R	0.52	0.74R	1.24R- 1.67F	1.01F
$e * f$, %	0.16R	0.13	0.10R	0.26F- 0.69R	0.16F
\dot{e} , %/hr	0.85	0.74	0.76	0.77	0.71
G_s	(1.51)	1.50	(1.51)	(1.51)	(1.51)
γ , g/cm ³	1.38	---	1.37	1.36	1.32
γ_d , g/cm ³	1.16	---	1.09	1.07	1.07
w(sample), %	18.3	---	24.0	27.5	20.0
w(ends), %	16.8	24.1	23.7	---	20.3
S_g , %	95.1	---	95.3	100.0	72.6
Void ratio, %	29.1	---	38.1	41.3	41.5
% (estimated), %	70(±)	75	85	50	85
β , (°) angle between Joint and sample axis	30	30	29	31	30

(±)...approximately

xxx...extrapolated

(xxx)...assumed value

?...questionable data

xxx...interpolated

R...during relaxation test

for definition of strain terms see Chapter 3.

2.3.4.3 Triaxial Compression Test Results

The strength data are summarized in two Mohr diagrams (Figures 2.2 and 2.3). Figure 2.2 includes strength data from tests TR-1A, 1B and 1C, and from all repeated relaxation tests reported in Chapter 3. Figure 2.4 summarizes the corresponding stress-strain curves and volume change-strain plots if the latter was recorded. The individual curves are shown later together with a detailed description. A picture of sample TR-1B is shown in Plate 2.2. Figure 2.3 summarizes data of the high pressure tests.

Figure 2.2 shows the stress circles at failure. The stress state on the failure plane is indicated at the failure strain as well as at 2% and 3% total axial strain. The peak failure envelope from Figure 2.1 (the direct shear test data) are shown by dashed line for comparison. This comparison is possible since all triaxial test samples failed along a predetermined plane of weakness. The failure stresses measured in the direct shear test can be compared with the stresses acting on the failure plane of the triaxial test samples. Applying the same principle as used during the discussion of the direct shear test results, the fundamental shear strength for confining pressures up to 1 MPa and a degree of separation between approximately 50% and 85% ranged from 2.05 MPa to 0.7 MPa at peak strength, 1.5 MPa to 0.16 MPa at 2% total strain and 0.84 MPa to 0.14 MPa at 3% total strain. The fundamental shear strength

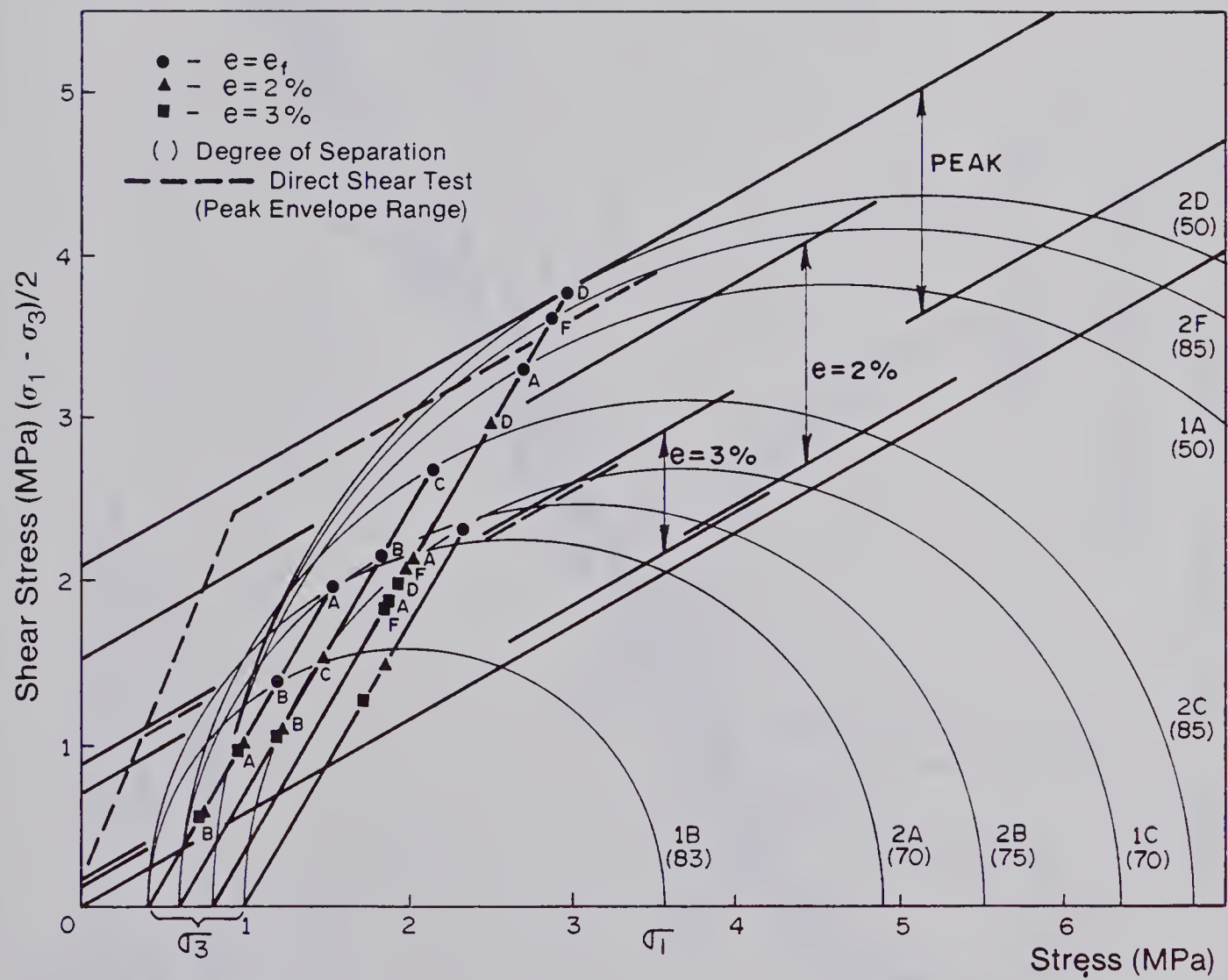


Figure 2.2 Mohr Diagram for Triaxial Compression Test Data
($\sigma_3 < 1$ MPa)

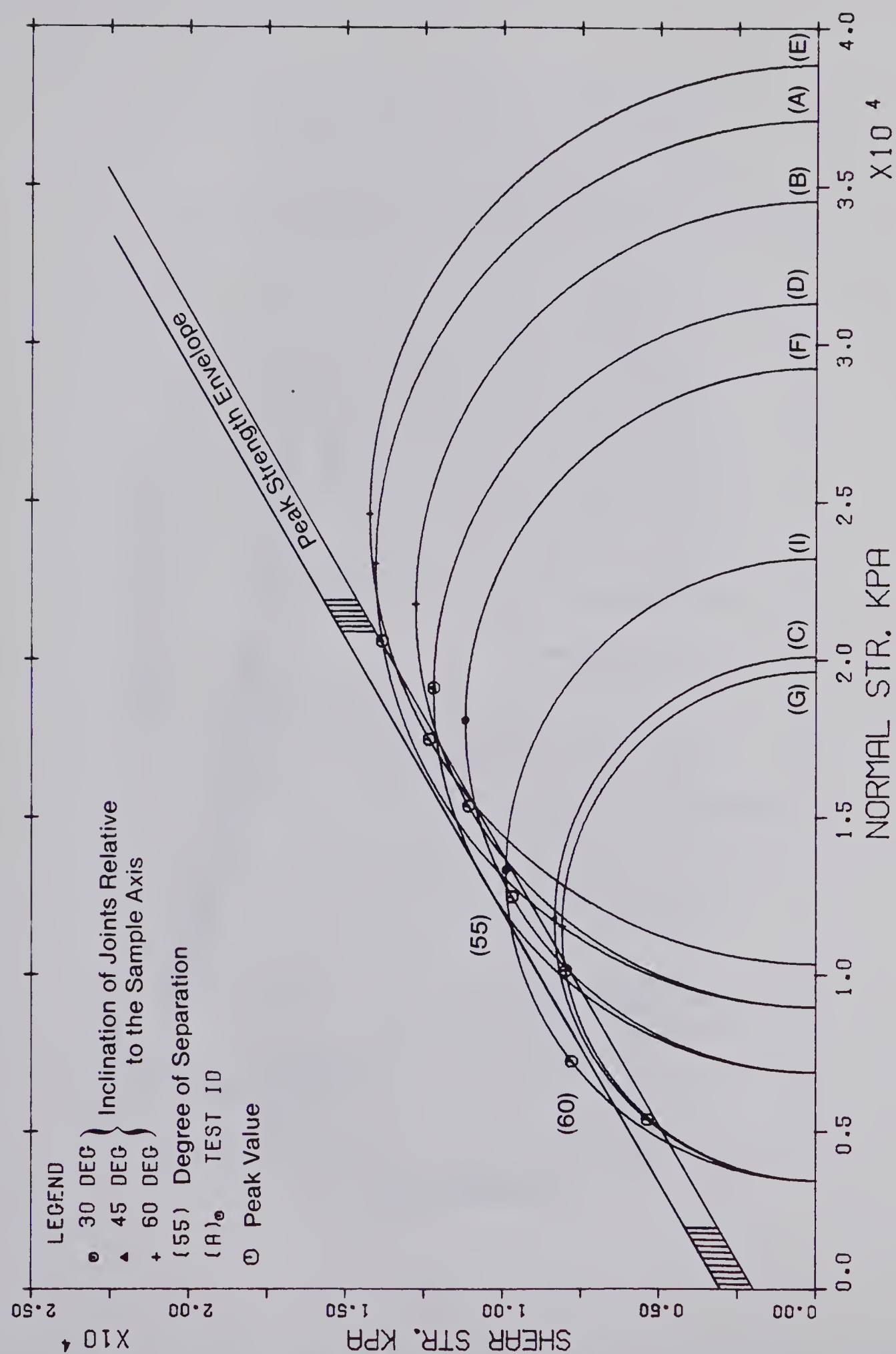


Figure 2.3 Mohr Diagram for Triaxial Compression Test Data
($\sigma_3 = 3.5$ to 10.0 Mpa)

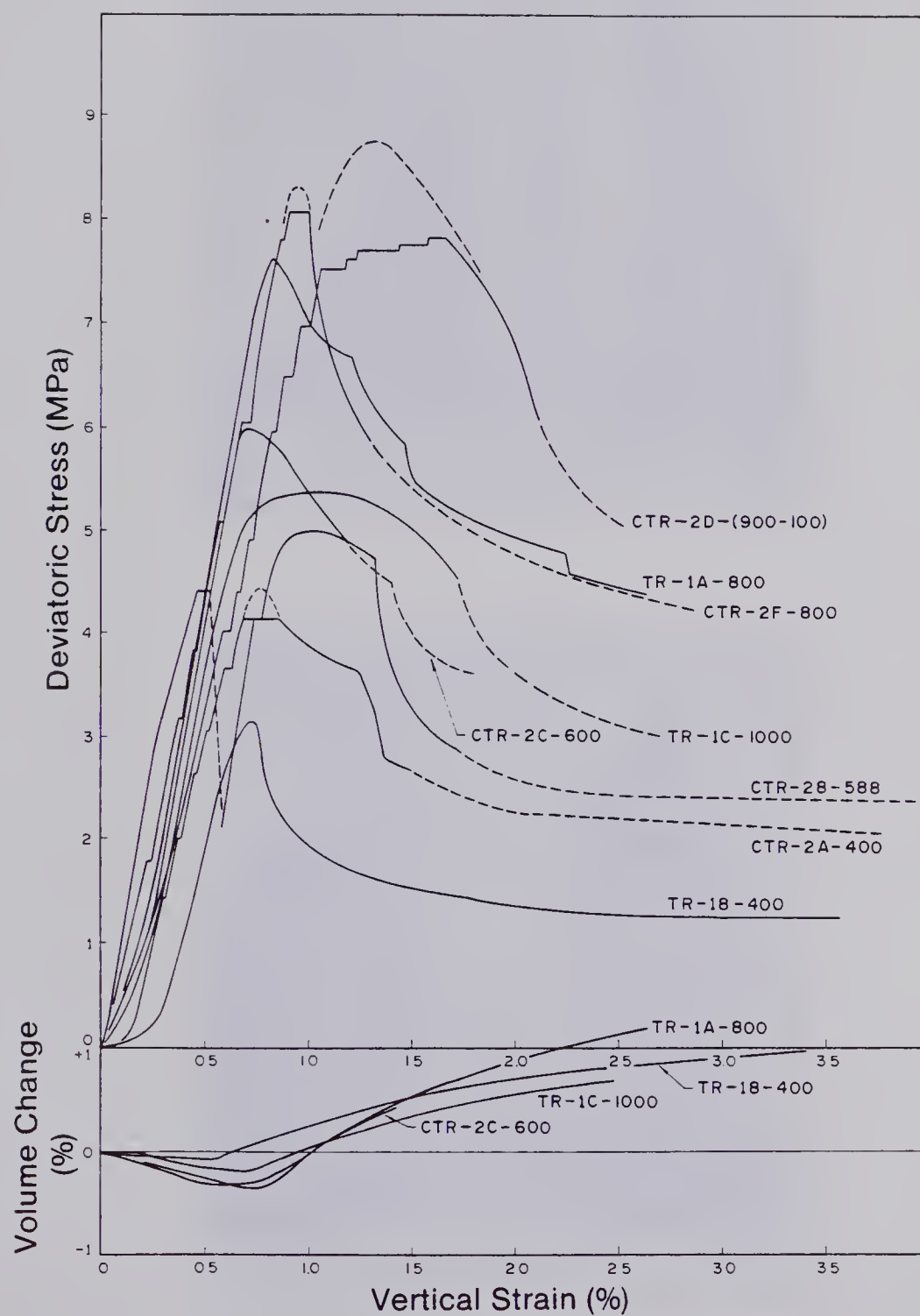


Figure 2.4 Summary Plot of Stress-Strain and Volume Change Data from Triaxial Compression Tests

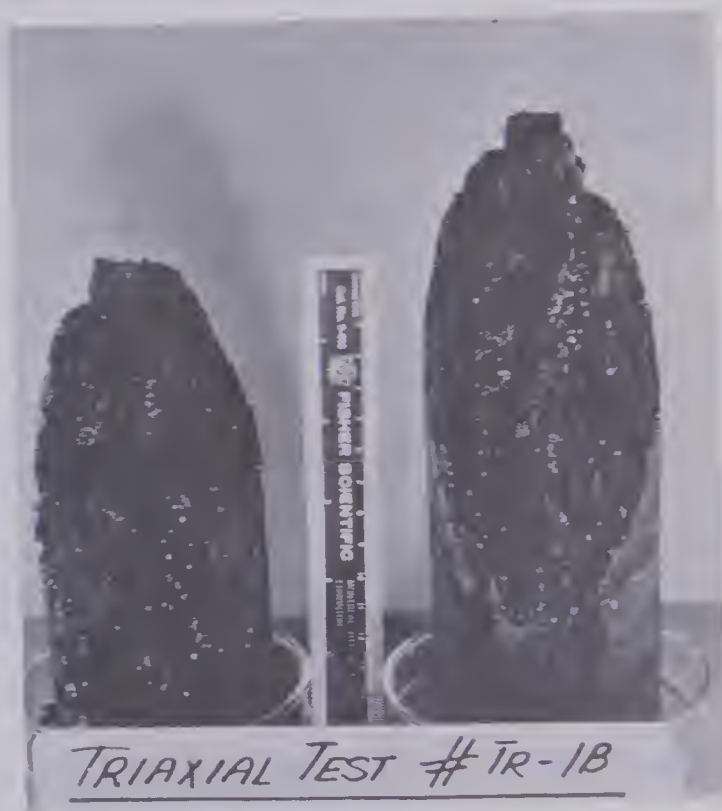


Plate 2.2 Sample No. TR-1B after Testing

determined from triaxial tests includes a strength component due to dilation. A curved failure envelope seems more logical but there is not enough data to support either assumption.

Figure 2.4 indicates that the coal is a brittle material and linearly elastic (after an initial non-linear stress-strain curve due to closure of cracks) up to stress levels close to the rock strength. During the failure process the coal dilates. It is not reasonable to draw other general conclusions because of variability among specimens and their failure modes. Each curve has to be considered separately. Both samples TR-1A and 1B indicate (Figure 2.5, Figure 2.6) a continuous linear volume decrease up to the point where the stress-strain curve deviates from linearity. Subsequently the sample dilates with a maximum dilation rate at or after peak strength followed by a continuously decreasing dilation rate towards the ultimate strength. Sample TR-1A shows the most dilation with 1.2% volume increase. This volume increase is composed of two parts, the dilation of the shear plane and the opening of vertical bedding planes (at low confining pressures). Volume increase due to crack opening within the "intact" coal can be assumed to be small. Loading parallel to the bedding planes causes tensile stresses at the ends of vertical cracks. As a consequence bedding plane separation occurs except if failure occurs first along an inclined plane of weakness. This bedding plane separation was observed in some samples.

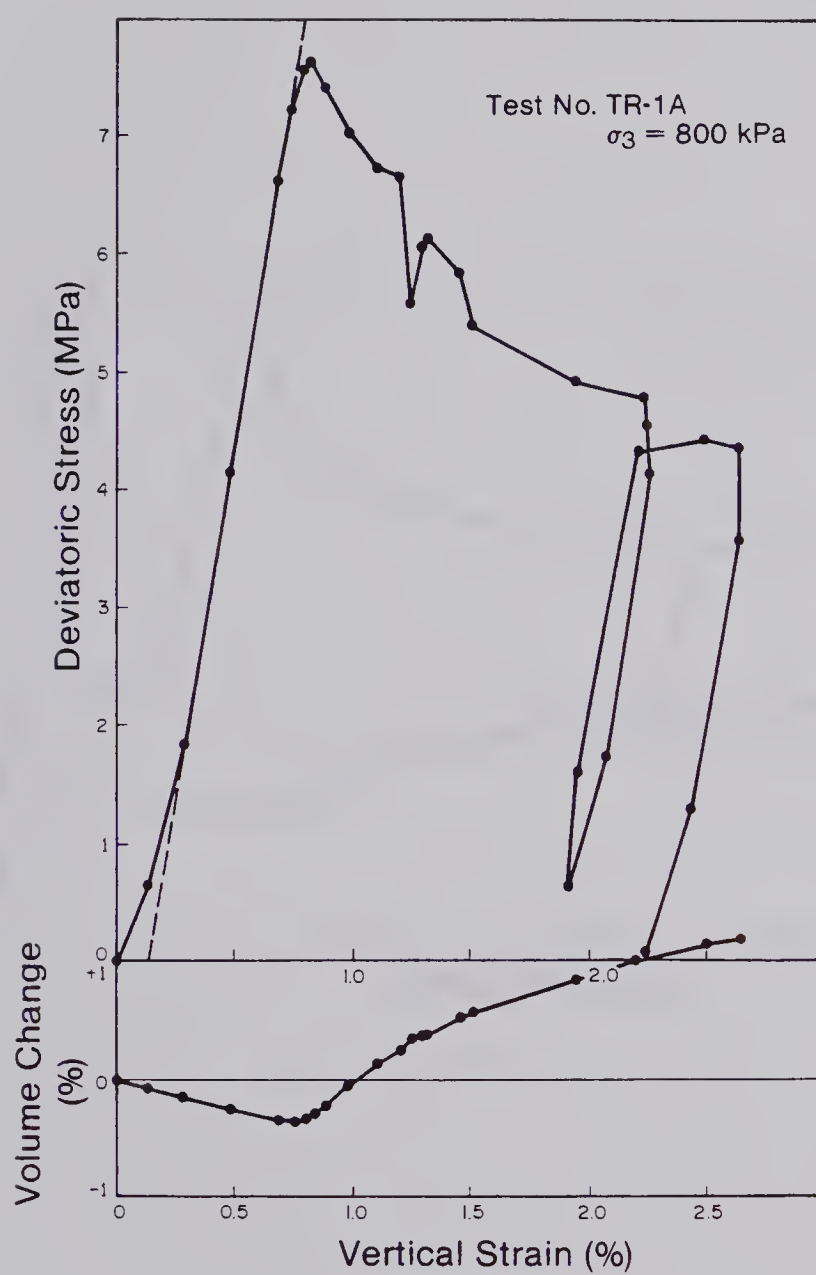


Figure 2.5 Stress-Strain and Volume Change Data of Test No. TR-1A

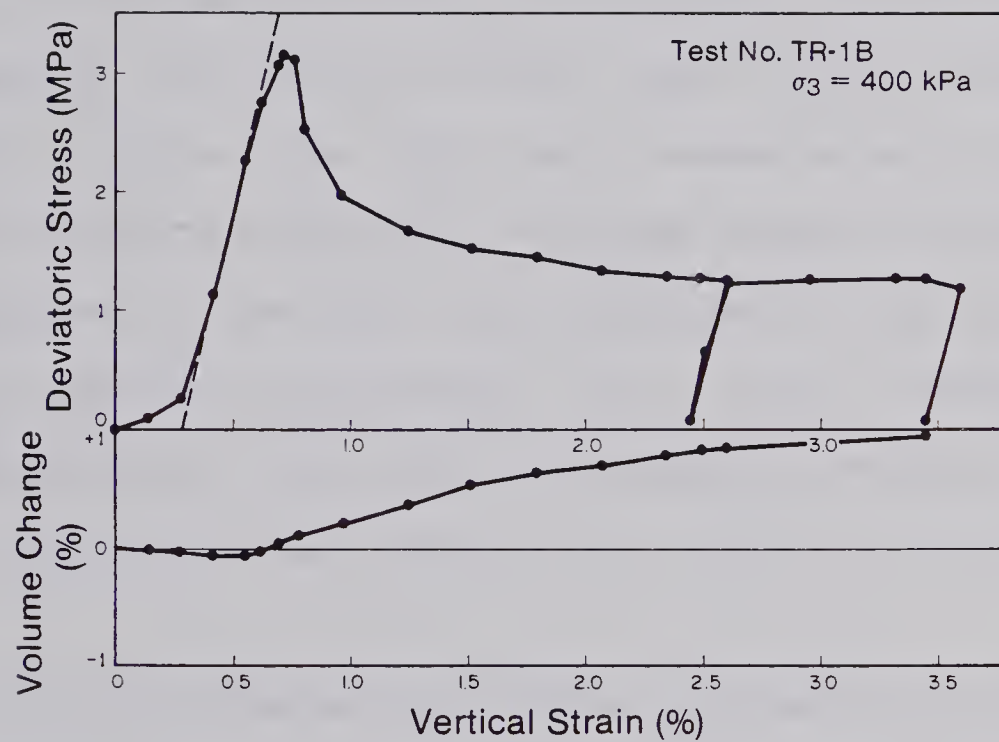


Figure 2.6 Stress-Strain and Volume Change Data of Test No. TR-1B

The almost constant loading, unloading, and reloading moduli indicate that slip occurred during failure. This cannot be considered to be a typical behaviour of a rock mass. Immediately after the peak strength, non-slip behaviour is believed to dominate in rock masses, as indicated by Mueller and Goetz(1973) and analytically modeled by Teeni and Staples(1969) .

Sudden drops in the after peak range indicate that the stiffness of the machine was lower than the stiffness of the tested coal at this point. In most cases it was possible to continuously follow the after peak stress-strain curve. It is believed that in particular the high capacity machine was stiff compared to the after peak stiffness of the coal. The machine stiffnesses determined from strain measurements during relaxation tests were approximately 80 MN/m for the 250 kN compression test machine and 40 MN/m for the 100 kN machine.

Sample TR-1C (Figure 2.7) failed initially as described earlier along a joint intersecting the load cap. Rotation of the load cap, stress transfer to the unfailed portion with increasing strain, and crushing of this overstressed area until failure occurred along a newly created shear plane is the reason for the rather ductile behaviour indicated in the stress-strain curve. These data are of rather limited value and are included only for completeness.

For confining pressures between 3.5 MPa and 10 MPa the fundamental shear strength ranges from $S_0 = 2.0$ MPa to 3.0

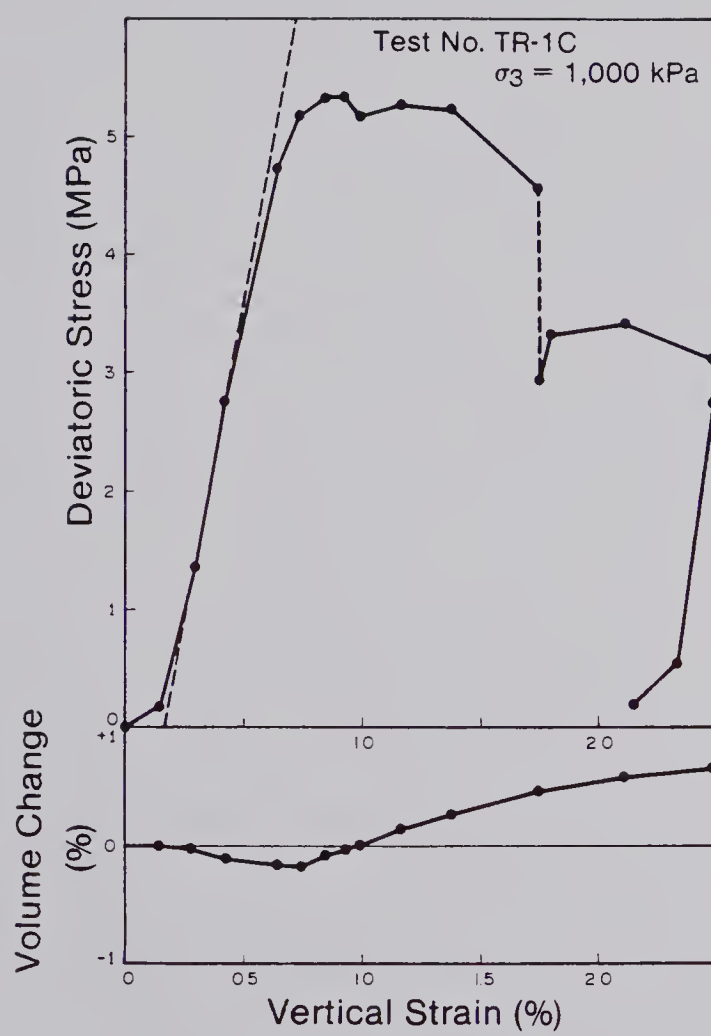


Figure 2.7 Stress-Strain and Volume Change Data of Test No. TR-1C

MPa (Figure 2.3). At total strains in excess of 5% this fundamental shear strength S_0 was reduced significantly to values between 0.0 and 1.5MPa. The fundamental shear strength increases with confining pressure as the strength of the jointed rock approaches the strength of the intact rock. Shear resistance along discontinuous joints becomes increasingly dominated by the rock bridges .

CHAPTER 3

MULTIPLE-STAGE REPEATED RELAXATION TESTS (MSRRT)

3.1 Introduction and Background

In Chapter 1 it is illustrated that it is of interest to investigate the time-dependent deformation characteristics of rock in the unstable zone of its stress-strain curve. It is assumed that a change in stress within the stable zone will generate terminating, time-dependent deformation, and an applied, constant displacement will cause a terminating, time-dependent stress change. A change of stress to a stress level inside the unstable zone will eventually lead to failure and a stress change within this zone will result in a change of time to failure. Application of a fixed displacement in the unstable zone will either directly cause failure or a new stress equilibrium will be established with time due to relaxation. The writer assumes that all brittle rocks have time-dependent properties and possess a stable zone in their stress-strain curve. Changes in properties and deformations with time might be sufficiently small to be neglected within a time scale relative to the life time of engineering structures, but cannot be disregarded when dealing with problems within a geological time scale. The same arguments apply to the second more controversial statement on the existence of a stable zone. Hofer(1958) believes that every rock body will fail if the stationary creep zone is reached;

it is then only a function of the applied stress when the tertiary creep stage or failure is initiated. It follows that there is no failure as long as there is a continuous decrease in strain rate ; i.e., a stable zone would exist. Denkhaus(1958) and Talobre(1957) agree and state that creep does not always lead to failure under moderate forces where deformations stabilize. Salustowicz(1958) disagrees and is of the opinion that creep always leads to failure under any sustained load. This implies that there is no stable zone except if a creep limit exists below which the material behaviour is time-independent. Nadai(1952) states that materials in the earth's crust behave viscously or deform plastically even under stresses as low as 500 kPa, if applied over geological times of tens of thousands of years. Rheological models for rock masses often include a viscous element in series with others; e.g. Burgers model or the modified Burger model with a number of Kelvin elements in series (Hardy and Chugh(1959)). This would indicate that these rocks do not have a stable zone. Nevertheless the simple fact that rock slopes and cliffs exist and do not deform significantly over large periods of time justifies the assumption of a stable zone for brittle rocks.

The stable zone, the unstable zone and the interface between them is to some degree history-dependent. The strength and the response of the rock at a given stress and strain level depend on its current structure. This structure is primarily a function of (a) the past rate of deformation

and (b) the confinement history during this deformation. The confinement is controlled by the stiffness of the loading system, the surrounding rock. The existing stress field is altered (e.g. during the construction of a tunnel) as a function of time (e.g. advance rate, time of lining installation) resulting in different stress histories. Because of non-linear, time-dependent rock properties and their variability on a micro- and macroscopic scale, the magnitude of stress concentrations, the local strain pattern, and the location of overstressing (failure initiation and propagation of failure zones) are affected by the loading rate. Different rock structures are created even if the total accumulated deformation is the same. The two factors of confinement and system stiffness are interrelated in most field situations but detached in triaxial compression tests with constant confining pressure. If confined rock deforms under an instant change in stress, the stress field will be altered with time since reactions vary as a result of time-dependent deformations (viz. K_0 is not the same in elastic and visco-elastic materials). Moreover, these deformations are a function of the ability of the loading system to store energy. The resulting rock structure is therefore a function of the system reaction which in turn is a function of the system stiffness. The phenomenon of rock bursts is an excellent example illustrating the relevance of the system stiffness. The same rock responds differently depending only on the surrounding rock mass and

the stored energy (Walsh et al., (1977) ;Walsh(1977)). Effects of system stiffness and behaviour at high confinement pressures have not been investigated during this research project. The failure plane was always forced through a plane of weakness inclined at 30^0 to the sample axis. The results presented should therefore be applied only to a corresponding failure mode. Nevertheless, it is believed that the observed behaviour can be generalized as long as the mechanisms and physical processes remain the same.

As a consequence of structure and system dependence there is no such thing as an absolute long-term or short-term strength. Only for a given state of deformation can we identify both a strength for instant loading and loading at an infinitesimal rate. The term "current" was introduced to specify this fact. The current short-term strength or current available strength (CAS) refers to the strength which could be reached, independently of time and deformation history up to this point, if the specimen were loaded instantaneously. Accordingly, the current long-term strength (CLS) refers to the strength which could be reached at an infinitesimal loading rate. It vanishes for a viscous fluid and has a finite value for a viscous solid. The current available strength can be determined by instant loading from a given point or by interpolation between two points where the current available strength was determined for different times and strains. The current long-term

strength can also be determined in a similar manner. The current strength is therefore a function of the present structure of the material.

The significance of this postulate is best illustrated by Figure 3.1 (Bieniawski(1970)). This Figure shows two stress-strain curves from uniaxial compression tests on a fine-grained sandstone at a constant strain rate between A and C, followed by an increased or decreased strain rate after C. After point B, corresponding to the stress level of the peak long-term strength, any fixed strain rate test follows a stress-strain pattern somewhere between the current available strength and the current long-term strength. A hypothetical range between current available strength and current long-term strength is indicated. The stress-strain curve for an instantaneous increase in strain rate at point C approaches the current available strength curve whereas it approaches the current long-term strength curve for a decrease in strain rate. New hypothetical ranges between current available strength and current long-term strength are indicated after a deformation of 0.15mm for the new strain rates. If we consider this rock strained with the four rate histories to a point D (same accumulated strain) we can see that the four ranges do not correspond. A stronger structure with a higher current available strength and current long-term strength is created at a lower strain rate (curve 1) and more damage resulting in a weaker structure with a current available strength even below the

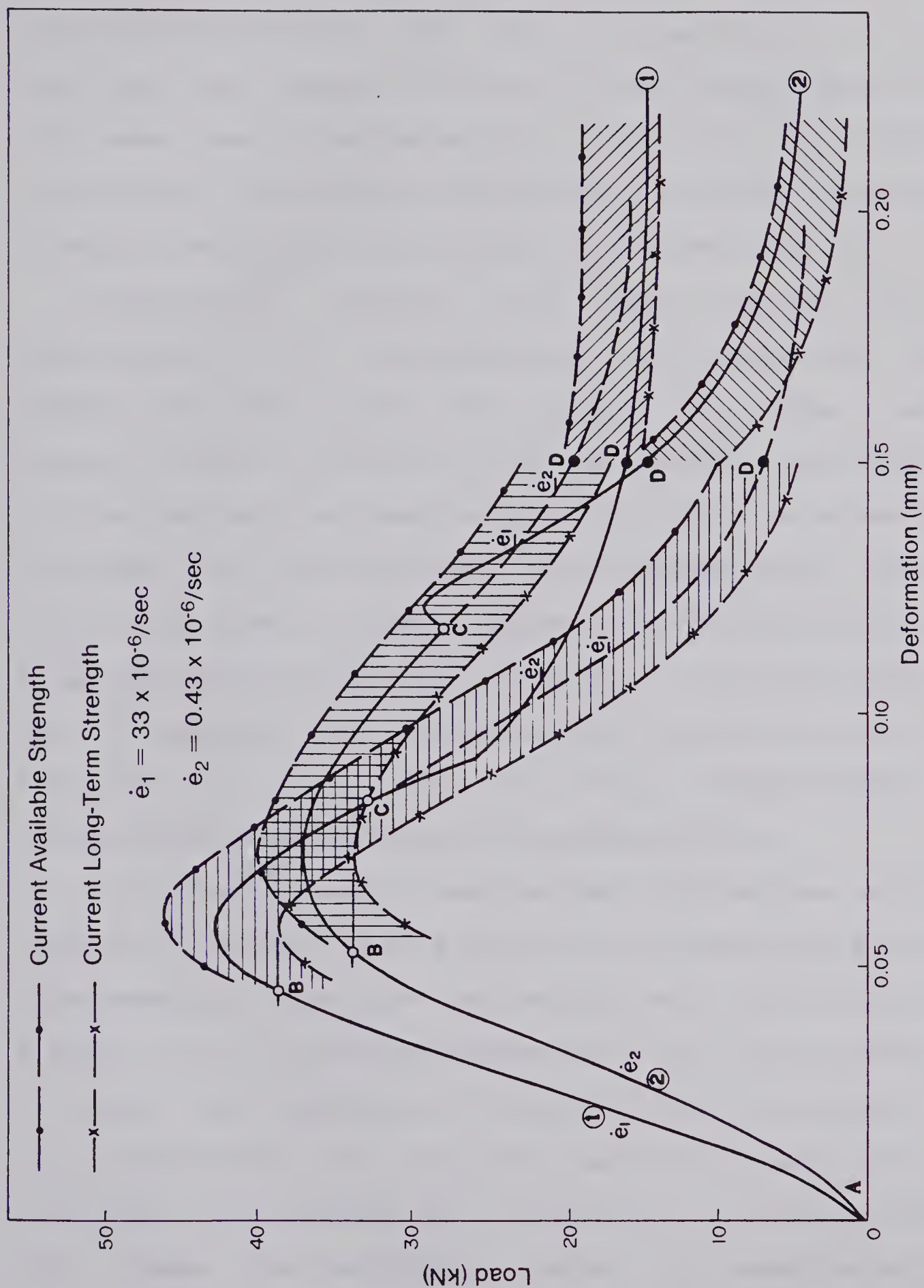


Figure 3.1 Uniaxial Compression Test on a Sandstone; Data from Bieniawski(1970)

current long-term strength of curve 1 is created at high strain rates (curve 2). This concept is applicable to intact rock and rock masses in general since the behaviour of a rock mass can be considered to correspond to the behaviour of an intact rock reloaded after it was strained beyond peak strength (see Figure 3.2) (Mueller and Goetz(1973)).

Considerable research has been devoted to the investigation of time-dependent rock properties. Most testing has been done with creep tests. Creep tests, however, cannot be used to study the post-peak behaviour of brittle rock and are inappropriate for this study since they correspond to an infinitely soft loading system. Results from creep tests on brittle material should only be applied to appropriate problems where initiation of failure leads to the collapse of the structure (e.g. infinite slope). The literature on creep tests and their interpretation is enormous and is reviewed by da Fontoura(1980) .

The time-dependent post-failure process has not been studied in detail, and as a result, our understanding of the time-dependent behaviour of yielding rock, particularly of brittle rock in confined conditions (e.g. around cavities) is poor. The majority of researchers have concentrated on the determination of the peak long-term strength and only relatively few attempts were undertaken, by variable strain rate tests and relaxation tests, to investigate the post-peak behaviour. Singh and Bamford(1971) reviewed and compared short-term test procedures to predict the long-term

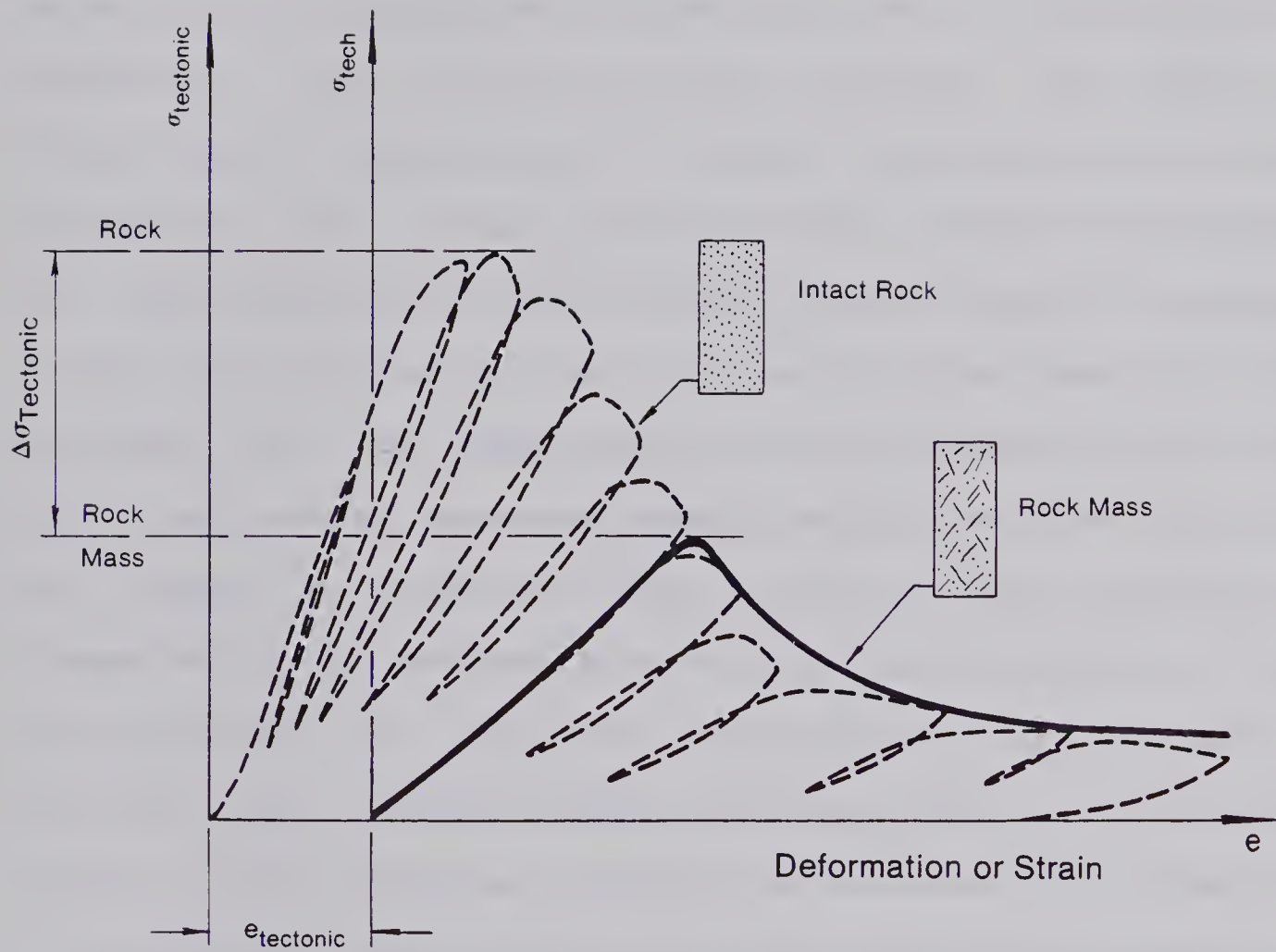


Figure 3.2 Interpretation of Uniaxial Compression Test on Sandstone (Data from Bieniawski, 1970) by Mueller and Goetz (1973)

peak strength of rocks by various indirect methods. They observed a considerable scatter between the various predictions ($\pm 4\%$ with an average long-term peak strength of 90% short-term peak strength) and they found best agreement with the loading rate method suggested in their paper. They also pointed out correctly that these short-term methods of predicting the long-term peak strengths are based on Bieniawski's hypothesis of crack initiation and crack propagation for intact, brittle rock. A direct application of these methods to rocks failing along a plane of weakness could be erroneous. No effort to predict the long-term peak strength will be made because of this reason and the fact that the natural variance between samples was too large and the number of tests too small. A similar test procedure as described in the following section was used by Pushkarev and Afanasev(1973) to determine the long-term peak strength of ductile rocks. Using the same test procedure in direct shear tests of rock contacts, Afanasev and Abramov(1975) found for a particular coal a friction angle for long-term shear of 83% of the short-term friction angle. As a result of further testing Afanasev and Pushkarev(1976) suggest a simplified method of determining the long-term peak strength of rock.

With the development of stiff, servo-controlled testing machines, a tool to obtain meaningful data in the post-peak range became available. Testing with various rates of loading was undertaken by Bieniawski (1970), Wawersik and Fairhurst(1970) , Wawersik(1973) , Rutter(1972) , and

Peng(1973) to mention only a few relevant contributions. Each of these tests shows that the post-peak behaviour is stress history-dependent and that different categories can be identified (Wawersik(1970)). Wawersik and Fairhurst(1970) illustrated how the fractured rock structure develops during shear before and after the peak strength is reached. Each test at a given loading rate followed a stress-strain path somewhere between its current available strength and current long-term strength path. Both the current available strength and current long-term strength as well as the test curve itself are a response to the continuously changing rate-dependent structure. These tests therefore give information about the development and strength of fractured rock structures as a function of loading history, but do not yield any information on the time-dependent properties or the response of a given structure at a given strain or stress level. They support the earlier statement that the rock structure at a given deformation is history-dependent.

The only way to investigate the time-dependent properties of brittle rock in the post-peak range is to unload samples and to conduct creep tests from stress levels within the stable or unstable zone, or to allow the sample to relax at various stages along a certain stress-strain path. The first procedure has been executed by Lama(1974) and will be approximated by the multiple-stage repeated relaxation tests discussed in the following paragraphs.

The time-dependent behaviour of failed rock was

investigated by multiple-stage relaxation tests and constant load tests in a stiff testing machine by Peng and Podnieks(1972) , Hudson and Brown(1973) , and Bieniawski (1970). Bieniawski (1970) determined the lower bound of the unstable zone, the current long-term strength which he called the long-term stability curve, and speculated that this limit might be parallel to the constant strain rate curve. He showed clearly that this lower bound depends on the strain rate. His test results indicate that the ultimate strength is rate-dependent and support the assumption that the ultimate strength of rock is not a material constant. No conclusions about the time-dependent behaviour within the unstable zone were drawn.

Hudson and Brown (1973) showed that slow strain rate tests followed a path close to a current long-term strength as would be expected. No general conclusions were drawn. Peng and Podnieks (1972) investigated the relaxation behaviour near peak strength, the strain rate effects before and after peak strength, and developed another theory of time-dependent peak strength. They indicate that the stress relaxation could be related to the crack propagation velocity and conclude that this stress relaxation is the reason for the stepwise drop in load at slow strain rates. Their data shows that the inelastic strain $e^* = e - e_c - e_0$ (for definitions see section 3.3) at failure is a function of strain rate and increases for the brittle tuff with increasing rate of strain. This contradicts the speculation

by some authors that the inelastic strain at failure is constant but it does not necessarily contradict the assumption of a critical inelastic volumetric strain at the onset of failure (Kranz and Scholz(1977)). Pushkarev and Afanasev (1973) used multiple-stage relaxation tests to develop a rheological model for a weak ductile rock but did not investigate the post-peak range in detail and no attempt was made to model this portion of the strength curve. Their model includes the existence of plastic deformations below the creep limit, the transition of visco-plastic to plastic deformations, and correspondence between the long-term strength and the stress level where irreversible visco-elastic deformation begins.

The aim of this section is to investigate the time-dependent transition from one rock structure, a discontinuously jointed rock, to another rock structure, a sheared continuous plane of weakness. The relaxation behaviour of a rock is an excellent indicator of the present state of the rock but assumptions about the strain-dependence of the material (e.g. strain- or time- hardening) have to be made, or a series of repeated relaxation tests at increasing strain are needed to evaluate this strain-dependence. The variability from sample to sample makes comparison difficult without a large number of tests and this provides an incentive to obtain as much information as possible from a single specimen, particularly where long-term testing does not allow large numbers of tests to

be conducted. Therefore multiple-stage testing has some advantages. The multiple-stage repeated relaxation test meets these requirements. The first part of this investigation has been published by Kaiser and Morgenstern(1979) .

The literature provides information on time-dependent properties of coal in the pre-failure range (i.e. Evans and Pomeroy(1966) , Pomeroy(1956) , Kidybinski(1966) , Morlier(1964) , Terry(1956) , and Ko and Gerstle(1977)) but no data are available for coal yielding at strains exceeding the failure strain. Most studies conducted in the pre-failure stage conclude that the rheological behaviour of coal can be simplified and modeled as a four-parameter fluid (Burgers model). Therefore coal would not have a stable zone or a current long-term strength and clearly would not give an adequate description of the failure process, particularly for a jointed mass. For a time scale relevant to engineering projects it is reasonable to neglect the viscous element in the Burgers model. Coal is therefore a good model of a typical rock mass.

3.2 Test Procedure and Factors Affecting the Results

3.2.1 Test Procedure

The test equipment used is described in Chapter 2. Here the test procedure during the multiple-stage repeated relaxation test is explained. The relaxation behaviour of the equipment and its effect on the data interpretation are

summarized. The problem of gas release from the coal and possible effects on the material behaviour are discussed.

All multiple-stage repeated relaxation tests were conducted under triaxial stress conditions with confining pressures below 1 MPa. The samples were fully consolidated under a constant confining pressure before loading at a constant rate of 1.52 mm per hour to a stress level above the crack closure range in the linear portion of the stress-strain curve. When a predetermined stress level, D_0 , normally in the vicinity of 30% of the estimated peak strength, was reached, the machine was stopped and the stress drop δD together with the straining of the sample was recorded. After a certain relaxation period δt the sample was reloaded to the original stress level D_0 and the relaxation test was repeated but from an increased total strain. The time interval δt was originally selected to maintain an average, constant stress level throughout the duration of a stage. This required frequent reloading at the outset in order to maintain a limited stress drop until the specimen became stiffer with increasing strain and less frequent reloading was necessary. An example of this procedure is given in Figure 3.3 for sample CTR-2A. It was recognized that this really approximated a creep test in the limit and had no special merit. This procedure was subsequently abandoned in favour of essentially constant time intervals δt between repeated relaxations of approximately one day. Such a repeated relaxation test at a

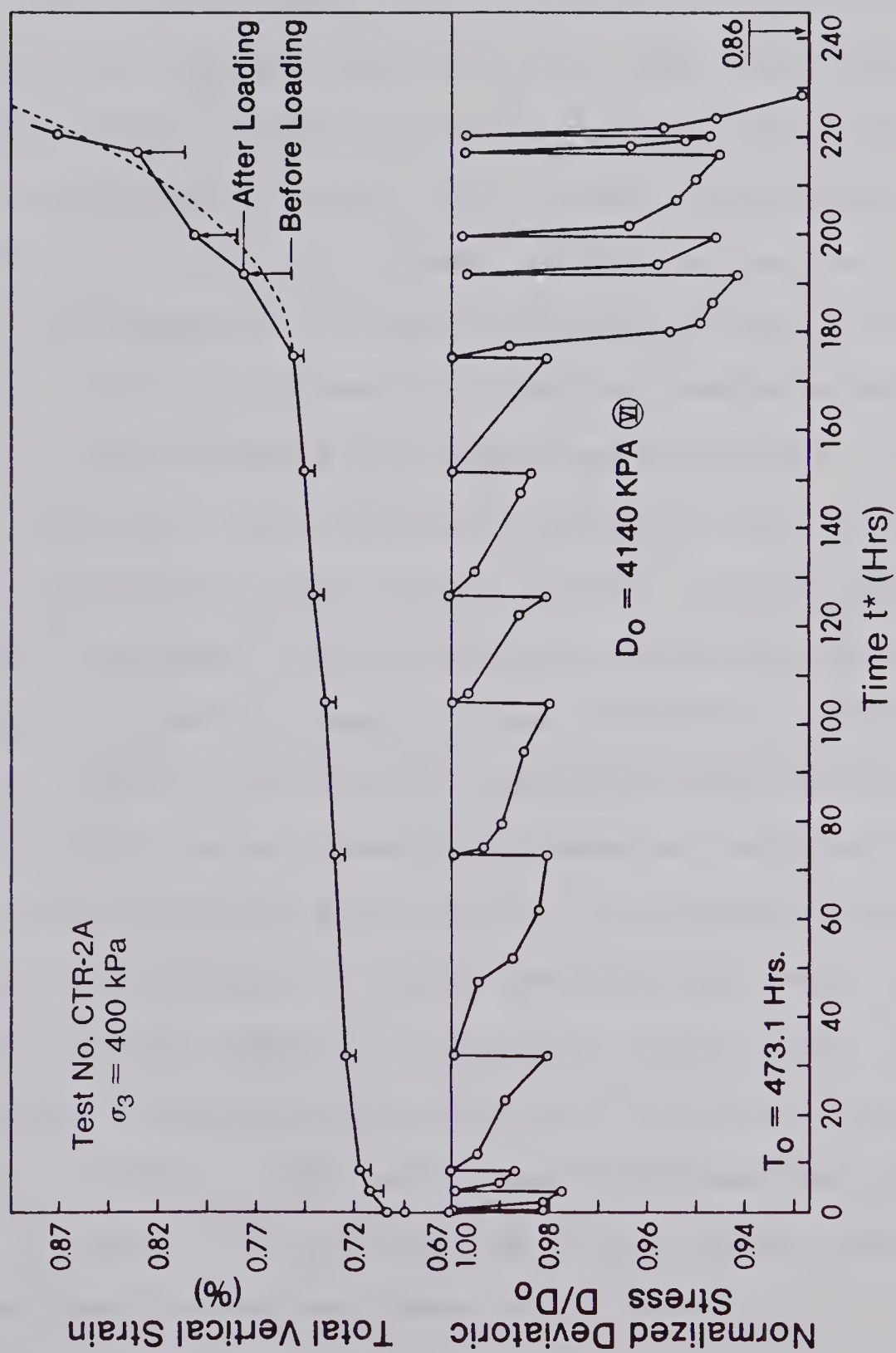


Figure 3.3 Normalized Deviatoric Stress and Total Vertical Strain versus Time of Test No. CTR-2A, Stage 6

fixed stage is illustrated in Figure 3.4. After a number of reloadings, normally five over a period of five days, the load was increased at constant rate to the next stage at a higher stress level and a new set of repeated relaxation tests were performed. If a constant relaxation rate was measured the load was increased by a small increment or left constant until failure occurred. Failure was indicated by a disproportionate stress drop during relaxation and an increase in vertical strain during reloading, or it was simply not possible to reach the original stress level D_0 . A similar test procedure was used by Pushkarev and Afansev (1973). After failure the sample was strained at a constant rate following the descending portion of the stress-strain curve. Unloading from stress levels beyond peak or near ultimate strength and reloading to stress levels below the current strength allowed the same relaxation test procedure to be repeated. Similarly, repeated relaxation tests could be conducted under stepwise decreasing confining pressure. This will be discussed during the interpretation of the test results. According to this procedure the test was called multiple-stage repeated relaxation test with the words "multiple" indicating step loading, "stage" referring to one specific stress level and "repeated relaxation" indicating that a number of relaxations were started from the same stress level within one stage of the test.

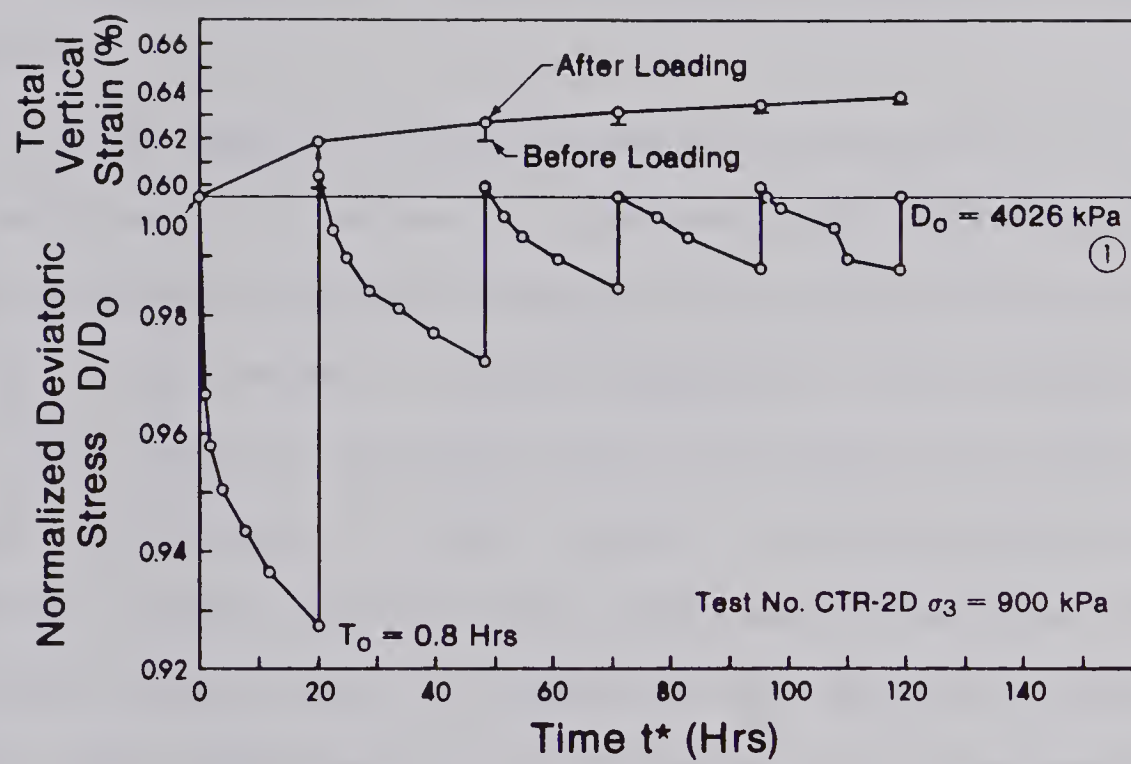


Figure 3.4 Normalized Deviatoric Stress and Total Vertical Strain versus Time of Test No. CTR-2D, Stage 1

3.2.2 Testing Environment

To reduce the effects of daily and seasonal air temperature fluctuations of up to about $\pm 3^{\circ}\text{C}$, an insulated box with a flowing water cooling spiral was built around the loading frame. This reduced the daily temperature fluctuation to approximately $\pm 0.5^{\circ}\text{C}$ and damped the seasonal variations significantly. The confinement of specimens in the triaxial cell eliminated the problem of humidity control.

It was observed that the moisture content at the end of a test was in general a few percent lower, and that gas bubbles appeared in the drainage lines which originally were filled with water. A back pressure of 100 kPa was used in one test (CTR-2D) to reduce the gas release from the coal. A brief discussion of the origin of these gases and their possible implications on the test results is given below. No attempt will be made to interpret the presented data in the light of this aspect, but it should be recognized that the moisture content and therefore the gas release affects the creep properties of coal. It is assumed that the failure mechanism was not affected. Nevertheless the rate of failure might have been reduced due to a reduction of the crack propagation velocity by the reduced gas pressure in the pore space.

During the deposition and compaction of plant material, large amounts of hydrogen-containing gases (mostly methane), along with carbon dioxide and traces of other gases are

produced, and some of the gases formed during the later stages of metamorphism are retained. Free gas within cracks, fissures and pores, adsorbed layers of gas at the surface of these openings and perhaps absorbed gas molecules dispersed between the coal molecules can be released if conditions are changed (e.g. free gas drains under a change in pressure gradient as a result of mine advance). In a triaxial test, openings close under increased pressure and free gas as well as adsorbed gas can be forced out of the sample. Similarly during dilation near failure more openings are created and adsorption is increased. The absorbed gas or gas in confined fractures can diffuse slowly in response to differences in concentration. This concentration difference may be caused by drainage of interconnected fractures or pore volume change. Because of the qualitatively observed slow but continuous rate of gas release it is believed that diffusion is one major reason for this gas flow. The problem of gas in coal is reviewed by Patching(1970) .

Ko and Gerstle (1977) conducted uniaxial creep tests on a subbituminous coal and found pronounced creep in wet coal with 35% moisture and negligible creep in dry coal with 3% moisture. Samples sealed against moisture migration for 481 days showed no creep until the seal was removed. The ultimate creep strain after approximately 2000 hours was the same independent of moisture history. This work indicates that the effects of moisture diffusion have to be contained in a realistic creep law for coal. It also indicates that

the time-dependent response of the coal could be affected by gas release since creep and long-term strength of brittle materials are controlled in part by stress corrosion at the crack tips. This corrosion is affected by the pore fluid or gas as indicated by strength tests on basalts in ultra-high vacuum by Krokosky and Husak(1968) . It is well known that the compressive strength of many rocks is decreased to as little as 50% of its dry strength by the presence of water in the pores space (e.g. Colback and Wiid(1965)). The mechanisms of rock strength reduction due to moisture in rock were reviewed recently by Ballivy et al.(1976) , Van Eeckhout(1976) and Kenney(1978) . The main causes can be attributed to fracture energy reduction, capillary tension decrease, pore pressure increase, friction reduction and chemical or corrosive deterioration. The first reason is most likely the dominating one for brittle rock where failure is a consequence of crack propagation due to tensile stresses exceeding the tensile strength at the crack tips. Water molecules reduce the surface free energy of rock and thus reduce its tensile strength. The opposite effect would therefore be expected if water in cracks is replaced by gas. The current strength would increase during this process, slow down creep or any time-dependent failure process, and increase the current long-term strength. On the other hand the strength could decrease if the gas diffusion causes a gradual change in pore pressure in closed pores or cracks. Whether one of these factors is the cause for the more

ductile behaviour of specimen CTR-2D, the only sample tested with back pressure (100 kPa), cannot be determined from the available data. The observed failure mode indicated crushing of a rock bridge near the top load-cap and it seems that this resulted in a different structure and consequently in a more ductile behaviour with large strain accumulation during repeated relaxation.

3.2.3 Relaxation of the Testing Machine

The testing system itself relaxes after application of a load due to relaxation of the "steel frame - load cell - ram - load cap" -assembly and slack in the gear box. A short testing program was undertaken to determine these effects. During this testing period a new data acquisition system (Fluke 2240B Datalogger) with higher recording accuracy of 0.001 mV was used, the temperature was not controlled and fluctuated approximately $\pm 2.5^{\circ}\text{C}$ over a period of one day. A steel block with the same dimensions was installed instead of the coal sample and preloaded to assure perfect seating of the load caps. The loading history consisting of twelve increments is summarized in Table 3.1 and the load-displacement curves for the ram relative to the base and the top of the cell as well as the absolute cell base displacement are shown in Figure 3.5 together with a schematic drawing of the test assembly. The various stress levels where relaxation tests were performed are numbered in sequence to facilitate comparison with Figure 3.6 and 3.7.

Table 3.1 Relaxation Test on Steel Block

LOAD INCREMENT NUMBER	DEVIATOR LOAD D_0 (kN)	LOAD INCREMENT ΔD (kN)	RELAXATION INTERVAL Δt (min)	LOAD DROP/ LOG CYCLE ΔD_0 (kN)	LOAD HISTORY
1	30.05	+30.05	1250	-0.1136	1.load.
2	30.10	+0.04	1400	0.0	reload.
3	34.20	+4.142	260	-0.0723	2.load.
4	34.25	+0.06	10	-0.0102	reload.
5	34.08	+5.80	260	-0.0224	un+reload
6	34.20	+5.80	1400	-0.0201	un+reload
7	25.25	-8.95	80	+0.0442	unload.
8	30.06	+4.81	3000	-0.0456	reload.
9	4.29	-25.78	1200	+0.0765	unload.
10	17.28	+13.00	800	-0.1029	reload.
11	17.25	-0.04	2500	0.0	reload.
COAL (CTR-2D)					
1	15.00	+15.00	1400	-0.4116	1.load.
2	15.00	+1.05	1400	-0.3044	reload.

s...slope of relaxation curve Lacerda and Houston(1973)
(Temperature effects approximately ± 0.05 to ± 0.1 kN)

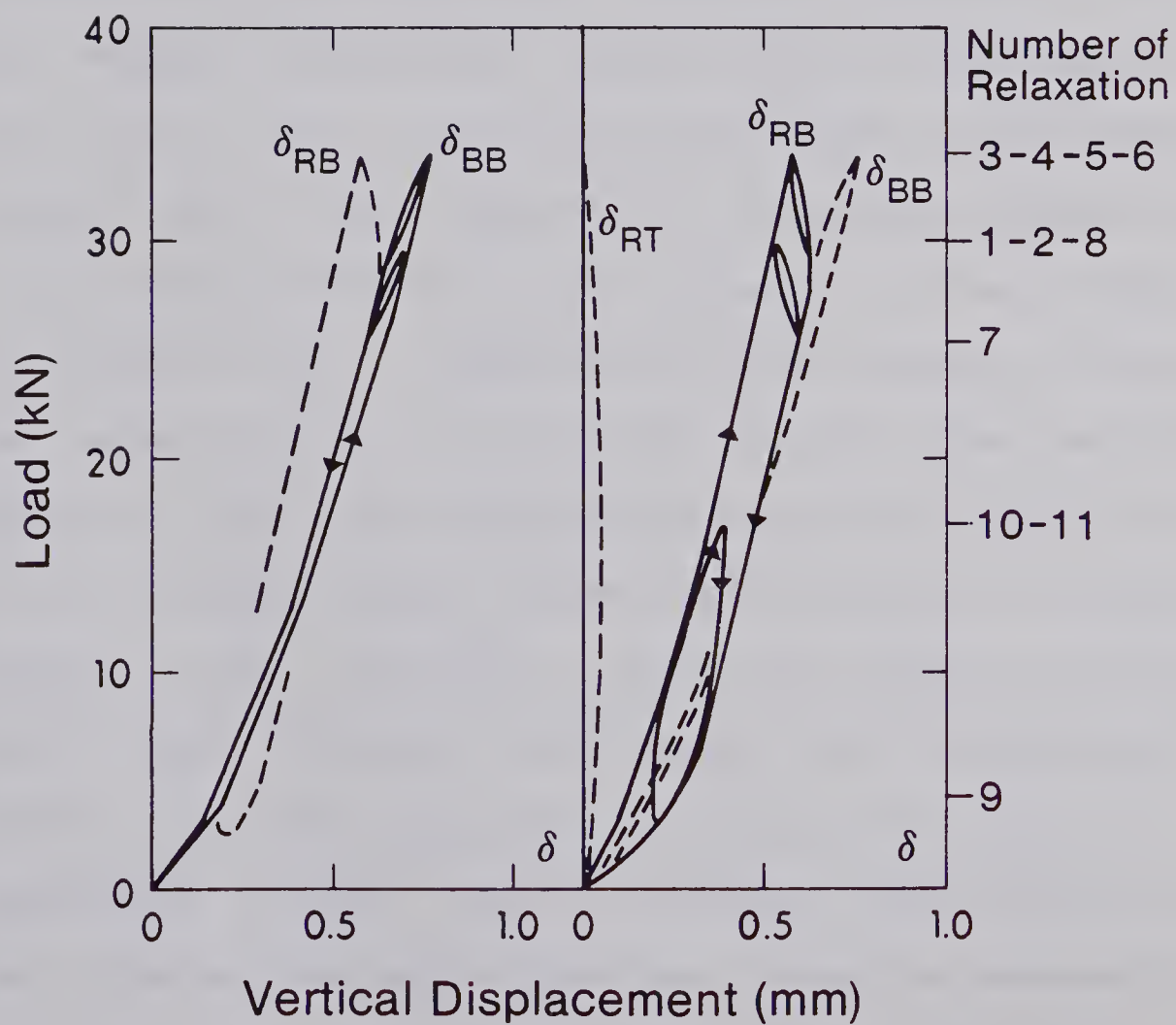
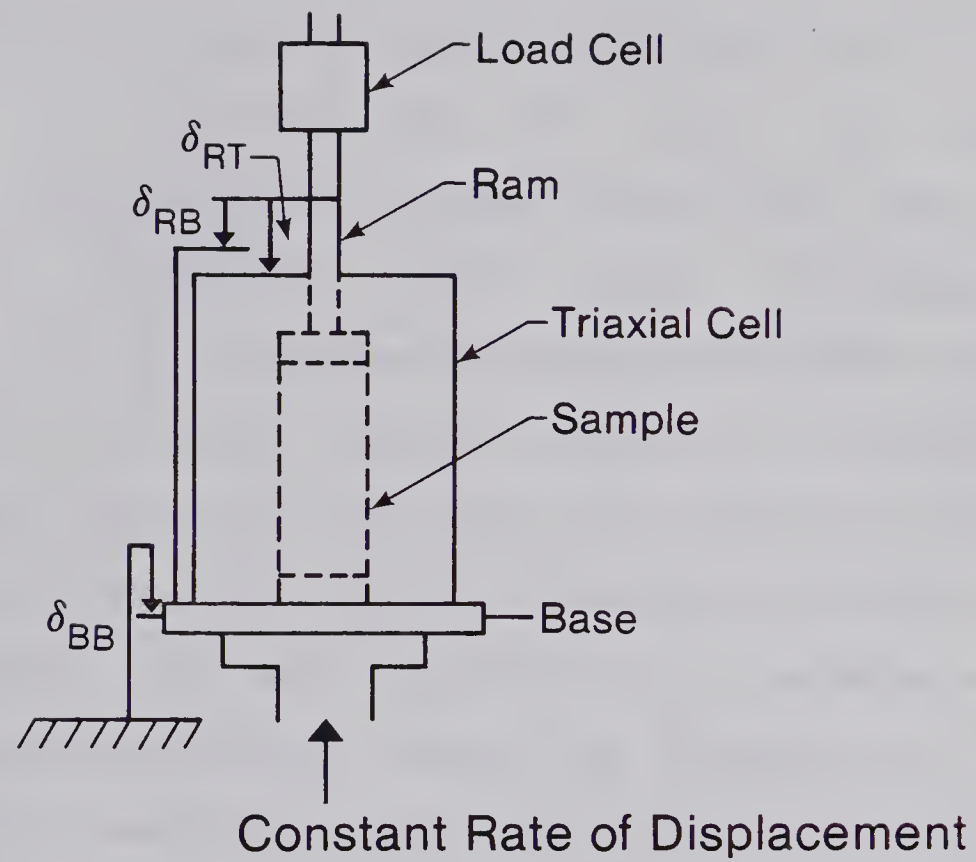


Figure 3.5 Test Assembly for Relaxation Test and Load - Displacement Diagrams for Test on Steel Block

The stiffness of the testing frame determined from cell base displacement is approximately 70 MN/m. The load - displacement curve measured between ram and cell base shows a pronounced hysteresis. Only after unloading by approximately 10 kN does the displacement between ram and base reverse. An almost immediate response is recorded at the load cell and at the cell base. The reason for this is not clear. Ram friction can be excluded since there is no movement between ram and top of the cell. Bending of the base plate and magnification through the extension rod could have caused this hysteresis. While the total displacement is affected by this behaviour it does not influence the stress drop during relaxation. About 0.2% of the measured total strain at 8 MPa (the maximum strength of the tested coal samples) has to be attributed to the system, resulting in a slight underestimation of the Young's modulus of the coal. The stress drop - logarithm of time diagram of the actual test data is given in Figure 3.6 and the linearized data in Figure 3.7. The load drop per log-cycle is included in Table 3.1. The loading system relaxes after loading is stopped and recovers after unloading. The first reading was taken one minute after loading was stopped. The load drop up to one minute was not included in Figure 3.6 and 3.7. The temperature effects start to dominate after four hours and load fluctuations after this time correlate reasonably well with room temperature. No cell fluid was used and the loading frame was not insulated. It can be assumed that the

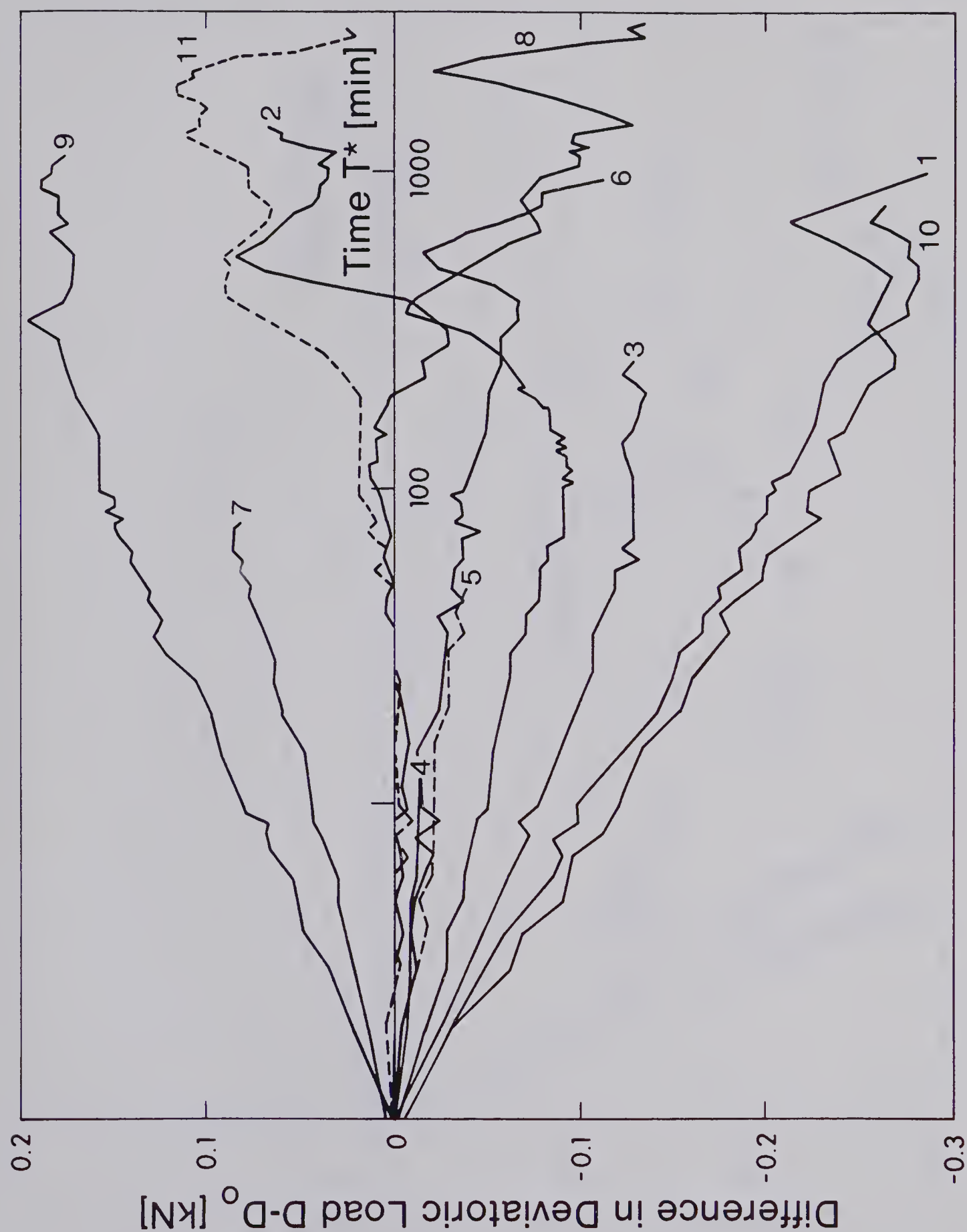


Figure 3.6 Load Change versus Logarithm of Time for Relaxation Tests on Steel

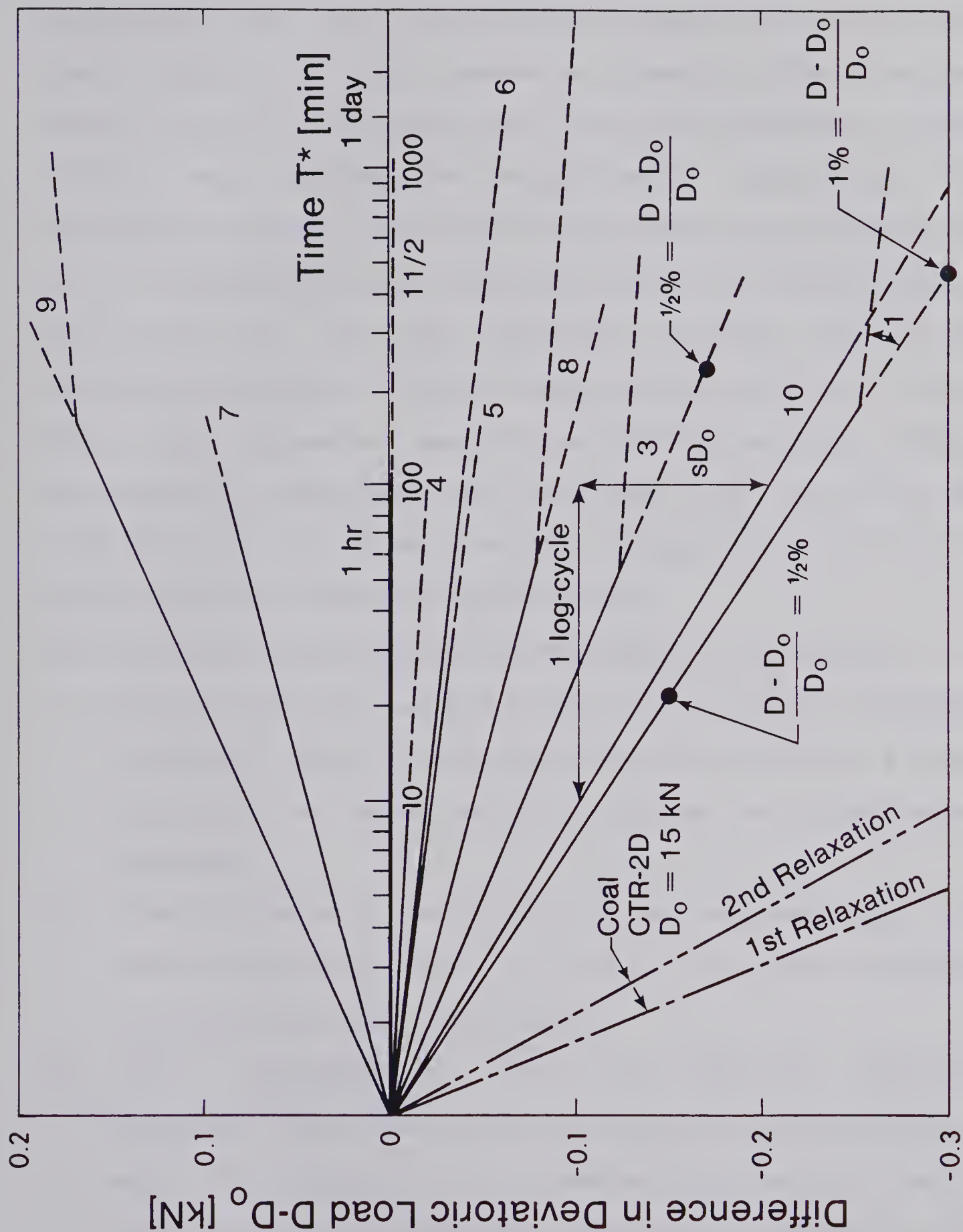


Figure 3.7 Linearized Data from Relaxation Test on Steel
(corresponding to data in Figure 3.6)

temperature of the whole system changed according to the room temperature. This temperature change caused a maximum stress variation of only about 1%. The temperature control during coal testing was significantly better and the recording accuracy was ± 0.01 mV or approximately ± 0.04 kN. As a consequence load variations related to temperature of less than ± 0.1 kN were estimated, a value close to the recording accuracy during coal testing. In Figure 3.7 the first two relaxation tests (load = 15 kN) on sample CTR-2D are shown for comparison. The load drop up to one minute was 1.35 kN and 0.2 kN for the first and second relaxation on coal, and 0.3 kN and 0.08 kN for steel.

The following observations and conclusions can be made:

1. After immediate application of the first increment (increment No. 1 to 30 N and No. 10 to 17.3 N) a total relaxation of approximately 1% during the first day was measured;
2. After subsequent reloading to the corresponding load level (increments No. 2 and No. 11) the relaxation within one day was almost zero;
3. After unloading by 17% and immediate reloading (increment No. 5 and No. 6) the relaxation was 0.15% per day. The purpose of this reloading cycle was to simulate the amount of gear movement necessary to reload the coal sample after each relaxation;
4. After increasing the load by 13.7% to the next stress level the relaxation within one day was about 0.5%

(increment No. 3) and 0.3% (increment No. 8).

It follows that the system relaxation would be in the order of 1% for the initial increment, 0.15% for the following increments and 0.5% for the first relaxation after loading to a higher stress level. The machine relaxation is not related to stress level or stress increment but to gear movement. Because of this fact a correction was not possible and the presented relaxation data includes therefore both system and coal relaxation. It will be seen that the conclusions drawn from the data interpretation are independent of the machine relaxation and that data from first relaxations do not correlate well with data from subsequent relaxations. The machine relaxation is not relevant near failure of the coal where large stress drops due to sample relaxation dominate. In multiple-stage single relaxation tests and during relatively short relaxation periods of a few hours the machine relaxation should be considered to eliminate possible misinterpretation.

3.3 Behaviour of Ideal Materials During Multiple-Stage Repeated Relaxation Tests

Multiple-stage repeated relaxation tests, their data and their interpretation are not conventional. In this section various ideal materials and their expected behaviour in multiple-stage repeated relaxation tests will be discussed. The actual test data will then be presented in the following section in corresponding diagrams to

facilitate their interpretation through comparison and to allow separation of zones of typical behaviour. An understanding of the response of some classical, ideal materials to multiple-stage repeated relaxation tests assists interpretation of tests when applied to natural rock.

Some symbols and their definitions are listed below to facilitate the discussion:

D_0deviatoric stress ($\sigma_1 - \sigma_3$) at the beginning of a stage of repeated relaxation tests;

Ddeviatoric stress at any time during relaxation;

δD_1 $D_0 - D$ after one day of relaxation;

D_{max} ...currently available strength, when, regardless of history, the rock is taken directly to failure by fast loading; D_{max} will in general vary with history;

D_{min} ...current long-term strength, when regardless of history, the rock is taken directly to failure by infinitely slow loading;

t^*time from onset of the first relaxation at a given stress level D_0 in each stage of the repeated relaxation test;

δttime increment measured from the beginning of each repetition of relaxation;

N_Rnumber of relaxation repetitions per stage;

evertical (or axial) strain determined by measuring the deformation in the direction of deviatoric loading divided by the length of the sample;

e_0linear elastic strain for loading rates that are fast compared with the average, and assumed to be identical with the initial loading curve;

e_cnon-linear strain at low stress levels due to crack closure;

e^*inelastic strain corrected for crack closure; i.e. $e^* = e - e_c - e_0$.

The definition of e^* as inelastic strain can only be applied if the material behaves linearly elastic up to the yield point. Otherwise e^* includes non-linear elastic strains. The inelastic strain e^* can be measured from any loading or reloading curve. The total inelastic strain would therefore be the sum of the inelastic strain prior to loading e_0^* , plus the newly accumulated inelastic strain e^* . This e_0^* is of particular importance if a rock mass is considered; there e_0^* includes past inelastic strains (e.g. tectonic strains). Increased damage and a weaker rock mass structure results as a function of the total inelastic strain (Mueller and Goetz(1973)).

The linear elastic stress-strain curve for instant loading is shown as a straight dashed line in all stress-strain diagrams. The inelastic strain e^* is measured from this line. It was assumed that the initial loading rate was relatively fast and that the deviation between instant and measured stress-strain curves could be neglected.

Ideal materials can be described as: (a) elastic or plastic with (b) strain-strengthening (often called

strain-hardening), (c) ideal plastic and (d) strain-weakening (often called strain-softening) characteristics (see Figure 3.8.I). A brittle rock with constant ultimate strength would be idealized by an elastic, strain-weakening, ideal plastic material. The time-dependent straining as observed in most rocks of the earth crust are (A) reversible, (B) partially reversible or (C) irreversible and the recovery can be (D) instantaneous, (E) delayed or (F) non-existent. The corresponding materials could be called (A) elastic, (B) partially elastic and (C) inelastic, (D) instantaneous-elastic (spring model), (E) delayed-elastic (Kelvin model) and (F) plastic (see Figure 3.8.III, 3.8.IV). Rheology deals with the time-dependence of materials (A) to (E). A solid will show terminating time-dependent strain (primary creep only) whereas a fluid will deform forever (primary and secondary creep). The use of these terms is in agreement with the accepted opinion that one should differentiate between delayed elastic behaviour (terminating deformation) and creep behaviour with continuous deformation eventually leading to failure. If a rock behaves like a fluid with a stress-dependent deformation rate it is called "ideal visco-plastic" (F) with "ideal" indicating rate-independent strength equal to the yield stress. Rock with a rate-dependent or time-dependent strength outside the yield surface (G), as observed in most rocks (Nadai(1952)), is generally called "visco-plastic" (e.g. Bingham model; see Figure 3.8.II). A rock mass behaves

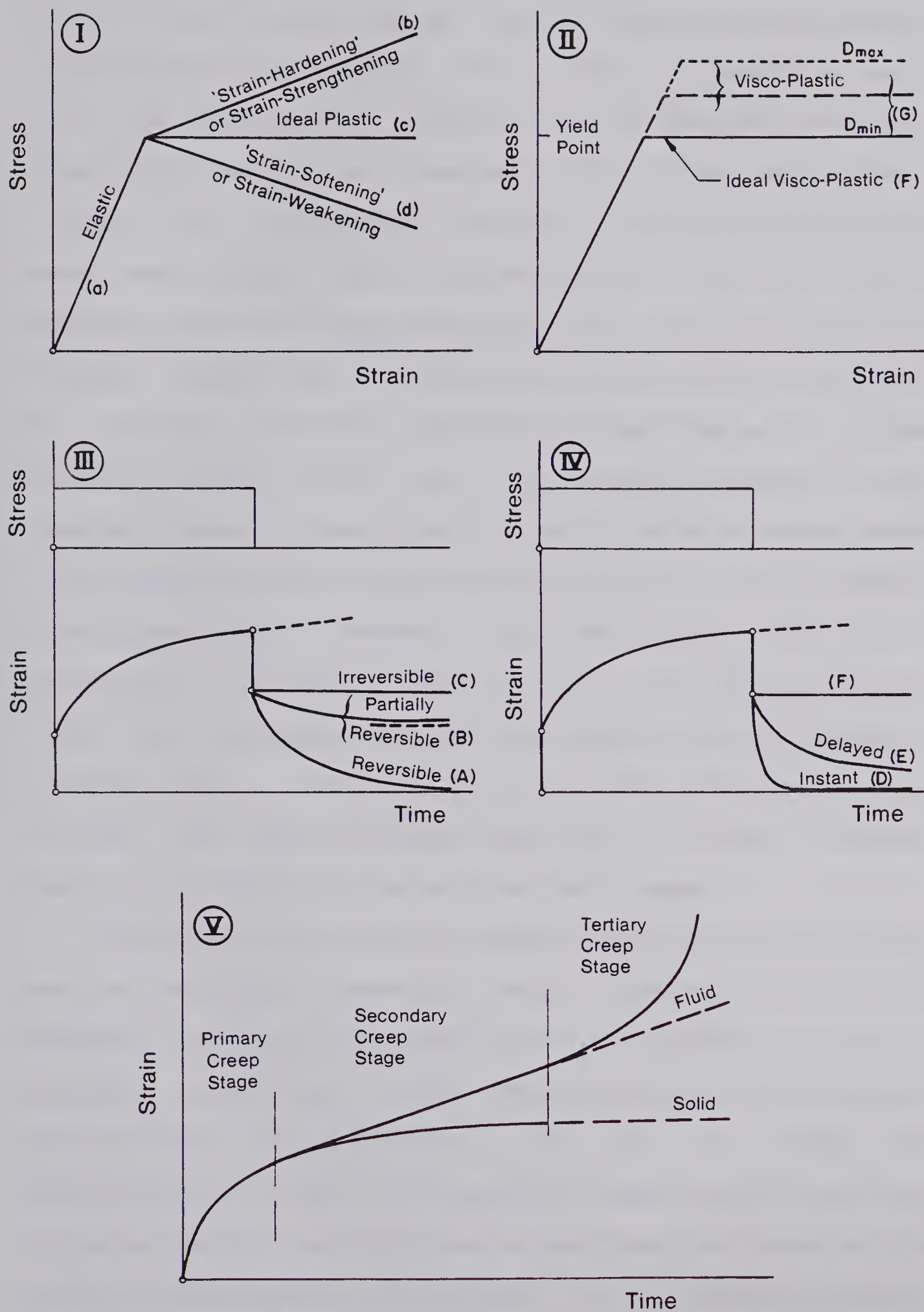


Figure 3.8 Schematic Stress - Strain - Time Diagrams for Ideal Materials

in a visco-plastic manner if (i) the rock itself deforms visco-plastically (shale, soft schist or swelling rock), (ii) the strength is reduced due to chemical alteration (weathered gneiss or granite), (iii) the rock mass is closely and continuously jointed, and (iv) the joints are open and filled with a visco-plastic material (clay or mylonite may be highly visco-plastic). As indicated by the Bingham model, the yield stress of a visco-plastic material is identical with the long-term strength D_{min} . The maximum possible stress level that can be reached depends on the loading rate. A visco-plastic material with an upper stress limit beyond which no additional load can be carried behaves visco-plastically between the two limits and can be simulated by a Bingham model in series with yield elements. This upper boundary is called available strength D_{max} . It follows that a material with a strain-dependent yield surface and upper strength limit has a "current" long-term D_{min} and a "current" available strength D_{max} .

Partially reversible and delayed elastic solids, fluids and visco-plastic materials with constant or decreasing strength will be discussed in the following section. No specific assumptions about the time-strain or time-stress relationship is necessary but it is assumed for simplification that a corresponding superposition principle could be found; e.g. Boltzmann's superposition principle for linear visco-elastic materials. It is therefore assumed, according to the behaviour of natural rock, that rock has a

memory. This memory can change or be lost during failure or plastic flow.

Figure 3.9 is a schematic diagram relating (a) stress level D_0 and (b) inelastic strain e^* to the normalized stress drop $\delta D_1/D_0$ where δD_1 is the stress drop during a unit period of time (e.g. $\delta t=1\text{day}$) starting from the time where loading is stopped. Among linear visco-elastic materials, the Maxwell model represents a simple two parameter fluid. If repeated relaxations were carried out from a stress level D_{01} , the stress drop per day is controlled solely by the viscosity and would be a constant that depends upon the stress level but is independent of the inelastic strain e^* . This may be represented by a horizontal line in Figure 3.9b.

An elastic, visco-plastic material where the behaviour within the rate-dependent plastic zone can be described by a Maxwell model, does not show any relaxation behaviour up to the yield point. At higher stress levels a stress drop proportional to the stress difference δD_{01} between the applied stress level D_0 and the yield stress can be observed. For an elastic, ideal visco-plastic material with no stress relaxation points plot on the abscissa (δD_1 is zero). The relationship between stress level and normalized stress drop for this material plots as an inclined line (Figure 3.9.a) whose slope depends on the viscous element and is independent of stress history or number of relaxation tests N_R . The simple linear visco-elastic solid is

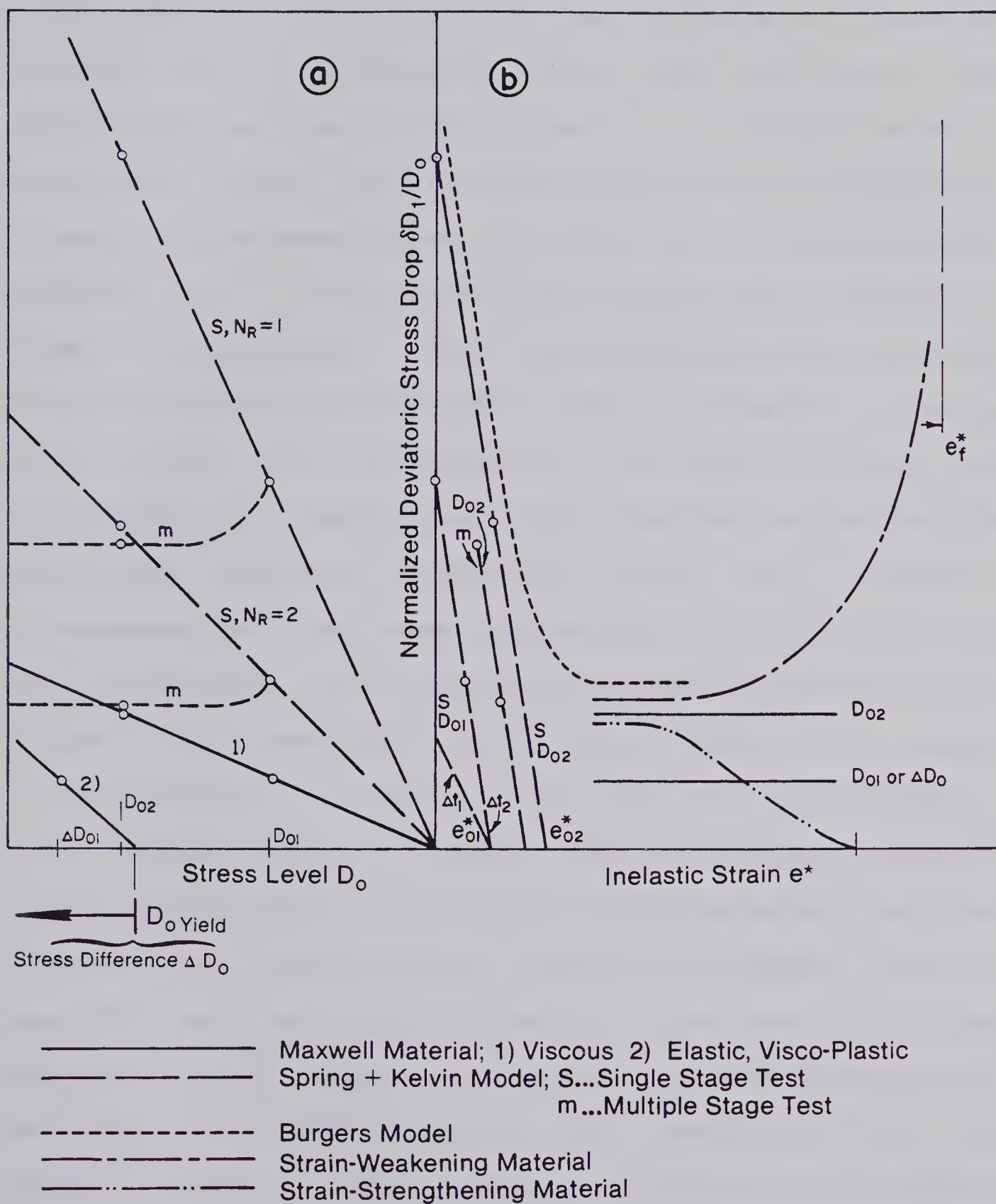


Figure 3.9 Schematic Diagram: Normalized Stress Drop versus Stress Level and Inelastic Strain for Ideal Materials

represented by a spring in series with a Kelvin model. In this case repeated relaxation from a given stress level D_{01} results in a decreasing stress drop per unit time, approaching zero at infinite time but at a finite inelastic strain e^* . This plots as an inclined curve (linear for a linear visco-elastic model) in Figure 3.9.b intersecting the abscissa at a maximum inelastic strain e^*_{01} . The shape of these curves depends on the loading history, but the maximum strain accumulated at infinite time is a function of stress level only and independent of stress history. The inclination of these curves decreases for decreasing time intervals between relaxations, and more strain is accumulated in the same time during relaxation tests with fast repetitions. If the maximum inelastic strain during one stage of repeated relaxations tests is reached (theoretically at infinite time) and the stress increment from stress level to stress level is constant, parallel curves displaced by a constant inelastic strain increment result. The loading curve between increments would be parallel to the initial loading curve and this ideal material would therefore resemble a strain-strengthening material (Finnie(1960)). If the normalized stress drop versus inelastic strain curves for subsequent relaxation stages are identical, as will be reported for some tests on coal, inelastic strain is recovered during loading and the maximum inelastic strain is stress independent (at least for a limited stress range). The behaviour discussed can be

illustrated by a series of curves indicated in Figure 3.9.a. For a single stage test with repeated relaxation each stress drop would fall on an inclined line according to stress level D_0 and number of relaxation NR . Relaxation decreases with accumulation of inelastic strain. In multiple-stage repeated relaxation tests only the first stage would plot on these lines and the results from later stages would fall on curves whose shape depends entirely on the stress history (the number of relaxations during earlier stages, the duration of each relaxation and the stress increment between stress levels). Again, for constant increments and complete straining per stage, parallel and horizontal lines would result. For a stress history similar to the one used in the coal testing a set of lines labeled with "m" would be expected. The reason for this shape is that there is a large first increment which is followed by smaller but constant increments.

The behaviour of a Burgers model which is often used for coal before failure, is indicated in Figure 3.9.b. At low inelastic strains and immediately after loading the Kelvin model dominates in coal, and later the viscous, Maxwell element controls the relaxation behaviour. For single stage tests (Figure 3.9.b), a set of inclined lines with a decreasing slope for an increasing number of relaxations NR would terminate at the line shown for a Maxwell material (and not at the abscissa as for the Kelvin material). For multiple - stage tests no schematic curves

can be included because of the complexity due to the history-dependence. Qualitatively linear superposition gives a good indication of the response which could be expected. For an elastic, visco-plastic material the same concept as discussed earlier would apply, and the behaviour would depend on the stress difference between the stress level and the yield stress rather than to the stress level itself.

For an elastic, visco-plastic material with a strain-dependent strength the stress difference $\sigma - \sigma_0$ changes gradually as a function of the accumulated inelastic strain even if the stress level σ_0 is kept constant. A decrease of the yield strength with strain in a strain-weakening material results in an increase in the stress difference $\sigma - \sigma_0$ up to a maximum at failure. On the contrary, for a strain-strengthening material the stress difference decreases as the stress level approaches the yield strength. The corresponding behaviour is indicated in Figure 3.9b with strain-weakening leading to failure at ϵ^* and strain-strengthening to a stable condition with no relaxation at a finite, inelastic strain. The shape of these two curves is controlled by the slope of the after failure stress-strain curve.

As soon as the relaxation becomes insensitive to the inelastic strain ϵ^* , as in the visco-plastic zone or near ultimate strength where the strength loss is small relative to a given strain increment, it is better to plot the stress ratio versus the normalized stress drop. The stress drop and

the stress level are normalized to the current available strength D_{max} to take into account a possible strength loss or the corresponding increase in stress level. This was not necessary in the previously discussed diagrams where D_{max} may be assumed constant for the prefailure range or at stress levels below D_{min} , the current long-term strength. In the following the relaxation behaviour in this zone of a few ideal materials is discussed and schematically illustrated in Figure 3.10.

A visco-elastic solid (e.g. spring + Kelvin model) shows a linearly increasing stress drop in single stage tests as indicated by the straight dashed lines. Subsequent relaxations from the same stress level will tend towards zero relaxation and at a fixed number of relaxations $N_R = n$ fall on a straight line between $N_R = 1$ and the ordinate. Because of the stress history dependence of this model the response at a higher stress level depends on the stress increments and time intervals between relaxations. An example is indicated for a three stage history (labeled I). After major relaxation during the first stage (after a large initial stress increment to stress level A) the relaxation decreases rapidly, even at slightly higher stress levels.

An elastic, visco-plastic material does not relax up to the yield point at stress level A. Above this level the relaxation is proportional to the stress difference between stress level and yield stress (Maxwell model) and the relaxation after infinite time is equal to this stress

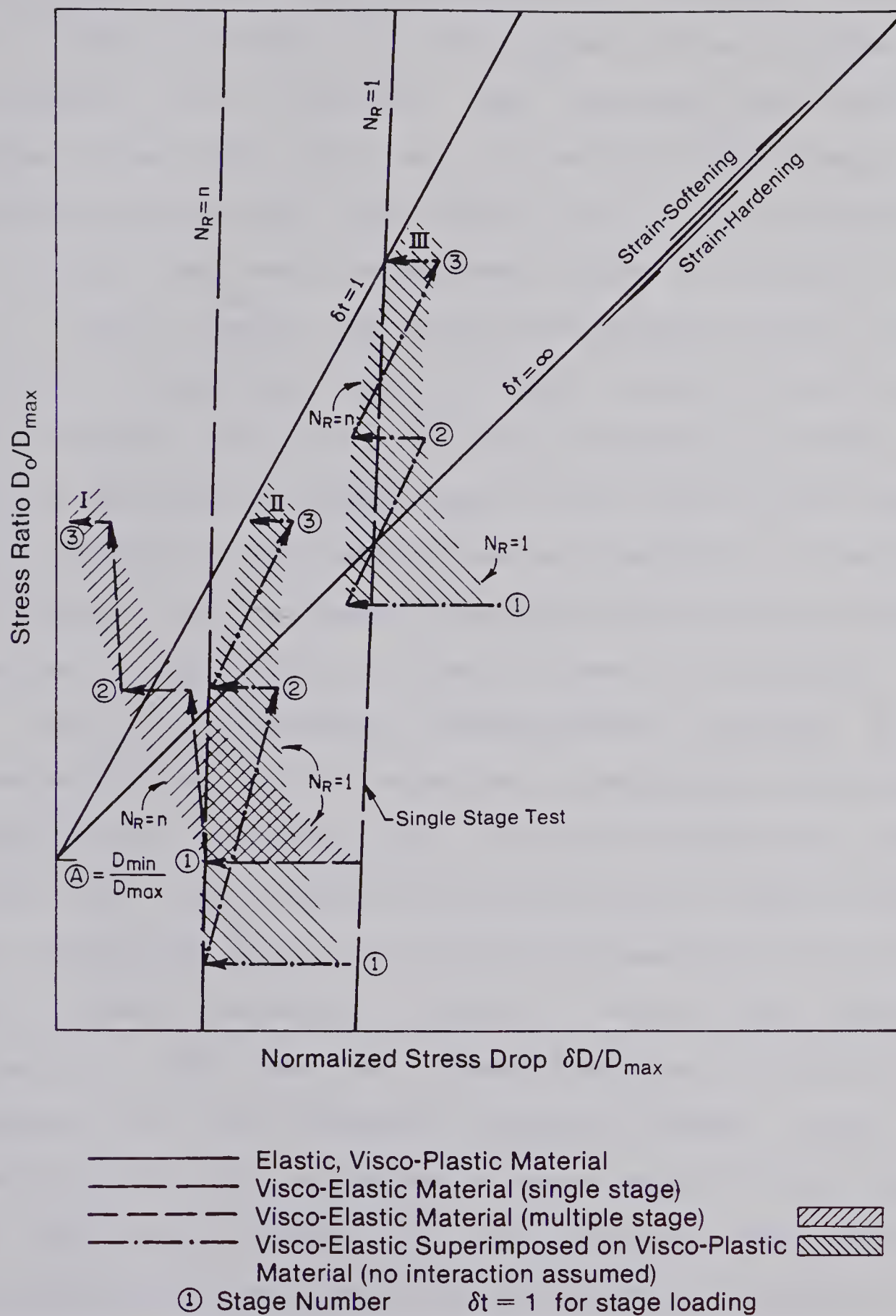


Figure 3.10 Schematic Diagram: Stress Ratio versus Normalized Stress Drop for Ideal Materials

difference. This type of material will therefore terminate at a line inclined at 45° (labeled for an infinite time increment), or at smaller time intervals the normalized stress drop will plot on an inclined line through A as indicated for a unit time interval $\delta t = 1$. It is assumed in this plot that the rate-dependent range is limited by D_{\max} (St. Venant element in series with Maxwell model). During repeated relaxations from a fixed stress level D_0 of a visco-plastic material with strain-dependent strength, the current available strength D_{\max} and the stress ratio change. This results in data points displaced parallel to the lines of constant time increment δt as indicated by the two arrows parallel to the relaxation limit δt equal to infinity.

For a visco-elastic, visco-plastic material it was assumed that the two processes were independent and could be superimposed directly. This is quantitatively not correct since the stress drop of the visco-plastic element affects the relaxation of the visco-elastic element and vice versa. The expected behaviour during a three stage repeated relaxation test for two stress histories (II and III) is indicated in the schematic diagram (Figure 3.10). The visco-elastic part dominates at early stages and low number of relaxations whereas the visco-plastic part dominates eventually when the visco-elastic element is strained to its limit. Figure 3.11 gives examples for linear viscous materials and variable stress histories using specific parameters:

1. Spring and Kelvin model

The stress after loading is stopped is given by Fluegge(1967)

$$D(t) = q_0 e_1 (1 - \exp(-t/p_1)) + D_0 \exp(-t/p_1) \dots \dots (Eqn.3.1)$$

and the normalized stress drop after unit time and instant loading is

$$\delta D_1/D_0 = (1 - (q_0/E_0))(1 - \exp(-1/p_1)) \dots \dots \dots (Eqn.3.2)$$

or for repeated relaxations, a constant loading modulus and a constant time increment equal to unity

$$\delta D_{1i}/D_0 = (1 - (q_0/E_0)(1 + \sum_1 (\delta D_{1(i-1)})/D_0))(1 - \exp(-1/p_1)) \dots \dots \dots (Eqn.3.3)$$

since e_1 at the beginning of each relaxation is

$$e_{1i} = (D_0/E_0) + \sum_1 (\delta D_{1(i-1)})/E_0 = e_0 + e^* \dots \dots \dots (Eqn.3.4)$$

(e^* is a function of the loading modulus),

where:

i ...number of relaxation test NR;

g_0 ... $E_0 \bar{E}/(E_0 + \bar{E})$, long-term stiffness (3.53×10^3 MPa);

E_0 ...stiffness of spring in series with Kelvin model (4.0×10^3 MPa);

\bar{E} ...stiffness of Spring in Kelvin model (30×10^3 MPa);

p_1 ...relaxation time (2.45 days);

\sum_1 ...summation from 1 to i .

The numbers in parentheses correspond to the values assumed for Figure 3.11. They are taken from tests on coal published by Morlier(1964) and Kidybinski(1966) . Data is indicated in Figure 3.11 for two cases; loading to one stage only, with five relaxations at D_{max} and

loading to a first stage at $0.9 D_{max}$ with five relaxations followed by loading to a second stage of repeated relaxations at D_{max} .

2. Maxwell fluid

The stress after loading is stopped is (Fluegge, 1967)

$$D(t) = D_0 \exp(-t/p_1) \dots \dots \dots (\text{Eqn. 3.5})$$

or for repeated loading and a constant time increment δt the normalized stress drop is

$$\delta D_1/D_0 = 1 - \exp(-\delta t/p_1) \dots \dots \dots (\text{Eqn. 3.6})$$

independent of number of relaxation N_R . The parameter p_1 was assumed to be 0.5 days for Figure 3.11. For a material with a yield point and a behaviour corresponding to the Maxwell model at higher stresses, D_0 is to be replaced by δD_0 , the stress difference above the yield stress. A series of curves for various time increments between six hours and infinity are given.

3. The previously discussed simplified assumption of superposition of the independent relaxation behaviour was used to illustrate the response of a visco-elastic material with viscous flow above a given stress level $0.9 D_{max}$. Three stress histories, all starting with a first stage of five repeated relaxations at $D_0 = 0.9 D_{max}$, are indicated. This first stage was followed by loading to a second stage of relaxations at D_{max} , $0.94 D_{max}$ or $0.92 D_{max}$. The latter was subsequently loaded to a third stage at $0.94 D_{max}$.

3.4 Results from Multiple-Stage Repeated Relaxation Tests

In this section the test results of five multiple-stage repeated relaxation tests on coal are presented. The specimens and their failure mode is described and a general description of the individual test is given. Difficulties during the early stage of this testing program and changes in the testing procedure did not allow a consistent analysis of all test results. Because of this fact no relaxation data are included for Tests CTR-2B and CTR-2C but a qualitative discussion of the stress-strain behaviour is given. The figures for the remaining three tests are located at the end of this section 3.4 in chronological order to facilitate comparison during the interpretation given in Section 3.5. The mechanical properties of all five samples were summarized in Table 2.2.

Test No. CTR-2B

This specimen was intersected by a number of joints and failed mainly along one joint intersecting the sides of the sample 6 mm below the load cap. The shear plane was inclined at approximately 65° to the horizontal plane and consisted of about 25% rock bridges only. One bedding plane separation was observed on one side of the shear plane. The stress-strain curve in Figure 3.12 seems to indicate that an initial failure occurred during stage one of repeated relaxation tests due to shear of the joint plane on one side of this bedding plane separation and that the remaining, intact part allowed reloading and failed at increased

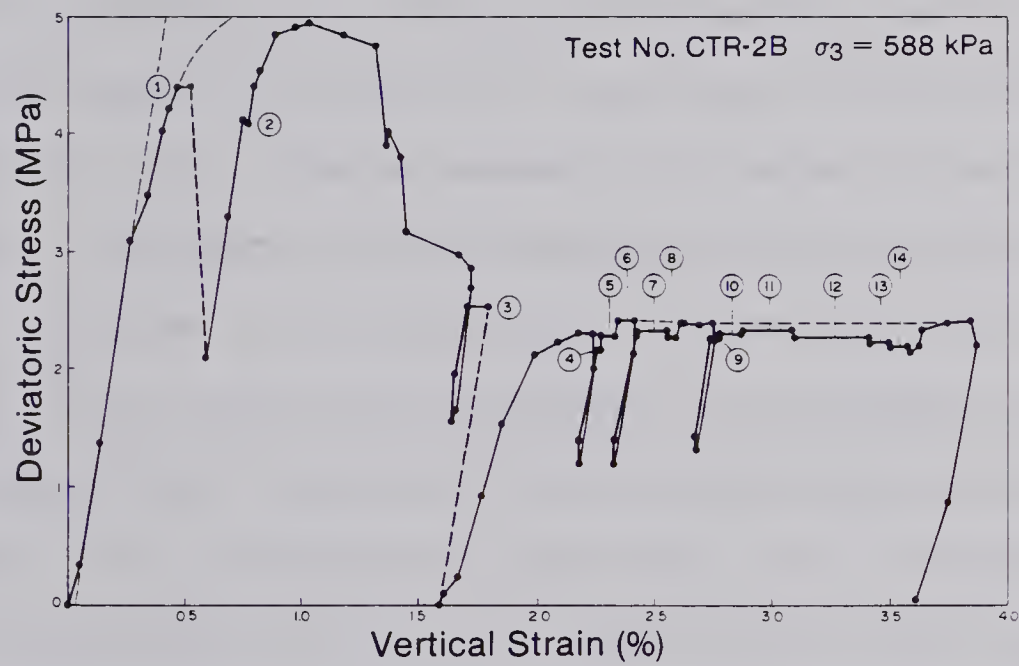


Figure 3.12 Stress-Strain Diagram of Test No. CTR-2B

strain. A sudden loss of confining pressure during stage three resulted in excessive shear of the sample and the total strain is therefore unknown. Two weeks later the pressure system was repaired, the sample was reloaded and relaxation tests were conducted near ultimate strength. The total testing time was 151 days. The data is not reported in detail because of two reasons: firstly, the total strain is unknown and secondly, the effects of shear on the rock structure during the loss of confinement and the two week unloading period cannot be evaluated. Nevertheless the results of the eleven stages of repeated relaxations near ultimate strength are consistent with the results of other tests, confirm the conclusions drawn in the following section and show a rate-dependent visco-plastic zone above 92% D_{max} . There was some indication that D_{max} is not only a function of accumulated strain but also a function of the time during which the normal stress acts on the shear plane. A strength increase with time might be explained by a time-dependent "over-closure", a term introduced by Barton(1974) to describe a stress-dependent interlocking of shear surfaces or rock mass structures. During reloading after stage three $D_{max} = 2.3$ MPa was reached. After unloading and reloading followed by two stages of repeated relaxations (4 and 5) a $D_{max} = 2.43$ MPa was reached at increased strain during stage six. No such effect was observed later and D_{max} was almost constant during accumulation of another 1% strain. This indicates that this

test series was conducted close to the ultimate strength of this specimen. D_{max} was determined three times after stage 6, 8 and 14 by fast straining at a rate corresponding to the initial testing rate.

Test No. CTR-2C

The failure plane along one joint inclined 59° to the horizontal plane emerged 10 mm below the load cap. No bedding plane separation was observed and only 15% of the shear plane consisted of rock bridges. Other visible joints were approximately 20 mm apart. The volume change of the cell was recorded during this test. During each stage of repeated relaxation tests the volume change indicator was closed because of a minor leak. The volume change behaviour (Figure 3.13) is similar to the one recorded in short-term tests. Failure occurred during stage five of repeated relaxation tests and the post-peak curve indicates a less brittle behaviour than during test CTR-2B (tested at the same confining pressure). The test had to be discontinued after 75 days due to a membrane failure. No valuable information was gained from stages 6 to 8 because of inconsistent testing procedures or loading too close to the current available strength.

In the prefailure range the following qualitative observations were made. Up to stage four continuously decreasing relaxation indicated a limited time-dependent zone with a behaviour similar to that of a rheological model with a spring in series with a number of Kelvin models

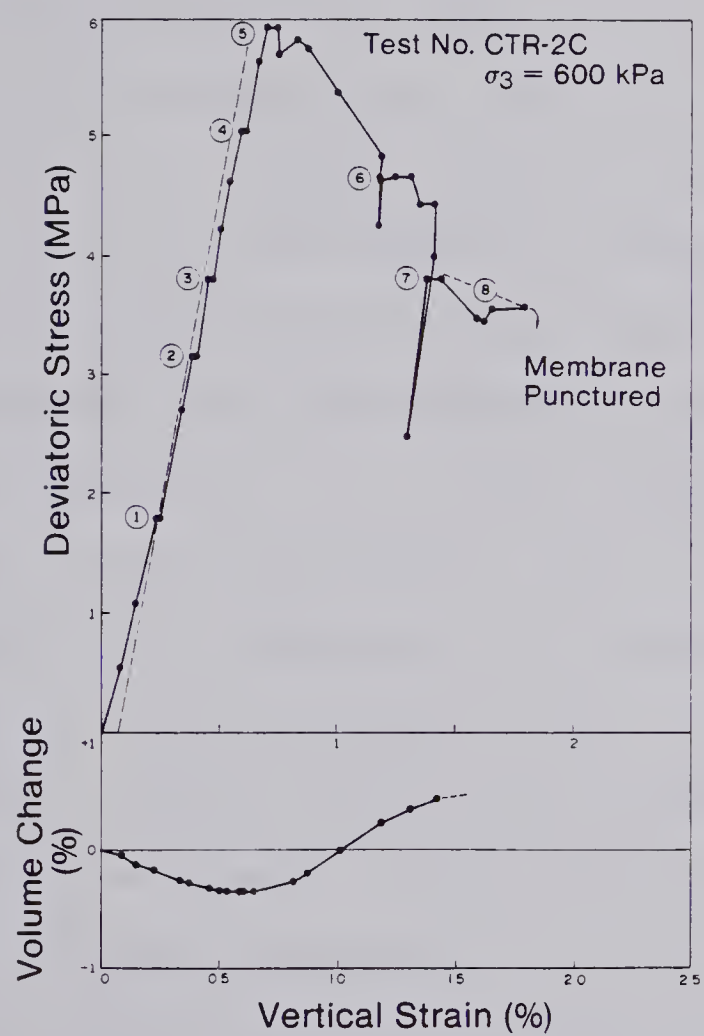


Figure 3.13 Stress-Strain Diagram of Test No. CTR-2C

(Hardy and Chugh(1959)). This zone would therefore be limited by a short-term modulus and a long-term modulus. During a load increase to the following stage the stress-strain curve was steeper and most of the creep strain was recovered if the increment was sufficiently large. From this observation it appears that the coal can neither behave like a time-hardening material, where the slope to the next stage would be reduced, nor like a strain-hardening material, where the slope would remain the same (Finnie(1960)). The time-dependent response seems to be proportional to the stress level and the inelastic strain ϵ^* . The model suggested by Hardy(1959) or Terry(1956) could describe the behaviour at a given stress and strain accurately but would not reveal the strain recovery behaviour since it simulates a strain-strengthening material. During loading to stage five the reloading modulus was approximately equal to the initial short-term modulus E_0 . Continuously increasing stress drops of three percent per 12 hours interval indicate that this stage was at a stress level well above the long-term peak strength.

Test No. CTR-2A

A picture of this specimen after testing is given in Plate 3.1. The shear plane developed along a joint plane inclined at 61° to the horizontal and a bedding plane separation similar to sample CTR-2B was observed. Crushing of the remaining part resulted in a rather ductile post - failure curve (Figure 3.14). The collapse of this separated



Plate 3.1 Sample CTR-2A after Testing

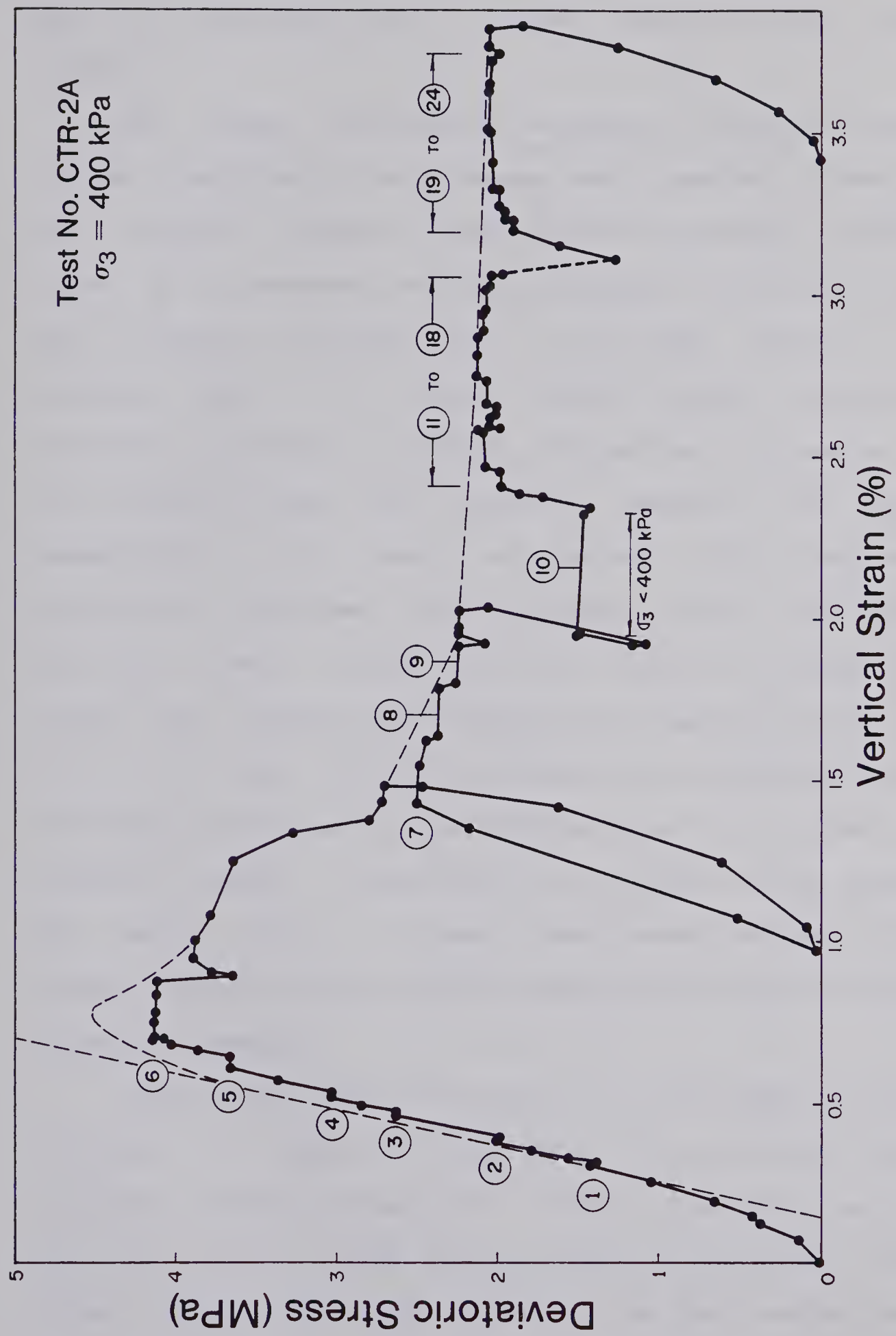


Figure 3.14 Stress-Strain Diagram of Test No. CTR-2A

part is indicated by a sudden change in post - failure slope.

Six stages of repeated relaxation tests at increasing stress levels before and through peak strength, three stages at decreasing stress levels after reloading (7 to 9), one stage at decreasing confining pressure (10), and 14 stages near ultimate strength were undertaken during a total testing time of 178 days. Between stage 19 and 20 the confining pressure accidentally dropped and the sample had to be reloaded after the original pressure was built up immediately. Two sets of typical test results with normalized deviatoric stress drop versus time and total vertical strain versus time are given in Figure 3.3 for stage six through peak strength and Figure 3.15 for stages 13 to 15 near ultimate strength. The first one shows the relaxation behaviour as the failure point is reached (from a primary through a secondary to a tertiary creep stage) and the second shows a linear relationship between time and strain during multiple-stage repeated relaxation tests near ultimate strength.

Figure 3.16 gives the data of two prolonged relaxations (5 days) at stage 14 and 24. It can be seen that the relation between normalized stress drop and logarithm of time is linear. This fact was used to determine δD_1 , the stress drop after unit time, if the test period was less than unity. The testing frame stiffness as determined from this diagram is approximately 50 MN/m. During stage eight

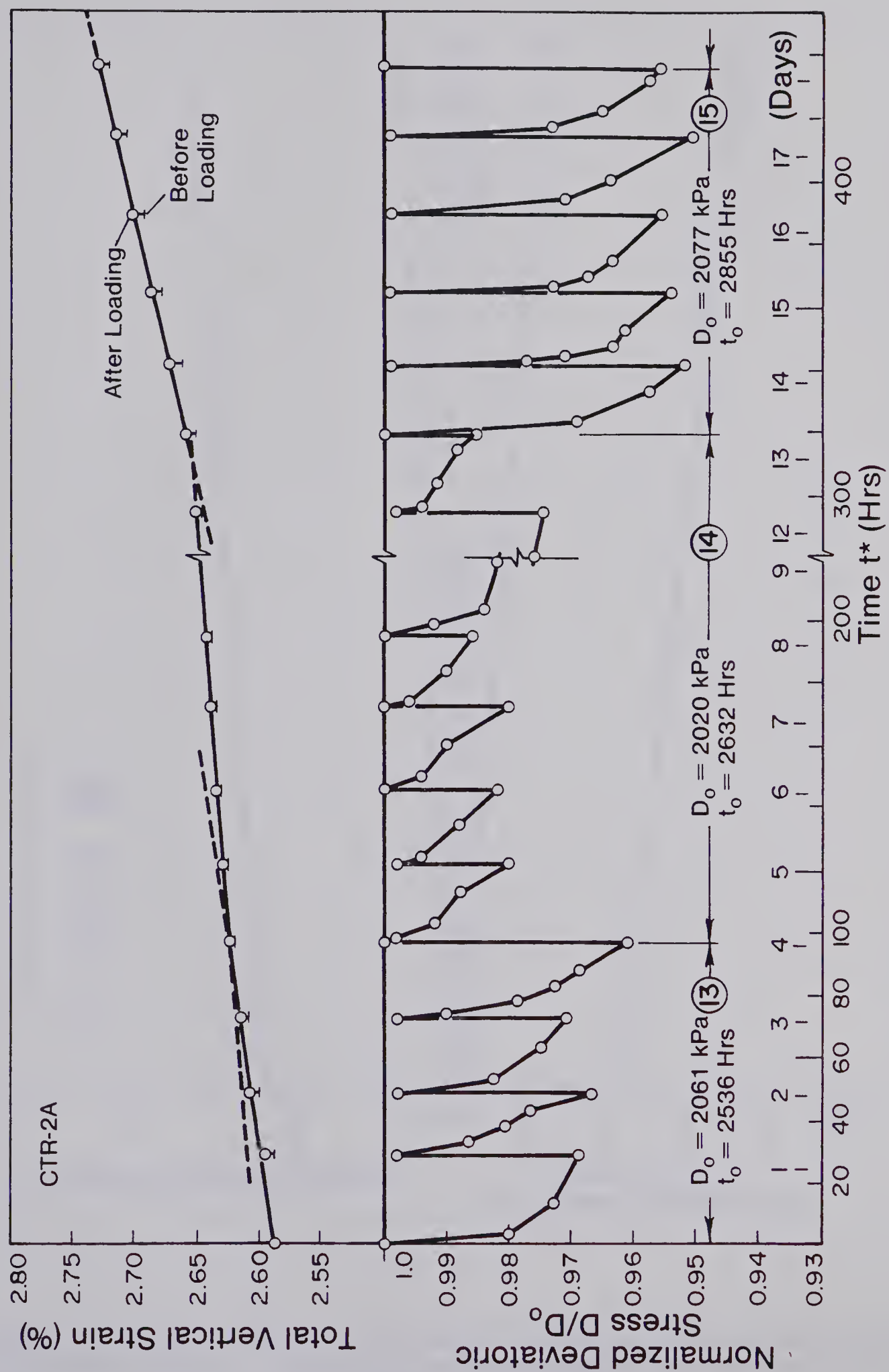


Figure 3.15 Normalized Deviatoric Stress and Total Vertical Strain versus Time of Test No. CTR-2A (Stages 13 to 15)

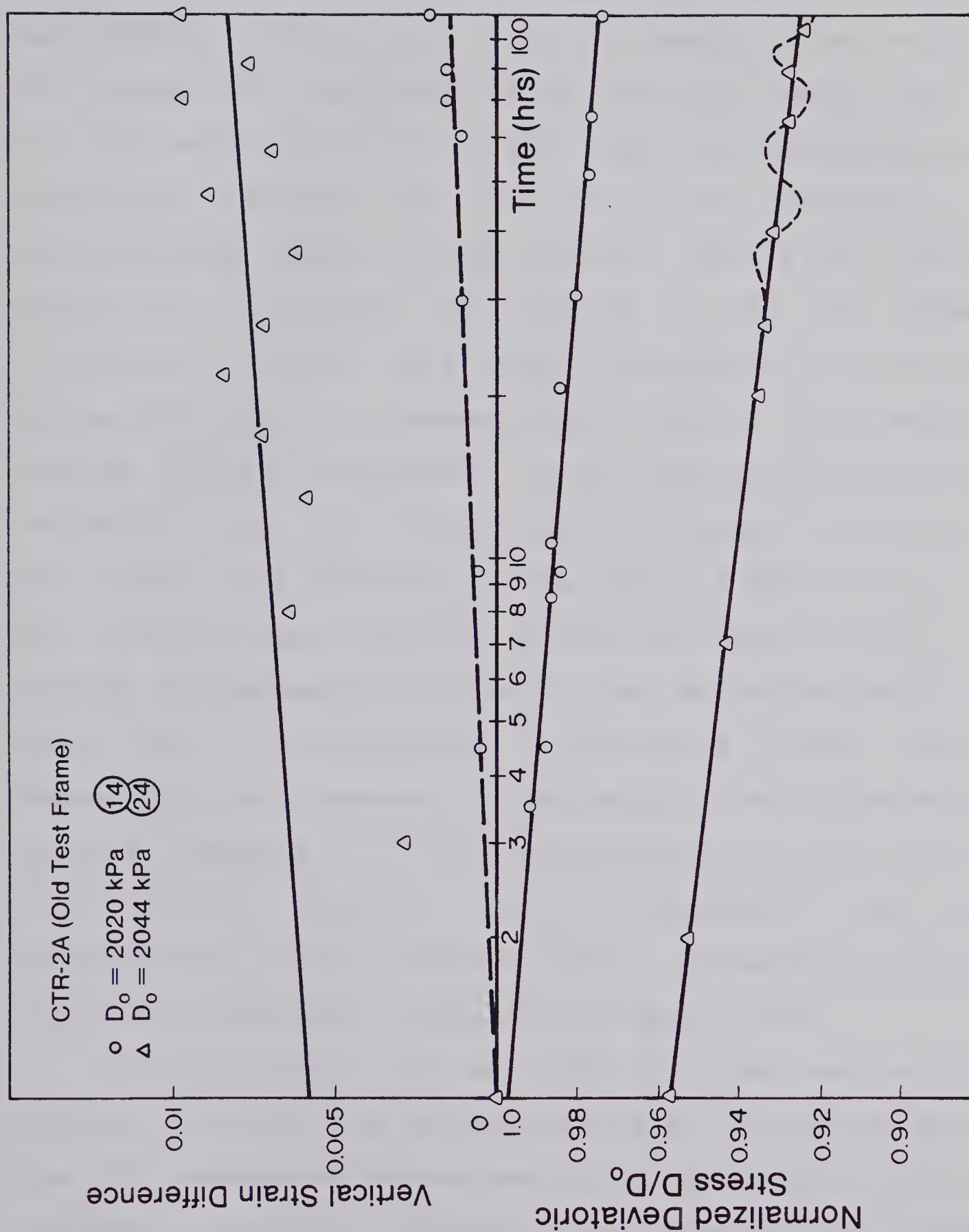


Figure 3.16 Normalized Deviatoric Stress and Vertical Strain Difference versus Logarithm of Time during Relaxation of Sample No. CTR-2A

the load was cycled at the initial strain rate and the accumulated strain versus number of loading cycles is given in Figure 3.17. The amplitude was 5% of the stress level $D_0 = 2.39$ MPa equivalent to the stress drop measured over a relaxation period of one day. For comparison the corresponding points during regular testing with one day relaxation intervals are plotted on the same figure (different scale). The strain accumulated during one relaxation cycle is approximately equal to the straining during the ten short-term cycles. Repeated loading after relaxation has some resemblance with fatigue testing with the major three differences being that the number of cycles in multiple-stage repeated relaxation tests is small, the cycles are asymmetric in time and that the stress range was kept below a few percent of the mean stress. Another observation of interest is that accumulated damage during cycling resulted in an increased relaxation (from 5.3% to 7.6% during a one-day relaxation increment) which was followed by a reduced relaxation due to strengthening before failure was initiated (compare with Figure 3.19).

Figures 3.18, 3.19 and 3.20 (at the end of this section) contain the relaxation data for the stages one to ten in normalized stress drop versus deviatoric stress or vertical strain ϵ^* diagrams. The stress ratio versus normalized stress drop for the stages 8 to 24 is given in Figures 3.21, 3.22 and 3.23. The current short-term strength D_{max} was calculated by interpolation between points where

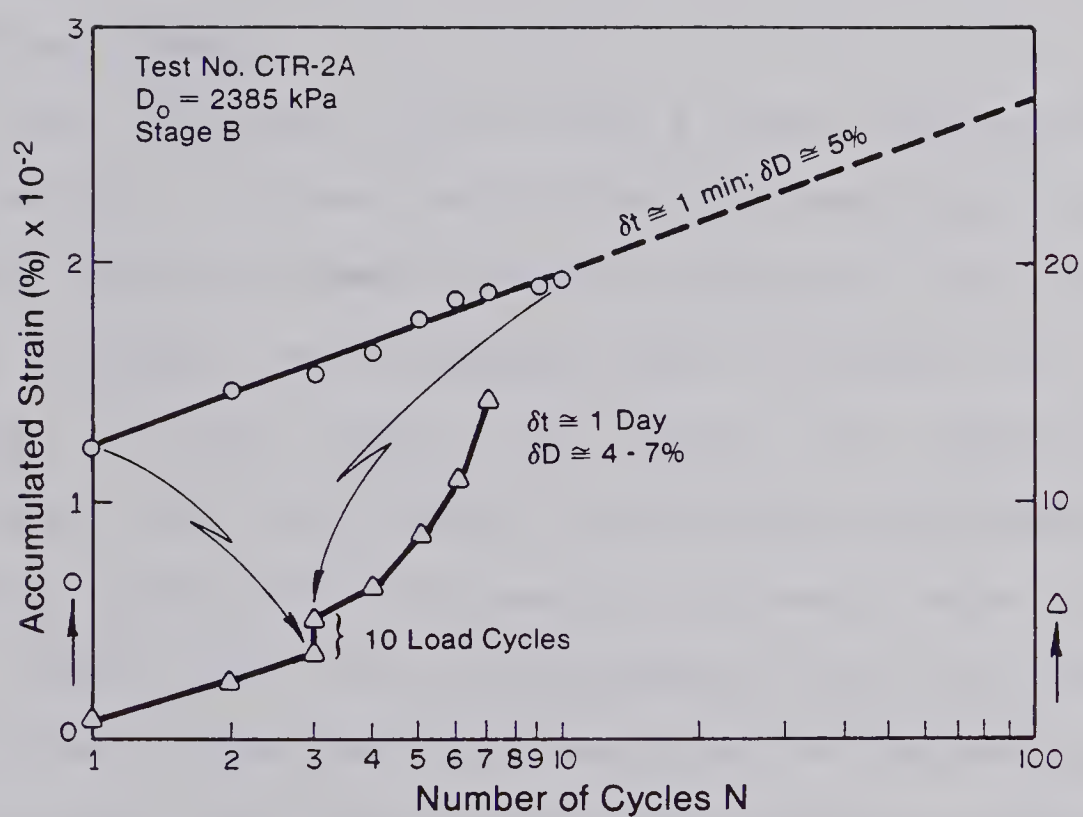


Figure 3.17 Accumulated Strain versus Logarithm of Number of Cycles, Test No. CTR-2A

D_{max} was known from rapid straining at a constant rate. Both D_{max} and ΔD , the stress drop, are affected by the loading rate and should theoretically be determined from instant loading. The rate of 1.52 mm/hour was kept constant throughout the testing program and is relatively fast. In principle the stress drop should be normalized to D_{min} , the current long-term strength, but this value is difficult to determine.

Test No. CTR-2D

This specimen failed along a joint inclined 57° to the horizontal. A strong rock bridge near the upper part of the joint caused a tensile crack to propagate towards the load cap. Loading, over-stressing and crushing of this rock bridge is most likely the reason for the more ductile behaviour of this sample. A minor part was sheared along a bedding plane which intersected the sample side 40 mm above the bottom load cap. Approximately 50% of the shear plane consisted of open joint surface. From the relaxation data it appears that the joint sheared when loaded to stage eight at an inelastic strain of $\epsilon_f = 0.26\%$ as indicated by the arrow in Figure 3.24.

Eleven stages of repeated relaxation tests at increasing stress levels before and through short-term peak strength were followed by five stages after unloading and reloading in the after failure range. The total testing time was 93 days. The membrane failed during the second unloading-reloading cycle at 2% total strain and no further

testing near ultimate strength was possible. Two sets of typical test results with time versus normalized deviatoric stress drop and total vertical strain versus time are given in Figure 3.4 for stage one before failure and Figure 3.25 for stages eight to ten near the long-term peak strength before collapse.

A diagram of normalized deviatoric stress and vertical strain versus logarithm of time for stages 1, 9 and 10 in Figure 3.26 indicates again a linear relationship and a machine stiffness of approximately 80 MN/m was calculated. All relaxation curves for the prefailure stages 1 and 5 are given in Figure 3.27; some non-linearity, most likely due to temperature effects, can be observed. Figures 3.28 and 3.29 contain the relaxation data for stages 1 to 11 and 12 to 16 in deviatoric stress and vertical strain ϵ^* versus normalized stress drop diagrams.

Test No. CTR-2F

A picture of this specimen after testing is given in Plate 3.2. The shear plane developed along four different joint planes inclined at 60 to 65 degrees to the horizontal. The left side of the sample sheared along one plane with some rock bridges whereas the right part sheared along three stepped joints. These steps were between 5 and 15 mm in height and they were created by tensile fractures approximately perpendicular to the joint planes. The lowest part of the shear plane intersected the load cap. Because of this irregular failure surface the sample was sheared along



Plate 3.2 Sample CTR-2F after Testing

a portion of a bedding plane. The overall degree of separation was roughly 85%. The stress-strain curve is given in Figure 3.30. Failure occurred during stage three and the post-peak curve is relatively steep. Between the two prefailure stages at stress levels above 75% failure stress only a portion of the accumulated inelastic strain was recovered. The sample was unloaded three times and reloaded in the post failure range. These loading cycles were followed by repeated relaxation tests at stage 4 and stages 5 to 8 at decreasing stress levels. Stages 8 and 9 involved testing at increasing confining pressure (contrary to Test No. CTR-2A) followed by a gradual cell pressure decrease to the original level and another three stages of repeated relaxation tests from decreasing stress levels near ultimate strength. The total testing time was 133 days.

Figures 3.31 and 3.32 contain relaxation data from stage 8 at increasing confining pressures and stage 9 at decreasing confining pressures. A linear normalized deviatoric stress-logarithm of time relationship is again obvious. Figure 3.33 summarizes the relaxation data from stages one to four in a vertical strain versus normalized stress drop diagram and the following Figures 3.34, 3.35 and 3.36 give the normalized stress drop versus stress ratio diagrams for the remaining stages 4 to 13.

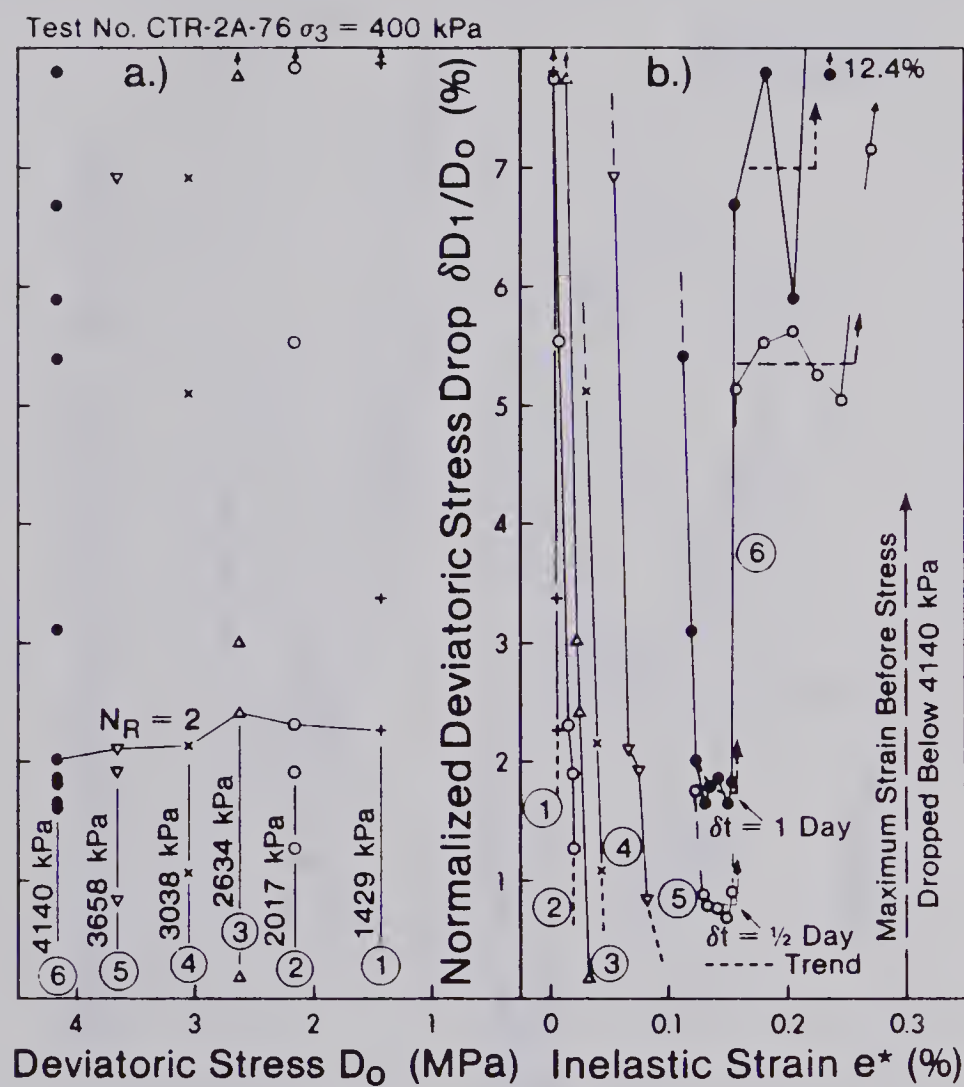


Figure 3.18 Normalized Deviatoric Stress Drop versus Deviatoric Stress and Inelastic Strain e^* , Test No. CTR-2A, Stages 1 to 6

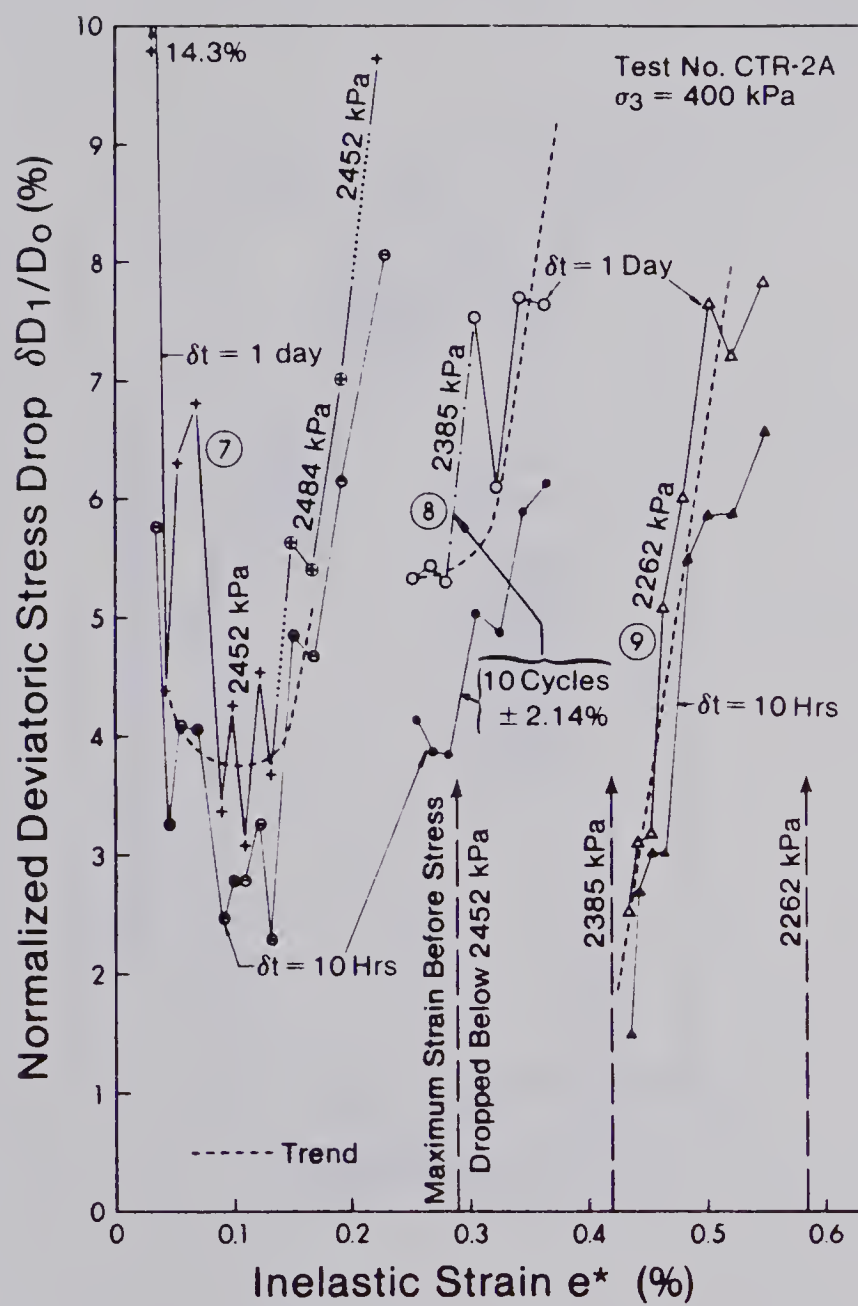


Figure 3.19 Normalized Deviatoric Stress Drop versus Inelastic Strain e^* , Test No. CTR-2A, Stages 7 to 9

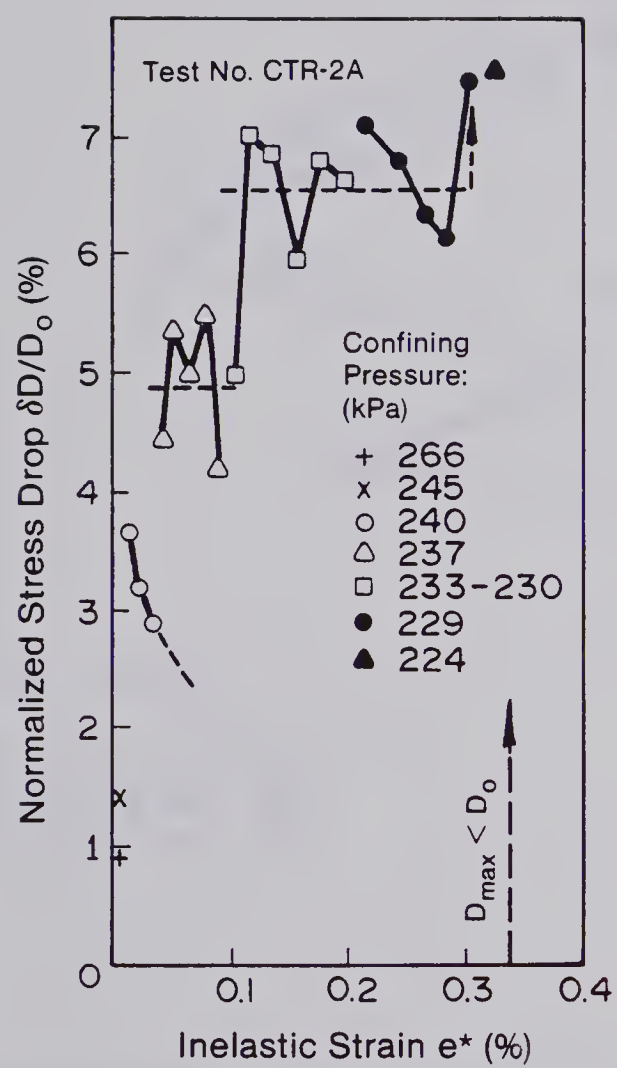


Figure 3.20 Normalized Deviatoric Stress Drop versus Inelastic Strain e^* , Test No. CTR-2A, Stage 10

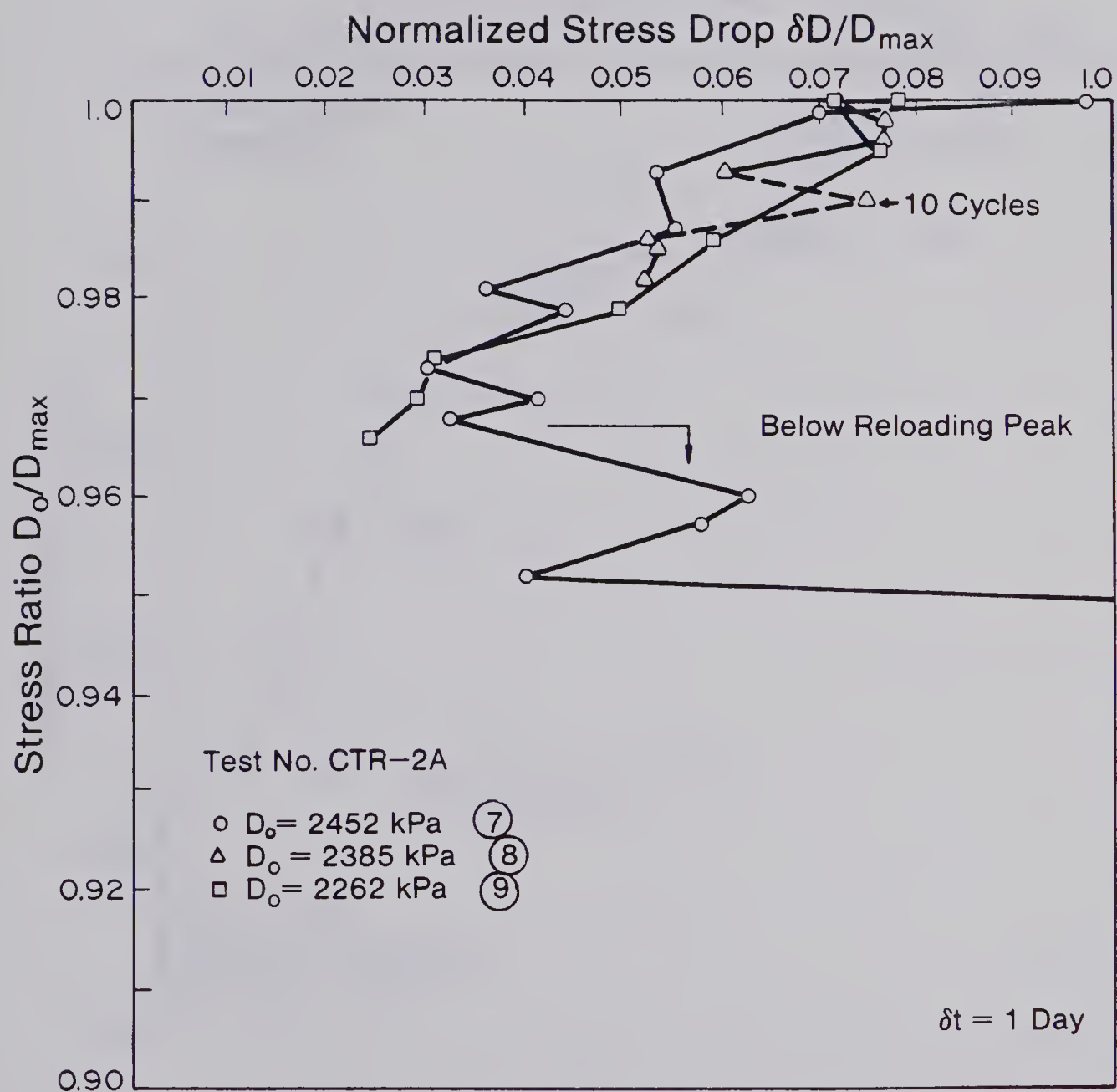


Figure 3.21 Stress Ratio versus Normalized Stress Drop, Test No. CTR-2A, Stages 7 to 9

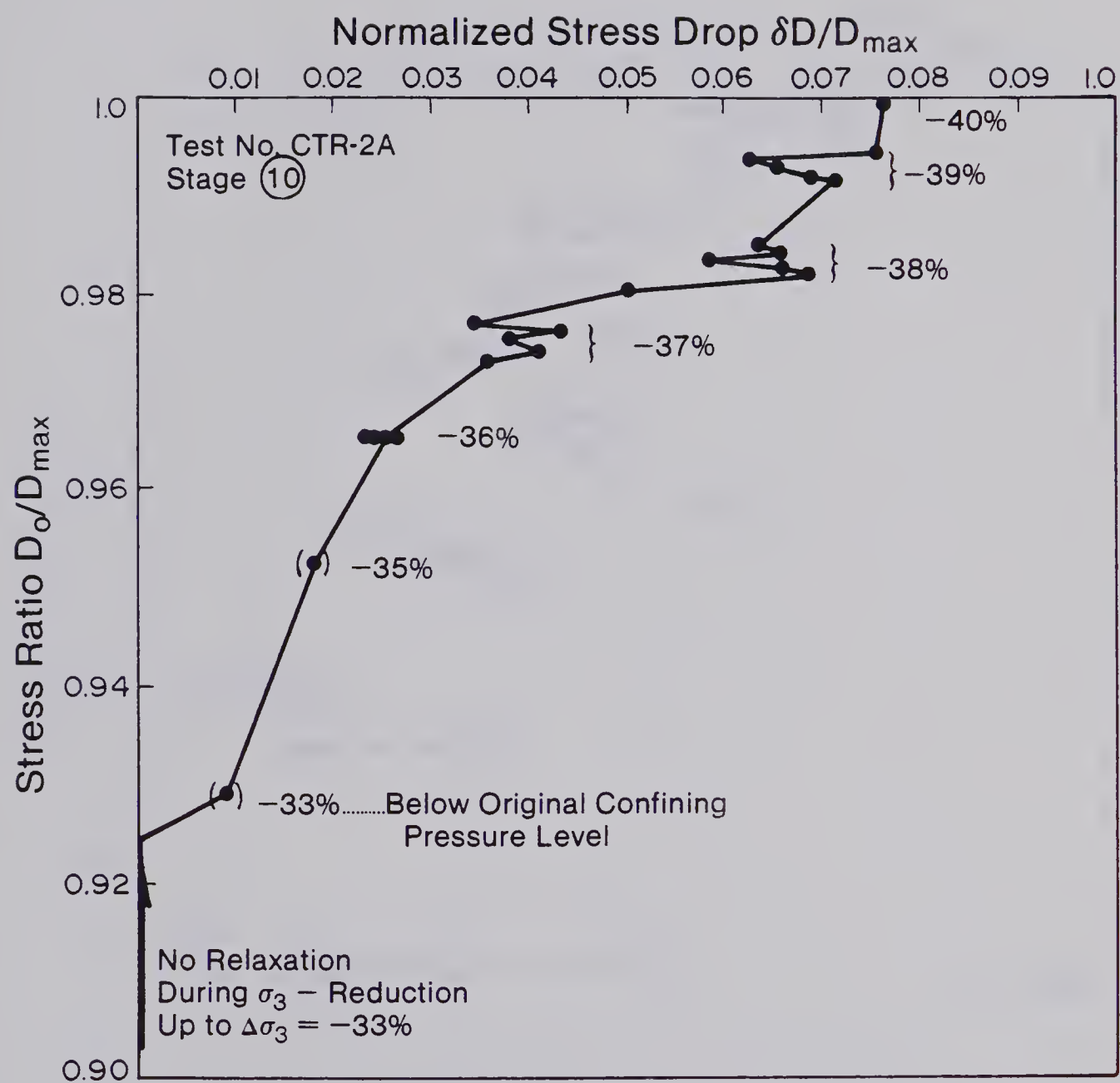


Figure 3.22 Stress Ratio versus Normalized Stress Drop, Test No. CTR-2A, Stage 10

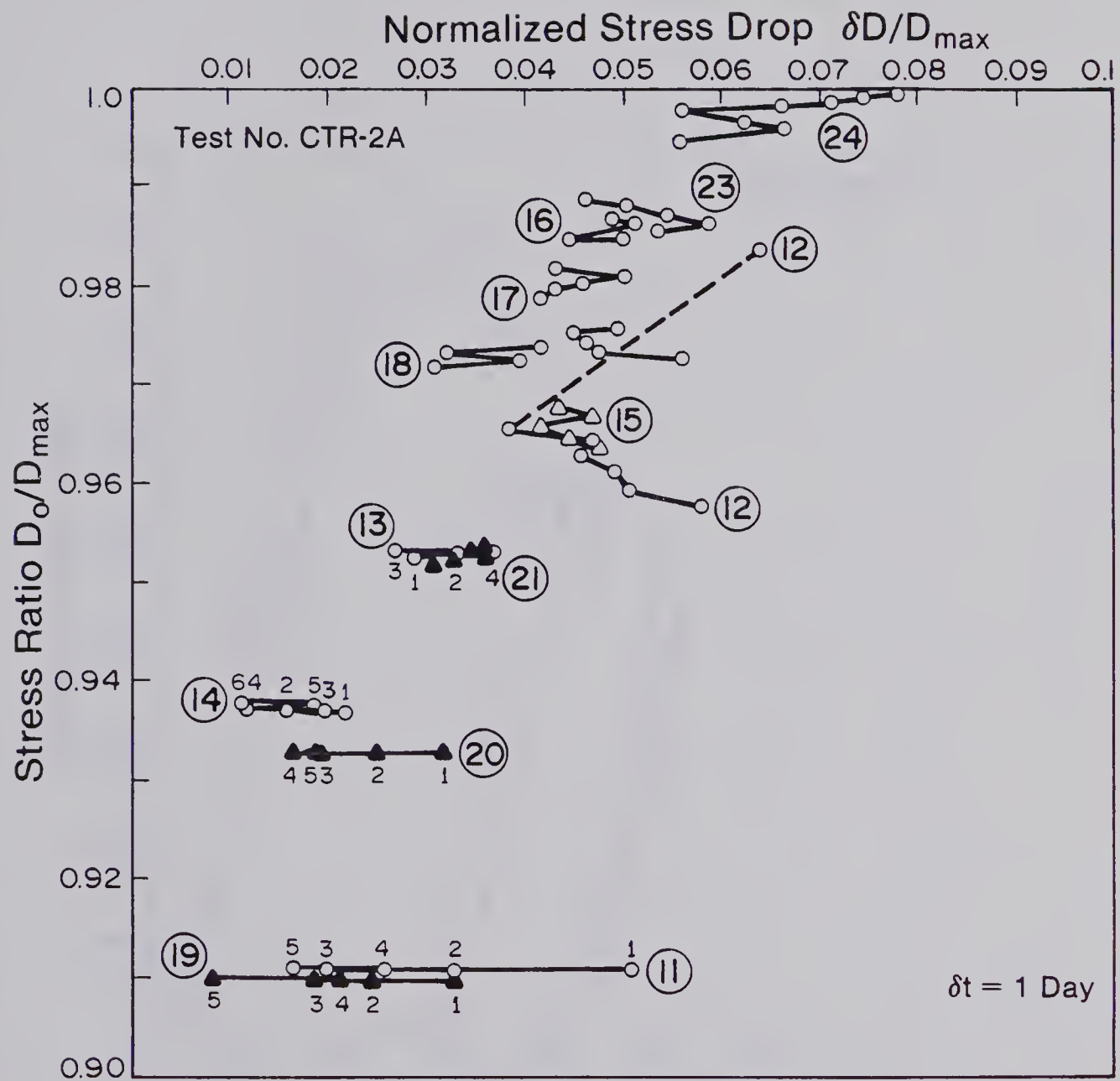


Figure 3.23 Stress Ratio versus Normalized Stress Drop, Test No. CTR-2A, Stages 11 to 24

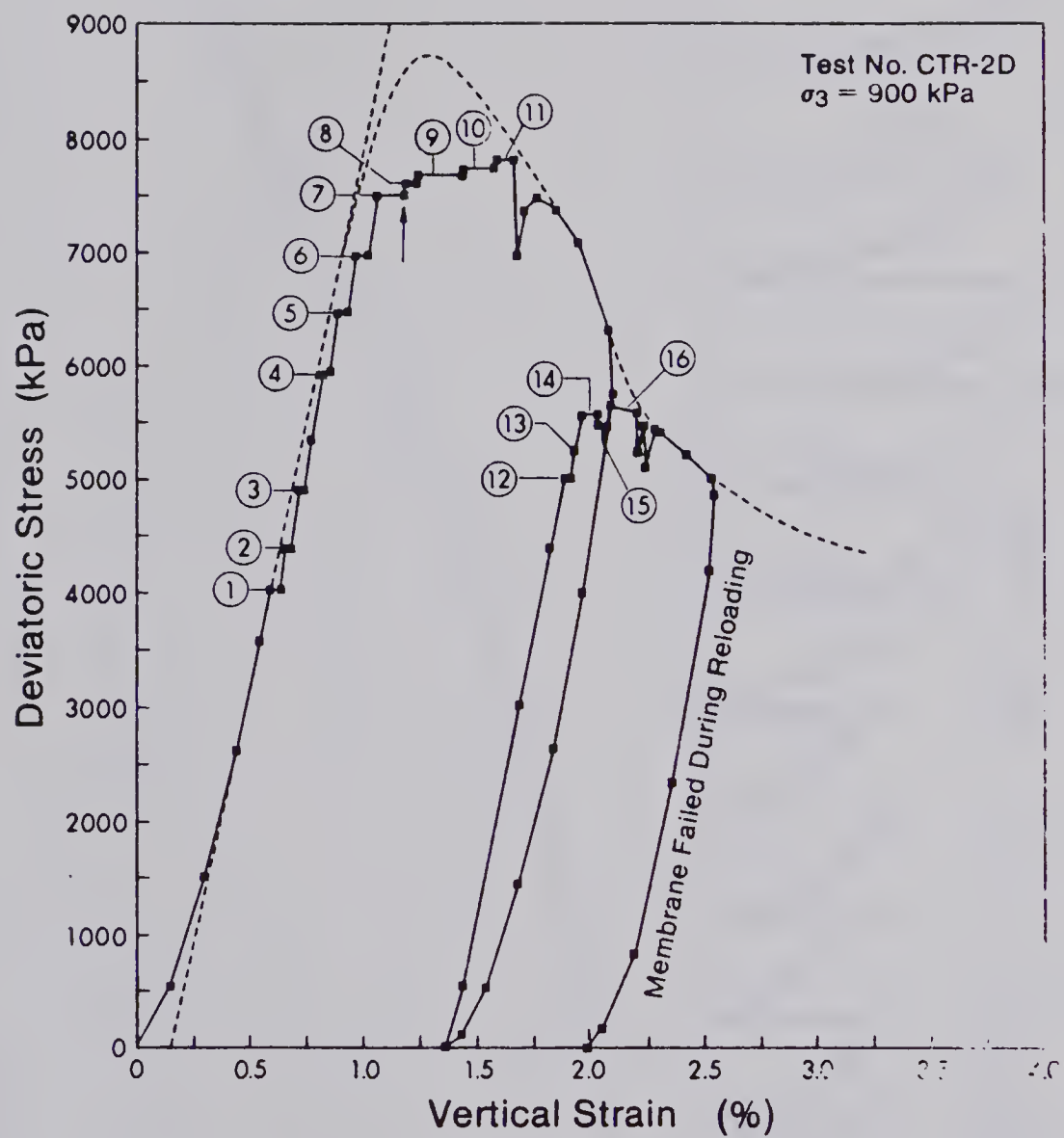


Figure 3.24 Stress-Strain Diagram of Test No. CTR-2D

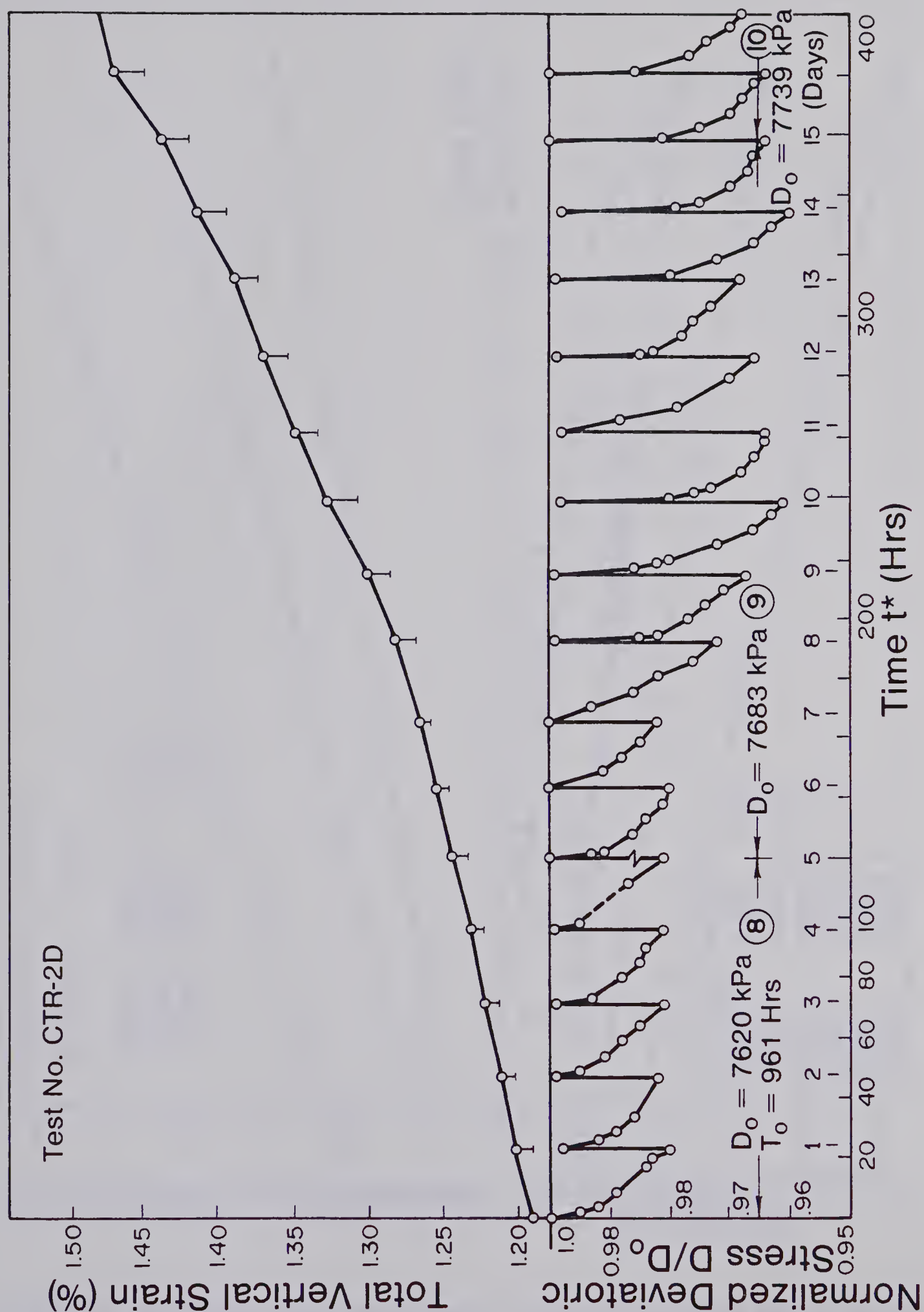


Figure 3.25 Normalized Deviatoric Stress and Total Vertical Strain versus Time of Test No. CTR-2D, Stages 8 to 10

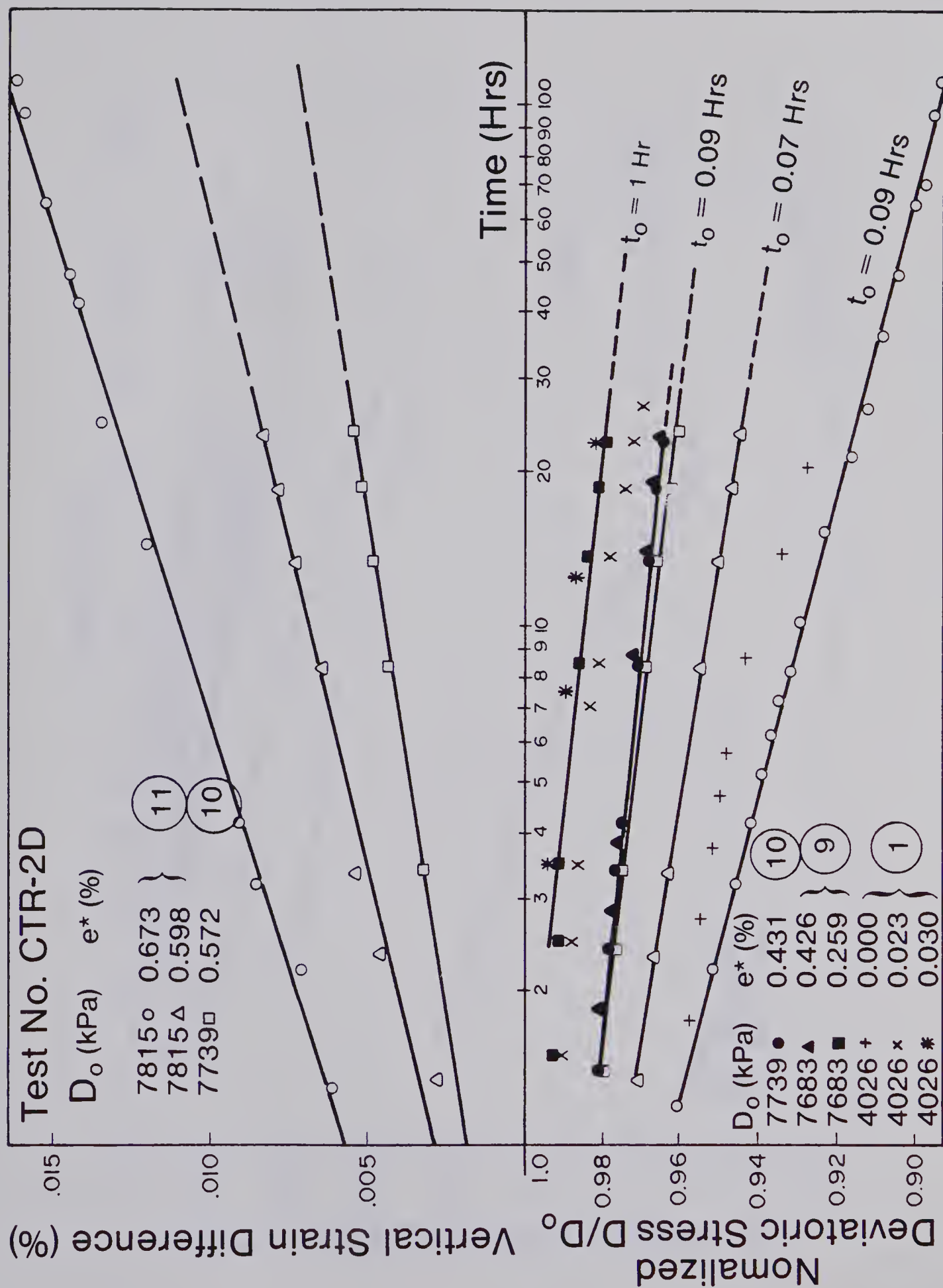


Figure 3.26 Normalized Deviatoric Stress and Vertical Strain Difference versus Logarithm of Time during Relaxation of Sample No. CTR-2D

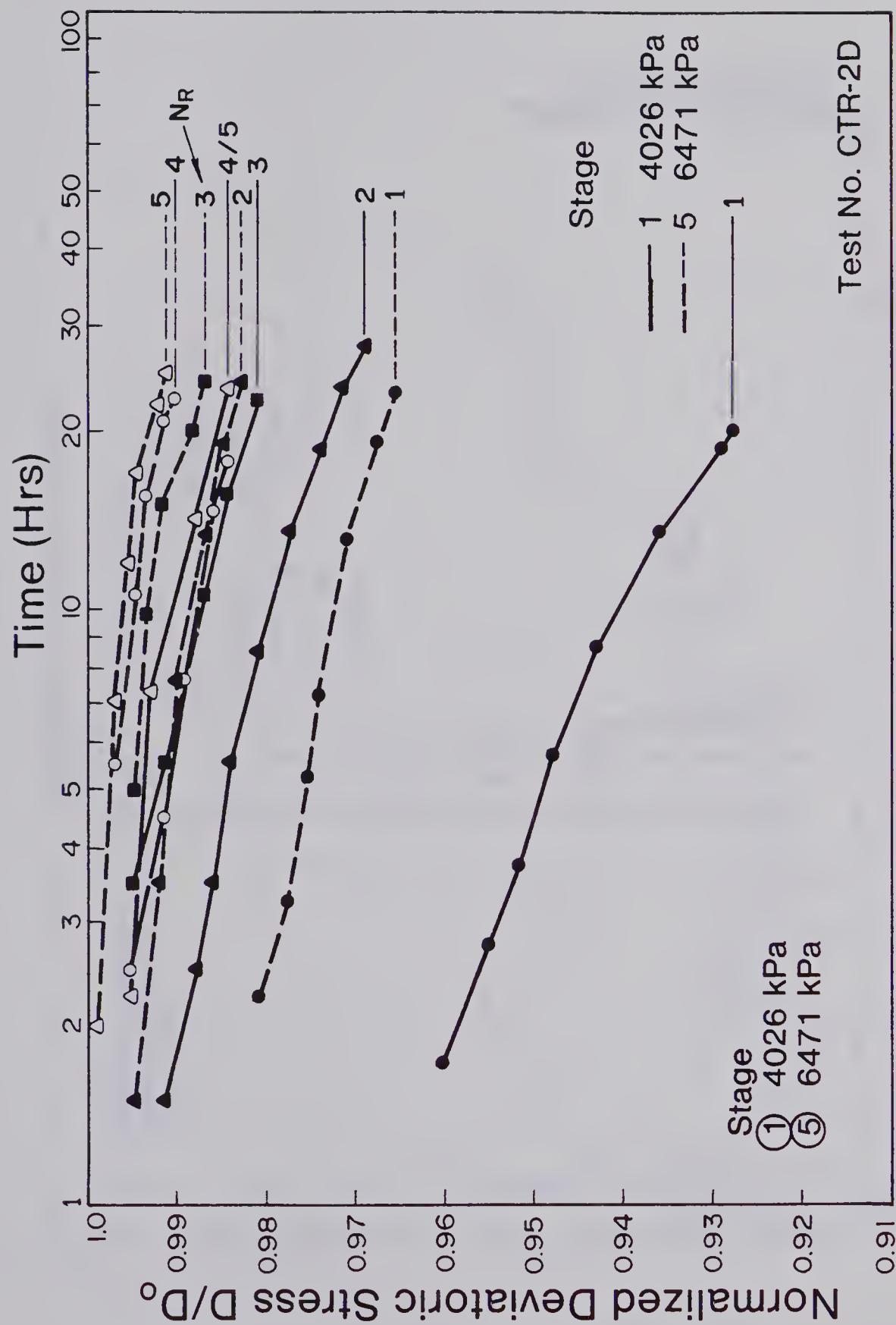


Figure 3.27 Normalized Deviatoric Stress versus Logarithm of Time, Test No. CTR-2D

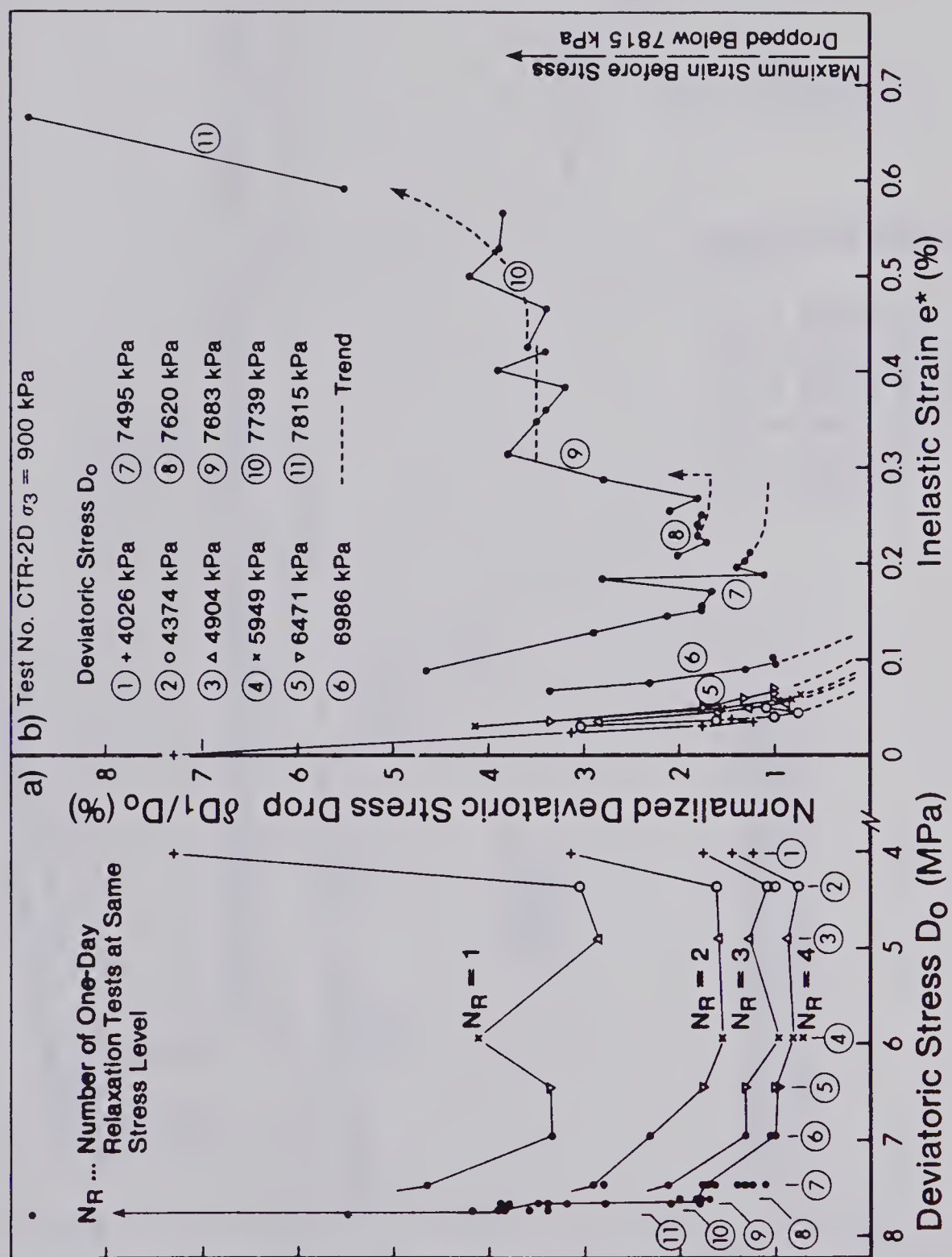


Figure 3.28 Normalized Deviatoric Stress Drop versus Deviatoric Stress and Inelastic Strain e^* , Test No. CTR-2D, Stages 1 to 11

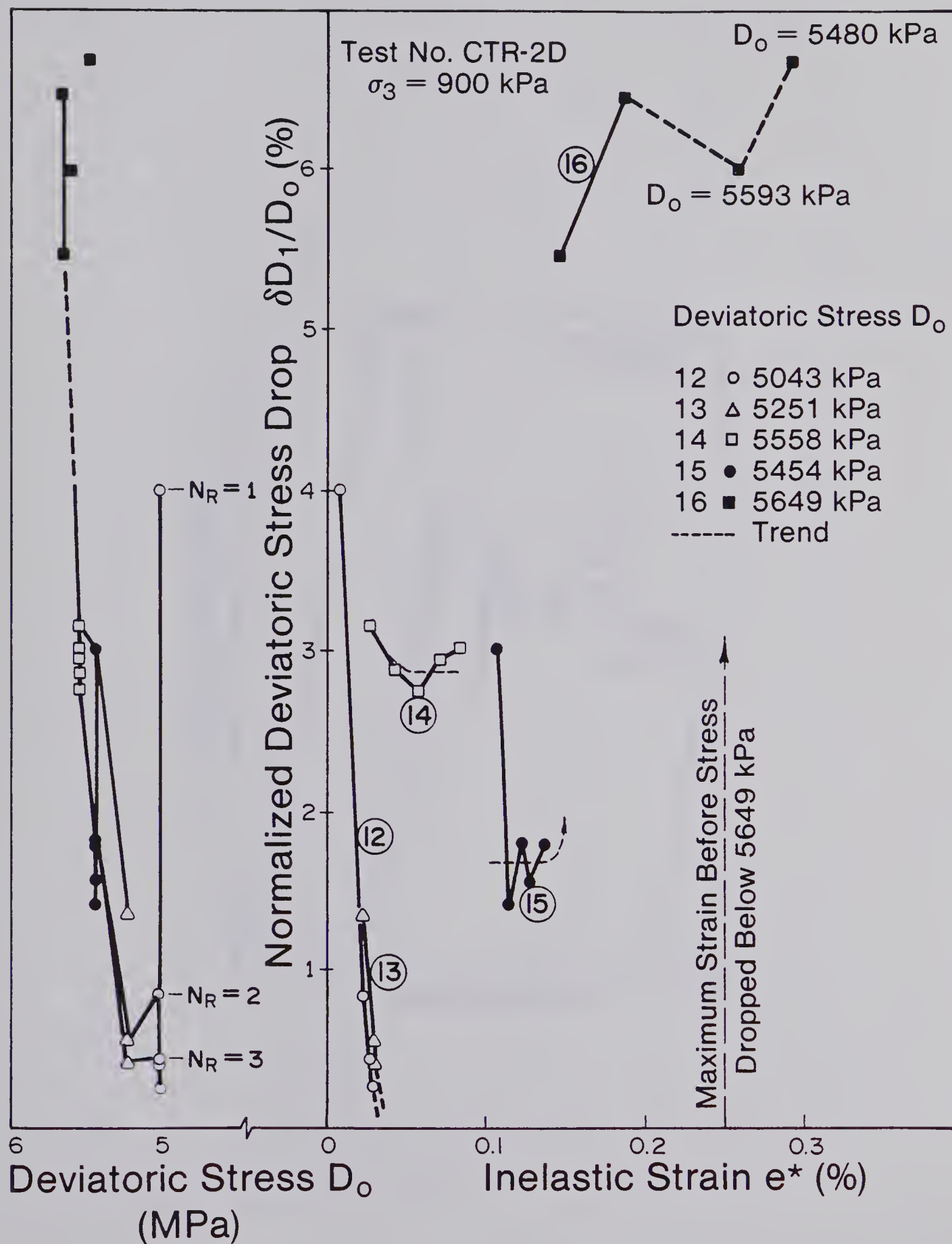


Figure 3.29 Normalized Deviatoric Stress Drop versus Deviatoric Stress and Inelastic Strain e^* , Test No. CTR-2D, Stages 12 to 16

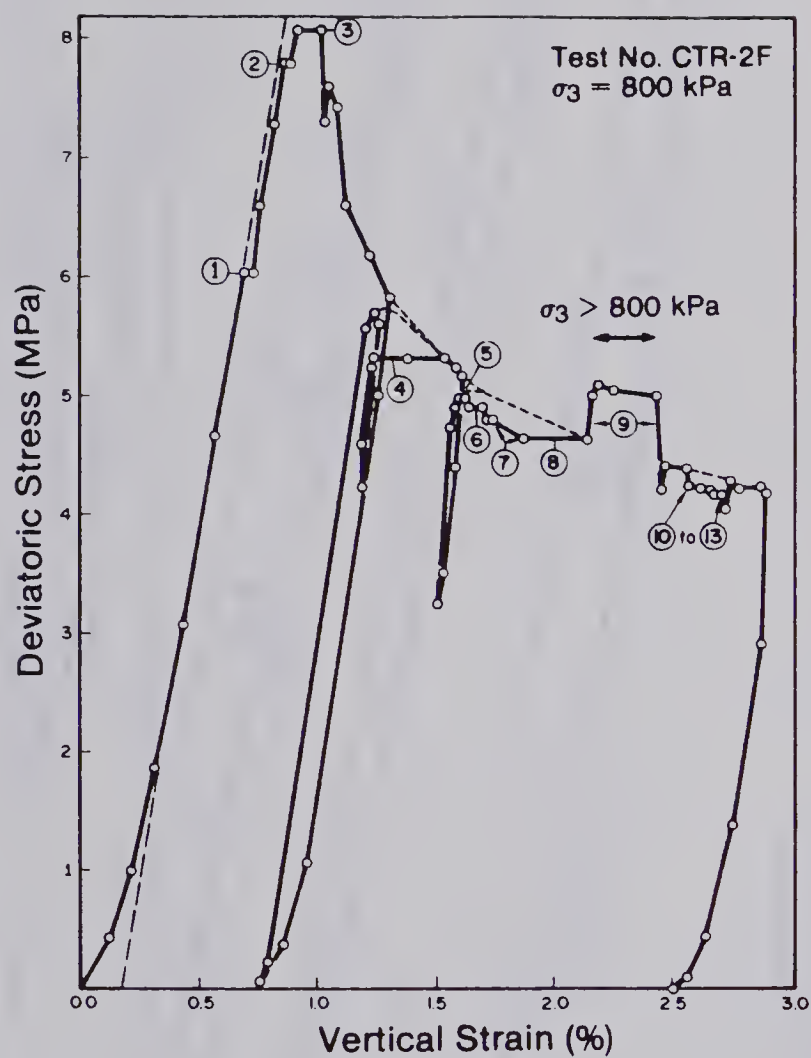


Figure 3.30 Stress-Strain Diagram of Test No. CTR-2F

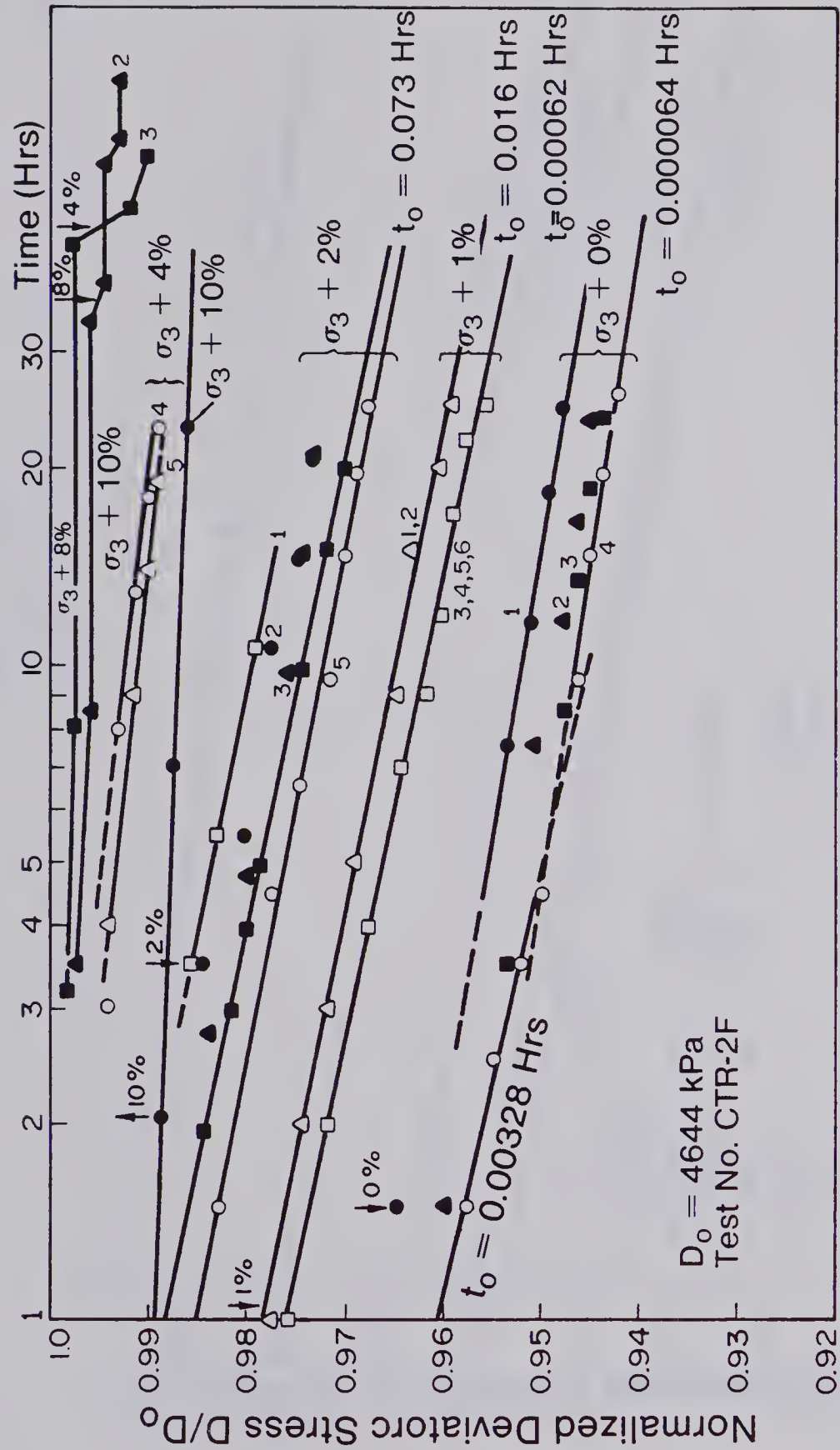


Figure 3.31 Normalized Deviatoric Stress versus Logarithm of Time, Test No. CTR-2F, Stage 8

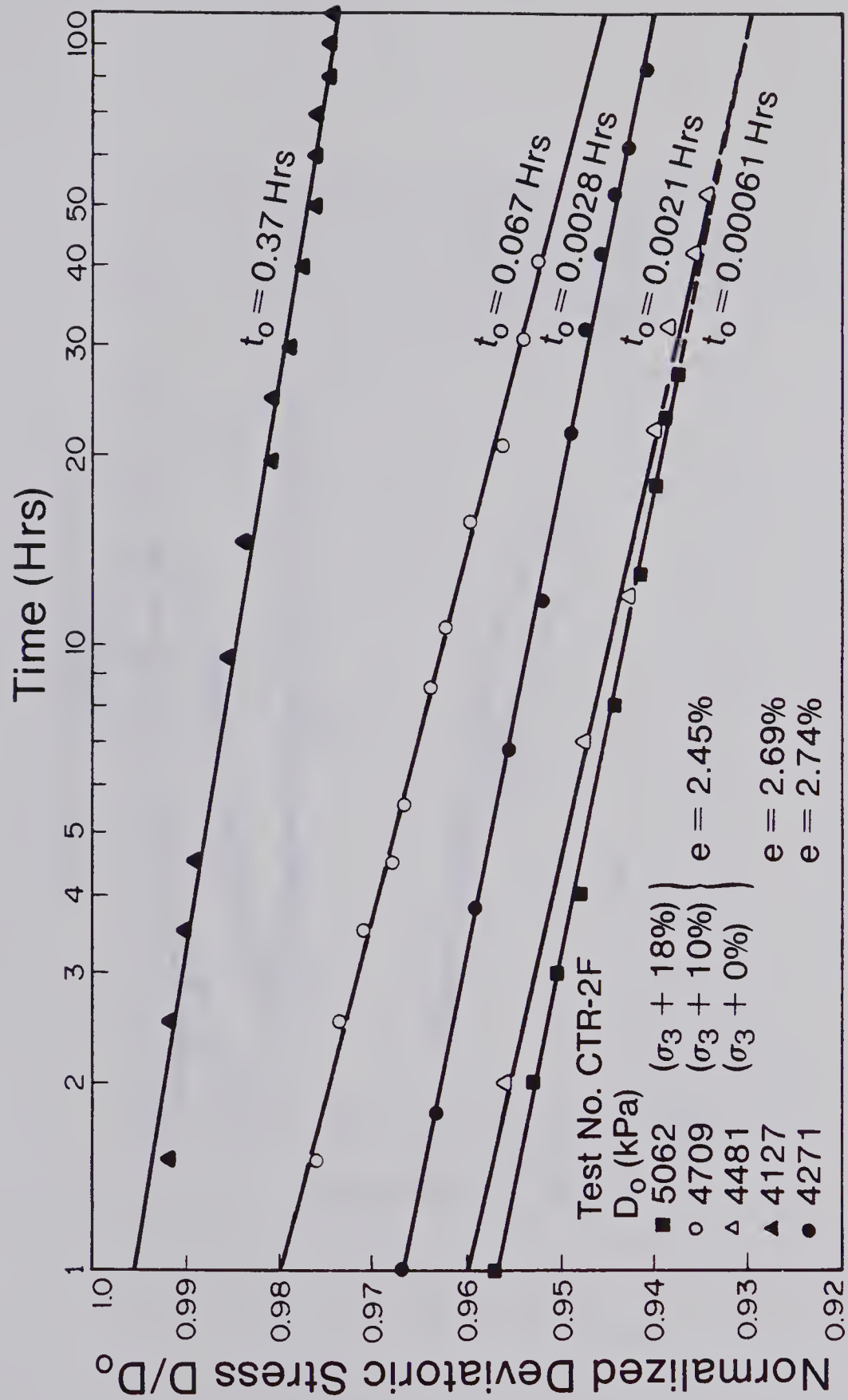


Figure 3.32 Normalized Deviatoric Stress versus Logarithm of Time, Test No. CTR-2F, Stage 9

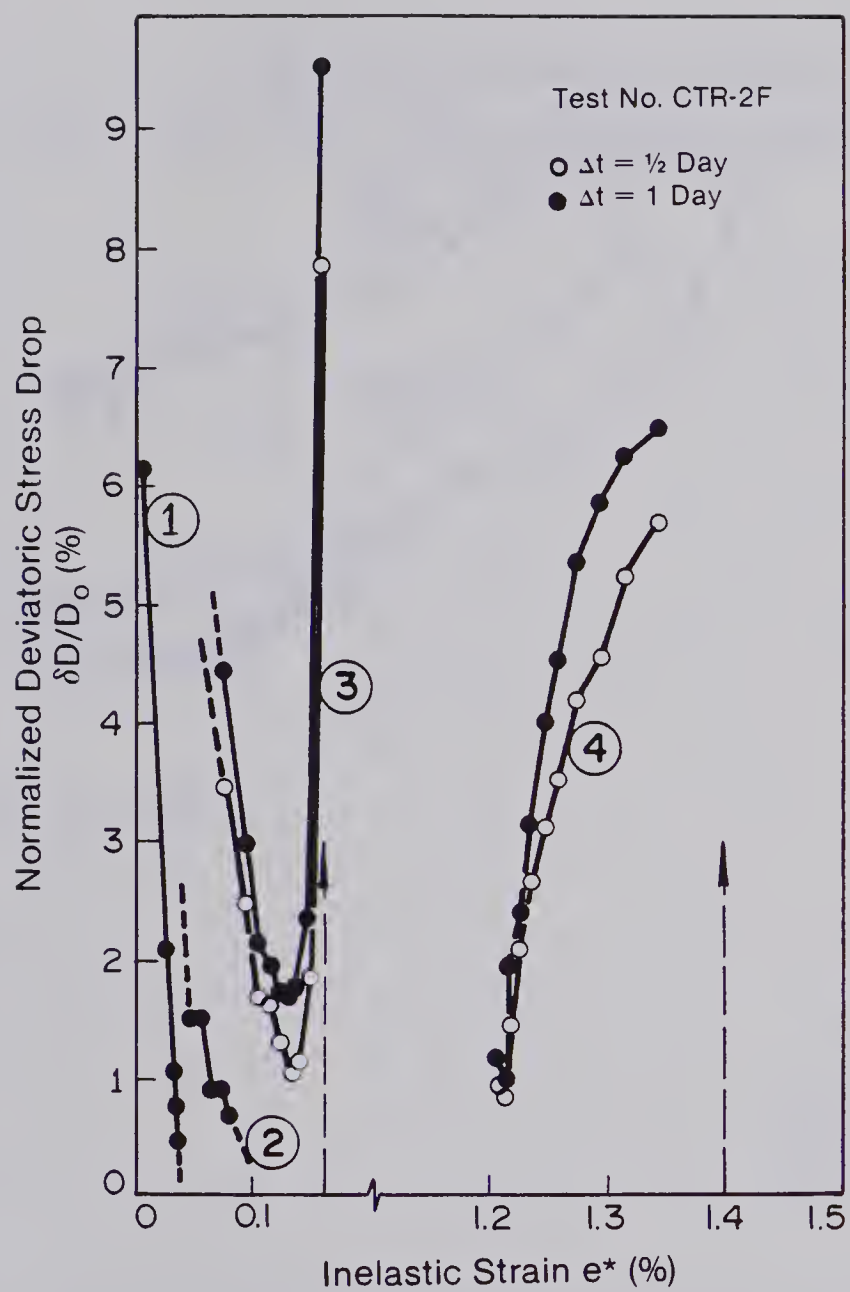


Figure 3.33 Normalized Deviatoric Stress Drop versus Inelastic Strain e^* , Test No. CTR-2F, Stages 1 to 4

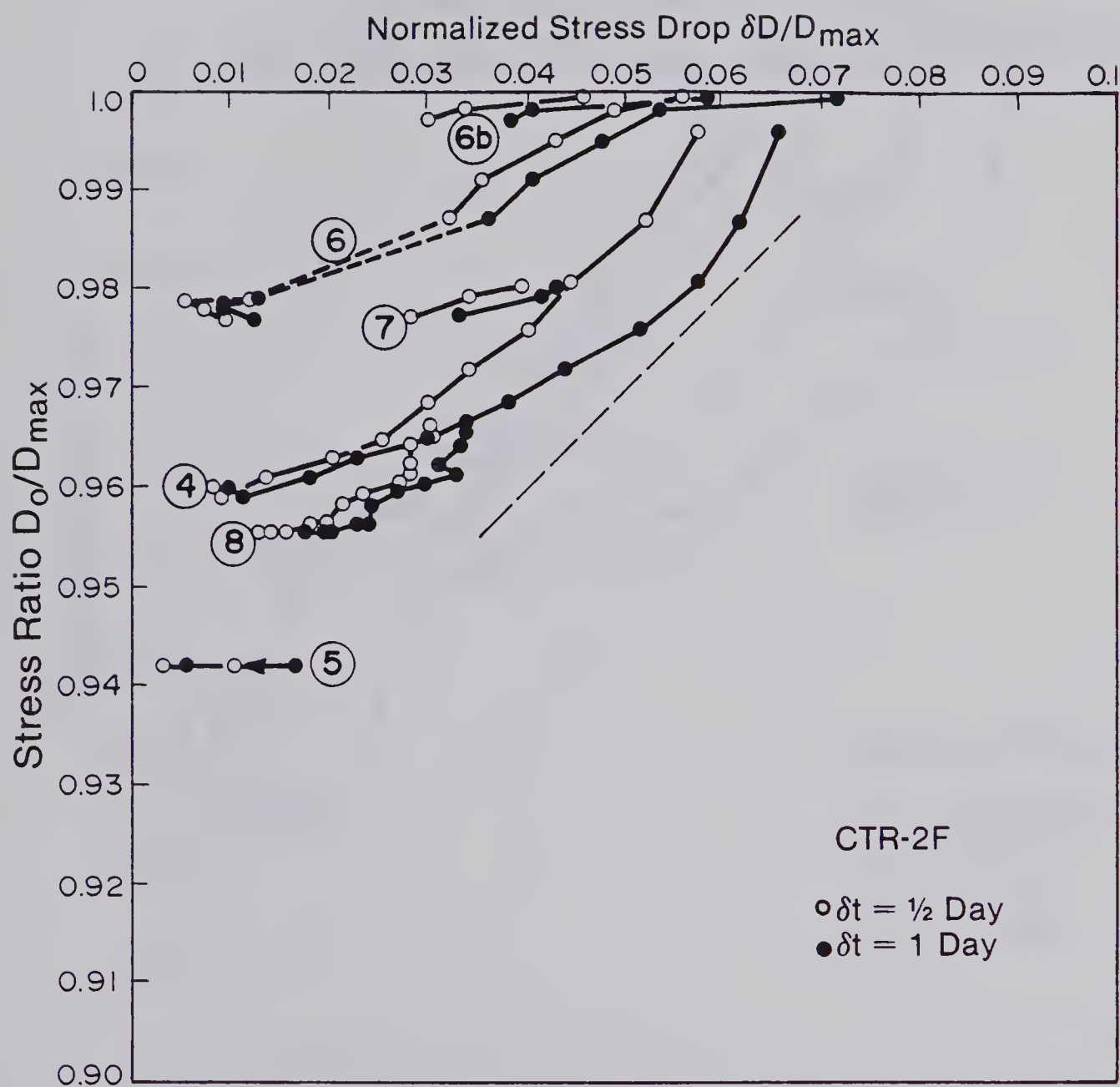


Figure 3.34 Stress Ratio versus Normalized Stress Drop, Test No. CTR-2F, Stages 4 to 8

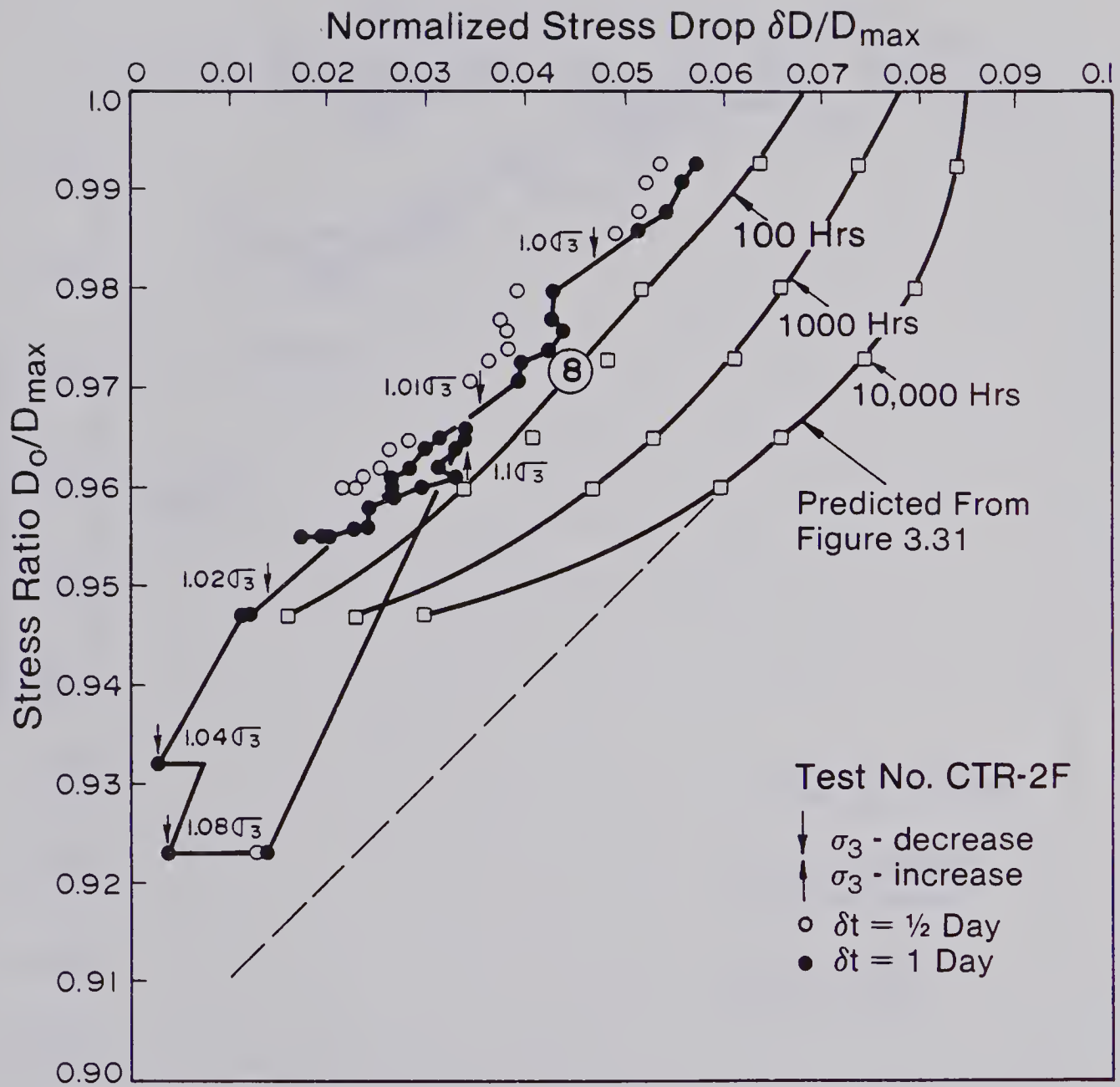


Figure 3.35 Stress Ratio versus Normalized Stress Drop, Test No. CTR-2F, Stage 8

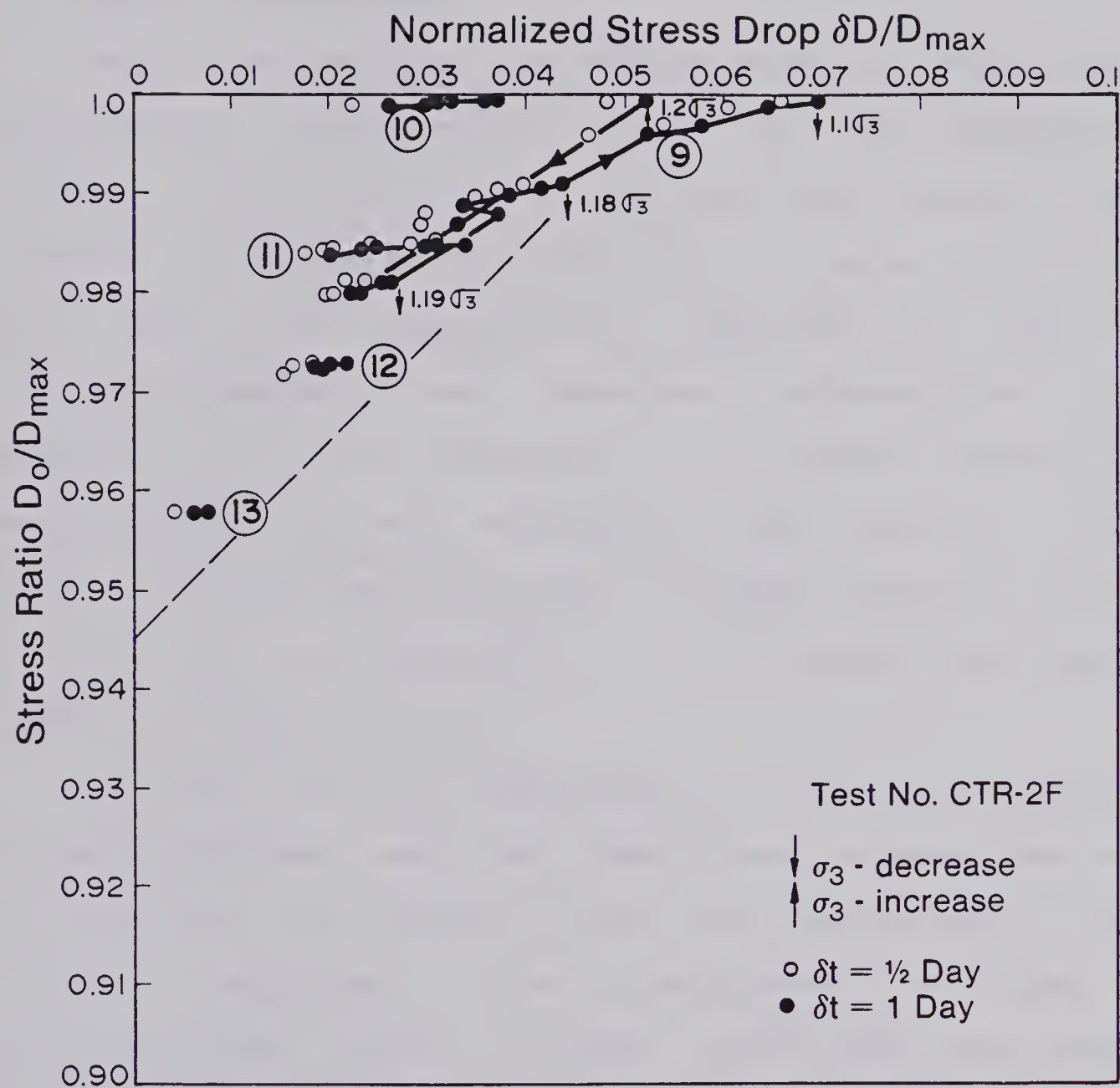


Figure 3.36 Stress Ratio versus Normalized Stress Drop, Test No. CTR-2F, Stages 9 to 13

3.5 Interpretation of Results

3.5.1 Introduction

During deformation, the microstructure of rock changes continuously. Crack closure occurs at the beginning of loading, shear displacement develops along cracks, cracks propagate and finally the confluence of cracks results in a shear zone. The time-dependent properties of rock are structure-dependent and therefore extrapolation from behaviour at one structure to another requires an understanding of this dependence. The rheology of rock cannot be effectively described in simple terms as a time-, stress-, or strain-dependent material except over limited ranges of stress or strain.

In this section a description is offered of ranges of typical behaviour and the transitions between them as a brittle rock is deformed over the peak strength to the ultimate resistance. This description is given in phenomenological terms in order to delineate the various processes involved. It should be noted that the recognition of transitions from one type of time-dependent behaviour to another is of particular interest for constrained rock structures such as underground openings where the interaction between elements strained to different levels is important and portions of the rock are stressed beyond their capacity.

In order to separate zones of typical behaviour, it is first of all necessary to decide whether the coal has a stable zone below a current long-term strength or not. If a current long-term strength exists, terminating creep or repeated relaxation and finite yield should be measured at stress levels below this current long-term strength. As indicated earlier many authors represented coal by a Burgers model, a fluid with no current long-term strength. Using the data given by Kidybinski (1966), which is comparable with parameters given by others and which predicts the relaxation during multiple-stage repeated relaxation tests at low stress levels reasonably well, a minimum creep rate of approximately $10^{-5}\%/hr$ under a stress of 1 MPa would be reached after more than 250 hours. The daily relaxation at this time would be less than about 0.024%/day, values well below the limits of the test accuracy. Most of the repeated relaxation tests at low stress levels were extended over a period of five days and showed stress drops in the order of a few percent. These drops are dominated by the Kelvin element and coal therefore behaves initially like a viscous solid. Kidybinski's tests indicated an asymptotic long-term strength of approximately 50% of the short-term strength after a test period of 1550 hours. Considering this information, it is impossible to determine whether a test is conducted below or above the long-term strength by extrapolation from one-day relaxation tests or five repeated relaxation tests at one stage. However, if tests are

conducted above the current long-term strength, a "constant" or increasing stress drop per unit time or a "constant" or increasing creep rate is measured after an initial decrease. If a current long-term strength exists, these rates will decrease as the stress level approaches the current long-term strength and vanish at the current long-term strength. It is therefore evident from the test results that a current long-term strength exists and that relaxation and creep must terminate at stress levels below the current long-term strength. This assumption is only supported by data within comparable time intervals and an extrapolation to geologic time scales is not permissible.

The normalized deviatoric stress is plotted in Figures 3.16, 3.26, 3.27, 3.31 and 3.32 against the logarithm of time. A linear relationship without termination is evident even in relaxation tests over an extended period of 100 hours. The non-linearity in Figure 3.27 can most likely be attributed to temperature effects. The same is valid for the bi-linear relationship indicated in Figure 3.31. Comparable trends can be observed in accumulated strain versus time plots (e.g. Figure 3.4) which indicate continuously decreasing strain accumulation. While neither set of data proves termination, the assumption of termination is strongly supported by the linear relationship between normalized stress drop and vertical strain e^* and a definite trend (indicated by dashed lines) towards a maximum e^* . The Figures 3.18 (curves 1 to 4), 3.28 (curves 1 to 4 (or 6)),

3.29 (curves 1 and 2) and 3.33 (curves 1 and 2) illustrate this point.

During test CTR-2A, the sample was unloaded after stage nine and no relaxation was measured over a period of several days. The confining pressure was decreased in steps resulting in a stepwise decrease in D_{max} . No relaxation was observed until the stress ratio reached about 0.92 (Figure 3.22). This behaviour is only possible if the sample had been loaded to a stress level below the current long-term strength. The existence of a current long-term strength is further supported by the data shown in Figure 3.23 where stages 11 and 19 show continuously decreasing and stages 14 and 20 constant stress drops. The current long-term strength is therefore higher than 0.90 D_{max} and most likely approximately 0.92 D_{max} . Additional support is given by the data shown in Figure 3.35 where an increase in confining pressure resulted in an immediate decrease in stress drop and only above a stress ratio of 0.94 was increased relaxation measured. Figure 3.31 shows the corresponding data in a normalized deviatoric stress versus logarithm of time plot. The stress drop at unit time, time t_0 (Lacerda and Houston(1973)), decreases with increasing confining pressure as well as with the number of relaxations undertaken at the same stage. The slope of the stress drop versus logarithm of time curve remains constant until it decreases after a confining pressure increase of more than 4% and becomes almost zero at confining pressures 8 to 10%

above the original stress level. At this stage an initial stress drop, which is most likely due to the testing system relaxation, is followed by an extremely small relaxation.

3.5.2 Schematic Stress-Strain Diagram for Rock

Based on the assumption that a current long-term strength exists a schematic stress-strain diagram has been developed in Figure 3.37 . Three zones can be identified. Zone A is characterized by a decreasing stress drop during repeated relaxations (or creep rate) if loaded to stress levels below the peak long-term strength (point (a) on $\dot{\epsilon}=0$ -curve). Above this level, the strain will accumulate until the limit a-a is reached at which the available resistance begins to change. Zone B is a rate-dependent yield or visco-plastic zone with strain-dependent upper and lower boundaries (current available strength and current long-term strength). The ratio between the current long-term strength and current available strength (D_{min}/D_{max}) increases and it is expected that this ratio becomes unity at large strains where both limits coincide. Highly strained rock would behave like a visco-plastic material and the ultimate strength would be time-independent. This point was not proven since the maximum strain was limited. Lines of equal creep rate or stress drop per unit time can be found between these limits. Constant stress tests or repeated relaxation from a constant stress level will lead to relaxation or creep rate increases and to failure as these

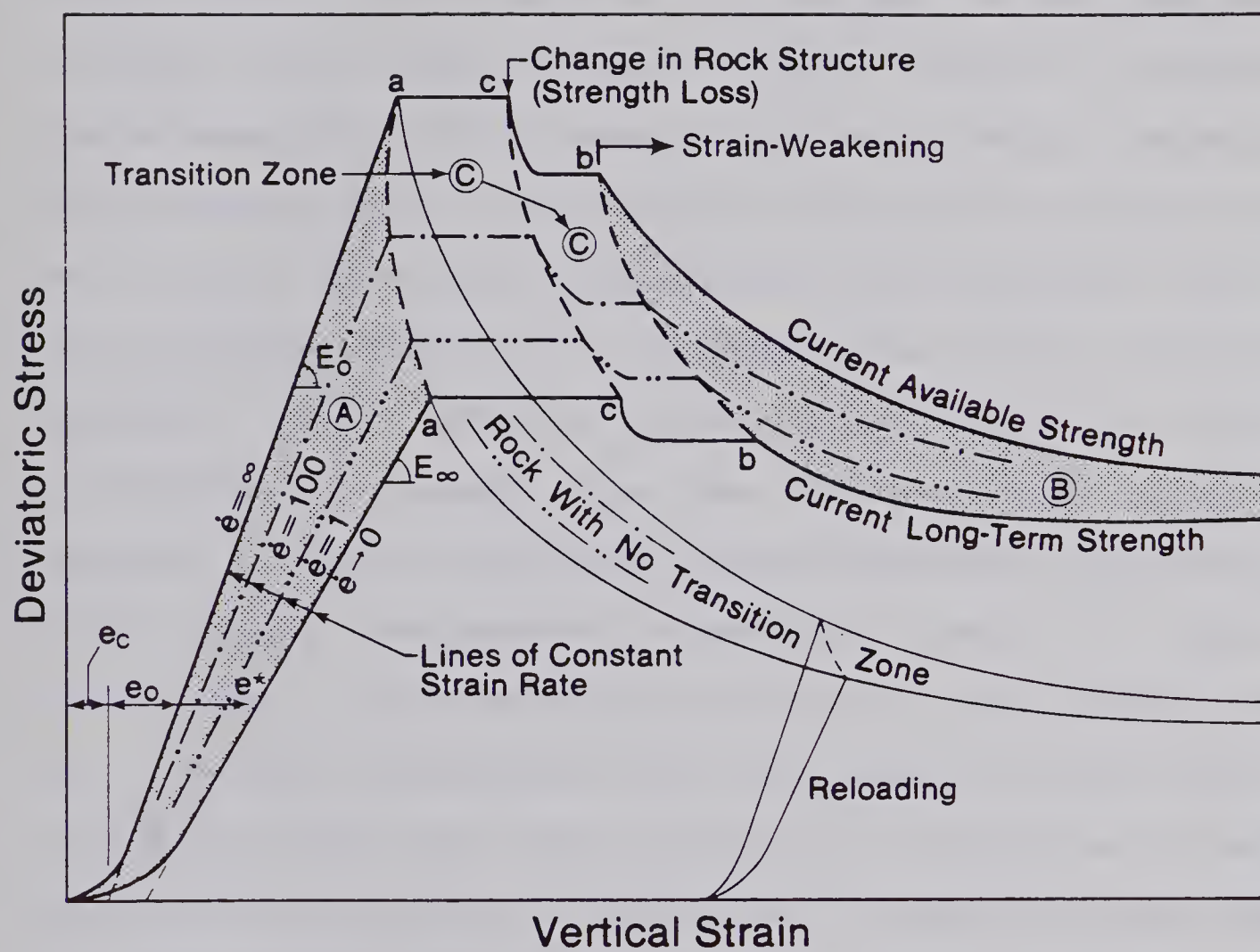


Figure 3.37 Schematic Stress-Strain Diagram of Rock

lines are crossed and the current available strength is reached. Similarly, a stress-strain path crossing lines of constant strain rate in descending order will approach the current long-term strength. Zone C is a transition zone whose extent depends upon the ductility of the rock. The behaviour in this zone is a function of the available strength which may increase, remain constant or change instantaneously. If the current available strength decreases continuously zone B is reached. For brittle materials the two limits a-a and b-b coincide and the transition zone is non-existent. Failure is reached if the current available strength drops below a given stress level by either instantaneous strength loss due to structural change or gradual strength loss during strain-weakening. The tertiary creep stage, accelerating deformation stage or failure initiation, is reached as soon as lines of equal strain rate are crossed in ascending order. The inelastic strain ϵ^*_{f} at this point, where the first significant stress drop increase was observed, is given in Table 3.2. It varied between 0.05% in sample TR-1A and 0.26% in CTR-2D.

Kranz and Scholz(1977) suggested that the inelastic volumetric strain at the onset of tertiary creep should be a constant critical value. A direct comparison with their results is not possible. Kranz and Scholz tested intact rock (granite and quartzite) and measured the volume change, whereas in the tests presented here, only the vertical strain during failure of a jointed rock was measured. If it

can be assumed that straining of a joint is directly related to volume change of a sheared joint, a similar relationship between inelastic vertical strain and onset of failure would be expected. The reported inelastic strain at failure initiation is not constant and varies within a wide range. The writer believes that the inelastic strain at failure and failure initiation is a function of the present rock structure. This structure varies from sample to sample and as a function of the loading history. It is therefore not surprising that there is no direct correlation. The same is to be expected for a rock mass where the failure is controlled by the structure within the overstressed zone.

3.5.2.1 Behaviour in Zone A (below peak long-term strength)

At stress levels below the current long-term strength, time-dependent deformation terminates. The deformation contains both recoverable and irrecoverable components, and, in the case of repeated relaxation testing, yields a continuous decrease of stress drop per unit time tending towards zero stress drop at a finite inelastic strain ϵ^* as illustrated by curves 1 to 5 in Figure 3.18, 1 to 6 in Figure 3.28, 12 and 13 in Figure 3.29, and curves 1 and 2 in Figure 3.33. The expected trend is indicated by the dashed lines. The exact amount of irrecoverable strain would have to be determined from unloading and recovery tests but yielding may be observed in the figures mentioned above. The increasing separation between the curves connecting points

of normalized stress drop during one stage of a multiple-stage repeated relaxation test and the increasing curvature indicates that more inelastic strain is accumulated during similar loading history but increased stress levels. It has to be recognized that this separation includes recoverable, stress-dependent strain and depends on the estimated slope of the fast loading curve. An over-estimation of the short-term stiffness would lead to a linear increase of this separation with stress. A corresponding behaviour was found during reloading tests (e.g. stages 12 and 13 in Figure 3.29).

The near parallelism of these curves reveals that the relaxation response during this mode is essentially independent of the irrecoverable strain accumulated prior to the particular loading stage, even though this strain is increasing throughout the test. An attempt was made to analyse the prefailure stages of sample CTR-2D by fitting a relationship similar to the one suggested by Lacerda and Houston (1973) to the data from each relaxation test (Hungry (1977)). It was found that relaxation tests starting from parallel linear stress strain curves showed the same time-dependent response at least up to stage 5(CTR-2D). These lines were inclined at a lower angle than the fast loading curve. The slope would have to be equal to the long-term stiffness because of the parallelism. This predicts a time-dependent behaviour independent of stress level and stress increment but dependent on the strain

remaining to the long-term stress-strain curve. Even though the analysis showed good correlation with correlation coefficients ranging from 0.85 to 0.99 this approach proved not entirely satisfactory because of the difficulty in selecting the correct origin of the time axis.

Similar to the problem of strain recovery in multiple-stage creep as indicated in Figure 3.9 there might be full or partial stress recovery between relaxation tests. Therefore, the stress measured at the beginning of a relaxation test is only the true D_0 if the test is started from the instantaneous loading curve after full recovery in multiple-stage tests. This means that functions were fitted through data without knowing the exact location of the origin of the coordinate system. Nevertheless, this suggests that the time-dependent deformation of coal at stresses below the current long-term strength can be expressed simply by relating it to the remaining time-dependent deformation or the distance from the long-term stress-strain curve. The more detailed investigation of the time-dependent prefailure behaviour by means of multiple-stage creep tests on the same coal, conducted by da Fontoura(1980), supports the view that the creep relations are independent of the accumulated strain.

It is not the purpose of this work to develop rheological models for this coal but it is of interest to check the data against the available models. Since not enough data was collected to determine the parameters for

the Burgers model and due to the fact that both Kidybinski (1966) and Morlier (1964) determined very similar parameters for coals completely different in origin, average parameters from these two publications were used. The relaxation behaviour during the first three stages was calculated by linear superposition (Boltzmann's principle). Good agreement with the measured data was found in the shape of daily stress-drop versus time as well as in magnitude of the relaxation after each relaxation test with the exception of the first increment of each stage. This deviation of the first relaxation test on each stage was also detected by Hungr (1977) and can be attributed to an additional initial relaxation in the gear box of the testing machine after major straining to a new load increment. The shape of each relaxation curve was found to be linear in the stress drop versus logarithm of time plot which indicates that a Burgers model is an oversimplification and that a model with a number of Kelvin models in series and a certain retardation spectrum (Terry(1956)) would have to be used to describe the coal accurately. The most important point, mainly for the interpretation of the model test data, is that the behaviour in the prefailure range, well below the long-term peak strength can be predicted by linear superposition since the coal behaves like a linear visco-elastic material.

3.5.2.2 Behaviour in Zone B (near ultimate strength)

Tests are conducted "near ultimate strength" if a strength loss can be achieved only during extensive straining. The behaviour in this zone is evaluated first because of the strain independence. Two major factors will be discussed besides the general behaviour in this zone; the effects of repeated loading with variable time-delays in between loadings, and the effects of confining pressure changes.

(a) Slow versus fast repeated loading:

From the brief test with enforced loading and unloading (Figure 3.17) it appears that the rate of deformation or strain accumulation in Zone B is directly related to the locally concentrated stress causing failure of asperities or extension of cracks and the time period over which this stress is acting. Straining of this brittle coal is only possible if cracks or fractures extend and relative displacement along the crack planes occurs. Crack initiation, crack propagation, and crack propagation velocities are controlled by the stress concentrations at the crack tips. Each loading cycle induces stress concentrations high enough to cause crack extension. In the case of fast cycling the time over which high stress concentrations are maintained is small, and the accumulated strain, proportional to the product of time and crack velocity, is also small. On the other hand, during repeated relaxation the product between time and crack velocity is larger since the stress drops slowly during relaxation as a

function of crack extension. This results in higher accumulated strains and therefore leads to failure in fewer load cycles.

If these stress concentrations diminish due to redistribution or other factors, strain accumulation decreases and the stable zone is entered. This happens during a relaxation test and as a consequence the stress at the end of a relaxation test is below the current long-term strength. Figure 3.35 shows a series of curves predicted by extrapolation which illustrate this point clearly. It was assumed that normalized deviatoric stress versus logarithm of time could be extrapolated linearly from Figure 3.31. During repeated relaxation tests the stress drop per unit time has to decrease in the stable zone and increase or be at least constant in the unstable Zone B.

(b) Zone B as a rate-dependent visco-plastic zone?

This sub-title is formulated as a question in anticipation of the conclusions drawn from the following discussion. Because of the novelty of the test procedure and the complexity of the test data presentation, it is more convenient to discuss the data in the light of the conclusions rather than in general terms. The diagrams with stress ratio on one axis and the normalized stress drop on the other (e.g. Figure 3.21) are used for this purpose. A general discussion and illustration of ideal materials has been given in section 3.3. Comparable stages of repeated relaxation tests are normally summarized on the same diagram

and the stress drop after half a day and one day are indicated by empty and full circles respectively. The dependence of Zone B on strain will be discussed later.

A comparison of the schematic diagram in Figure 3.11 and the Figures 3.21, 3.22 and 3.23 for sample CTR-2A or 3.35 and 3.36 for sample CTR-2F shows a remarkable similarity indicating that the coal behaves like a visco-plastic material when strained beyond a certain stress level D_{min} . Before each figure is examined individually and in detail it is necessary to consider certain factors which could affect the behaviour.

Measurements of stress level or stress drop are normalized to D_{max} , the current available strength, a parameter which has to be determined by interpolation. D_{max} is therefore relatively inaccurate, particularly if the stress-strain curve is discontinuous or strongly curved. Linear interpolation between known values was normally used. It is necessary to normalize these parameters for comparison to either the upper or lower boundary of the Zone B. The upper boundary was selected because of two reasons: (a) the upper boundary, the current available strength, can be determined quickly by fast straining and (b) one aim of this thesis is to define and find the lower boundary D_{min} , the current long-term strength. The advantage of this diagram is that for a visco-plastic material, the measured data at a constant time increment should fall on a straight line and the slope of this line should be 45° at a time interval

equal to infinity. Lines for constant time increments should intersect the abscissa at a stress ratio D_0/D_{\max} equal to D_{\min}/D_{\max} , at the current long-term strength ratio.

Inaccuracies in the determination of D_{\max} affect the magnitude of the stress ratio much more than the normalized stress drop. This means that points calculated with an overestimated D_{\max} are plotted too low or, if underestimated, too high. For example, an initial underestimation of D_{\max} would lead to curves shaped like the ones plotted on Figure 3.34 (but this is not the reason for the curvature in this figure). The major two reasons for underestimation of D_{\max} are (a) the difference between the static and dynamic friction and (b) the possibility of over-closure or interlocking. Both mechanisms lead to a local peak strength, an additional resistance above the current available strength. A different response would be expected for stress level increases approaching the visco-plastic zone than for stress level decreases approaching the current long-term strength from inside the visco-plastic zone. These mechanisms might explain the non-linear shape of stage 10 in sample CTR-2A (Figure 3.22), but in general no clear evidence can be found in the data to support this process. D_{\max} could have been overestimated if the stress-strain curve was strongly non-linear or discontinuous.

Depending on the stress history, the observed relaxation is a combination of relaxation due to the

visco-elastic and the visco-plastic element. The effects of this factor were illustrated in Figure 3.11 for ideal materials. Only if the time-dependent deformation from the stable portion has terminated, as in the case of incremental loading with extensive repeated relaxation tests, can the pure visco-plastic behaviour be observed. Particularly close to the current long-term strength decreasing stress drops are often observed due to the superposition of visco-elastic and visco-plastic rock properties. As long as the stress drop per unit time decreases, the current long-term strength is either higher than the stress level or the terminating deformation has not yet stopped. In the first case, the abscissa will be reached eventually and in the second case, a constant stress drop value will be approached from the right side (see stages 11, 19 and in Figure 3.23). The terminating portion is small and can be neglected after a few stages of repeated relaxation within the visco-plastic zone.

Machine relaxation is another factor which could affect data. It was not possible to correct the data for the machine related stress drop as discussed earlier, but it can be assumed to be constant for each relaxation during testing within the visco-plastic zone. The stress level and the amount of straining between increments is more or less constant and all data points would therefore be shifted to the left by a constant amount.

During repeated relaxation tests, strain accumulation

results in a decrease in D_{\max} . If it is assumed that D_0 is kept constant and repeated relaxations are conducted to failure, D_{\max} decreases continuously and lines of constant stress drop are crossed. Transformed into the stress ratio versus normalized stress drop diagram this means that the curves for constant relaxation time increments should theoretically (visco-plastic material) be linear and intersect the abscissa at the long-term strength ratio D_{\min}/D_{\max} . Such test data are given in Figure 3.34 for stage four in Test CTR-2F. Possible reasons for the non-linearity were discussed earlier. It was possible to illustrate the linearity of such curves when the straining was kept low and D_{\max} was reduced by lowering the confining pressure (e.g. Figures 3.35 and 3.36).

The width of Zone B should decrease with increasing strain and eventually disappear. As a result D_{\min} would approach D_{\max} and data would be displaced parallel to a 45°-line towards the upper left corner of the stress ratio versus normalized stress drop diagram. This trend can be observed by comparison of Figures 3.35 and 3.36 where an estimated D_{\min} decreases from about 7% to 5% D_{\max} . These data were observed relatively close to the peak strength where a relatively rapid decrease in strength and extent of Zone B would be expected. A similar trend can be observed in Figure 3.23 but it is not consistent, possibly because of other more dominating factors. These data were collected in Zone B where almost no strength loss occurred. The

estimation of D_{\max} was difficult due to local D_{\max} increases and the change in zone width would be expected to be small except if strained extensively.

Zone B can be crossed by single relaxation, by repeated relaxation from a constant stress level, or by reduction in confining pressure. This latter path was studied at two locations in Zone B.

(c) Effects of confining pressure changes:

1. Stage 10, sample CTR-2A: the sample was unloaded after stage 9 and partially reloaded (Figure 3.14). The confining pressure was decreased in steps and repeated relaxation tests were started as soon as a stress drop was measured. The data is summarized in Figure 3.23.
2. Stages 8 and 9, sample CTR-2F: a series of normal repeated relaxation tests at stage 8 was followed by an instant confining pressure increase of 10% and a stepwise decrease to the original pressure. The data is shown in Figure 3.35. After the confining pressure was increased by 20% the sample was loaded into Zone B and repeated relaxations at 119% and 118% confining pressure lead to failure. The data, during stepwise relaxation to the original confining pressure, is summarized in Figure 3.36.

With this background information it is now possible to discuss each Figure, compare them and illustrate that Zone B can be considered as a visco-plastic zone.

Sample CTR-2A:

Repeated relaxation tests at three stages cross Zone B during strain accumulation. Figure 3.21 shows three almost identical curves. Stage 7 was initially below the reloading peak and decreasing relaxation resulted in points converging towards the lines indicating visco-plastic behaviour. Similarity with ideal visco-plastic materials is obvious. A D_{min} of less than $0.92 D_{max}$ was estimated by drawing a line through the data with a slope greater than 45° (since the relaxation is measured after one day). The extent of Zone B seems constant over the limited strain range.

Figure 3.22 contains data from confining pressure reduction tests at stage 10. No relaxation was observed up to $0.92 D_{max}$ giving a lower bound for the current long-term strength. The two points in brackets are data points from a single relaxation test. The non-linearity, mainly the small stress drop at 0.64 and 0.63% of the original confining pressure, can most likely be attributed to the phenomenon of over-closure. The sample did not relax significantly until the additional resistance due to interlock or increased adhesion was overcome. This argument is supported by the data in Figure 3.35. Over-closure could not occur during this test because of the opposite stress path. The confining pressure was increased until relaxation vanished. It was also observed that a higher percentage of the total one-day stress drop occurred during the first twelve hours at the highest two stress levels (0.62 and 0.61% of the original confining pressure). This indicates that these points are

closer to the current long-term strength, after one day of relaxation, than the others after the same time. D_{min} estimated from this figure is $0.92 D_{max}$, slightly higher than estimated from Figure 3.21. No conclusions should be drawn from this fact since stages 8 and 9 were started from stress levels significantly higher than the current long-term strength which had to be determined by extrapolation.

Figure 3.23 contains a large number of stages from a zone with almost constant strength. Reloading was necessary after stage 19 because of an accidental loss of confining pressure. Corresponding stages 11 and 12, and 19 and 20 show decreasing relaxation and converge towards the abscissa (stages 11 and 19) or towards a finite stress drop (stages 12 and 20). The current long-term strength has to lay in between these two stress levels. All other stages show a more or less constant stress drop per unit time. In the first section (stages 13 to 18), the first three stages 13, 14 and 15 fall on a line intersecting the abscissa at about $D_{min} = 0.915 D_{max}$ and stages 16, 17 and 18 fall on a line intersecting at approximately $0.93 D_{max}$. In the second section (stages 20 and 21 to 24) all stages fall on a line intersecting at about $0.91 D_{max}$. The estimated current long-term strength is $0.92 \pm 0.01\% D_{max}$. Even though the data are scattered over a wide range this figure supports the working hypothesis of the existence of a visco-plastic zone. This scatter can be explained by the factors discussed

earlier.

Sample CTR-2F:

Figure 3.34 summarizes data from comparable stages. Figure 3.30 gives the loading history. All stages were started after the stress level was lowered and in an area where a significant non-linear strength drop has to be assumed. It was difficult to estimate D_{max} and the calculated stress ratios are somewhat questionable. Failure during stage 4 occurred due to strain-weakening. The non-linearity in Figure 3.34 can be explained by the curvature of the current long-term strength curve. If repeated relaxation is undertaken through the peak strength, the current long-term strength starts to drop gradually and levels off after a maximum post-peak slope is passed. If relaxation tests are started from a constant stress level the stress drop will increase according to the stress difference to the current long-term strength and result in a non-linear curve. Test at stages 5 to 7 were undertaken within a transition zone. At stage 8, where the current long-term strength shows less curvature, this non-linear behaviour disappears gradually.

The first 12 relaxations of stage 8 are included in both Figures 3.34 and 3.35. After a series of repeated relaxation tests, the confining pressure was changed as indicated in Figure 3.35. Figure 3.31 shows the normalized deviatoric stress versus logarithm of time of the individual relaxation curves. An almost perfect linear relationship is

observed which supports the assumption of a visco-plastic zone. The deviatoric stress versus logarithm of time curves were used to predict (by linear extrapolation) the relaxation after 100, 1000, and 10,000 hours. These predicted curves are included in Figure 3.35. The non-linear shape supports first of all the earlier statement that relaxation close to the current long-term strength will terminate at the current long-term strength and that relaxation from high stress levels can cause stress drops below the current long-term strength. These predicted curves show, corresponding to the assumed linearity, continuous relaxation and contradict the assumption of a long-term strength. Nevertheless, the definite trend towards zero relaxation near a long-term strength ratio of 0.93 strongly supports the assumption of a current long-term strength. Some indication of termination of relaxation can although be detected in Figure 3.31.

Figure 3.36 again confirms the existence of a visco-plastic zone and it can be seen, by comparison with Figure 3.35, that the extent of this zone decreases with increasing strain. The extent of Zone B dropped from about 7 to 5% of D_{max} .

3.5.2.3 Behavior in the Transition Zone C

The transition from terminating creep at low stress levels to the visco-plastic behaviour in the strain - weakening range is best discussed by reference to the

idealization in Figure 3.37. Above the long-term peak strength, the strain will accumulate until the limit a-a is reached at which the available resistance begins to change. It is understood that these limits may not be as abrupt as indicated. In Zone B, the visco-plastic behaviour discussed previously dominates beyond the limit b-b. For brittle materials the limits a-a and b-b coincide. Zone C is a transition whose extent depends upon the ductility of the rock. The behaviour in this zone is a function of the available strength. If this strength is constant for a certain strain increment, the stress drop per unit time in a repeated relaxation test will also be constant. If creep tests were performed at the stress level of this stage, decelerating creep would be observed at the outset with a transition into steady-state creep. In most rocks the available strength is not constant and a steady-state creep stage does not exist. The stress drop per unit time during repeated relaxation tests changes discontinuously if the rock strength decreases in a discontinuous manner. This type of deterioration is illustrated by the limit c-c in Figure 3.37. A creep test would display a transition into tertiary creep at this limit. The details of the behaviour during the transition from zone A to zone B will be governed by the development of the microstructure formed by crack propagation. The behaviour in the transition Zone C observed in the tests is illustrated in Figures 3.18, 3.28 and 3.33. These figures show normalized stress drop versus deviatoric

stress in part (a) and versus inelastic strain e^* in part (b). Curve 6 in Figure 3.18 and curve 3 in Figure 3.33 display brittle behaviour with only a small inelastic strain increment δe^* of less than 0.05% separating diminishing relaxation per unit time from large increases in the normalized stress drop. Hence the transition Zone C is narrow. Curves 7 to 11 in Figure 3.28 represent the more ductile failure - at peak strength of sample CTR-2D. The extent of the transition Zone C is about 0.4% e^* and the discontinuous nature of the failure process is exhibited by the sudden increase in stress drop per unit time found during stage 9, Figure 3.28, and similarly during stage 6, Figure 3.18. In the more ductile transition zone of sample CTR-2D, almost constant relaxation corresponding to secondary creep was observed at stage 8 (Figure 3.28) and at stage 9 and 10 after a discontinuous strength loss. This sample would have entered the tertiary creep stage after approximately 0.3% inelastic strain and would have failed in a creep test because of the soft loading system. During repeated relaxation tests the sample does not fail. A new rate of relaxation corresponding to the available strength will be established after the strength loss and failure occurs only if the current available strength drops below the stress level D_0 .

Similar behaviour is found during a reloading cycle of the same sample after straining beyond the peak strength (see Figures 3.19, 3.29 and 3.33 (stage 4)). The behaviour

in these areas is normally more ductile and the transition zone is often continuous without instant strength losses. As indicated in Figure 3.29, a decrease in stress level causes a reduced relaxation or correspondingly a reduced strain rate. This fact in combination with all other observations resulted in the schematic stress-strain diagram (Figure 3.37). Lines of constant strain rate or lines of constant stress drop per unit time are indicated.

The data of stage 10, sample CTR-2A, are presented in Figure 3.20. The stepwise decrease in confining pressure causes a translation of the lines of constant relaxation and less strain is needed to reach failure. This results in a contraction of the strain axis and a stepwise curve with increasing, but almost constant, relaxation per confinement level.

With this information and an understanding of the behaviour in Zone A, C, and B near ultimate strength, it is easy to connect Zone C and B and understand the behaviour in the strain-weakening portion of the visco-plastic Zone B. The two boundaries, current long-term strength and the current available strength as well as the lines of constant relaxation or creep rate are sloped and curved. To maintain a constant rate of deformation, the stress level has to be lowered continuously. Terminating deformation can be expected if the stress drops faster and below the current long-term strength curve. Failure occurs if the stress decreases slower and the current available strength is

reached. The Zone C is a special case of Zone B.

3.6 Conclusions

Multiple-stage repeated relaxation tests constitute an effective test procedure for investigating the time-dependent behaviour of natural, intact or discontinuous rocks. The test procedure is too time-consuming for commercial use but this could eventually be improved by a reduction of the time intervals. Interpretation has to be improved by further research. Data from several tests on fractured coal have been reported in detail and it is seen that such tests can be conducted over the full range of behaviour, prior to peak strength, through the strain-weakening zone, and close to the ultimate resistance. From these tests a consistent pattern of time-dependent behaviour has been identified. In particular, decreasing stress drops, which are associated with decreasing creep, characterize the time-dependent response if the long-term strength curve is approached, at which creep terminates, or if the transition zone is approached where the strength of the rock begins to deteriorate. At these stress levels, above the peak long-term strength, the time-dependent behaviour depends upon the extent of the transition zone which in turn is a function of the microstructural weakening process. Within the strain-weakening zone and towards the ultimate resistance, the time-dependent behaviour is dominated by the rate-dependent available shearing

resistance or visco-plasticity. This implies that there is a possible stress-strain path along which the rock deforms at a constant strain rate, or, in terms of repeated relaxation tests, shows a constant stress drop per unit time. This does not imply that a constant strain rate test would follow this line. The available shearing resistance declines to the ultimate with increasing irrecoverable strain. The distinction between the various processes governing the time-dependent behaviour of rock is important and comprehensive experimental programs will be needed to characterize them in more detail.

The conclusions from this chapter are summarized and implemented in a schematic stress-strain diagram in Figure 3.37 and the most important conclusions are summarized and described below. The schematic stress-strain diagram, and therefore the conclusions, are based on the assumption of the existence of a stable zone with terminating time-dependent deformation. A phenomenological model for rock will be developed on the bases of the following conclusions in Chapter 4.

1. A current long-term strength exists below which time-dependent deformation terminates. This conclusion should not be extrapolated to far beyond a time interval comparable to the test duration;
2. A current available strength exists as an upper strength limit which constitutes the locus of strength for instant loading;

3. Both limits are stress-history-dependent, are functions of the current structure and circumscribe a time-dependent failure zone. They define the limits of a rate-dependent failure envelope. Any rock strained under any stress-history will yield between these current limits and a change in rate will cause a shift towards either limit. At a given strain the extent and magnitude of the time-dependent range is history-dependent.
4. This time-dependent zone can be split into two sections: Zone A where any stress path causes intersection of lines of constant strain rate, or constant stress drop per unit time, in descending order, and Zones B and C where lines of constant strain rate, or constant stress drop per unit time, are intersected in descending or ascending order or followed depending on the stress path. In Zone C the current available strength may increase, remain constant or decrease discontinuously whereas it decreases continuously in Zone B;
5. The data reported allows one to separate these zones and to describe the time-dependent behaviour within each one. Within Zones B and C, the stress-history-dependent rock structure development (fracture process) has been tested. In this research program only one rock structure development with shear failure along a originally discontinuous joint under low confining pressure was investigated. It is believed that the process studied is representative of a rock mass under similar confinement

conditions;

6. The relationship between stress drop and logarithm of time is linear;

For Zone A:

7. Finite yielding can be observed;
8. The time-dependent response at a given point (e.g. stress drop per unit time) could be predicted by linear superposition. It was found (Hungry(1977)) that the relaxation behaviour at low stress levels was proportional to the inelastic strain remaining between the current state and the long-term stress-strain curve. This is consistent with the behaviour found in the model tests where almost identical curves (with constant slope and intercept) were found for subsequent creep stages, when logarithm of strain rate was plotted versus logarithm of time;
9. The stress drop per unit time during multiple-stage repeated relaxation tests did not terminate in zone A above the long-term peak strength. An almost steady state was reached or acceleration led to failure. This observation allows the determination of the long-term peak strength by increasing or decreasing stress levels;

For Zones B and C:

10. Above the current long-term strength a strain-dependent visco-plastic zone exists within which the time-dependent deformation behaviour associated with rock structure changes can be related to the stress

difference between stress level and current available strength or current long-term strength;

11. A transition Zone C exists where the available strength increase is reduced, becomes zero, and a discontinuous loss in current available strength occurs. This partial strength loss causes acceleration of relaxation or creep but may not lead to failure immediately. This zone is encountered whenever the unstable zone is entered (e.g. reloading) and its extent depends on the ductility and total accumulated strain;

12. Near peak strength, lines of constant strain rate or constant stress drop per unit time are convex. They change gradually to concave curves near the ultimate strength. These lines will be crossed during a particular stress path leading to failure or stable conditions. During a creep test these lines are crossed at a large angle near peak and a small angle near ultimate strength. As a result, rapid acceleration leads to failure after little strain near peak strength and slow acceleration causes collapse after extensive straining near ultimate strength. The time to failure is a function of the slope of these lines relative to the applied stress path as well as the extent of the visco-plastic zone. As in any visco-plastic material the yield strain accumulated is a function of the stress increment applied beyond the yield stress and the time this stress is acting;

13. The behaviour in the visco-plastic zone and the extent of this zone are sensitive to such processes as over-closure or interlocking, local and global stress alteration allowing instant structure changes and any other factor which causes similar effects (e.g. weathering).

Several implications follow from these conclusions:

1. 'If rock is deformed plastically beyond its peak strength under a given stress-history, it will follow a curve between the current available strength and the current long-term strength. Further, if the system is statically determined (no stress change results from deformation) this rock cannot fail without acceleration in deformation rate and before the time-dependent zone vanishes. The deformation in a creeping, unconfined slope must accelerate before collapse and deform sufficiently to reduce the extent of the visco-plastic zone.
2. A rock element stressed to a stress level inside the visco-plastic zone deforms in a stable or unstable manner depending on the ratio between stress change and enforced strain change. If rock is unloaded by stress transfer to stiffer zones, the current long-term strength is approached and deformation terminates. On the contrary, if a yielding element is loaded or the stress reduction is not sufficient, the current available strength will be approached, the deformation

rate increases and the element will eventually fail. This process is affected by the development of the confining pressure. Confined slopes, rock pillars and tunnel faces are three of the most important examples where this process can be observed. In a confined slope, originally overstressed zones deform with time but will be unloaded gradually due to stress transfer to the confining boundaries. Similar processes may go on in unconfined slopes where deformations are mobilized in a non-homogeneous manner; i.e., arching within the slope mass. In a pillar, original loading causes stress concentrations near the pillar walls which cause yielding of elements with low confinement. This strength loss causes a stress transfer to the center of the pillar. This process of unloading near the walls and loading at the centre is a function of time. Depending on the total load on the pillar (which may also be a function of time) and the ratio between load and overall strength of the pillar, this process may lead with time to a stable, but almost continuously deforming, or unstable pillar. At the tunnel face, or in general at the mining face, the stresses increase during excavation according to the advance rate and drop in between face advances due to stress redistribution. This loading history may cause an element to be stressed into the visco-plastic zone and subsequently to be unloaded causing stabilisation, constant rate of deformation, or

failure. During continued advance the stress range during each cycle will decrease but the stress level and the accumulated strain will increase. Due to the convex shape of the lines of constant deformation rate near peak this process may be more catastrophic near peak strength due to the fact that the same stiffness relationships may lead to failure near peak strength and stable conditions near ultimate strength. These processes are discussed in more detail in Chapter 1 and supported by Cogan(1978) .

3. The existence of a transition zone with strength plateaux indicates that an instant but partial loss of current available strength does not lead to immediate collapse. A stress reduction may lead to a stable condition.

The fact that the transition zone becomes more ductile with increased straining combined with the assumption (Mueller and Goetz(1973)) that a rockmass behaves as reloaded, fractured rock, lead to the view that tectonically deformed and largely overstressed zones behave in a visco-plastic manner with less pronounced strain-weakening.

4. The fact that the post-failure behaviour is stress-history dependent has implications for both, the model test and tunneling in real rock masses. The development of a plastic zone will be rate-dependent and both the time-independent and time-dependent

deformations will be affected by the stress-history. For the model this means that measured deformations cannot be directly compared with reality since the loading path is different, and for an actual tunnel this implies that the excavation history affects the development and extent of the plastic zone. Consideration of the final (limit equilibrium) state only may lead to misleading results.

5. Since the visco-plastic zone is sensitive to stress changes and other factors affecting rock structure, the following parameters have an influence on the time-dependent failure process: vibrations due to blasting, drilling and construction traffic as well as earthquakes; weathering of rock and rock joints; and effects of water flow, e.g. outwash of infilling.
6. Numerical methods for visco-plastic materials (Zienkiewicz et al.(1975)) can be used to consider the time-dependent failure process in the post-peak range if connected with strain-weakening material properties.

CHAPTER 4

PHENOMENOLOGICAL MODEL FOR ROCK WITH TIME-DEPENDENT STRENGTH

4.1 Introduction

In this chapter the principles established in the preceding chapters are used to develop a phenomenological model which describes the time-dependent failure of rock and rock masses. Such a model will be useful in three ways: it will help to characterize the time-dependent failure process through interpretation of existing data; it will help to direct future research programs as well as assist in the development of numerical models; and, if expanded to rock masses, it will allow the prediction and interpretation of rock mass behaviour under various conditions. The purpose of this chapter is to develop the model in general terms, to prove its validity by a qualitative discussion of data available in the literature, and to suggest a possible way to transform the phenomenological model into a mathematical model. This last point is formulated as a recommendation for future research.

From the results of multiple-stage repeated relaxation tests on jointed coal it was concluded that the response of rock at a given stress and strain state depends entirely on the current rock structure. Therefore the behaviour during any particular stress-history depends on the development of the rock structure during deformation. This has led to the conclusion that the rock behaviour is a function of the

current available strength. This point illustrated in the schematic stress-strain diagram in Figure 3.37 and will be clarified further by the proposed phenomenological model.

Time-dependent rock properties are in general evaluated by one of the following three approaches:

1. Empirical fitting of exponential or power laws to experimental data: this approach is based on interpolation and any extrapolation from such laws is hazardous (Price(1969) especially where the deformation mode changes. It is most justified where creep terminates but any extrapolation into the near failure range (e.g. prediction of time and strain to failure) is difficult since it has to be based on assumptions about the rock structure change, a process which is not completely understood at the present time.
2. Mechanical or mathematical models or analogues: this approach allows one to describe all stages of time-dependent deformation up to failure but does not explain the mechanisms of rock deformation, even though it may be related closely to the physical processes. In reality, the models might be composed of complex elements whose parameters are difficult to determine. Simplifications, necessary to overcome this difficulty, may again lead to unrealistic predictions. Many models are only applicable for restricted zones, e.g. the Burgers model for coal is valid only for the pre-failure stage and limited time intervals.

3. Theories of physical processes or statistical mechanics: many theories were developed for different rock types, e.g. dislocation theories for crystalline rocks, and crack propagation theories for brittle rock (e.g. Bieniawski(1967)). It is believed that processes such as time-dependent crack initiation, crack propagation and, in general, stress- and time-dependent structure changes result in creep with time and time-dependent strength of brittle rocks. No attempt was made to elucidate these physical processes here. Nevertheless, the proposed model will reflect to some extent the process of time-dependent crack propagation. During loading of rock a non-uniform true stress field is created and certain areas (e.g. grain contacts or crack tips) are highly stressed and will relax due to strength loss or stiffness changes with time.

The physics of the failure process has been thoroughly investigated by many authors. However, the application of the knowledge gained has been slow, partially because of the fact that there is no model available to describe the observed behaviour during time-dependent failure of rock. If the initial state of the rock and the change in boundary conditions can be described, a model would be most useful to evaluate the controlling parameters, their dependence and significance. It would be possible to make predictions from information gained during the early stages after boundary conditions are changed and apply them to later stages in the

deformation history.

4.2 Required Properties of Model

The data presented in the preceding chapter and results from rock testing in general reveal the following major facts:

1. Rock deforms elastically over a limited stress range;
2. Rock deforms with time even below the yield limit, but deformations terminate below the yield point;
3. The yield limit is rate-dependent, but in general there is a minimum long-term yield point;
4. The yield limit is strain-dependent;
5. The strength limit is rate- or history-dependent; the range between both the upper and lower limit is variable in extent;
6. The resistance of rock is composed of frictional and cohesive (or intrinsic) strength.

Any model should possess these properties, be applicable to intact rock and rock masses at low or high confining pressure and at any accumulated strain. It follows that a model which can satisfy these requirements will consist of at least three types of elements:

1. Elastic elements (E);
2. Time-independent yield elements (Y);
3. Time-dependent yield elements (T) with loading rate-dependent strength.

4.3 Proposed Model and its Element Properties

Figure 4.1a shows a schematic diagram of the proposed phenomenological model. It consists of a block of two types of parallel units; (m) A-units with time-independent properties only, and (n-m) B-units with both time-dependent and time-independent properties. The individual elements are described below in general terms and illustrated by simple mechanical elements possessing the corresponding properties. Non-linearity can be achieved by superposition of linear units in parallel or by using elements with non-linear properties.

1. Elastic elements $E(A_i)$ or $E(B_i)$: a linear or non-linear elastic element.

Mechanical model: Spring with stiffness $E=f(\xi)$. The stiffness of these elements may vary from unit to unit and is best described by a stiffness distribution function. This is called a parameter distribution function and assigns a specific value to each unit.

The E-elements may be extended to include limited, partially irreversible or reversible yield elements to model crack or joint closure.

2. Time elements $T(B_i)$: an element which transmits load to the yield elements as a function of loading rate; zero load at an infinitesimal loading rate and maximum load for instantaneous loading.

Mechanical model: dash pot.

Termination of strain under a constant stress below the

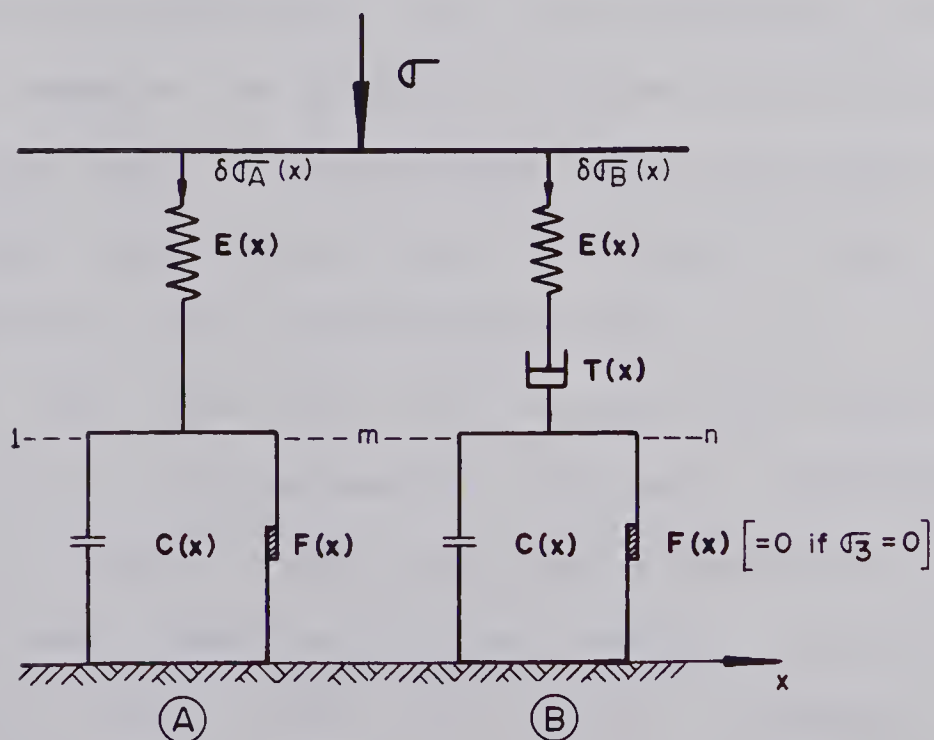
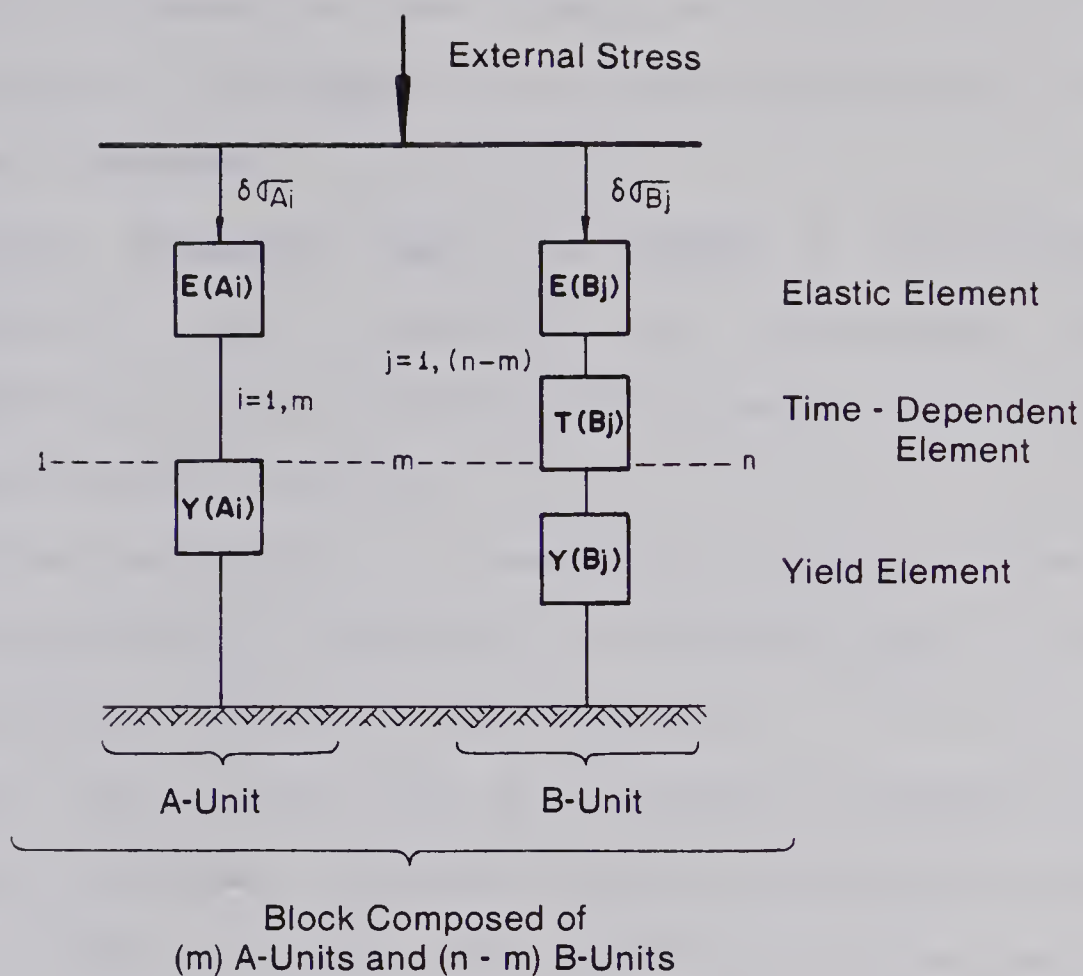


Figure 4.1 a) Schematic Diagram of Model
b) Simple Version of Model with Mechanical Elements

yield stress of the block of units is achieved by parallel arrangement of A- and B-units due to internal load transfer.

3. Yield elements $Y(A_i)$ or $Y(B_j)$: a time-independent element with cohesive and frictional strength components. Both resistances are described by a strength distribution function.

Mechanical model: a cracking element C, with brittle stress-strain behaviour, in parallel with a plastic or frictional element F (St. Venant).

The yield strain may be partially recoverable to model the hysteresis observed during unloading and reloading of rock. A spring in parallel with the cracking and frictional element would have to be included in the mechanical model.

The behaviour of natural rock can be modelled by a number of A- and B-units in parallel. If the relevant parameters of each unit can be determined this model will predict the short-term and long-term strength, the accumulated deformations, the deformation rate after a certain load history, and the time to failure. The simplest possible model, with the mechanical elements described above, is shown in Figure 4.1b and the stress-strain curves for instant and infinitely slow loading (labeled "fast" and "slow") of this model are given in Figure 4.2. In this figure the internal stress, the stress carried by individual units, is plotted against strain in the upper diagram (a)

and the external stress, which is the sum of the internal stresses of all units, is plotted against strain in diagram (b). This model is assumed to consist of one elastic, brittle, time-independent A-unit, which exhibits an instant strength loss at ϵ_{Af} of magnitude C_A and a constant ultimate strength F_A , and one time-dependent B-unit. Two cases of B-units are shown: The first case where unit B fails before unit A is labeled B1 and the second case where the unit B fails after unit A is labeled B2. Both B-units show an instant strength loss C_B and possess a constant ultimate strength F_B .

Three loading histories (I to III) are superimposed in Figure 4.2 and described in the legend. The following observations are of interest:

1. Only the unit A carries load if the loading rate is infinitesimal (I);
2. The failure strain, where the first inelastic deformation occurs or the peak strength is reached, depends on the loading rate and the properties of the time-dependent B-units. In loading history II failure occurs at a lower strain but higher stress than in loading history III and a block composed of A + B1-units fails before a block composed of A + B2-units.

By increasing the number of units and by selecting a proper parameter distribution function for the elements E , T , C and F almost any stress-strain-time relationship can be modelled. This simplified model indicates that the

resistance of the B-units is only lost during stressing at a finite loading rate whose lower limit is controlled by the properties of the T-element. This does not correspond in general to observed rock behaviour and a different T-element might be necessary to model natural rock. This point will be ignored during the following discussion but it could be included by gradually changing the properties of the element YB, as a function of the total accumulated strain, to maintain the model's validity over a large range of strain. Because of the arrangement of both the frictional and cracking elements in series with the time element T, it is assumed that a portion of the frictional resistance is time-dependent. This point has to be proved by testing and the frictional element FB might have to be eliminated.

Hudson and Brown(1973) describe the shape of the stress-strain curve of brittle rocks on the bases of crack propagation as follows:

"The shape of the complete stress-strain curve will depend on the variability of the microstructure. If the rock is composed of a uniform structure of elements that have the same elastic-brittle characteristic, the test specimen will behave elastically until all the elements fail simultaneously and the load-bearing capacity of the specimen drops instantly to zero. Conversely, if the rock is composed of different elements in a random structure and with extreme strength variations, the test specimen will fail very gradually as the displacement is progressively increased. It is this principle of progressive destruction that produces the basic shape of the complete stress strain curve."

This description fits the proposed model especially if it is added that some elements (called units in this model) may fail as a function of time due to a time-dependent load

transfer from softening to stiff elements. Various physical processes are the reason for this weakening of elements with time.

Hudson and Brown's description can be expanded to describe the behaviour of rock masses if the microstructure is replaced by the macrostructure and the sample size is increased accordingly. Other physical processes may be the cause for the material behaviour but the rock mass response is comparable and can be described by the proposed model.

Kovari(1977) has developed a model which he called a "micromechanics model of progressive failure in rock" for rock with time-independent properties. A comparison of this model with the proposed model for time-dependent rock shows that they are identical for the case of instant loading. Kovari's model is a special case of the proposed model if the T-element is assumed to be infinitely stiff or the B-units are eliminated. Because of this similarity and the description given by Kovari, the following discussion concentrates on the time-dependent properties of the model. An explanation of the effects of confining pressure and parameter distribution functions on the shape of the stress-strain curves is not repeated. The same terminology, as far as applicable, is used to simplify comparison.

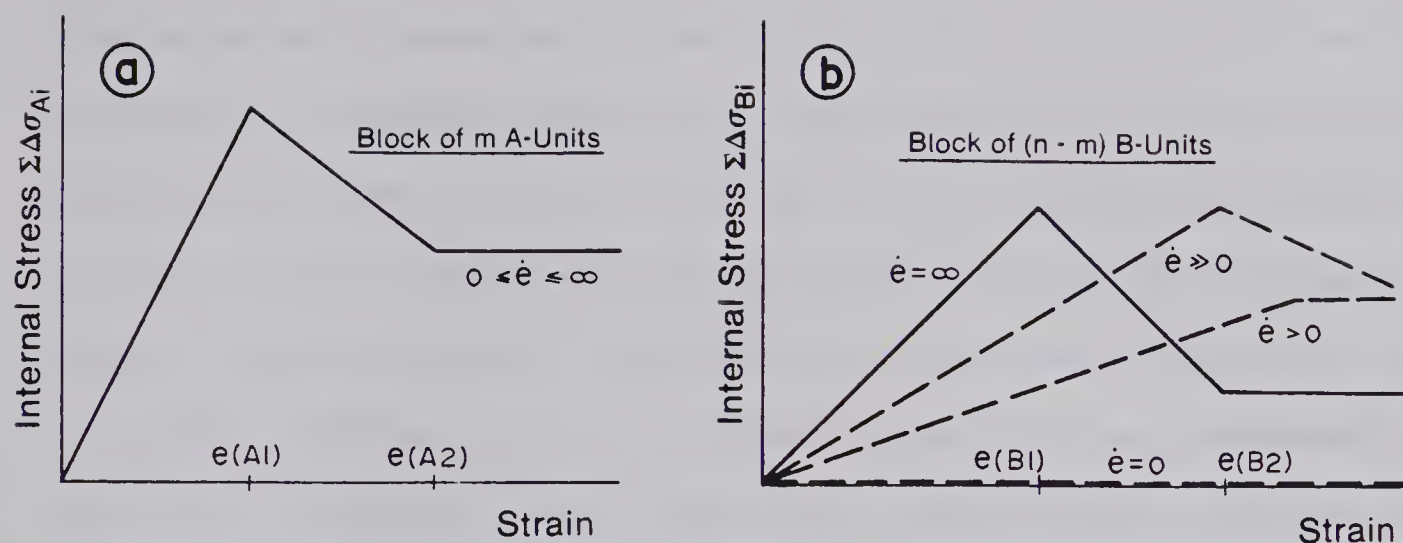
Many rheological models have been developed for various rock types to describe the response of a material within a specific stress or strain range. These models were often created to fit test data up to failure. Yield elements have

been included and assumed to have a constant time - independent strength and could not be overstressed (e.g. Cohen(1978)). In other models (e.g. complex Bingham model (Price(1969) or Broadbent and Ko(1972)) the yield elements are time-dependent, due to a viscous element in series after the yield element, but exhibit an unrealistic infinite strength for instantaneous loading. Even the model suggested by Pushkarev and Afanasev (1973) simulates in principle a visco-elastic, visco-plastic material only. The proposed model overcomes these limitations. It is applicable to various rock types, for the pre-failure and post-failure range, and it is valid after the rock is overstressed as long as the same stress history is applied to the model as experienced by the rock.

4.4 Comparison of Model with Published Test Data

4.4.1 Special Case of Model

In this section the general model composed of one block of A-units and another block of B-units will be tested on data reported from single- and multiple-stage creep tests, single- and multiple-stage relaxation tests, and constant and variable strain rate tests. As a special case it will be assumed that the number of units and their parameter distribution functions are selected such that both blocks of units show a linear strain-weakening behaviour as indicated in Figure 4.3(a and b). If the model is loaded infinitely slowly the B-units will not carry any load and the



Assumed stress-strain curve for m Type A and $(n - m)$ Type B Units in parallel:

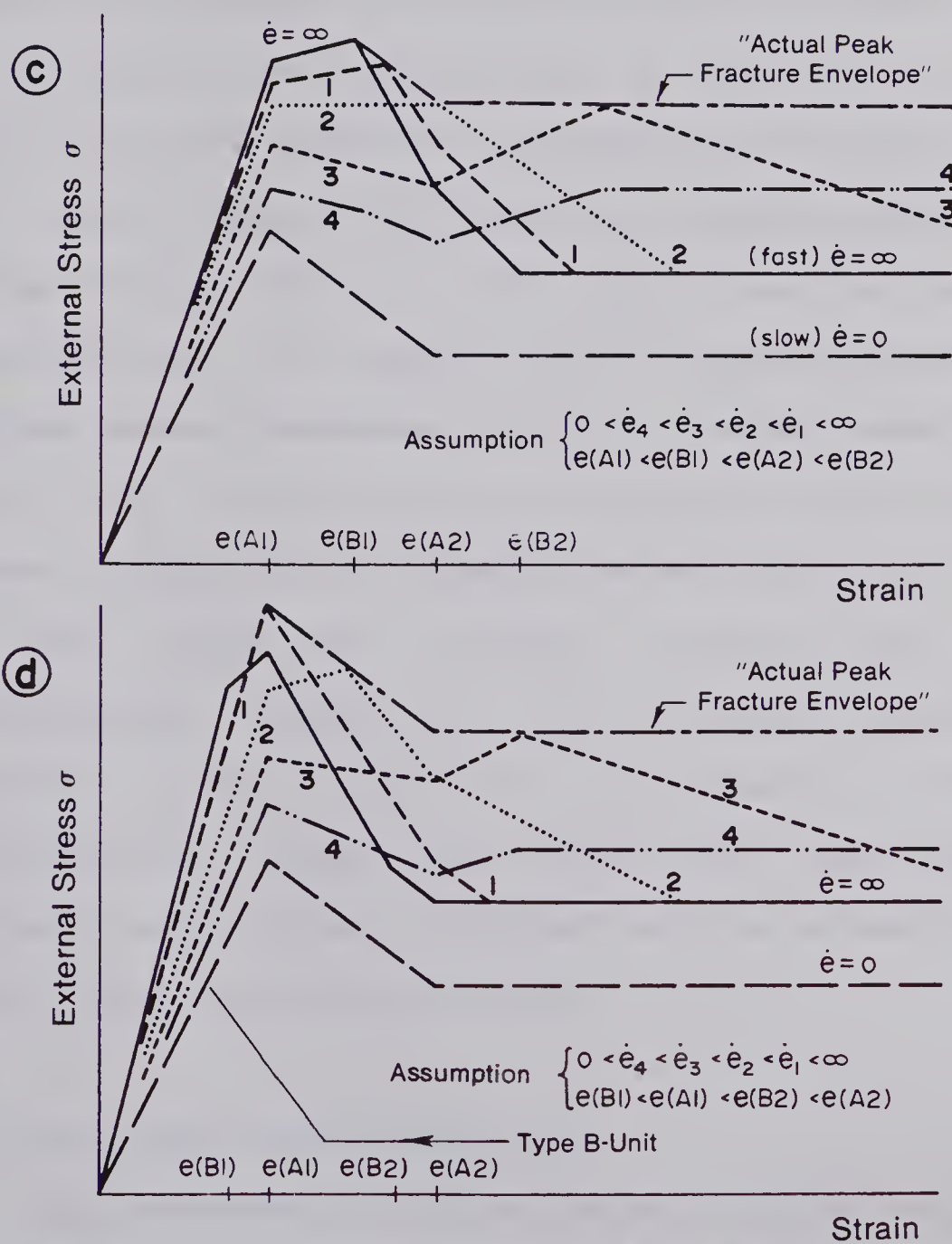


Figure 4.3 Special Case of Phenomenological Model

stress-strain curve in Figure 4.3.c will be identical to the one given in Figure 4.3.a. On the other hand, at an infinite loading rate the two types of units will carry their maximum loads and the resulting stress-strain curve can be found by direct superposition of Figure 4.3.a and the curve for infinite strain rate in Figure 4.3.b. At an intermediate rate the B-units may reach the same peak strength and residual strength but at larger strains as indicated in Figure 4.3.b. They will always exhibit a lower stiffness as a function of the loading rate. If this rate is too slow to reach the peak strength of the block of B-units, this block will show plastic yielding at a reduced stress level. The stress-strain curve of the model can be determined by superposition. In Figure 4.3.c superpositions for four loading rates (numbered 1 to 4) are shown together with the curves for instantaneous and infinitely slow loading. This figure is based on the assumption that yielding occurs first in the block of A-units. Figure 4.3.d gives the corresponding curves for the opposite assumption that yielding occurs first in the block of B-units. All stress-strain curves fall within an area limited by the "actual peak fracture envelope" and the stress-strain curve of the time-independent units.

4.4.2 Constant Strain Rate Test

The stress-strain behaviour of the simplified model was illustrated in Figures 4.3 (c and d). The particular shape

of the intermediate strain-rate tests depends on the properties of the T-element and the relative strength of the A- and B-units. Because of the selected stress-strain curve, composed of linear segments for both types of units, the resultant stress-strain curve is composed of linear segments. The stress-strain curve would show continuous curvature if continuous parameter distribution functions had been selected. For decreasing loading rates the model predicts (Figure 4.3.c) several phenomena:

1. Decreasing peak strength;
2. Increasing ductility with decreasing post-failure slope of the stress-strain curve;
3. A rate-dependent ultimate strength which may be higher than the ultimate strength for fast loading or at least higher than the ultimate strength for infinitely slow loading;
4. All stress-strain curves lie within an "actual peak fracture envelope";

and (from Figure 4.3.d):

5. The instantaneous loading curve may not touch the "actual peak fracture envelope". The peak strength determined from a intermediate loading rate may be slightly higher than for infinitely fast loading.

The "actual peak fracture envelope" can be determined if it is assumed that the time-dependent units are loaded to their peak strength and remain at that stress level during further straining without losing strength. Figure 4.4.a shows a copy

of data from uniaxial compression tests conducted on a sandstone with various constant strain rates (Bieniawski, 1970). The similarity to the predicted curves in Figure 4.3.c is obvious. A very similar trend was found by Ruesch (1960) from tests on concrete (Figure 4.4.b). From his test data it can be seen that the peak strength was almost constant. This would indicate that the block of A-units was composed of frictional elements only and did not possess any or only very little cohesive resistance.

Another typical response of rock to various constant loading rates is illustrated in Figure 4.4.c. These data, from uniaxial compression tests on tuff by Peng and Podnieks (1972), are similar to results from tests on other rock types reported by many authors (e.g. Wawersik (1973) and Peng (1973) on marble and sandstone). To predict this type of behaviour the model must be modified slightly to reproduce the rate-independent stiffness up to a certain stress level (22 MPa in Figure 4.4.c). This can be achieved if it is assumed that the time-dependent B-units are only activated after the A-units have been strained to their peak strength or by introducing a second yield element in parallel with the time-dependent element. The B-units would have to be visco-plastic units with or without strain-weakening. The behaviour of these units and the predicted response of the corresponding model is shown in Figure 4.5. To model the data presented in Figure 4.4.c beyond a total strain of 0.45% the B-units would have to be assumed as

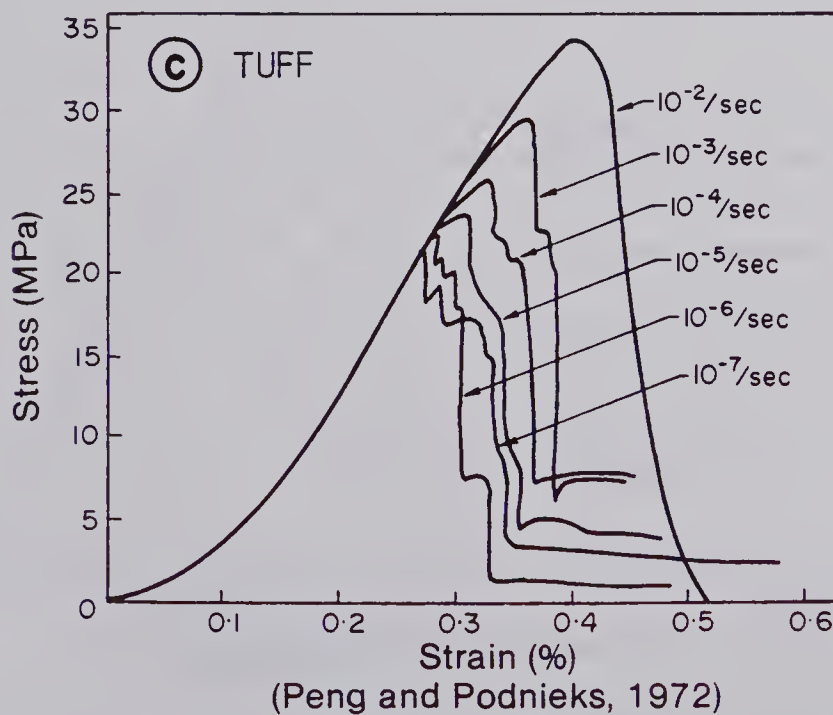
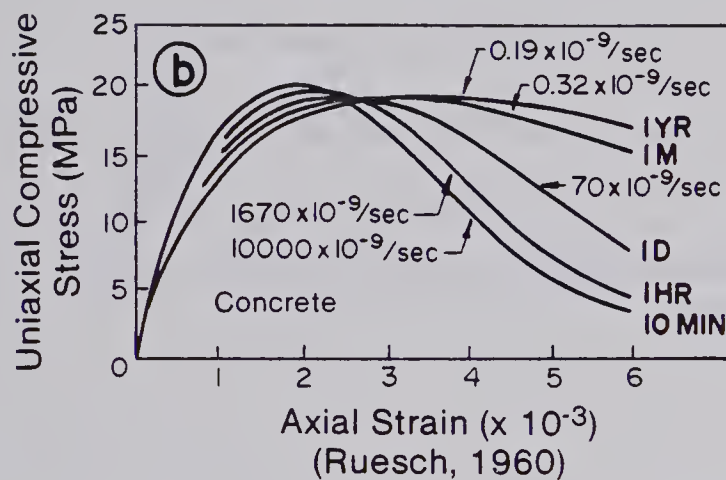
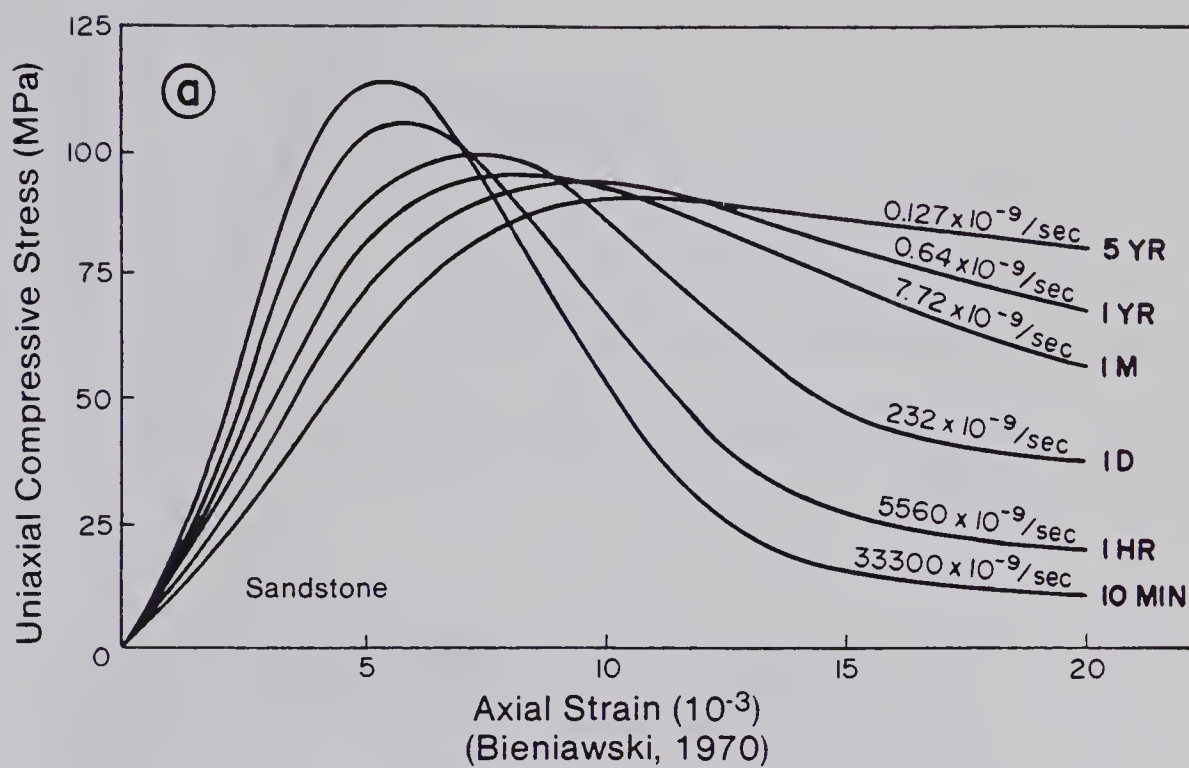


Figure 4.4 Stress-Strain Diagram from Uniaxial Compression Tests reported by a) Bieniawski (1970), b) Ruesch (1960) and c) Peng and Podnieks (1972)

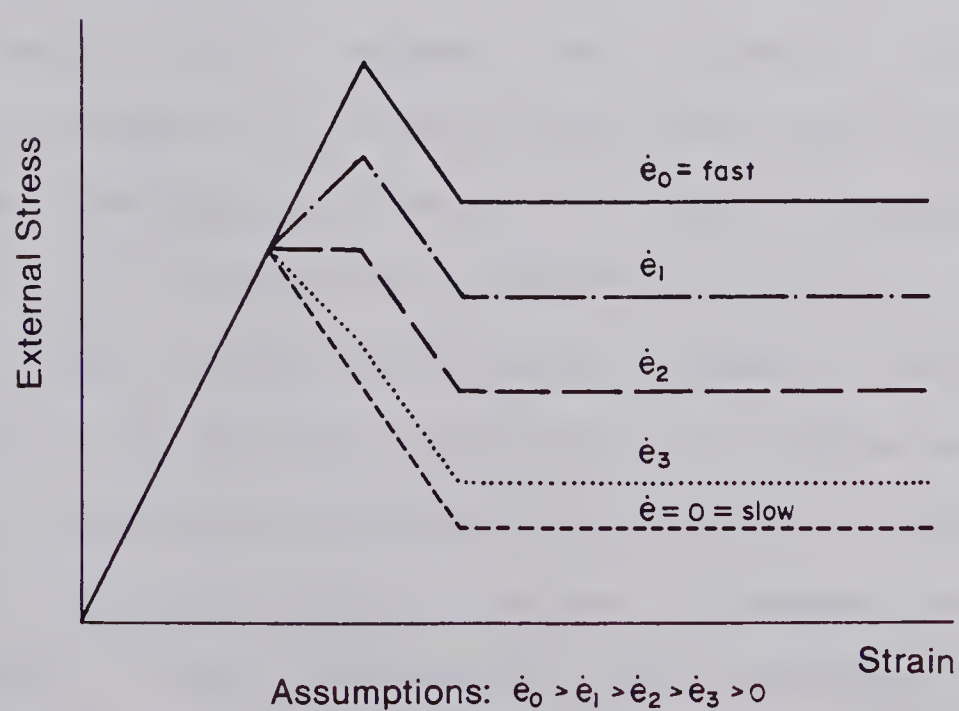
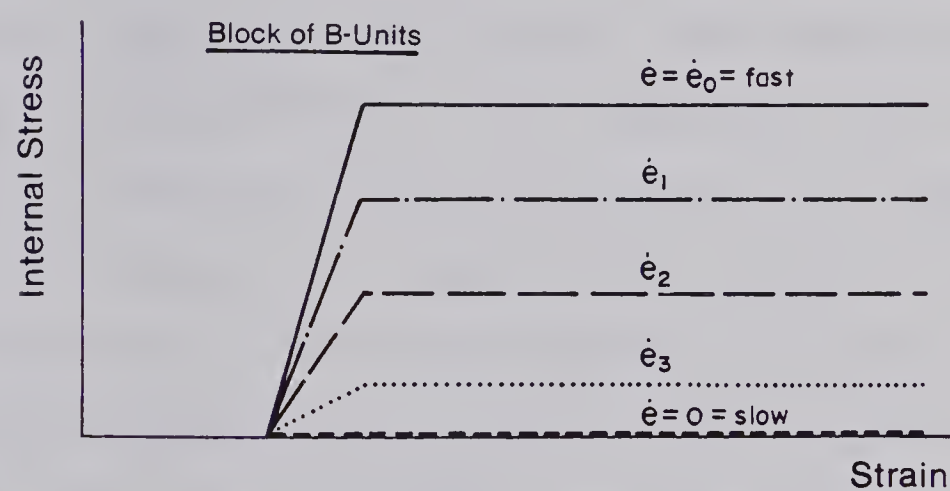
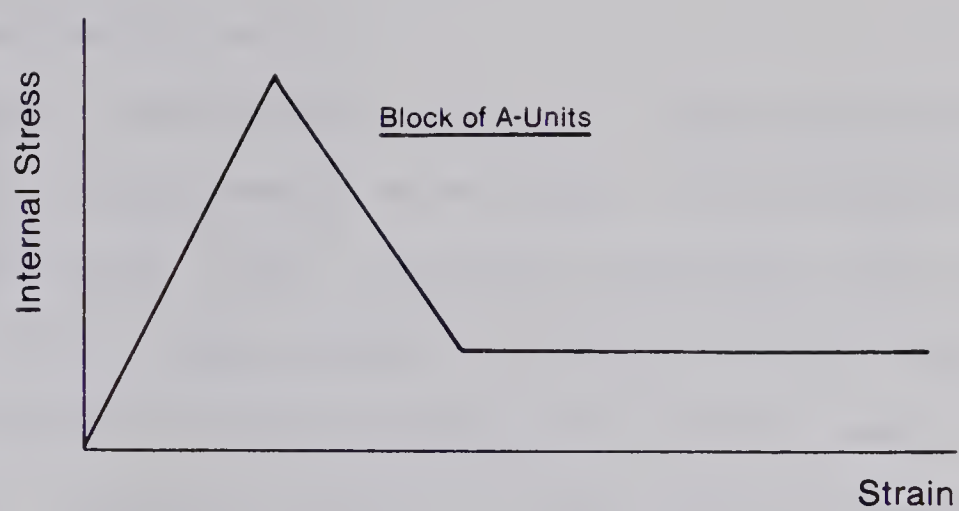


Figure 4.5 Special Case of Model for Rock with Time - Independent Stiffness below the Yield Strength

strain-weakening units.

Other observations made by Peng and Podnieks (1972, Figure 7) on the strain rate effect in the post-yield region are consistent with the model behaviour; the slope of the stress-strain curve beyond a certain stress level (about 22 MPa in Figure 4.4) decreases if the strain rate is decreased and even becomes negative if the strain rate drops below a certain critical value.

Another set of test results from tests on Solenhofen Limestone (Rutter(1972)) is summarized in Figure 4.6. Diagram (a) shows the brittle behaviour at a relatively low confining pressure (30 Mpa). This could be modelled by introducing mainly frictional elements as yield elements for the A-units and mainly cracking elements for the B-units. As a result the block of A-units would be elasto-plastic with little strain-weakening and the block of B-units visco-plastic with almost no ultimate strength. The following diagram (b) contains data from tests with the same effective confining pressure but with an equivalent back pressure. At a strain rate of 10^{-6} /sec or lower the results indicate that the law of effective stress is applicable and the model can be used accordingly. At higher strain rates dilatancy hardening (Brace and Martin(1968)), due to a pore pressure reduction during volume increase in this low permeability rock, increases the frictional resistance causing a similar response as a confining pressure increase (compare with diagram (c)). This pore pressure decrease is a

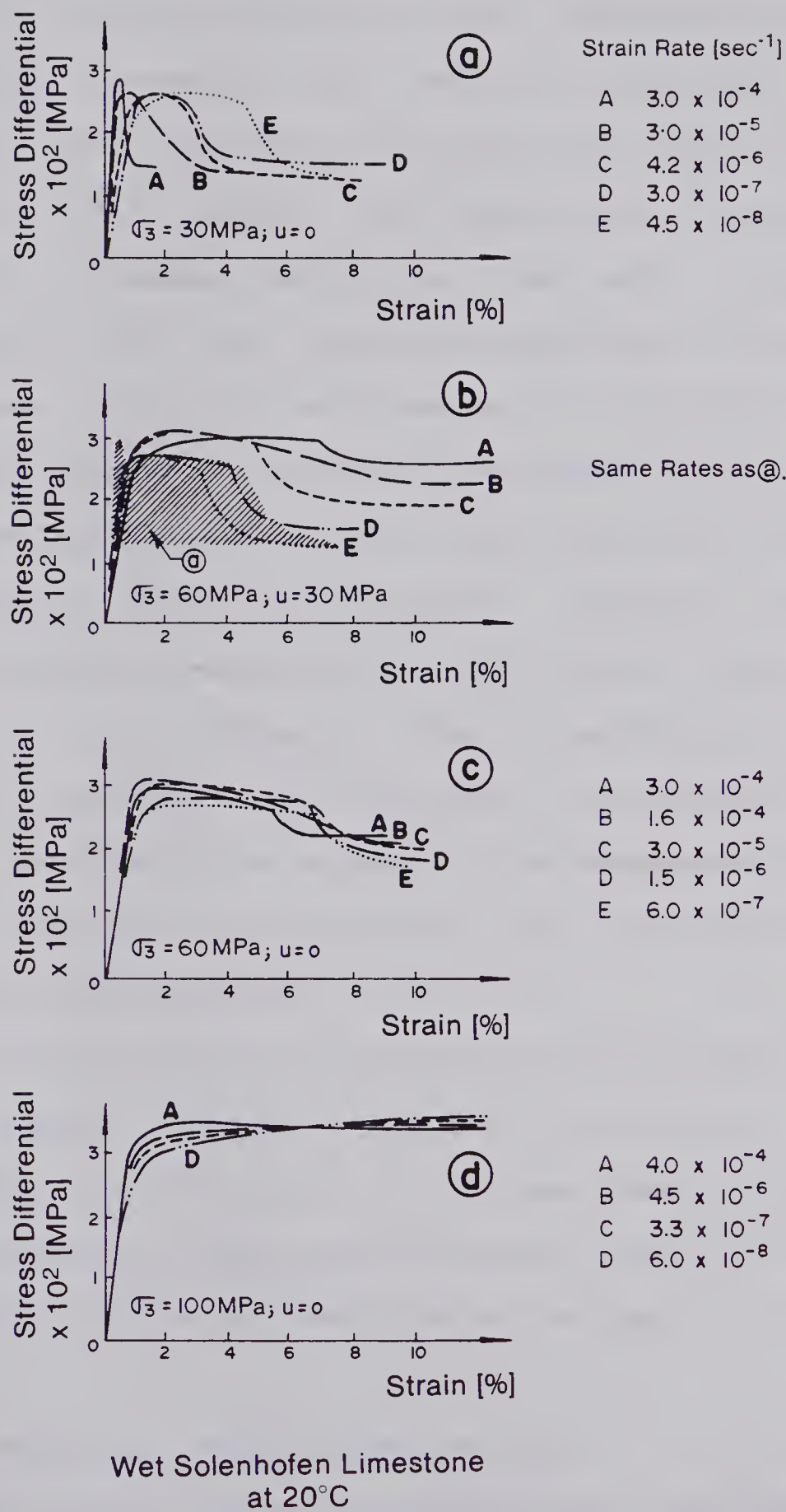


Figure 4.6 Stress-Strain Diagrams from Tests on Solenhofen Limestone (Rutter, 1972)

function of the loading rate and the rock permeability. In the model the yield element F is a function of the effective confining pressure. The process described above would increase the strength of the model and make it more ductile as the ratio between the resistance of the cracking and friction elements decreases. The model again shows good agreement with the observed behaviour. At high confining pressures (d) the rock behaves in a ductile manner with a somewhat higher yield point for rapid loading and strength loss at increased strain. This indicates a visco-plastic behaviour where frictional elements control the time-dependent response at low strain and some cracking elements are activated after significant straining. A detailed analysis is necessary to evaluate whether these data can be modelled by one set of parameters. The proposed model describes qualitatively all observed variations in strength and ductility.

From this brief discussion it follows that the proposed model with properly selected parameter distribution functions can describe the various observations of strain rate-dependent behaviour of failing rock. This model should therefore explain the response to changes in strain rate.

4.4.3 Tests with Varying Strain Rate

The tests reported by Bieniawski (1970) were conducted with varying strain rate to determine the behaviour of fractured rock. To the author's knowledge these are the only

variable strain rate tests documented in the literature. The shape of the stress-strain curves from tests on a sandstone are shown in Figure 3.1. Two pertinent observations can be made:

1. A decrease in strain rate in the post-peak zone results in an initially faster stress drop with a subsequent leveling off at a higher ultimate strength;
2. An increase in strain rate in the post-peak zone results in an secondary peak. The slope of the stress-strain curve changes to a positive slope immediately after the rate increase and a steeper, negative slope, leveling off at a lower ultimate strength, can be observed after this secondary peak.

The corresponding behaviour for the model discussed in Figure 4.3 (special case c), which was found to fit the constant strain rate data from tests on the same rock (Bieniawski(1970)), is illustrated in Figure 4.7. Four stress histories are illustrated in this figure: the two cases of infinitely fast and slow loading, which have already been discussed in Figure 4.3, and two additional cases (I and II) with intermediate strain rates $\dot{\epsilon}_1$ and $\dot{\epsilon}_2$ (where $\dot{\epsilon}_1 > \dot{\epsilon}_2$). If it is assumed that an original strain rate $\dot{\epsilon}_2$ is selected so that the B-units do not fail (case II) and that the strain rate after a total accumulated strain $\epsilon(\text{II})$ is increased to infinity or decreased to a lower strain rate $\dot{\epsilon}_3$, the resulting stress-strain curve can be found by superposition of figure 4.7.a and 4.7.b. The predicted

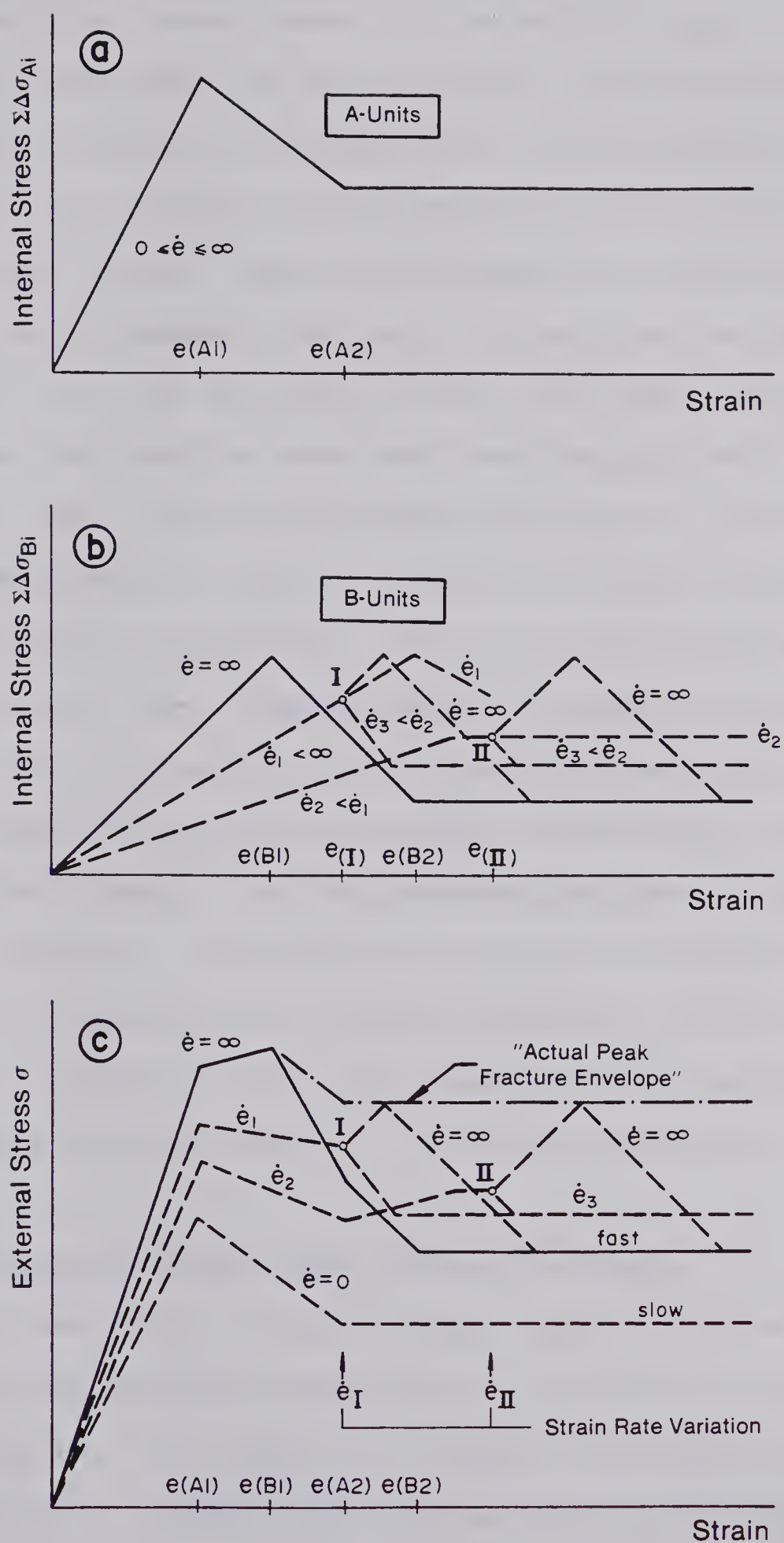


Figure 4.7 Special Case of Model for Rock in Variable Strain Rate Tests

stress-strain curve shows a secondary peak, due to the strength reserves of the B-units, and leveling off at a different ultimate strength level. The predicted behaviour is given in Figure 4.7 (c) together with another case (I) where the strain rate was changed at a total accumulated strain $\epsilon(I)$ before the peak strength of the B-units was reached. It can be seen that the model duplicates the behaviour observed by Bieniawski surprisingly well. The model supports the conclusions drawn in Chapter 3 that different rock structures with variable ultimate strength and time-dependent properties can be created during loading. Depending on the stress-history, B-units may or may not fail. The response at a given strain is controlled entirely by the current available strength; specifically, the current available strength of the B-units. The special case of the model predicts a structure independent, constant long-term ultimate strength, but a history-dependent current available strength. This is the case because of the assumption that the time-dependent element T is a viscous dash pot.

4.4.4 Multiple-Stage Single Relaxation Tests

As mentioned earlier, this type of test is a special case of the variable strain rate test where the strain rate is reduced to zero at various locations along the stress-strain curve. Such test procedures were reported by Bieniawski (1970), Peng(1973), Hudson and Brown(1973) and others. This loading history applied to the model means that

the B-units are loaded to a certain stress level, before or after their peak strength, and then allowed to relax gradually as soon as loading is stopped. These units will not carry any load at infinite time (Figure 4.8.b). The relaxation will therefore terminate at the current long-term strength which is controlled by the strength of the A-units. This process is shown for three single relaxations with instant loading in between them in Figure 4.8 for the special case described in Figure 4.3.c. During the first relaxation (I) the load carried by the B-units drops to zero. These units will therefore possess an unchanged strength reserve as long as they have not been overstressed. During loading to the second stage (II) the A-units start to fail at a strain $e(A_1)$ but the B-units can take further load until they start to fail when the "actual peak fracture envelope" is reached. If the loading rate between relaxations is high enough, the B-units will reach their peak strength and reach the "actual peak fracture envelope" independent of loading history. Stages II and III, illustrate relaxations within the zone where some of the B-units are overstressed. The available strength after relaxation is equal to the stress carried by these units before relaxation was started.

Again excellent agreement with documented observations can be found by comparison of the model behaviour with results published by Peng(1973) (e.g. Figure 4.9.a), Bieniawski(1970) or Hudson and Brown(1973). From these three

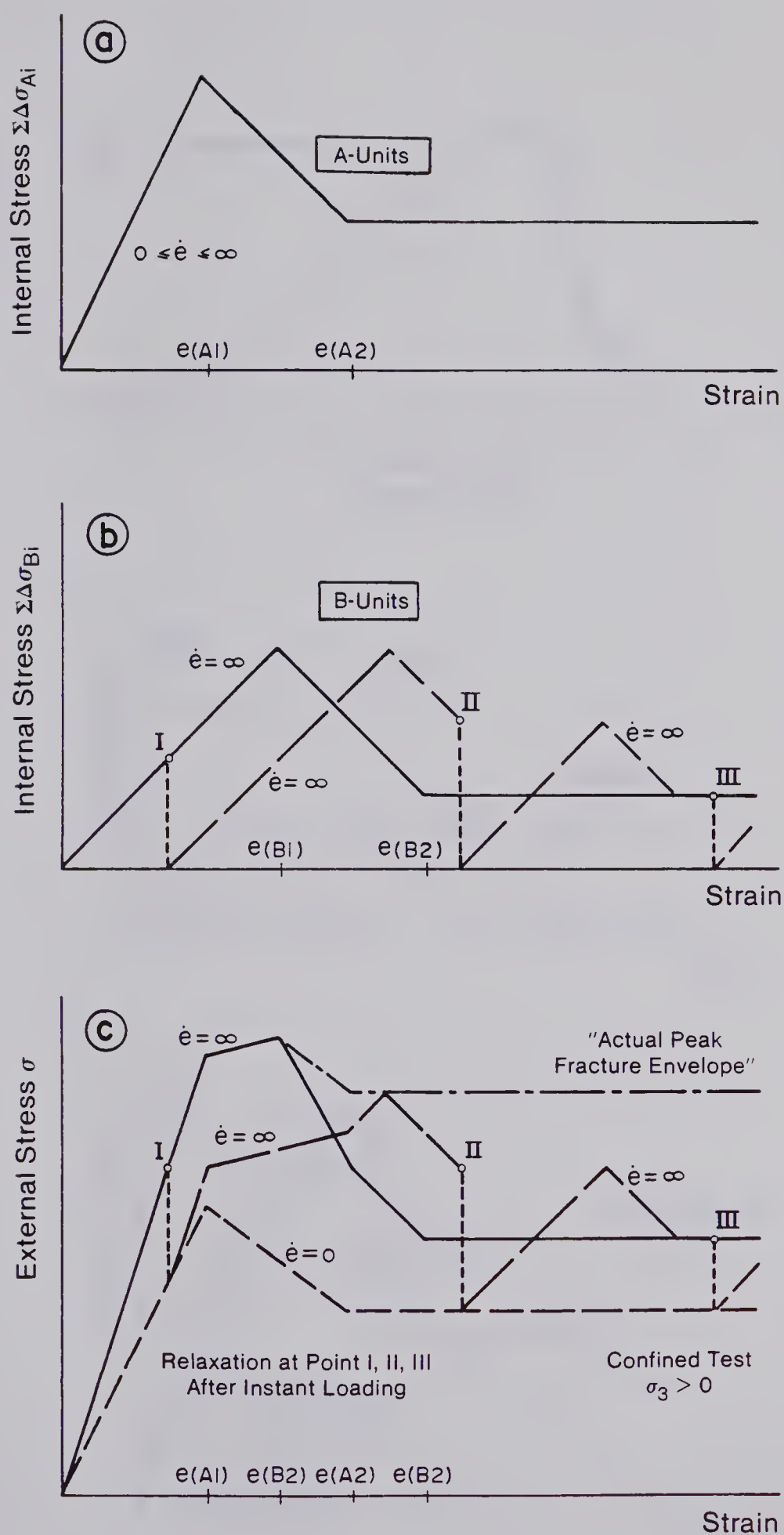


Figure 4.8 Special Case of Model for Rock in Multiple-Stage Single Relaxation Test

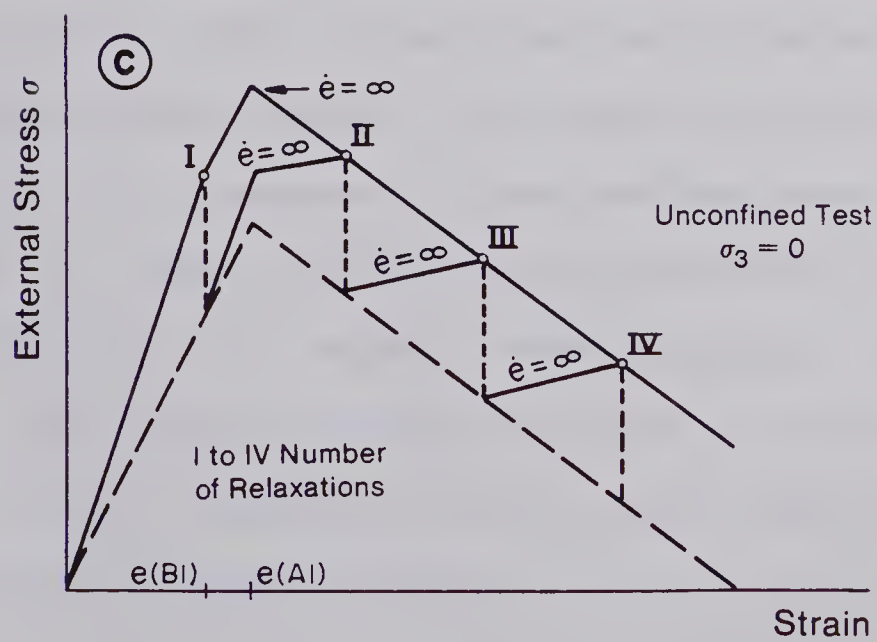
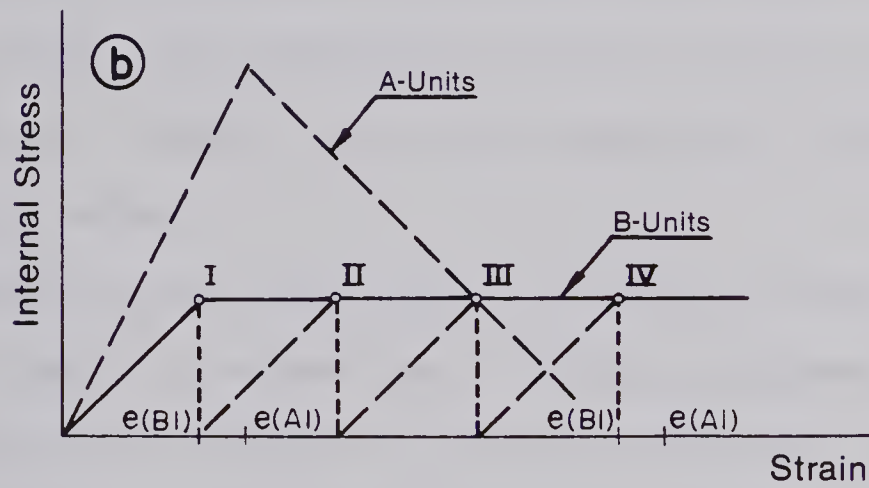
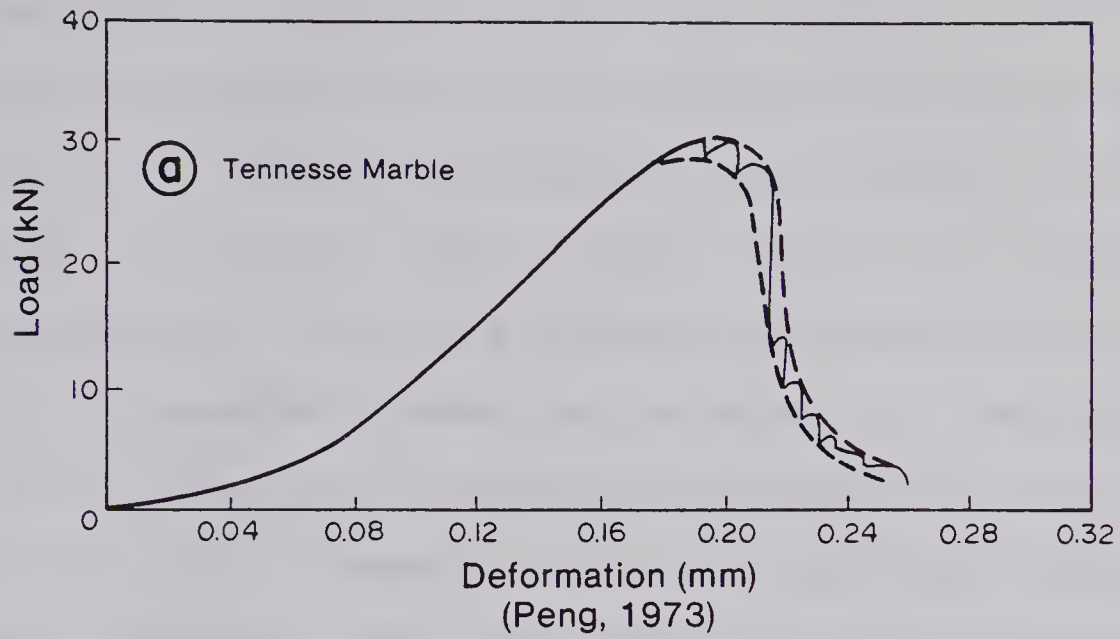


Figure 4.9 Special Case of Model during Relaxation for Comparison with Test Data (Peng, 1973)

publications it appears that the B-units of the tested materials possess only a minor cohesive resistance and that they can be modeled as elastic, visco-plastic units. (The sandstone tested by Peng (1973, Figure 3) shows some strain-weakening of the B-units). The behaviour of a model with corresponding properties is shown for comparison with the real behaviour in Figure 4.9 (b and c). It is assumed that the yield elements of the A-units are composed of cracking elements only and that reloading is undertaken after complete relaxation. A yield element must be added in parallel to the time-dependent element (or the B-units must be delayed) to model the time-independent portion of the stress-strain curve.

The effects of the machine stiffness on the behaviour of failing rock in connection with the proposed model have been discussed in detail by Kovari(1977) for the case of time-independent rock. These effects have to be considered when the results from relaxation tests during unconfined uniaxial compression tests are compared with the model. Depending on the parameter distribution functions of the elements E, C and F, it may be possible that B-units fail during relaxation if stress redistribution within the B-units or excessive strength loss of A-units leads to a loading of other B-units. In both cases sudden changes in relaxation rates may be observed.

4.4.5 Multiple-Stage Repeated Relaxation Test

The major difference between the single relaxation test and the multiple-stage repeated relaxation test is that the rock is not reloaded to the current available strength during testing within one stage. The model has to be compared with the data presented in Chapter 3. Because the model was developed on the basis of this information, the following discussion cannot be considered as a proof of its validity, but it illustrates another case where the model predicts the real behaviour. The model can be used to describe the behaviour in the three Zones A, B and C (see Figure 3.37).

In Zone A relaxation decelerates and terminates at stress levels below the long-term peak strength. All units in the model are loaded to stress levels below their capacity and the predicted behaviour corresponds to the behaviour of a number of spring elements in parallel with a number of Maxwell elements. Below the long-term peak strength this will lead to terminating creep or relaxation and above the long-term peak strength stress transfer from the B-units to the A-units will eventually, at the limit between Zone A and C, lead to collapse of some A-units (or B-units). The response of the model during stage testing in Zone A can be determined by linear superposition. At strains beyond the peak failure strain but at stresses below the current long-term strength the model predicts a behaviour similar to that observed in Zone A. No additional yield

elements fail and the time-dependent behaviour is controlled by the E and T elements.

In Zone B near the ultimate strength most or all cracking elements are exhausted. If the yield elements in the B-units consist of frictional elements the material will behave in a visco-plastic manner as soon as zone B is entered. On the other hand, if the yield elements in the B-units are cracking elements only, the material will show a time-independent ultimate strength as soon as the last yield element of the B-units has failed. The behaviour within a strain-weakening zone B follows as a logical consequence. Yielding of all yield elements is superimposed on the visco-plastic behaviour and the extent of Zone B decreases with increasing strain as the number of failed cracking elements of the B-units increases.

The behaviour within the transition zone C is dominated by the sudden breakdown of major load carrying regions within the rock structure. The resulting discontinuous stress-strain relationship is simulated by a model with groups of elements possessing similar parameters which leads to an even loading of these units and simultaneous collapse of groups of units. The condition of constant current available strength and therefore secondary creep is a special case and can only be modeled by specific parameter distribution functions.

The view expressed in Chapter 3 that the results from relaxation tests near failure cannot be used to predict

creep behaviour without making assumptions about the failure process is strongly supported by the model. A single relaxation is a response to the current state of rock (or model) whereas creep describes the transition from one state to another during the specific stress history of constant load. Different stress histories result in a different stress distribution at a given strain (Kranz(1979)). The same units that will fail during relaxation are not the same as those which would fail under constant load at the same accumulated strain. Two relaxations executed immediately after each other could show completely different behaviour. If a unit just failed during reloading, relatively little relaxation will be observed, whereas a major stress drop is recorded if a unit collapses during relaxation. This drawback is overcome in repeated relaxation tests where (a) decreasing relaxation means that units are loaded and capable of carrying load transferred from the time-dependent units, (b) constant relaxation means that elements fail but in a stable manner with load transfer to stronger units and (c) increased relaxation means that unstable conditions exist where more load is transferred than can be carried. The latter case may become stable if strong units can be mobilized at increased strain. Repeated relaxation tests in a stiff testing frame show essentially the same advantages over a creep test as does strength testing with a stiff testing machine over testing with a soft testing machine. The energy release of the test frame is controlled and

little damage is created due to the test system; pure rock response is observed.

4.4.6 Single-Stage Creep Tests

Single-stage creep tests at stress levels below the long-term peak strength, where none of the yield elements are overstressed, can be used to investigate the properties of the assembly of E and T elements. Creep will terminate at these stress levels. The model assembly corresponds to a three-parameter solid with constant parameters. Consequently it does not predict a linear relationship between the logarithm of strain rate and the logarithm of time as observed for coal by da Fontoura(1980). A variation of the parameter distribution functions does not affect this predicted non-linear trend. It is necessary to alter the type and arrangement of the E and T elements to satisfy linearity at these pre-failure stress levels. For coal, a number of Kelvin elements in series, with a retardation time spectrum (Terry(1956)), will be required.

Above the long-term peak strength the model will initially predict a decrease in creep rate followed by acceleration leading to collapse. Only as a special case, with a certain arrangement of distribution functions, might it be possible to model a secondary creep stage with a constant creep rate. It follows from the model that secondary creep is not characteristic of failing brittle rock. Many types of strain-time relationships have been

observed in creep tests on rock. The various types can be simulated by a model with the right parameter distribution functions. The following example will serve to illustrate this.

Data from creep tests on shale and marble by Singh(1975) are reproduced in Figure 4.10. Three typical behaviours are revealed: (a) sudden increases in strain rate on generally decelerating creep curves; (b) gradual failure by continuous strain rate increase; and (c) almost instant failure after a sudden strain rate increase during continuously decreasing creep rate. A similar stress-strain curve was observed during coal testing. The model explains these three cases:

1. A stress transfer between B-units and a collapse of these units will result in a momentary strain rate increase. Subsequent deceleration is caused if the A-units are never loaded beyond their capacity;
2. Gradual failure is caused if the stress transfer is slow and the B-units are able to carry temporarily the strength losses due to the collapse of A-units;
3. Stress is transferred to A-units and their strength loss leads to an overstressing of the B-units, resulting in collapse within a very short time span.

Another feature of the proposed model is that it can predict the total strain to failure. Depending on the selected parameter distribution functions, collapse occurs at a strain corresponding to the accumulated strain for rapid

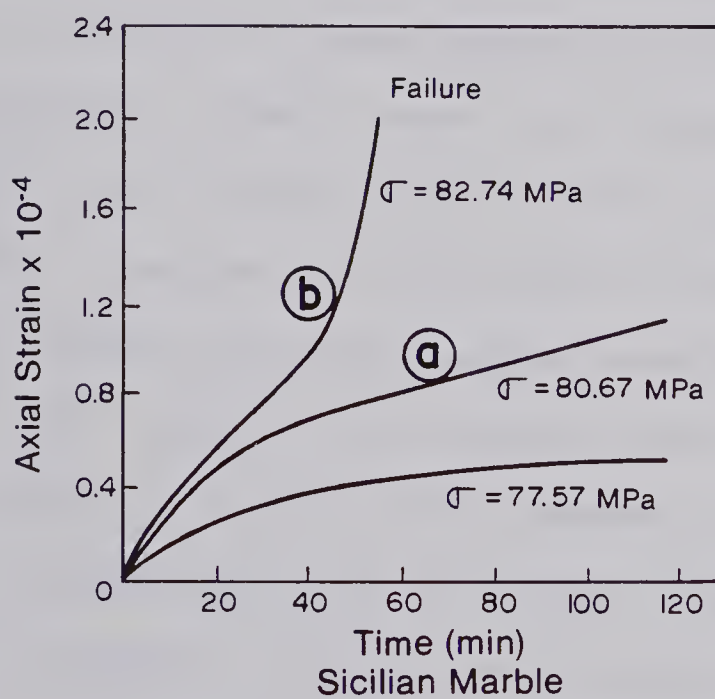
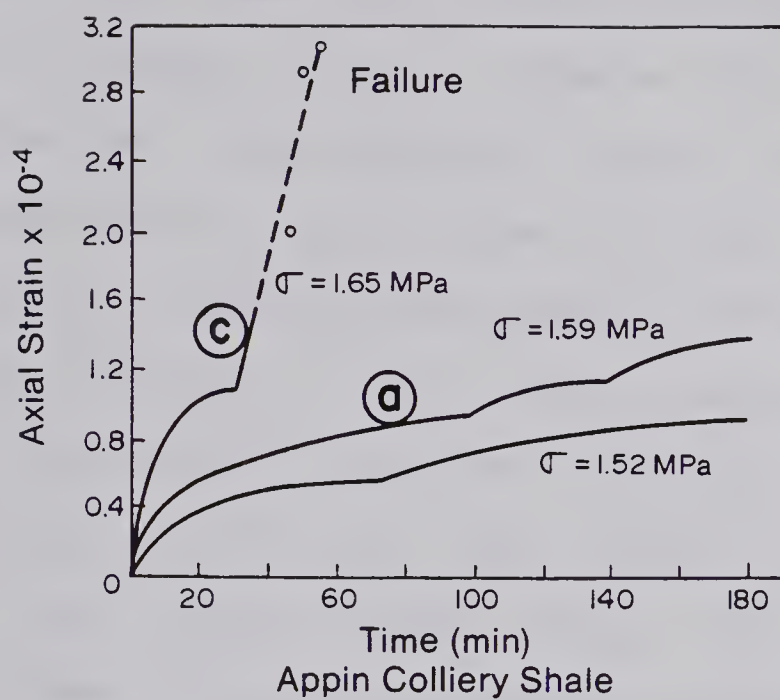


Figure 4.10 Axial Strain versus Time Curves of i) Shale and ii) Marble (Singh, 1975)

loading or at much higher strains. Both types of behaviour may be observed during testing of rock. A schematic model behaviour (for the same case as shown in Figure 4.3.c) is illustrated in Figure 4.11. A similar diagram, for a material where the time-dependent units fail before the time-independent units is given later in Figure 4.13.

Figure 4.11.a includes stress-strain curves for loading at minimum and maximum strain rate (called "slow" and "fast") and the "actual fracture envelope" (Lama(1974)) which is not identical with the "actual peak fracture envelope" if the A-units yield first. The "actual peak fracture envelope" can only be reached if the B-units have not been damaged during the loading and the "actual fracture envelope" can be reached if some damage has been done during loading. Single-step creep tests are conducted at stress levels(I), (II) and (III). Figure 4.11.b gives the stress carried by the B-units as a function of strain for these three cases. A constant maximum loading rate up to the creep stress level was assumed. At stress level (I) all stress initially carried by B-units will transfer to the A-units, the creep rate (Figure 4.11.c) will drop to zero, and creep will terminate (Figure 4.11.d) at the long-term strength curve (Figure 4.11.a). At stress level (II) (above the long-term peak strength) the creep rate decreases initially due to unloading of the B-units to a minimum at $e(A_1)$, the strain where the A-units begin to fail. This stage is followed by a rate increase due to stress transfer from A-

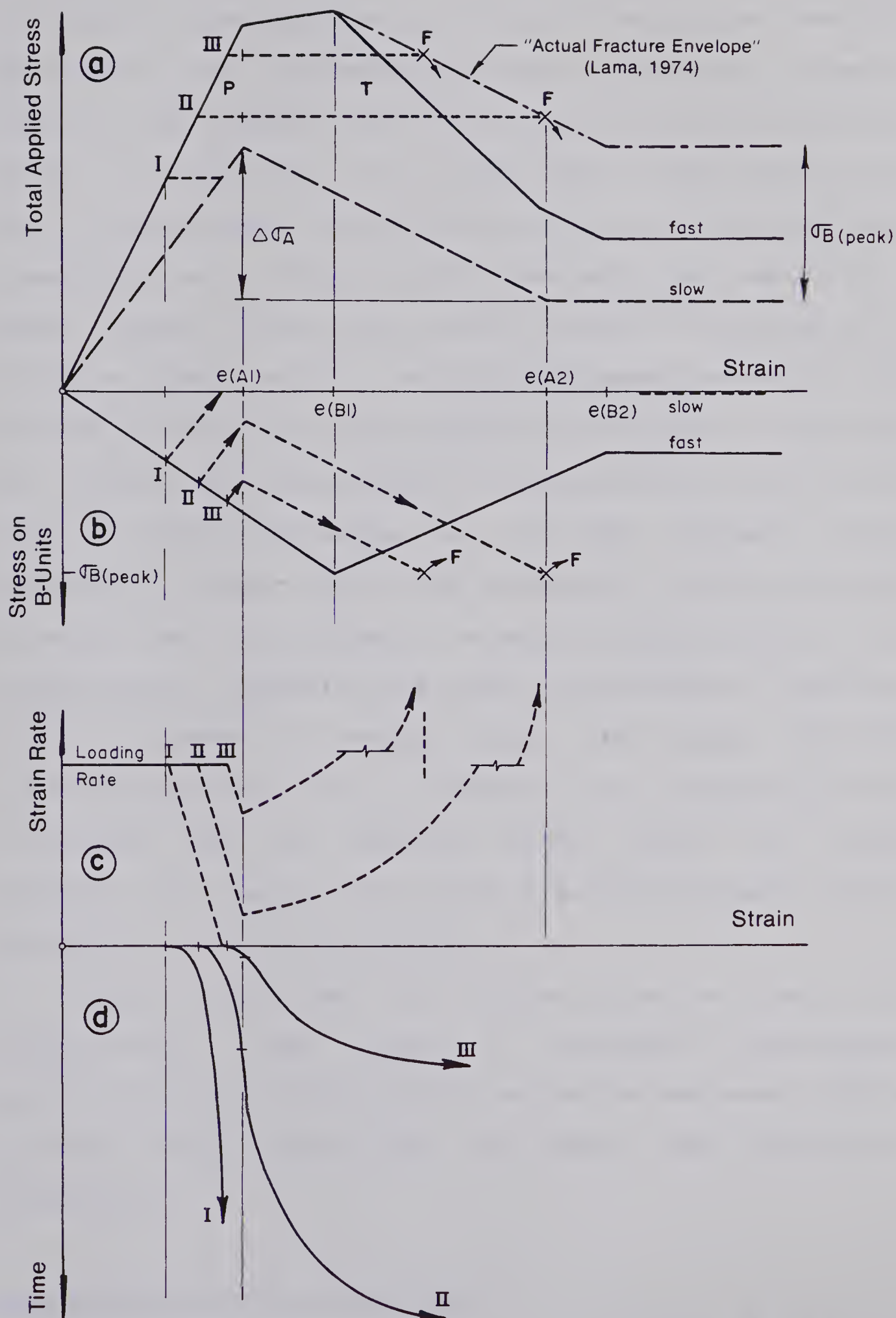
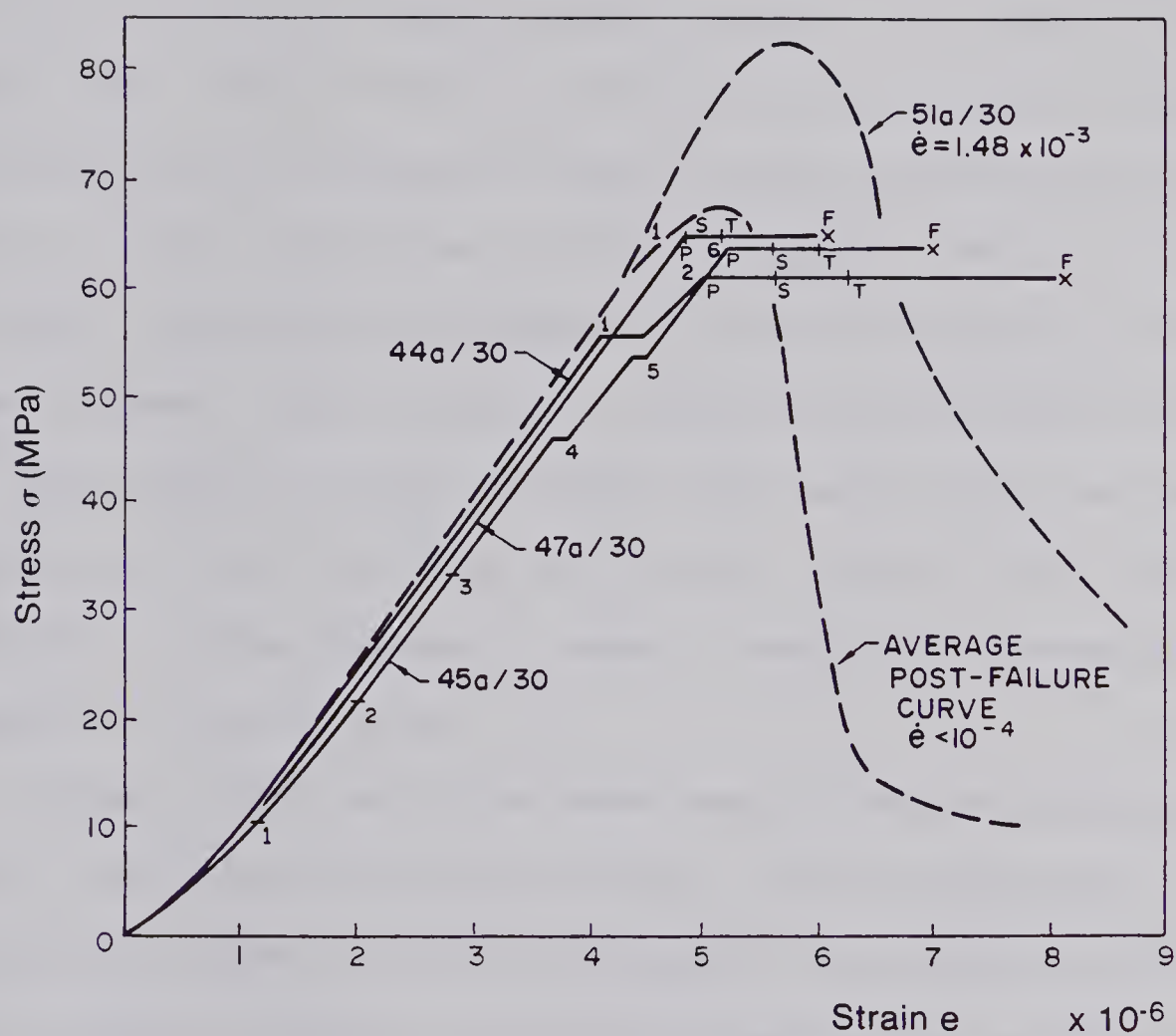


Figure 4.11 Special Case of Model for Rock in Single-Stage Creep Tests

to B-units and failure will occur at the "actual fracture envelope". The corresponding curves for internal stress on B-units and strain rate as well as the creep curves are given in Figure 4.11. At an even higher stress level (III) only a minor stress transfer from B- to A-units is followed immediately by a stress transfer reversal. This results in a small primary creep zone before failure is initiated at a constant strain $\epsilon(A_1)$. Failure will occur beyond the fast loading stress-strain curve except in the special case where the B-units are represented by visco-elastic, plastic units with no strain-weakening. If the peak strength of the B-units is larger than the difference between the peak strength and the ultimate strength of the A-units, it is theoretically possible that creep will not lead to failure. After a period of primary creep, the creep rate will gradually increase to a maximum level, depending on the T-elements and the relative stress level, and remain constant as long as the current available strength remains constant.

Figure 4.12, Test No. 47a/30, gives an example of a single-stage creep test. It provides experimental verification of the behaviour predicted by the model (Figure 4.11.a). These creep tests on marble were reported by Lama(1974) .

4.4.7 Multiple-Stage Creep Tests



Sample	Time to Failure
44a/30	10 min
47a/30	290 min
49a/30	480 min

Figure 4.12 Stress-Strain Diagram of Multiple-Stage Creep Tests, Lama (1974)

Creep tests are undertaken from increasing or decreasing stress levels (stages) until failure is reached at the final creep stage. The stress-strain curves from such tests with increasing stress levels (Lama(1974)), together with an average stress-strain curve for tests at strain rates less than 2.5×10^{-4} (units not given in Lama's publication), are shown in Figure 4.12. One test at a higher strain rate indicated higher strength with an almost parallel post-peak stress-strain curve. It appears that all three creep tests failed at stress levels relatively close to the long-term peak strength. This means that no load was carried by the B-units at rates below 2.5×10^{-4} . The observed stress-strain curve describes therefore the response of the A-units.

Other multiple-stage creep tests from reloading curves after the long-term peak strength showed comparable results (Lama(1974), Figure 11). This supports the view that the rock mass should behave in a manner similar to reloaded failed rock.

Before Lama's data can be compared with the proposed model, a few observations must be made. It seems impossible to predict the stress level of the creep stages relative to the peak strength determined for constant strain rate tests due to a considerable variation in strength between samples. To connect the failure points by an "actual fracture envelope" seems questionable. Furthermore, because of the previous statement that a secondary creep stage exists only

under very special conditions, it is necessary to reinterpret the given limits between primary, secondary and tertiary creep. The minimum creep rate should lie somewhere within the "secondary" (S) zone and acceleration must have been obvious at or beyond the limit between the (S) and "tertiary" (T) zone. The model in Figure 4.11 predicts that the transition point between primary and tertiary creep would correspond with the long-term peak strength and that creep tests closer to the long-term peak strength would show a more pronounced primary creep stage and more strain to failure. This is very similar to the behaviour observed by Lama.

The schematic diagram for multiple-stage creep tests on a material whose B-units fail before the A-units is given in Figure 4.13. Three single-stage creep tests (I), (II) and (III) (similar to the ones in Figure 4.11) are included in this figure. It can be observed that a single-step creep test at stress level (III), (beyond failure initiation in the B-units), will not reach the "actual peak failure envelope" due to some strength loss of B-units before the creep level was reached (Figure 4.13.b). On the other hand, it can be seen that multiple-stage creep tests with failure at the same stress level may fail at the "actual peak fracture envelope" if the B-units did not lose any strength during the previous loading history (both V and VI). The loading history (VI) indicates that loading beyond the limit called "actual fracture envelope" by Lama (1974) may be

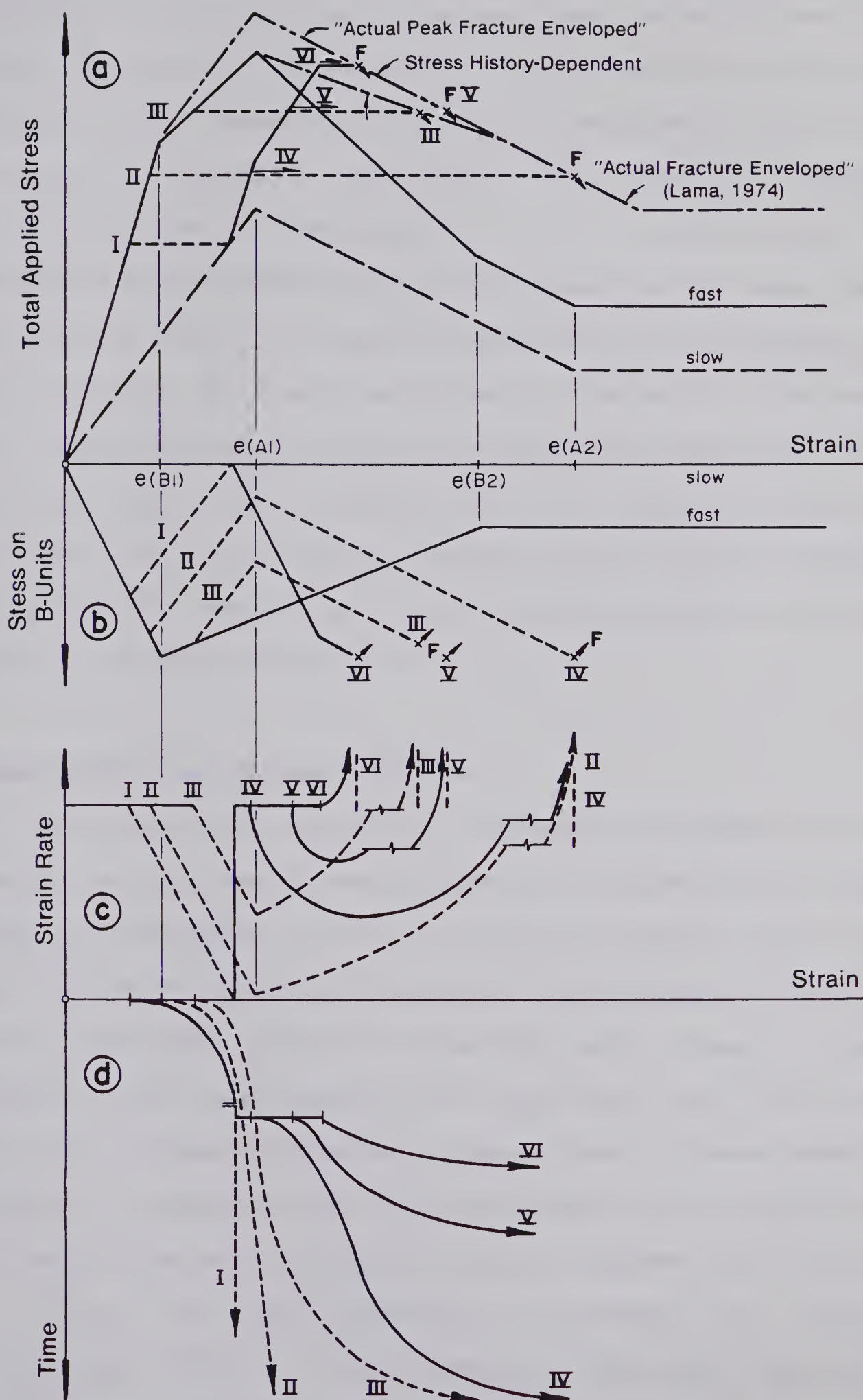


Figure 4.13 Special Case of Model for Rock in Multiple-Stage Creep Tests

possible. It follows that there are some rocks (Figure 4.13) where the strain to failure is history-dependent and others (Figure 4.11) where it is history-independent. The "actual fracture envelope" introduced by Lama is therefore history-dependent. Moreover, it is possible, as was mentioned during the discussion of single-stage creep tests, that this limit is never reached during creep tests. The term "actual fracture envelope" is therefore questionable and has been replaced by "actual peak fracture envelope" to indicate that this envelope can be reached if the peak strength of the B-units is mobilized. No further attention is given to this limit since it does not seem to have any practical implications.

4.4.8 Static and Dynamic Fatigue

The proposed model as discussed in connection with single-stage creep tests (Figure 4.11) shows clearly static fatigue behaviour. The time to failure (Figure 4.11.d) is a function of the applied stress level and fatigue failure has to be expected above the long-term peak strength. Dynamic fatigue could be explained by this model too, but it will not be discussed in detail. Stress level, stress range and loading frequency can easily be identified as some of the relevant parameters by examination of Figures 4.11 and 4.13.

It is of some interest to evaluate the model in connection with the brief testing program undertaken during Test No. CTR-2A, Stage B. A comparison of repeated

relaxations with enforced rapid cycling was given in Figure 3.17. This test was performed near failure above the long-term strength. Rapidly enforced cycling may therefore cause some elements in both types of units to yield due to minor stress redistributions between the time-dependent units or from the time-independent units. The total testing time during cyclic loading is relatively short compared with the time needed for the same number of load cycles during repeated relaxation tests. As a consequence, only minor straining occurs during rapid cycling since not enough time is given for the T-elements to deform and less damage is done to the rock structure. On the other hand, during repeated relaxation, a major unloading of the B-units over an extended time interval combined with loading of the A-units will result in strain accumulation at the T-element. Furthermore, during reloading between relaxation, more and more load will be carried by the A-units and overstressing will result in strength loss and strain accumulation. This behaviour is clearly supported by the observations reported in Chapter 3 and by Kranz (1979).

Further support for the proposed model may be found in many other publications, but because of incomplete information it is often difficult or impossible to evaluate the data in detail. For example, John(1974) published very interesting results on single-stage creep and constant strain rate tests on norite but reported only time to failure and strength at failure. His data indicate that

additional strength can be mobilized if rock is loaded relatively fast or after a creep test of limited time. He notes that, in a strength versus time to failure diagram,

"...the strength for continuous loading lies always above the strength for constant load tests by a constant amount."

He further explains:

"After failure initiation the deformation behaviour depends on the loading rate. This means that crack initiation and crack propagation are time - dependent."(Translated from German by the author)

This process is described by the suggested model.

Developments in other areas, e.g. geophysical research, indicate that time-dependent models can be used to describe fairly accurately several phenomena such as post-seismic creep, foreshocks and aftershocks (Cohen(1978)). The model used in Cohen's study is a special case of the proposed model with both time-dependent and time-independent elements connected to one frictional element. From the previous discussion it appears that even better agreement with observations might be achieved if the visco-elastic, plastic model would be replaced by a special case of the proposed model, a non-brittle visco-elastic, visco-plastic model. Application of the model to this area of research should be investigated in more detail.

4.5 Recommended Approach to Develop the Phenomenological Model to a Mathematical Model

The purpose of this section is to outline briefly a possible procedure to develop the proposed phenomenological model into a mathematical model. The recommended approach is based on the procedure outlined by Kovari (1977) which he used to analyse time-independent rock behaviour during the fracture process. To obtain a smooth stress-strain curve, Kovari assembled a large number of time-independent A-units with a continuous parameter distribution function into a "block" of units (Figure 4.14). The parameter distribution function gives the parameters for each element in the (m) A- and now (n-m) B-units. At the limit with an infinite number of units the distribution functions can be written as functions of one variable x : $E(x)$, $F(x)$ and $C(x)$, and new $T(x)$. Because of the dependence of the frictional resistance on the confining pressure p , the distribution function F depends on the two variables x and p , $F(x,p)$. Kovari calculated convex and concave post-peak stress-strain curves as a function of the ratio between the minimum and maximum value of the stiffness distribution function, which was assumed to be linear. Since most stress-strain curves are composed of a convex and a concave portion, two blocks of units with different parameter distribution functions had to be superimposed. The confining pressure effects were simulated by expressing the strength of the cracking elements and the strength of the frictional elements as a

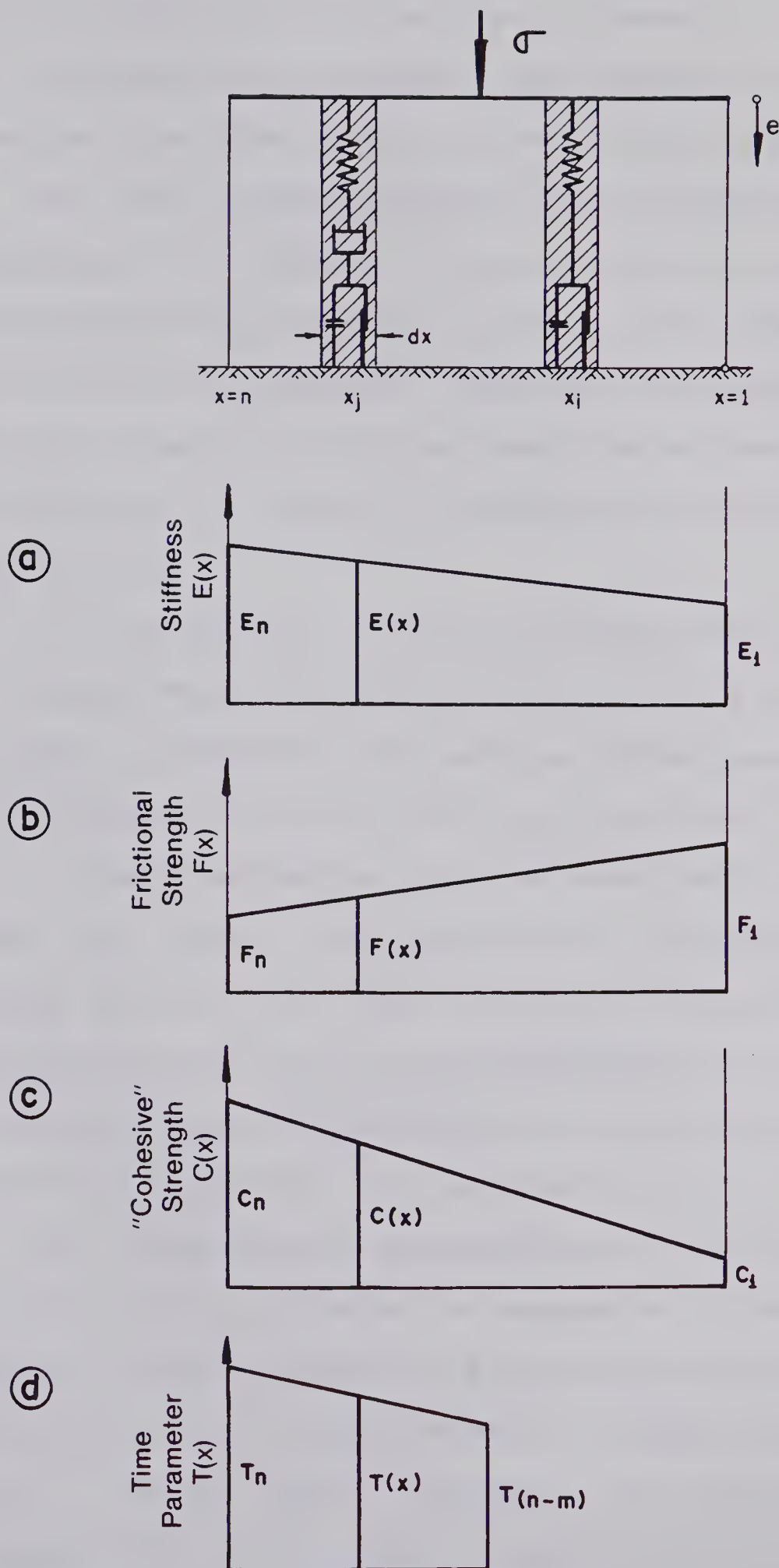


Figure 4.14 Continuous Parameter Distribution Functions
(a,b,c after Kovari, 1977)

function of a hydrostatic pressure p . In summary, this model allowed the simulation of uniaxial and triaxial compression test results from test on various rock types, particularly for the two rock classes suggested by Wawersik(1968). The model explains the effects of machine stiffness, does not include hysteresis in a reloading cycle and describes only a so-called "no-slip" material, where the reloading modulus decreases as a function of accumulated strain. Some of these deficiencies could be overcome by adding new elements to the individual units.

From the discussion of the proposed time-dependent model it follows that a portion of the units in a block have time-dependent properties. For the simplified assumption of a viscous T-element in series with one elastic and one yield element, a fourth parameter $T(x)$ for $(n-m)$ units has to be added when (m) units are assumed to be time-independent. (See Figure 4.14). With this addition it is possible to calculate the stress-strain-time relationship as a function of the stress-history. The formulation adopted by Kovari can be expanded to calculate the internal state of stress as well as the corresponding deformation at a specific time. For variable loading histories an incremental approach will be necessary. This process is illustrated graphically in Figure 4.15 for the special case of a single stage creep test on a rock model composed of elastic $E(x)$, time-dependent $T(x)$ and cracking elements $C(x)$ only.

If this model is loaded instantaneously to a certain

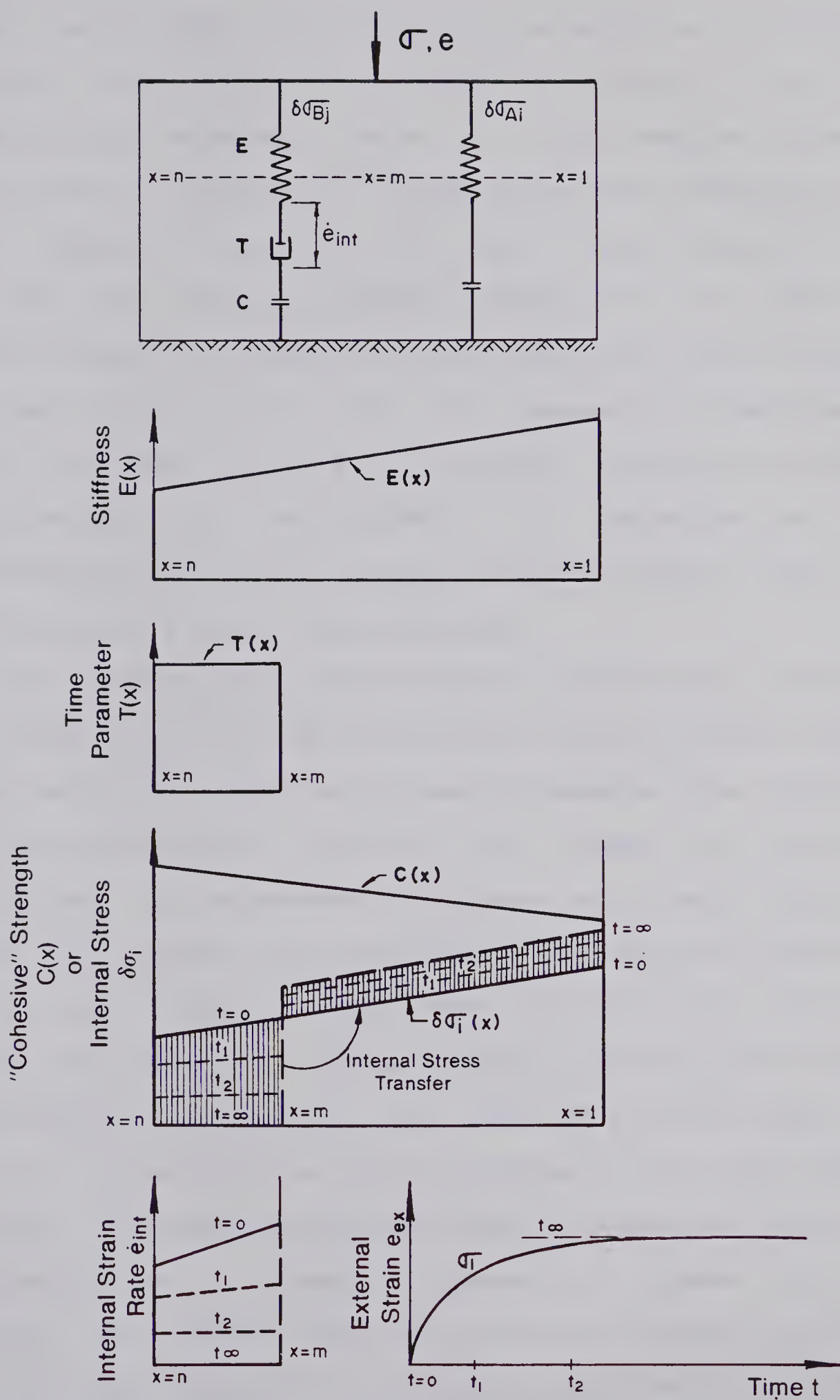


Figure 4.15 Creep Test on Model with Continuous, Linear Parameter Distribution Function; $\delta = \delta_1$

stress level $\sigma = \sigma_1$ the stiffness E_0 is given by the elastic elements in parallel $E_0 = \sum E_i(x)$, (where $i = 1, n$), the corresponding external strain $\epsilon_0 = E_0^{-1} \sigma$, and the internal stress $\sigma_i(x) = \epsilon_0 E_i(x)$. At infinite time the stiffness will be $\bar{E} = \sum E_i(x)$, (where: $i = 1, m$), the external strain $\bar{\epsilon} = \bar{E}^{-1} \sigma$ and $\sigma_i(x) = 0$ for $i > m$ or $\sigma_i(x) = \bar{\epsilon} E_i(x)$ for $i \leq m$, since the elastic elements in series with the dash pots will not carry any load. The strain rate will gradually drop from an initial maximum to zero at infinite time. The external stress-strain-time relationship is controlled by the differential equation of a three parameter solid $\sigma + a \dot{\sigma} = B \epsilon + c \dot{\epsilon}$, where a , b , and c are constants.

At a higher stress level $\sigma = \sigma_2$ the model might initially still behave elastically but internal stress transfer during creep will cause yielding of some C-elements. The constants in the differential equation will change as units are eliminated. An incremental approach will most likely be needed to analyse the model behaviour during this process. At an even higher stress level σ_3 stiff units will fail during the initial loading process and constants in the differential equation at the onset of a creep stage will have to be derived from the properties of the still active elements. The response and behaviour at these two levels is illustrated in a schematic diagram in Figure 4.16. To simplify the diagram the stress level is assumed to be the same for both cases but two strength distribution functions $C(x)(II)$ and $C(x)(III)$ have been used. The stress level

$E(x)$ and $T(x)$ same as in Figure 4.15

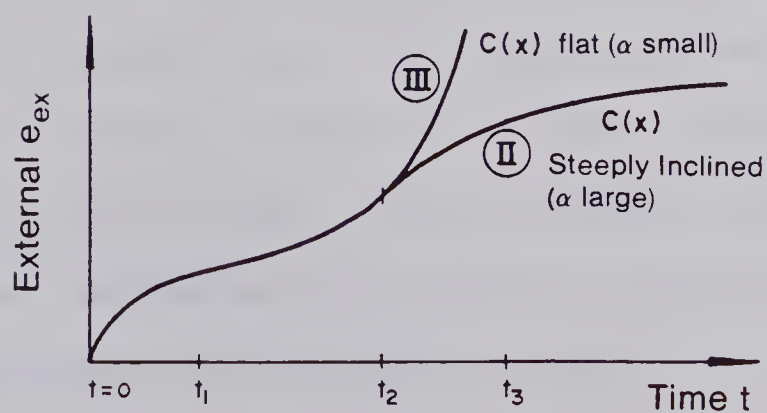
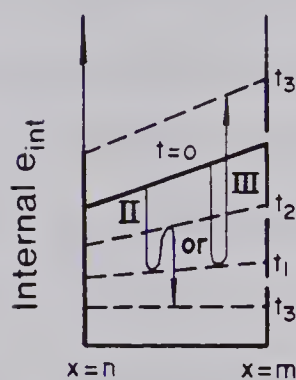
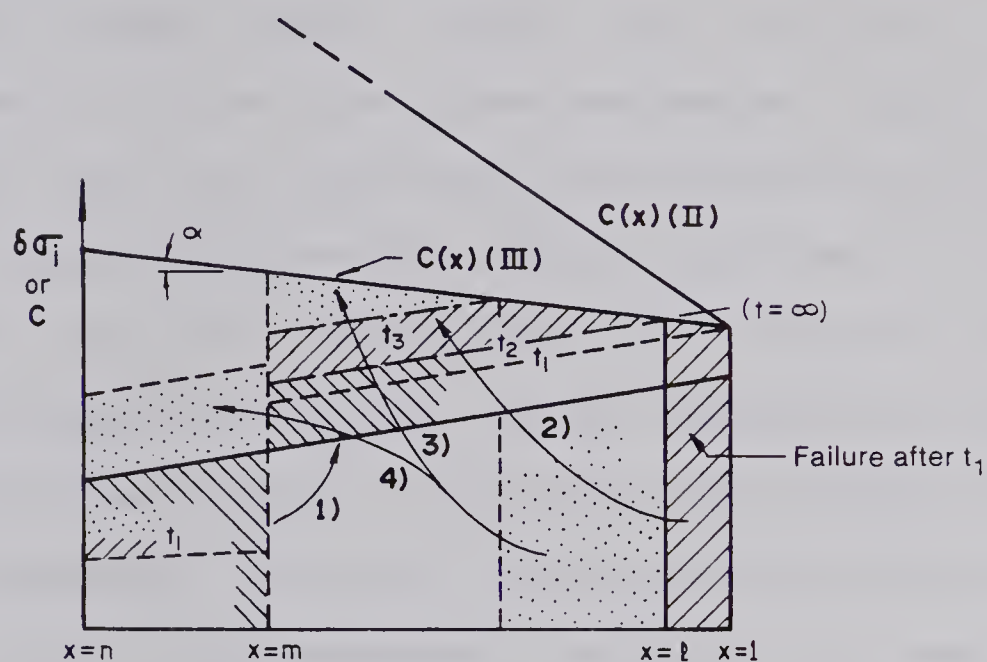


Figure 4.16 Creep Test on Model with Continuous, Linear Parameter Distribution Function; II) $\delta=\delta_1$, III) $\delta=\delta_2$

5(II) is therefore lower, relative to the model strength, than the stress level 5(III). Up to time t_1 stress is transferred (1) to the time-independent units and the behaviour can be described by the differential equation. Further stress transfer will lead to collapse of a number of elements (e.g. (1) elements). This changes a) the model parameters and the constants in the differential equation of the model and causes b) an additional stress transfer to time-independent units (2 and 3), and if the rate is high enough, to time-dependent units(4). A numerical and iterative program could be developed to model this process.

Depending on the parameter distribution functions (e.g. $C(x)$) different strain-time relationships will result. For example, as shown in Figure 4.16 failure will start in both cases at time t_1 as soon as the unit $C(n)$ is overstressed. In case (III) strain will gradually increase and collapse occurs. In case (II) the strength of the remaining units is high enough even at infinite time to carry the applied load and the deformation rate will increase initially and then decrease during stress transfer. The deformation will terminate eventually. More complex models and effects of different parameter distribution functions can be evaluated by the proposed mathematical model.

4.6 Summary and Conclusions

A phenomenological model for time-dependent failure processes in strain-weakening rock has been presented, described and tested qualitatively on published test results from creep tests, relaxation tests and variable strain rate tests. The model indicates that rock basically consists of a time-independent and a time-dependent resistance to deformation. The time-independent resistance is mobilized and the strength is lost as a function of total accumulated strain. The time-dependent resistance is a function of stress-history. Various parameter distribution functions are necessary to model different types of rocks but it was found that the proposed model can describe essentially any observed time-dependent rock failure behaviour. Figure 4.17 summarizes in schematic stress-strain diagrams the predicted response of the model to various stress histories. In each diagram hypothetical curves for

- the "actual peak fracture envelope";
- the current long-term strength (a);

and

- the current available strength (b)

are shown to facilitate comparison. Curve (b) represents the current available strength for the special case of instant loading. Any other stress-history creates its own current available strength curve. It may be observed from Figure 4.17 that:

- Constant strain rate tests may or may not reach the

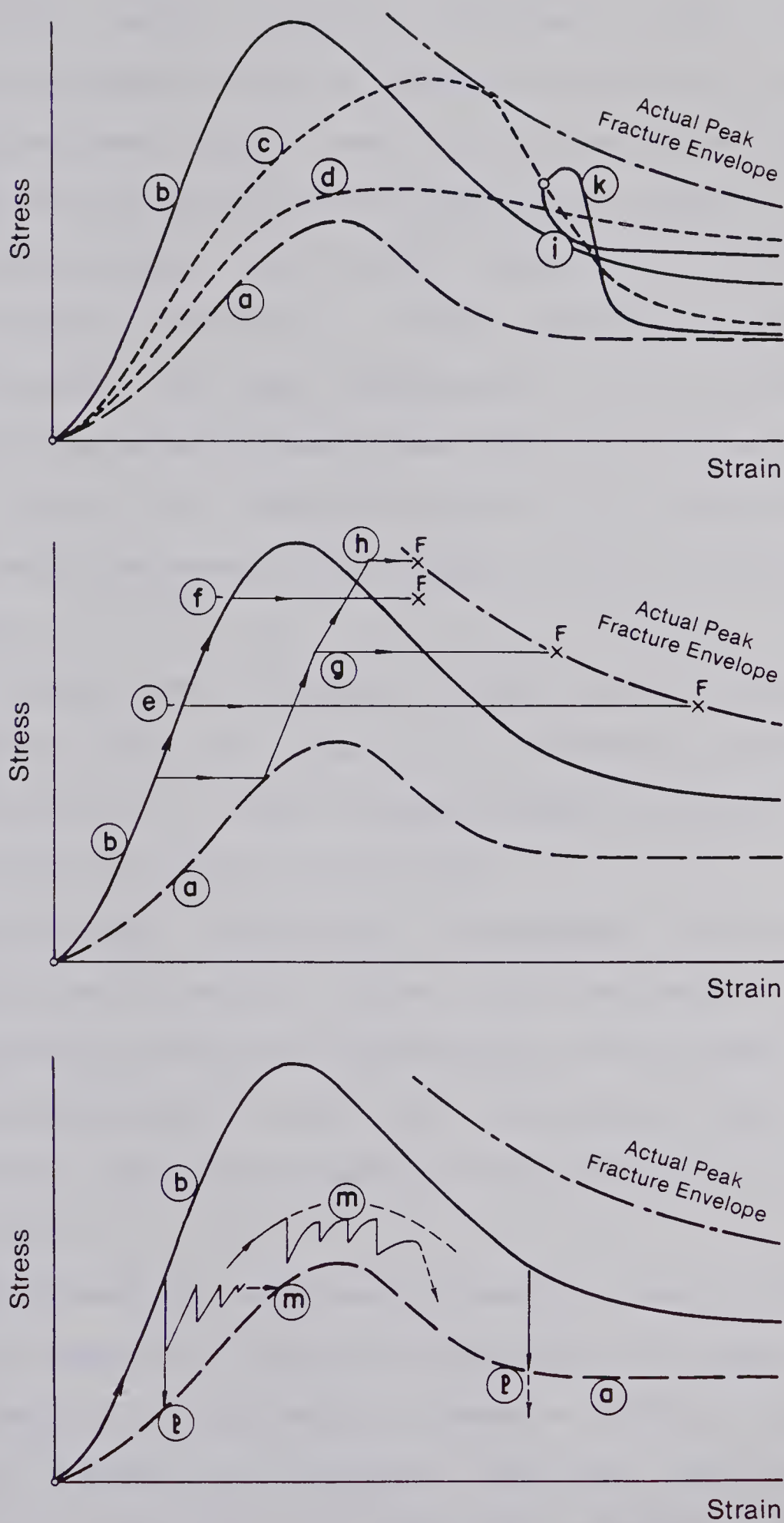


Figure 4.17 Schematic Stress-Strain Diagrams Predicted by Proposed Model

- "actual peak failure envelope". They exhibit a rate-dependent ultimate strength (curves (c) and (d));
- Single-stage creep tests fail at or below the "actual peak failure envelope" (curves (e) and (f));
 - Multiple-stage creep tests fail, as a function of stress-history, at or below the "actual peak failure envelope", but not necessarily at the same failure strain as single-stage creep tests (curves (g) and (h));
 - A strain rate decrease results in an initially faster strength decrease with a higher ultimate strength (curve (i)).
 - A strain rate increase results in a secondary peak strength (or at least in a reduced strength loss) followed by a more rapid strength loss and a reduced ultimate strength (curve (k));
 - Single-stage relaxation terminates at the current long-term strength (curve (l)). Relaxation beyond the long-term strength is possible in the post-peak range if time-independent units are overstressed due to energy release from time-dependent units during the relaxation period;
 - Multiple-stage repeated relaxation tests terminate at the long-term strength curve before the long-term peak strength is reached and thereafter follow a path (curve (m)) between the current long-term strength and the current available strength. The relaxation rate varies as a function of the stress level relative to the

current available strength and the extent of the range between the current available strength and the current long-term strength.

An extensive research program is necessary to test this model, to extend the phenomenological model into a mathematical model, and to determine the parameter distribution functions for various classes of rock. A possible procedure for the development of the mathematical model was discussed briefly.

The implications of the proposed model with respect to the behaviour of rock masses are numerous. Rock masses behave in a manner similar to overstressed "intact" rock specimens (Mueller and Goetz(1973)) and exhibit, in general, a less brittle stress-strain relationship (Reik and Zacas(1978)). The model may be used to simulate rock masses if the stress-history, which was experienced by the rock during tectonic and man-made stress changes, is applied to the model or if the stress-strain curves for the time - independent and time-dependent units are selected so that they correspond to the rock mass properties. The model should predict adequately the response of a rock mass with time due to a given stress change whenever the behaviour is dominated by the properties of overstressed rock. A general discussion of the implications of the time-dependent failure process is given in Chapter 1.

Areas of application of the presented model may be separated into three classes:

- unconfined failures (e.g. rock slope stability);
- progressive failures;
- confined failures (e.g. underground excavations).

From the model it can be concluded that unconfined failures are controlled largely by the long-term peak strength. Failure initiation leads to a rapid collapse. This failure mode is similar to failure mode during creep testing and therefore is adequately described by creep tests.

In natural materials, even under uniform load conditions (e.g. gravity), complex stress distributions are created within the rock mass due to stiffness variations, discontinuities and the roughness of such discontinuities. Local overstressing and stress-redistribution as simulated by the model explains progressive failure modes in materials with time-dependent strength and strain - weakening characteristics.

High stress concentrations are created near openings and may cause overstressing of rock in the low-confinement area near the opening. As a consequence of time-dependent failure or yielding, stresses are transferred away from the opening to high-confinement areas. Several protective shells are developed around an opening (Mueller et al. (1978)). The proposed model will be extremely useful in numerical simulations to describe this process.

In opposition to the case of unconfined failures the time-dependent stress-redistribution in confined conditions is largely controlled by the visco-plastic, strain-weakening

post-peak stress-strain behaviour. The proposed model constitutes therefore an essential element in support of current research efforts to explain time-effects on tunnel design in overstressed rock. Stress development within fault zones and related energy transfer or release constitutes another area where the process described by the model is of great importance.

CHAPTER 5

DEVELOPMENT OF GEOMECHANICAL MODELING TECHNIQUE

5.1 Introduction

5.1.1 Reasons for Geomechanical Model Studies

The main purpose of the geomechanical model studies reported here is to evaluate the behaviour of cavities in rock masses with time-dependent properties and particularly to study the time-dependent failure process in overstressed rock surrounding cavities. Our understanding of the behaviour of overstressed rock masses near underground openings is poor because the physical failure process is an extremely complex problem and is not fully understood.

Underground cavities are often expanded to collapse or they have to be supported to allow further excavation. As a consequence, the rock surrounding the opening is overstressed and will eventually fail. Because of the time-dependent strength of these rocks and the confined conditions around an opening, a progressive failure process and stress redistribution develops. This process controls the behaviour of an opening and depends largely on the following factors: natural state of stress in the rock mass; mechanical properties of the intact rock and the discontinuities of all sizes which control the properties of the rock mass; geometry of the opening; excavation method; support system; and construction sequence, with time as an important parameter. The importance of this process is

receiving increased attention by researchers but there have been only limited attempts to develop cavity support procedures based on an understanding of the time-dependent strength of rock.

There are two promising ways to attack this problem: a study of case histories, or the use of physical models. Ideal case histories are limited in number, are often not in the public domain, and extrapolation to other sites is often not possible. Model tests have the drawback that artificial materials have been used in the past, but this drawback has been overcome through the selection of a natural material (coal) which represents an almost ideal model material for a jointed rock mass possessing the required time-dependent properties. Mathematical or numerical models cannot be used at this stage since the purpose of this research is to delineate the failure process. Nevertheless, the results from Chapters 3 and 4 give some indication as to how the results from the model test might be simulated by numerical models. The required model for a strain-weakening, visco-plastic material for finite element modeling is not available at the present time and has to be developed for this purpose.

The most promising technique for the study of the time-dependent behaviour of openings in rock masses appears to be the use of geomechanical models. In the conventional technique, a small scale model is constructed in a material which accurately represents the properties of the actual

rock mass in the field. All other conditions such as stress state and boundary conditions are then selected so that the requirements of similitude are satisfied. The behaviour of the model then represents the behaviour of the prototype with respect to stress, strain and displacement distribution. There are relatively few theoretical limitations on this technique. Elastic and inelastic material as well as failure modes can be simulated. However, technical problems are often not insignificant and it is often not possible to satisfy all similitude requirements.

The model tests undertaken here differ from conventional tests. No attempt was made to model one specific prototype as far as mechanical properties, geometry and excavation process, are concerned. The purpose of these model tests is to simulate the time-dependent response of a rock mass to a given stress-history and to simulate the time-dependent failure process of an opening in a strain-softening or more accurately strain-weakening material with time-dependent deformation and strength properties.

The validity, usefulness and theoretical basis of model studies in general and of structural and geomechanical models in particular has been well established. Heuer and Hendron(1971) give a brief literature review and summarize the similitude considerations necessary for the study of underground openings in rock with time-independent properties. Mandel(1963) discusses similitude of time-dependent materials such as visco-elastic and

visco-plastic materials.

Many investigators did not satisfy some critical aspects of similitude requirements such as boundary loading conditions or material properties. Their work is therefore of limited value. The test system used by Heuer and Hendron (1969) overcomes many of these deficiencies and it was decided to rebuild and modify their test apparatus. The most important factors of this system are that it allows testing of materials with high friction angles in a plane strain condition while controlling friction along the loaded faces of the model. In addition, the system of load application makes strain measurements behind the tunnel wall possible.

5.1.2 Scope of Study

This study consisted of two phases: 1) the development and modification of the geomechanical modeling techniques, and 2) testing of coal samples to study the pre-failure behaviour of an opening in a rock mass with time-dependent deformation properties. The first phase included the development of: a) the test frame and the hydraulic pressure system, b) a sampling procedure and a method to prepare and instrument the sample, and c) the data processing system. In the second phase, model blocks of jointed coal, without or with a circular unsupported opening, were loaded in stages to external pressures of up to 15 MPa, more than two times the expected unconfined compressive strength of the coal. The tunnel closure and the strains within the model mass

were recorded as functions of time during 5-day periods of constant load. The ratio between the vertical and horizontal stress was varied between tests. The results of these tests are compared with solutions for elastic and visco-elastic materials to contribute to our basic understanding of the behaviour of underground openings. This information is most valuable in the evaluation of the results from a third phase on which Guenot (1979) has reported. He describes and discusses the data recorded during the collapse of a tunnel in a coal sample. The results from all three phases will be valuable in planning instrumentation programs for field measurements in real openings and assist in the development of the observational tunneling method.

5.2 Rock Modeling Materials

A mixture of water, plaster of Paris and sand (1.2/1/9) as designed by Heuer and Hendron (1969) was used for the preliminary testing to check the loading apparatus and the sample instrumentation. Since the results from these tests will not be reported in this thesis further details about this material are omitted. Nevertheless it is of interest to summarize the mechanical properties of this mixture as determined by Heuer and Hendron (1971) since it was used to calculate the capacity of the test frame. The mixture had an average angle of internal friction of 35 degrees and an average unconfined compression strength of 4.15 MPa. The ratio of Young's modulus to unconfined compression strength

was about 1500, which is higher than the average for rock. The Poisson's ratio was found to be strongly influenced by the loading path but assumed to be higher than 0.15.

The properties and origin of the coal used as a model material were discussed in detail in Chapter 2. The average angle of internal friction is 30 degrees and the average unconfined compression strength, which depends largely on the structure of the sample tested, was estimated from triaxial tests on jointed samples and at low confining pressure. It was found to be comparable to the unconfined compression strength reported for the sand-plaster mixture (Heuer and Hendron, 1969). After extensive testing of coal blocks it was realized that this value was underestimated significantly or that the stress concentration near the tunnel was much less than predicted from linear elasticity. The unconfined compression strength of the coal would have to lie between 8 and 12 MPa. The corresponding ratio of Young's modulus to unconfined compression strength is about 200 for instantaneous loading, similar to an average for rock, and 100 for infinitely slow loading, which is somewhat lower than average for rock. The Poisson's ratio, calculated by Guenot (1979) from tests on blocks without a tunnel and subsequent tests on blocks with a tunnel, increases with stress level from close to zero to approximately 0.2 at field stresses of 6 MPa.

Without discussing in detail the theory of similitude it is of interest to mention a few of the more stringent

requirements on the behaviour of model materials as compared to real rock. The theory of similitude requires that Buckingham pi-terms containing all of the pertinent variables which influence the phenomenon under study have to be equal for the model and the prototype. For actual rock the most relevant pi-terms which have to be satisfied are: $5\% < (5_t/5_c) < 10\%$; $250 < (E/5_c) < 500$; $25^\circ < \theta < 60^\circ$; $0.1 < \nu < 0.3$. The model laws require further that, on any dimensionless plot of strength (e.g. normalized to 5_c), the data for both the model and prototype materials must collapse onto a single line. Similarly for the deformation characteristics, normalized stress-strain curves must coincide. This implies that the two materials must fail, under comparable confining conditions, at the same strain. Axial failure strains for natural rock range between 0.2 to 1.0% in unconfined compression tests and 1% to as high as 10 to 20% in triaxial compression tests at confining pressures equal to the rock's unconfined strength. For a model study in which inelastic deformations and failure conditions are important, the model laws must be satisfied as nearly as possible. Patterns of stress and strain distribution differ considerably from those of the prototype if these model laws are not satisfied accurately.

In summary, the static strength and deformation properties compare well with properties of real rock. A satisfactory degree of similitude is achieved but extreme care has to be taken when results of inelastic deformation

measurements and failure modes are applied to real conditions. Further testing to determine the time-dependent material properties and an extensive evaluation of similitude to time factors is relegated to further research.

5.2.1 Sampling Procedure

The origin, geology and location of the coal seam from which the samples were collected are described in Chapter 2. The following describes the procedure adopted to collect block samples of approximately 90 by 90 by 45 cm from the top of the upper main seam in the west pit at the Highvale Mine (Sundance).

The usual mining procedure of removing the overburden by dragline, immediate loosening of the coal seam by blasting and subsequent excavation of the coal by a power shovel, was altered to accommodate a one-week sampling period. Blasting was stopped about 50 to 100 m from the sampling site, the overburden was then removed by dragline and the coal surface was cleaned by a bulldozer. A pattern for 9 samples was outlined and a series of closely spaced holes ($d=6\text{cm}$) were drilled to a depth of at least 2 m (Plate 5.1.a). The rock bridges between the holes were removed by hand-drilling inclined 2.5 cm holes. In a later sampling program these rock bridges were broken to a depth of 50 cm by use of a pneumatic hammer (Plate 5.1.b). The coal was then excavated on two sides of the predrilled sampling area (Plate 5.2.a) to a depth of approximately 1.5 m by a



**Plate 5.1 Drilling of Holes along Sample Boundaries and
Breakage of Rock Bridges**



Plate 5.2 Excavation around Samples, Breaking off and Loading of Samples

bulldozer. Depending on the composition of the coal and particularly the location of clay-shale seams, one or two levels of horizontal holes were drilled to weaken the bedding plane. Two steel rods were inserted at these levels and a steel cable was connected to each end of these rods and to the blade of the bulldozer which broke the sample off and loaded it on to a truck (Plate 5.2.b). The samples were then trimmed to create a flat support area, positioned on foam to reduce vibrations during transportation, and strapped and prestressed with steel bands to inhibit tensile stressing. Upon arrival at the laboratory the samples were cleaned (all loose material was removed) and sealed with two coats of latex. The samples were stored in a humidified room.

Before testing, the samples were trimmed to size (61 x 61 x 20.3 cm) by Alberta Granite Marble and Stone Co. Ltd. This company owns the biggest rock saw (4 foot blade) in Edmonton. The two larger sides (61 x 61 cm) had to be cut from two sides. This created alignment problems and made additional (undesired) handling of the sample necessary. The coal possesses very little tensile strength perpendicular to the major joint set and perpendicular to the bedding plane. To reduce the possibility of breakage and to increase the recovery rate, samples were strapped after each cut parallel to the next cutting plane. Finished faces were covered with plywood to protect the sample corners and to distribute the prestressing stresses. This procedure resulted in a

reasonable recovery rate. Visual inspection of the samples during the trimming showed that all of a somewhat desiccated crust of approximately 5 cm thickness was removed. After trimming, the blocks were sealed with two coats of latex, wrapped in plastic, covered with plywood, strapped in the three principal directions, and stored at 10°C and 100% humidity.

5.3 Model Test Apparatus

5.3.1 Introduction

The general concept of the equipment described below was developed, tested, improved and modified by Heuer and Hendron (1969,1971). The extensive evaluation, description and discussion of this system, of all successful and unsuccessful alterations, and the consistent results produced by these authors showed that an extremely versatile model test apparatus had been developed which fitted the proposed research objective. Furthermore, it was felt that the development of a completely different system would cause a delay of at least one year. The strength of the proposed model material was estimated on the basis of direct and shear test data (Noonan(1972)) and found to be almost identical to the strength of the model material used for the design of the original test frame. As a consequence, it was decided to rebuild an almost identical test frame and to design an hydraulic system with a slightly higher capacity. A brief summary of the original design and a detailed

description of all alterations is given in the following sections.

Heuer and Hendron (1969,1971) discuss in detail the reasons for the selection of the final model configuration, boundary conditions, design criteria and various unsuccessful attempts to satisfy these requirements. The major points which were considered in the design of the model test system are summarized in the following list.

1. A circular, cylindrical opening can be excavated easily by coring and simple mathematical solutions are available for comparison.
2. The model should be as small as possible for economy but as large as possible for technical reasons. The only modeling requirements on linear dimensions are that the ratio of joint spacing to tunnel diameter be modeled accurately, and that the block be at least 4 to 6 tunnel diameters in width so that a relatively uniform "free field stress state" can be achieved. A tunnel opening of 10 to 15 cm is desirable to reduce complications during the installation of the instrumentation to measure tunnel closure.
3. Body forces are neglected as a matter of convenience. The position of the block with the tunnel vertical greatly simplifies the design.
4. Various N values ($N=5p/5y$) with uniform pressure distribution along the block sides are desirable.
5. Plane strain conditions with no strain in the direction

of the tunnel axis best represent the field conditions. Three possible techniques were evaluated: uniform pressure application, rigid heads and load-controlled rigid heads. The latter was selected after extensive evaluations.

6. Under plane stress condition shear failure into the unloaded face could develop but plane strain condition do not eliminate this possibility completely.
7. The frictional resistance between the model block and the rigid heads should be minimal. A extensive testing program showed that a waxpaper-teflon-teflon-waxpaper sandwich with a friction angle of 30° was the best solution.
8. On the basis of a minimum stress concentration factor of two and the assumption that the unconfined compression strength (4 MPa) should be exceeded by at least a factor of three, the load frame and hydraulic system have been designed for 7 MPa lateral or vertical field stress (Heuer and Hendron(1969), Figure 44). (The University of Alberta version of the loading frame was later strengthened to accommodate more than twice this design load and was used at field stresses of up to 16 MPa).
9. For a Poisson's ratio less than 0.25 and N greater than $1/3$, the longitudinal stress is the minor principal stress. Failure of the intact block should not occur except if N is less than one and if the joints have low cohesive and frictional resistance (Heuer and

Hendron(1969), Figures 45 to 48).

10. To maintain plane strain conditions the longitudinal expansion of the model should be restricted to the order of less than 0.01 mm (this value is a function of the material properties).
11. A flexible, lateral loading system (sets of triangles) was selected to accommodate 1 to 2 cm of lateral movement and non-uniform deformations.
12. The load is applied actively to all four sides of the block to maintain loading symmetry, to keep the tunnel axis stationary with respect to the loading frame and to have symmetric distribution of the frictional resistance between longitudinal loading heads.

Our experience shows that these criteria resulted in unsatisfactory conditions especially for long-term testing. Firstly, the sample, loaded by 8 "point loads", is free to rotate. Such a rotation actually occurred when the rams were not aligned perfectly or after some translational movement had occurred due to small load differentials between rams. These load differentials were not detected by Heuer and Hendron (1969, 1971) since they did not measure the load between ram and sample. During long-term testing the ram friction changes from static to dynamic friction as soon as the ram moves and may reach relatively high values if the direction of the ram movement is reversed. Translation of the sample causes a slight rotation of the rams

resulting in a force couple. The effects on the stress and strain distribution in the sample may be undetectable, but this force couple may cause rotation of the sample because of the low frictional resistance between the longitudinal loading heads ($\theta=3^\circ$, the longitudinal stress σ_l is small especially if the Poisson's ratio is small). Secondly, it was observed that the load measured between the sample and rams pressured from one pump varied up to about 10%. This occurred when the sample translated or started to rotate. Again, it is felt that the internal ram friction and particularly the difference between static and dynamic friction, as a function of movement direction, was the reason for this load variation. A test set-up with two passive reactions and individually controllable rams would be advantageous.

13. The stress distribution within a test block was evaluated by internal strain measurements and crack pattern studies of samples sprayed with a brittle lacquer coating. It was found that a uniform strain distribution was reached at less than 4 cm from the sample boundaries.

5.3.2 Description of the Model Loading System

The original design is described by Heuer and Hendron (1971). In the following only a brief description of the major unaltered parts together with a discussion of the modifications is given. Working drawings are given in

Appendix A5. An overview of the loading frame is given in Plate 5.3.

Longitudinal Restraint and Reaction Frame: The sample is oriented with the tunnel axis in the vertical direction and the plane strain condition is maintained by a controlled rigid longitudinal loading head (Figure A5.1). The sample sits on a passive reaction head composed of a concrete block (covered with a steel plate) above the lower longitudinal reaction head (Figure A5.2). On the opposite side a rigid loading head (Figure A5.3) is pressed actively by four rams against the upper longitudinal reaction head (Figure A5.4) and the sample top. Two channel irons instead of stiffener bars are used in our version of the upper reaction head to facilitate testing of smaller (1 x 1 foot) samples with only one ram per sample face. The displacement of the loading head is measured relative to the passive reaction head and longitudinal expansion is nulled by load application through the four rams. The deformation measuring devices (dial gauges and LVDTs) are mounted on rods which are fixed to the steel plate between the concrete block and the bottom face of the sample block. The loads are recorded on four load cells; this allows the calculation of Poisson's ratio in the longitudinal direction (perpendicular to the bedding plane). Values of less than 0.1 have been measured. The hydraulic system is designed to supply and maintain constant oil pressure for each ram or to pressure each ram individually by hand and lock in oil pressure. Even though the hydraulic

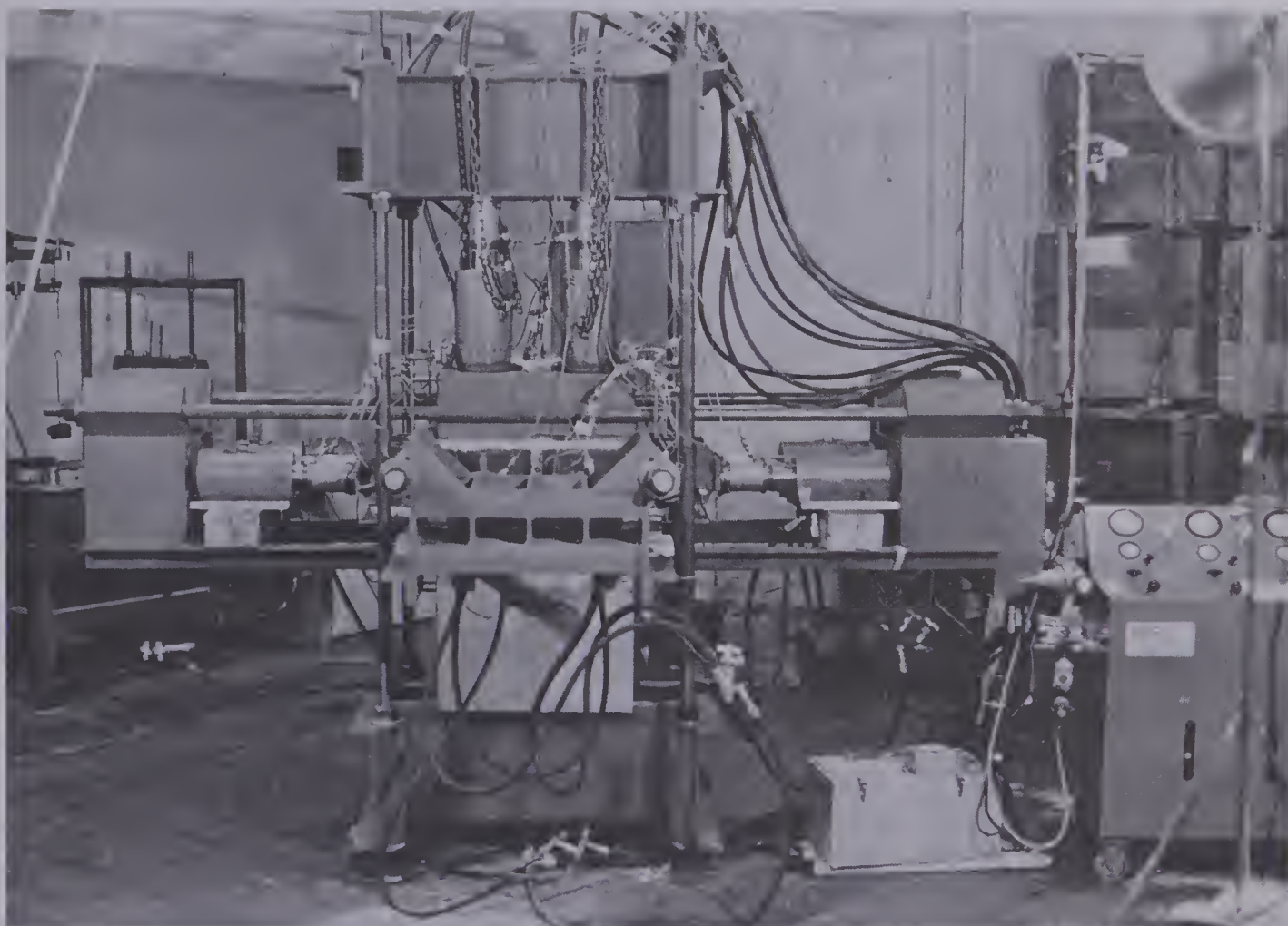


Plate 5.3 Loading Apparatus

system is quite versatile, a certain experience is necessary to prevent translational or rotational movement. Note that the loading head contains a removable steel plate. This allows pressurization of the full face during tests without a tunnel, or insertion and adjusting of instrumentation through a hole in the steel plate during testing with a tunnel, or visual observations of fracture development.

Cantilevered Lateral Reaction System: A symmetric cantilever with movable special steel tie rods was designed to inhibit bending stresses due to eccentric force application and for simplified sample installation. For those members in which deformation was not a controlling factor, the reaction frame was designed for extreme fiber stress of 138 MPa in both tension and compression in the rolled steel sections, which were of A36 steel. The horizontal and vertical tie rods were subjected to higher stresses in the threaded sections, and were of higher yield steel (H.T.SPS). The capacity of the original design was increased after an initial testing period by welding additional angle irons to the cantilever and improving the conditions at points of load transfer at the horizontal reaction heads. The modified design and a general view of the lateral loading assembly are shown in Figure A5.5, A5.6, and A5.7. The last figure indicates schematically and Plate 5.4 shows how the load is transferred from the rams through the load cell and a set of triangles to the sample. Heuer and Hendron (1969,1971) proved that this system leads to a



Plate 5.4 Lateral Load Distribution by Triangle System

satisfactory stress distribution within the test block. The load cells, which were added to determine the exact load distribution, are hollow aluminium cylinders with internally mounted strain gauges. These load cells are positioned on a flat surface on one side and on a lubricated, spherical seating on the other side to ensure that no bending moments are introduced.

Hydraulic Loading System: This system consists of three major parts: 12 rams; a pressure console with three Haskel-pneumatic pumps; and a safety system to prevent damage of the instrumentation during tunnel collapse, power failure or sample rotation.

The hydraulics was designed to our specifications by Northern Hydraulics Ltd., Edmonton. The double acting hydraulic rams, with a piston area of 129 cm^2 , have a capacity of 890 kN at 69 MPa maximum oil pressure. The rams are controlled in groups of four from a console with three pneumatic (air - over - oil) pumps with a pressure multiplication factor of 100. A schematic drawing of the hydraulics is given in Figure A5.8 and the console is shown in Plate 5.5. Air pressure of maximum 1.7 MPa is normally supplied by an air compressor or from a general air-supply-system (maximum 0.5 MPa) in case of a power failure. The switching is automatic if the required pressure is less than 0.5 MPa and manual with a 24-hour alarm system, otherwise. This is necessary since a small pressure drop below the required level may result in a differential load

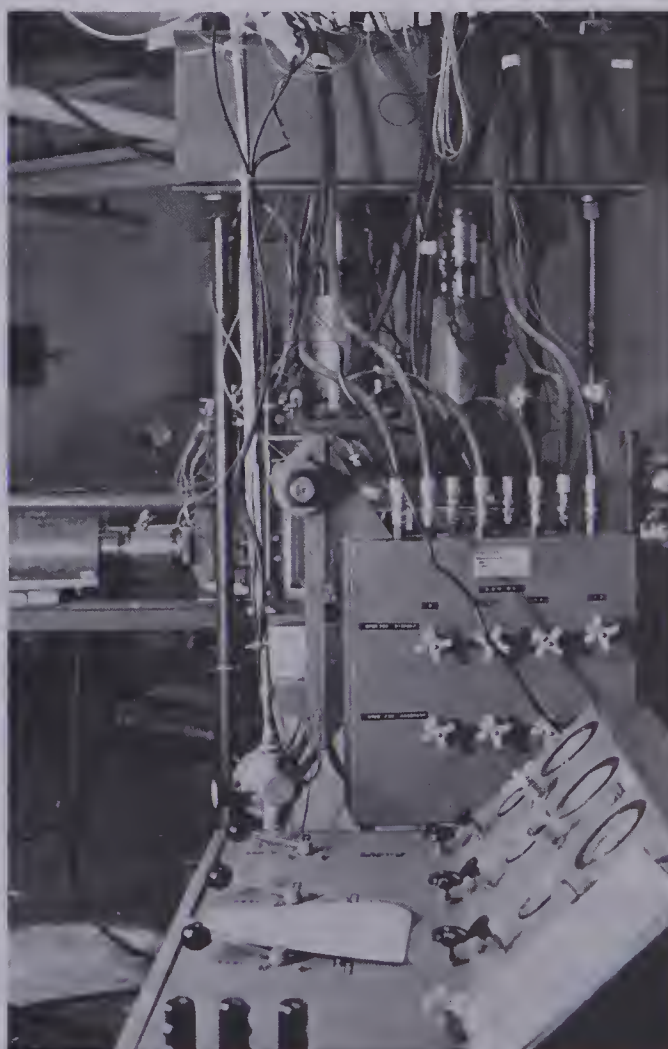
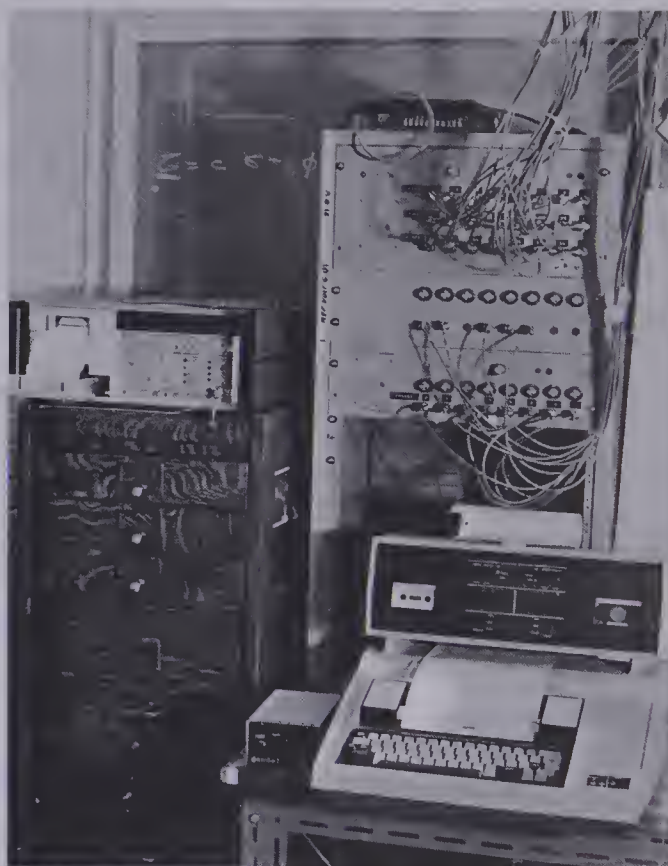


Plate 5.5 Pressure Control Systems and Data Acquisition System

on the rams if one ram is leaking internally.

The dewatered and cleaned air is regulated to the required pressure which is then multiplied 100 times by a pneumatic pump. A separate air line (not shown in Figure A5.8) is used to move a pilot valve in the pump which otherwise would move too slowly due to the air-flow-volume restriction in the regulator. From this pump the oil flows through a high pressure hose/valve system to the rams. The magnitudes of the air and the oil pressures are displayed on the console, a reversal valve allows retreat of the pistons and a fine bleed-by valve together with an air-pressure reduction is used to unload the sample. A hand pump was installed in parallel with the pneumatic pump to maintain the pressure during air pressure loss and to control each ram individually by locking the remaining rams. A special arrangement which allows operation of each ram without locking other rams was used for the longitudinal rams.

This system can maintain pressures over a period of five or more days with pressure fluctuations of less than one percent (see Figure 5.2). The cycling of the pumps introduces load variations of less than 0.1% and the number of cycles per hour depends entirely on the internal leakage of the rams and the leakage of the hoses. This points out the two most critical factors of the hydraulic pressure system. It is almost impossible to prevent these leaks at pressures of 70 MPa. Extreme care must be taken when handling high pressure hoses to prevent any bending near the

connections. As far as the rams are concerned, there is a trade-off between internal leakage and ram friction. It was found that: (a) low pressure seals are easily damaged after one or two loading cycles but prevent high ram friction; (b) high pressure seals are adequate at high pressures but are too stiff to provide a good seal at lower pressures, and high ram friction must be accepted. Two additional factors have to be considered in the design of high pressure rams for long-term use: (a) the wall thickness or the material type has to be selected such that barreling during operation is less than the tolerance required for the seals; (b) the ram should be short and capable of operating with the piston close to the bottom of the ram. This reduces the pressured section of the ram and prevents barreling and therefore leakage.

NOTE: All rams are designed for 69 MPa but the piping for pump number three, for the longitudinal rams, was designed for 41 MPa only. Eight new rams with high yield steel were built and are marked accordingly.

Safety System: Micro-switches were installed at each ram to turn off the air-pressure as soon as excessive movement occurs. This prevents damage of instruments during collapse of the tunnel, unexpected failure of the model block or undesired (but possible) rotation of the sample block. These switches are powered from a battery and are therefore active during power or air pressure failure. Another safety system turns off the high pressure air system

if the switch to lower air pressure was activated. This prevents uneven reloading by the automatic pressure system.

The system described has been used successfully during continuous test periods of more than three months.

Data Acquisition System: The data from all load cells and deformation measuring devices (LVDTs) are recorded automatically. About 50 instruments are scanned in even time intervals of less than a minute up to several hours by a Fluke 2240B Datalogger. The readings are recorded by a Silent 700 ASR terminal on tape and paper, and can be transferred to the central computer between recordings (Plate 5.5). The data may then be processed from the same terminal and the results may be plotted on a Tectronix 4014 or a hard copy may be obtained. The data transmission and processing takes in general less than one hour from the time the last reading was taken to the point where the processed results can be examined on the Tectronix. This procedure allows examination of data from a loading increment before the next increment is applied. Unprocessed data can be used in the meantime to evaluate the test performance.

5.3.3 Instrumentation, Preparation and Installation of Model Blocks

All model blocks of coal tested were installed with the following parameters fixed: unlined tunnel with a tunnel diameter of 12.5 cm, bedding plane perpendicular to the tunnel axis and major joint set inclined at 45° to the

tunnel axis. The following measurements were taken during the duration of each test: loads applied by each ram to sample, overall straining of the block, strain measurements inside the test sample by extensometers measuring over an average distance of 5 cm at distances of approximately 1.75 and 2.5 times the tunnel radius from the tunnel axis, and the tunnel closure in four directions (parallel, perpendicular and at 45^0 to the joint direction).

Sample Instrumentation: The tunnel closure was measured by LVDTs (with a range of ± 2.5 mm) mounted on a stand fixed to the steel plate below the sample. The cores of the LVDTs were spring loaded. The set up was such that two LVDTs mounted on one diagonal measured points on two circumferences approximately 1.5 cm apart and LVDTs oriented in different directions measured points on two circumferences approximately 2.5 cm apart. Closure measurements were therefore made over about 50% of the tunnel length. In a newer development, two LVDTs were mounted on the same axis with the cores pressured towards the tunnel wall by a spring in between the two LVDTs. A picture of this set-up is shown in Plate 5.6 The distance between the diagonals is about 2.5 cm. The tunnel closure has to be calculated in both systems from the difference between two LVDT readings.

The overall straining was calculated from the displacement difference measured from stands fixed to the steel plate, to pointers on opposite sides of the sample.

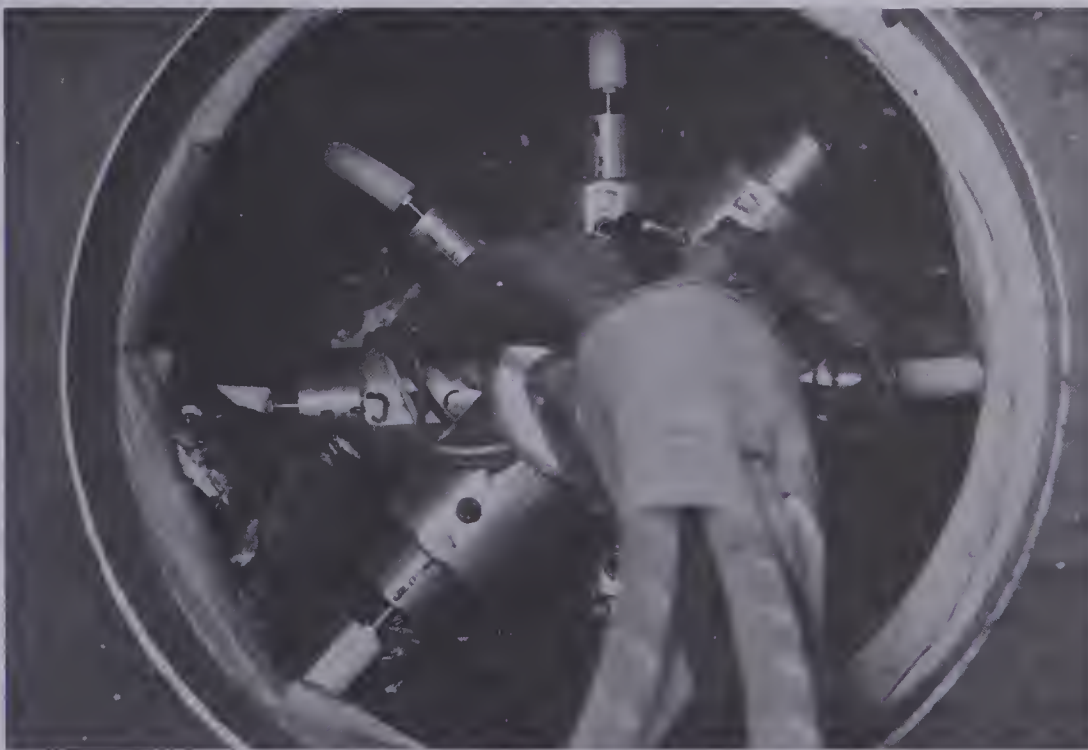
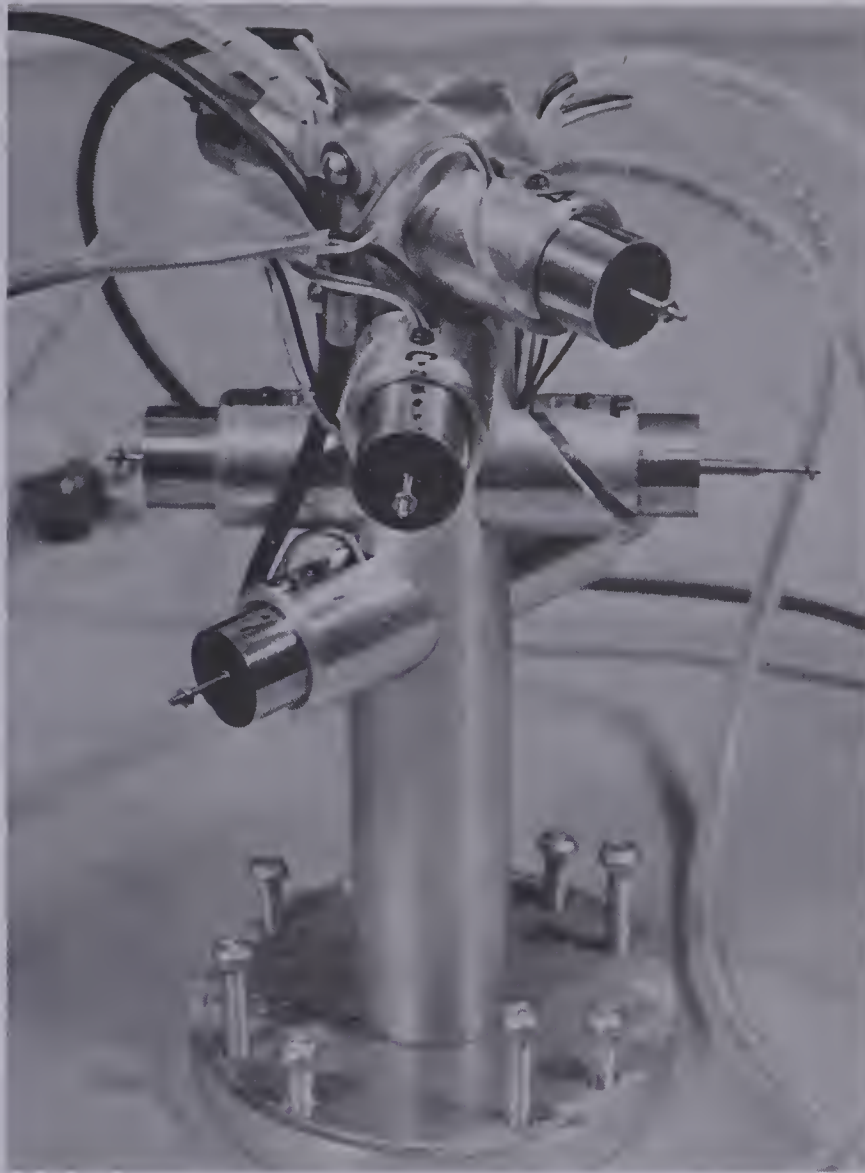


Plate 5.6 Instrumentation for Tunnel Closure Measurements

These pointers have been grouted into the sample at a depth of 3 cm.

Extensometers were used to measure average radial strain within the sample mass. The system which was used initially is shown in Plate 5.7. Two 7 mm holes were drilled 2.4 cm apart, perpendicular to the tunnel axis to depths 5 cm apart. Two pipes with 3 mm outside diameter were inserted into these holes with washers fixed to them at a distance of 1 cm from the end. Five-minute-epoxy was then forced through this pipe to grout the split end of the pipe. The volume of the epoxy was controlled by filling the pipe before it was inserted into the hole. An LVDT was fixed to one pipe and the core of this LVDT was pressed by a spring onto a pointer mounted on the other pipe. This system worked in general satisfactorily except if one pipe was bent during the loading process. This rotational movement of the LVDT caused questionable radial strain measurements in some cases.

As a consequence, the following new system was developed and used since. One 10 mm hole is drilled first and then extended by a 7 mm hole. In this case, both anchors of the extensometer are installed in one hole. First, a stainless steel 1.2 mm rod is grouted to the end of the hole, then a stainless steel pipe (3 mm OD) is inserted over the rod and grouted 5 cm further back. The grouting procedure had to be altered since there was no space to inject glue besides the rod or the pipe. A tight teflon washer is located approximately 3 cm behind the tip of the

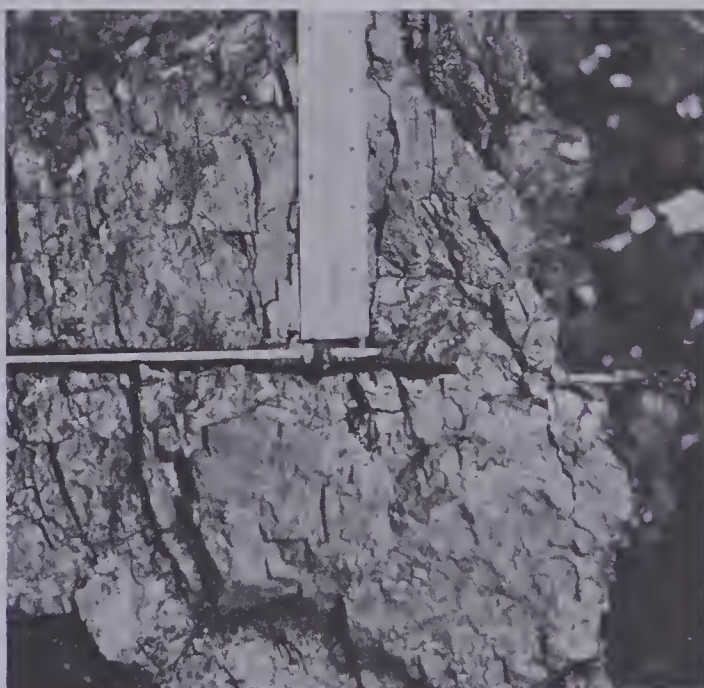
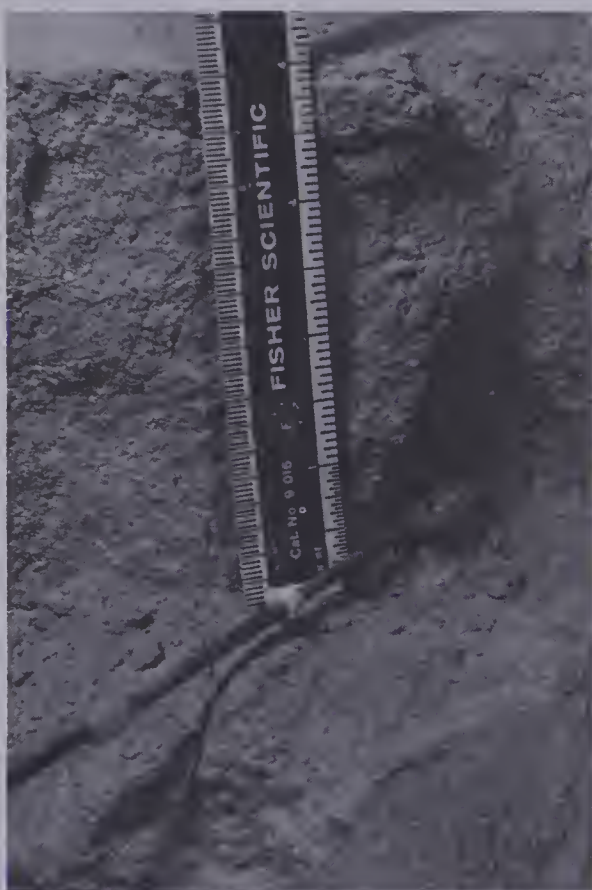
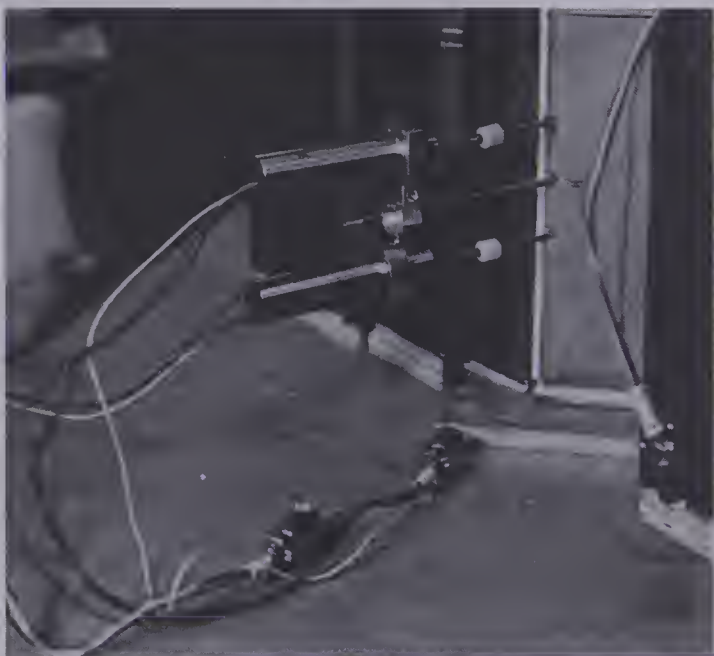


Plate 5.7 Old Extensometer to Measure Internal Strain

rod or pipe, Colma-Dur Gel, a paste-like glue, is then painted around the end of the rod (or pipe) and carefully inserted into the hole. The teflon washer is then pushed by a pipe of larger diameter. This teflon washer pushes the glue ahead and compacts it against the end of the hole. For the second anchor a rubber washer is positioned at 1 cm from the end of the pipe and the glue is forced towards this washer. After testing, all instruments were excavated and the bond between rod or pipe and sample was checked. The exact location of the first and second washer was measured before testing. A protection rod, with the same outside diameter as the hole, is inserted over the extensometer to reduce friction during testing and to reduce the effects of the holes on the sample stiffness. Outside the sample, the LVDT is fixed to the pipe and the core of the LVDT is connected to the rod. Plate 5.8 shows this set-up and a rod which was excavated after testing.

Sample Preparation: The pretrimmed sample is taken from the moist-room and all sides are sanded with coarse sandpaper and to insure that all faces are planar. At this stage all surfaces are mapped carefully. Because of the low tensile strength of the joints and bedding planes it is often necessary to infill small broken off corners or joint blocks. Sulfaset 190 (a stiff, high strength grout) is used for these repairs. This may create some stress concentrations near the boundary but assures plane strain conditions. The sample is then placed in an aluminium mould

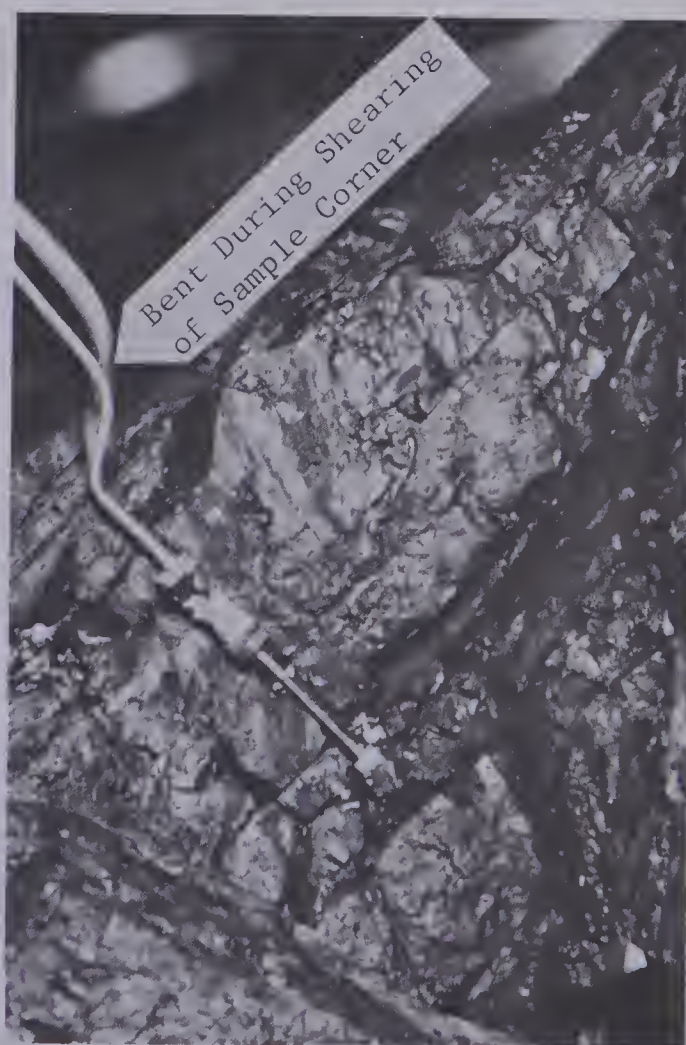


Plate 5.8 New Extensometer to Measure Internal Strain

with removable sides (Plate 5.9) . The top face is cast with plaster of Paris (about 3 mm thick) and covered with waxpaper - teflon - teflon - waxpaper sandwich before the mould is closed and loaded with the loading head. After one day the sample is turned over and the other face is cast. This time the loading head is put directly onto the waxpaper-teflon sandwich since this side will be the top face of the sample. After the plaster has gained its strength the loading head is removed, the mould is closed and the remaining faces are cast in a similar manner until the whole sample is covered with plaster of Paris and waxpaper. The sample is now ready to be instrumented. Holes are drilled parallel to the bedding planes near the centre of the sample. During the drilling the sample has to be confined to inhibit tensile cracking due to wedge action of the drill. The sample is then transported to the testing machine, the mould is removed (except the bottom plate), the holes are surveyed carefully and the extensometers and protection rods are installed. The sample is centered in the test frame and the vertical and lateral loading heads are installed. Finally the LVDTs are mounted. At this stage zero-readings for loadcells and LVDTs are taken.

5.3.4 General Loading History

The loading history consists of two phases. During phase one, the test sample is tested without a tunnel to determine the material deformation properties and their

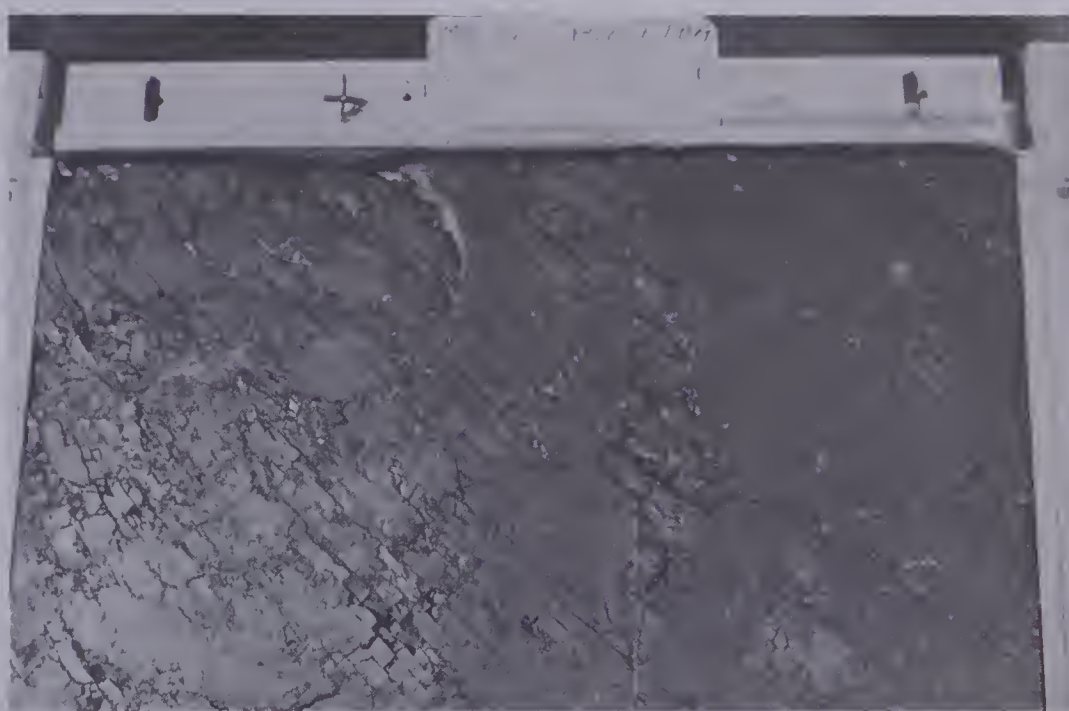
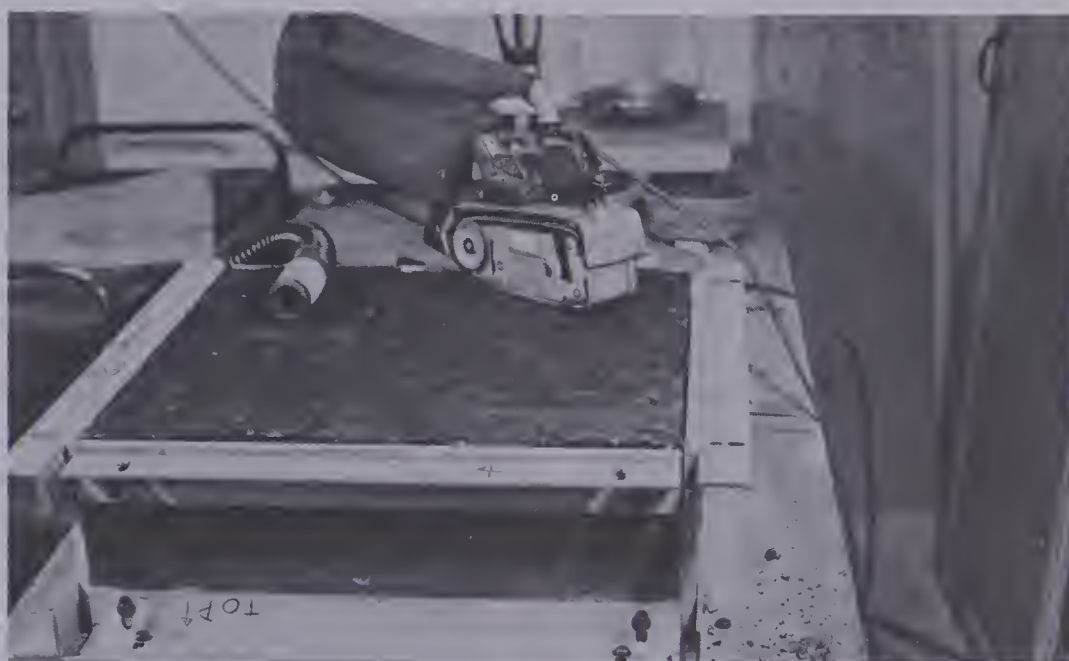


Plate 5.9 Coal Sample in Mould Ready for Casting

distribution within the sample. For a homogeneous, isotropic material all instruments should theoretically show identical stress-strain curves as long as the stress ratio between horizontal and vertical field stress is unity. In the second phase, after the sample is unloaded, the instrumentation and the loading heads are removed and the tunnel is drilled through the sample (Plate 5.10). The tunnel is sealed immediately after drilling with at least two coatings of latex and the sample is returned to its proper location, the instrumentation, including the tunnel closure measuring device and the loading heads, is then installed. The core recovered from the tunnel is mapped carefully and the moisture content is determined. The core was usually broken along bedding planes and could not be used for strength testing. After the zero-readings have been taken, the sample is loaded in small increments of 0.5 MPa to a certain stress level where the deformations are recorded during a constant load test for time intervals up to 5 (maximum 10) days. Further increments and creep tests follow until the capacity of the testing frame is reached or the tunnel collapses. Increments between stress levels and the length of creep periods are normally kept constant except near failure. After the test is terminated the sample is unloaded and the recovery behaviour is recorded for at least 5 to 10 days.

During loading the plane strain condition is maintained by application of a longitudinal load according to a precalculated value or until the dial gauge (with one

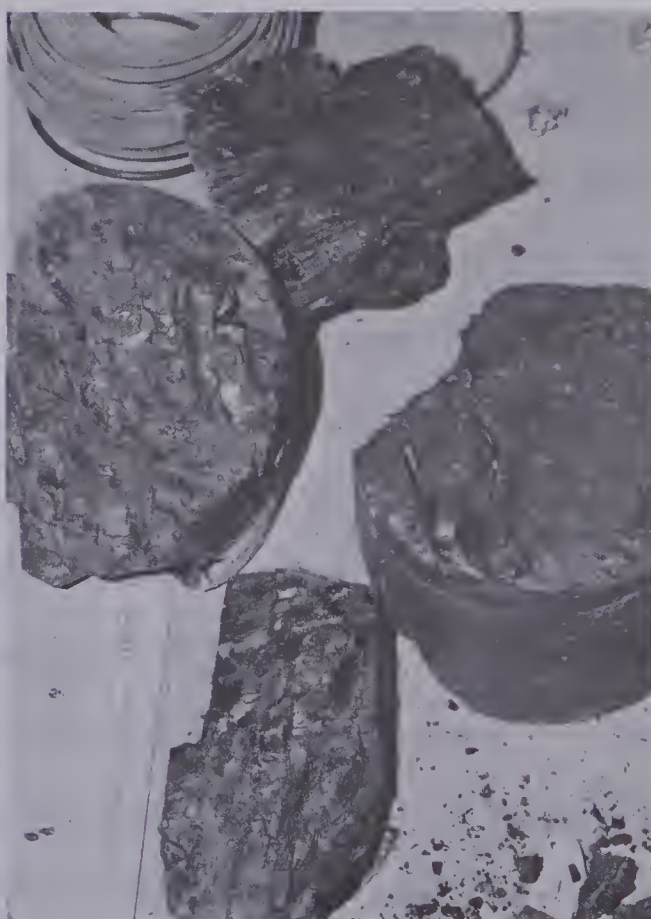
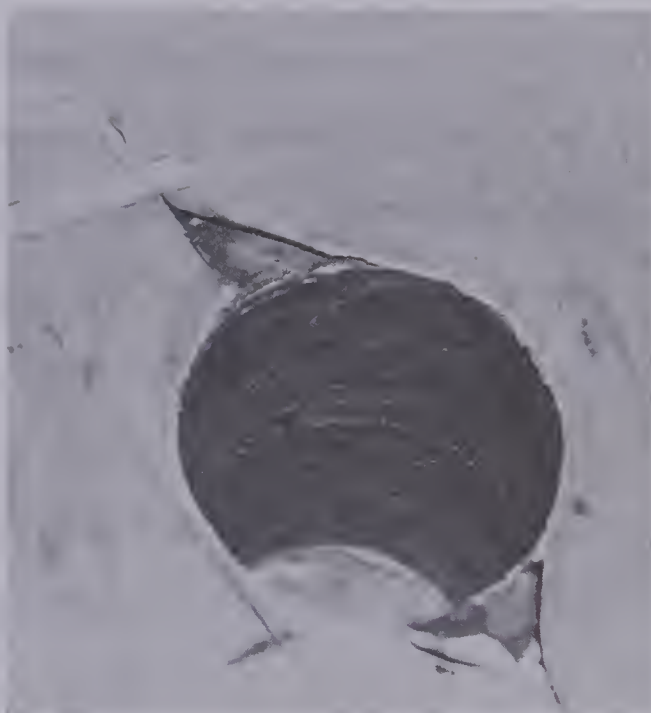
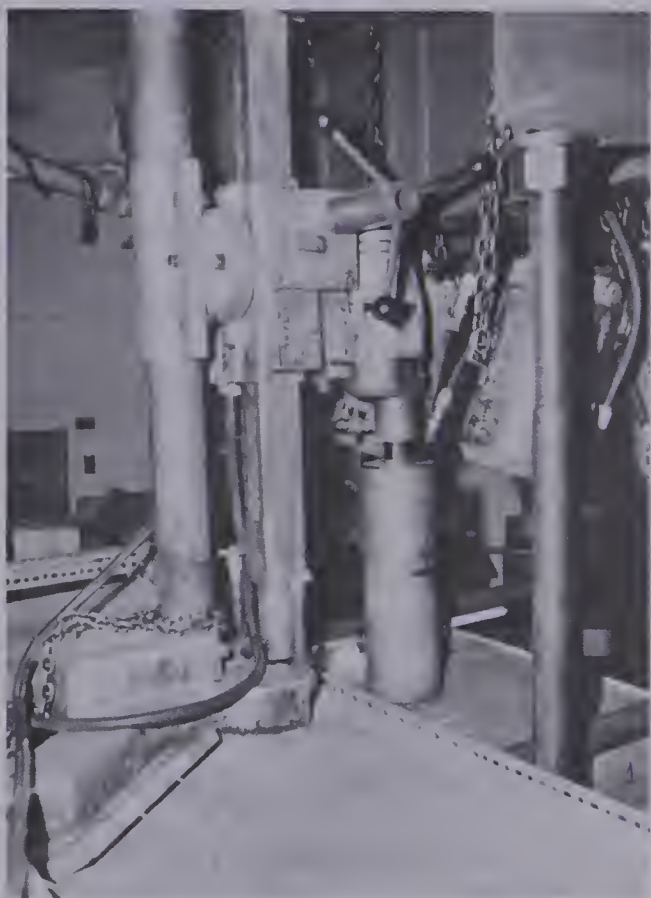


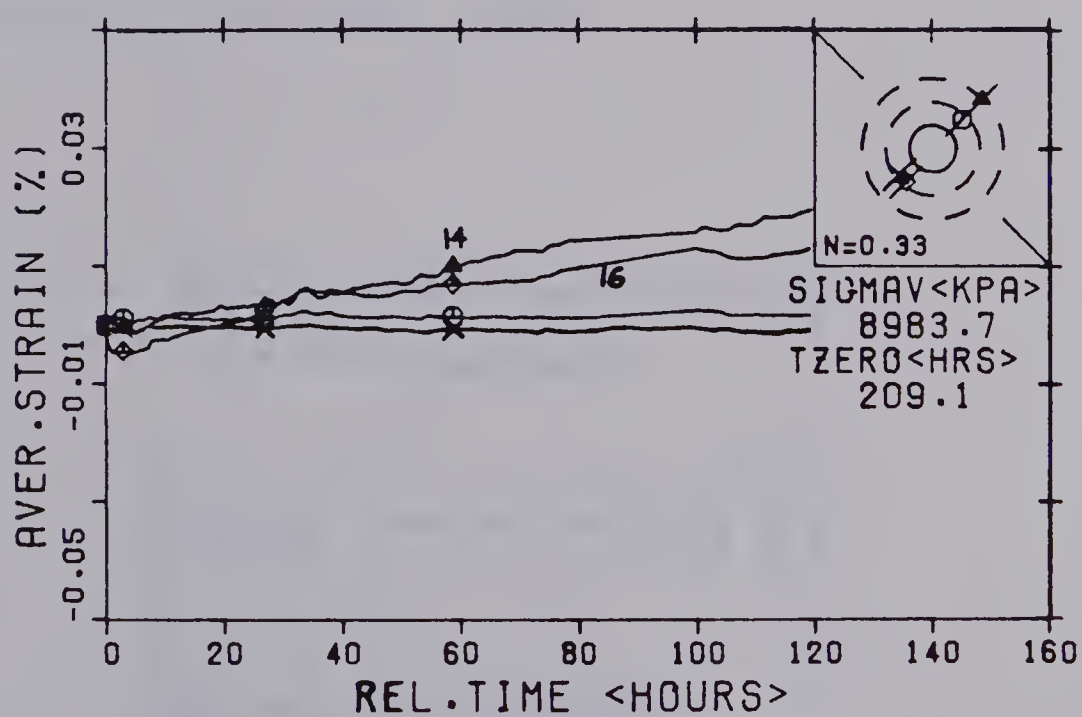
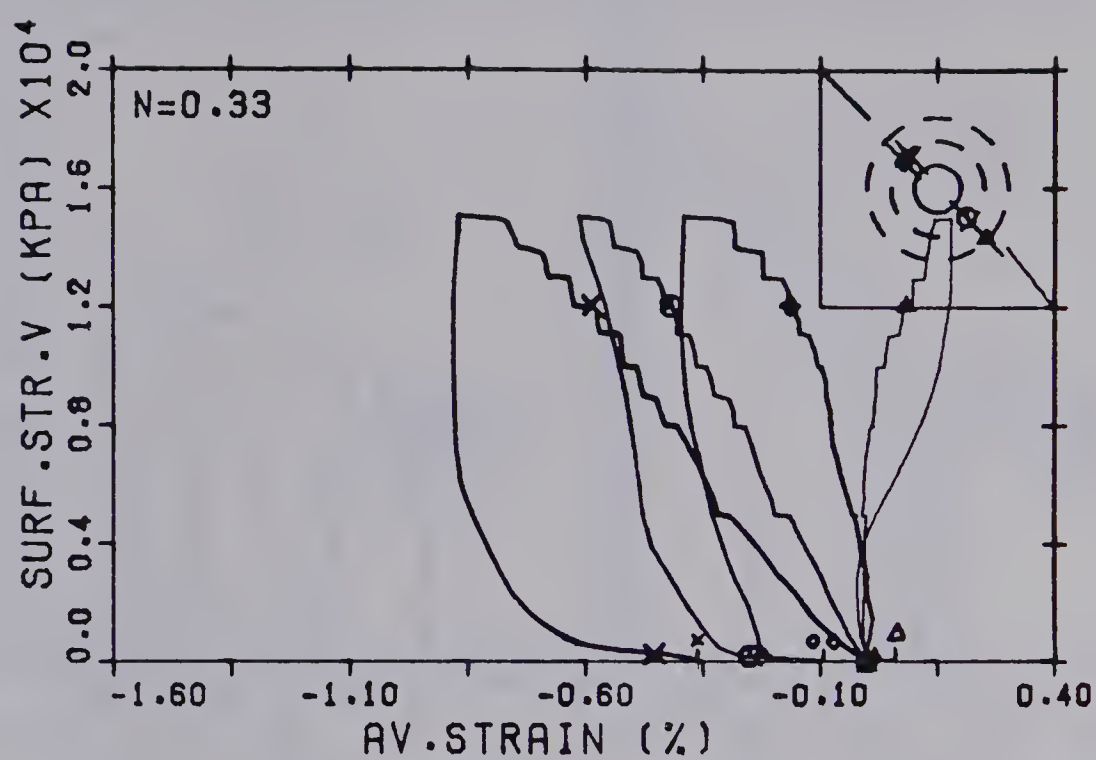
Plate 5.10 Drilling of Tunnel through a Coal Sample

hundredth of a millimeter accuracy) indicates compression. This load is normally high enough to prevent expansion during application of the lateral load increment. Friction in the rams prevents this expansion. The movement of the longitudinal loading head is recorded continuously and any movement is stopped immediately by load adjustment. Due to compaction of the coal with time it is often necessary to unload slightly during a creep stage.

If the tunnel has not collapsed and no plastic zone of significant extent has been created, the test procedure is repeated (after recovery) with a different N-value (for Test MC-2 with $N=0.75, 0.5, 0.33, \text{ or } 0.2$).

5.3.5 Data Processing

Several computer programs have been written to calculate and plot stresses and strains from recorded data. Calibration curves have been fitted by regression analysis with linear, bi-linear or power functions and these functions have then been used to calculate the load and deformations. The dimensions of the original sample and the measured distance between anchors before the test were then used to calculate stresses, strains or closure (=deformation of tunnel wall/tunnel radius). The results have been plotted on four types of diagrams as shown in Figure 5.1 and 5.2. It is the purpose of this section to familiarize the reader with the method of data presentation. Only specific points will be discussed on graphs presented later.



TEST #MC-2.8 WITH TUNNEL 1977

Figure 5.1 Typical Stress versus Strain and Strain versus Time Plot

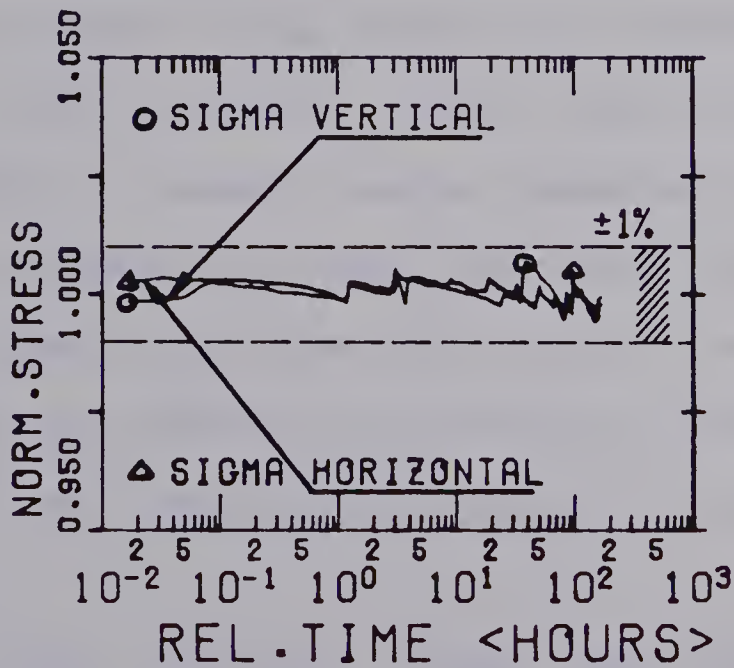
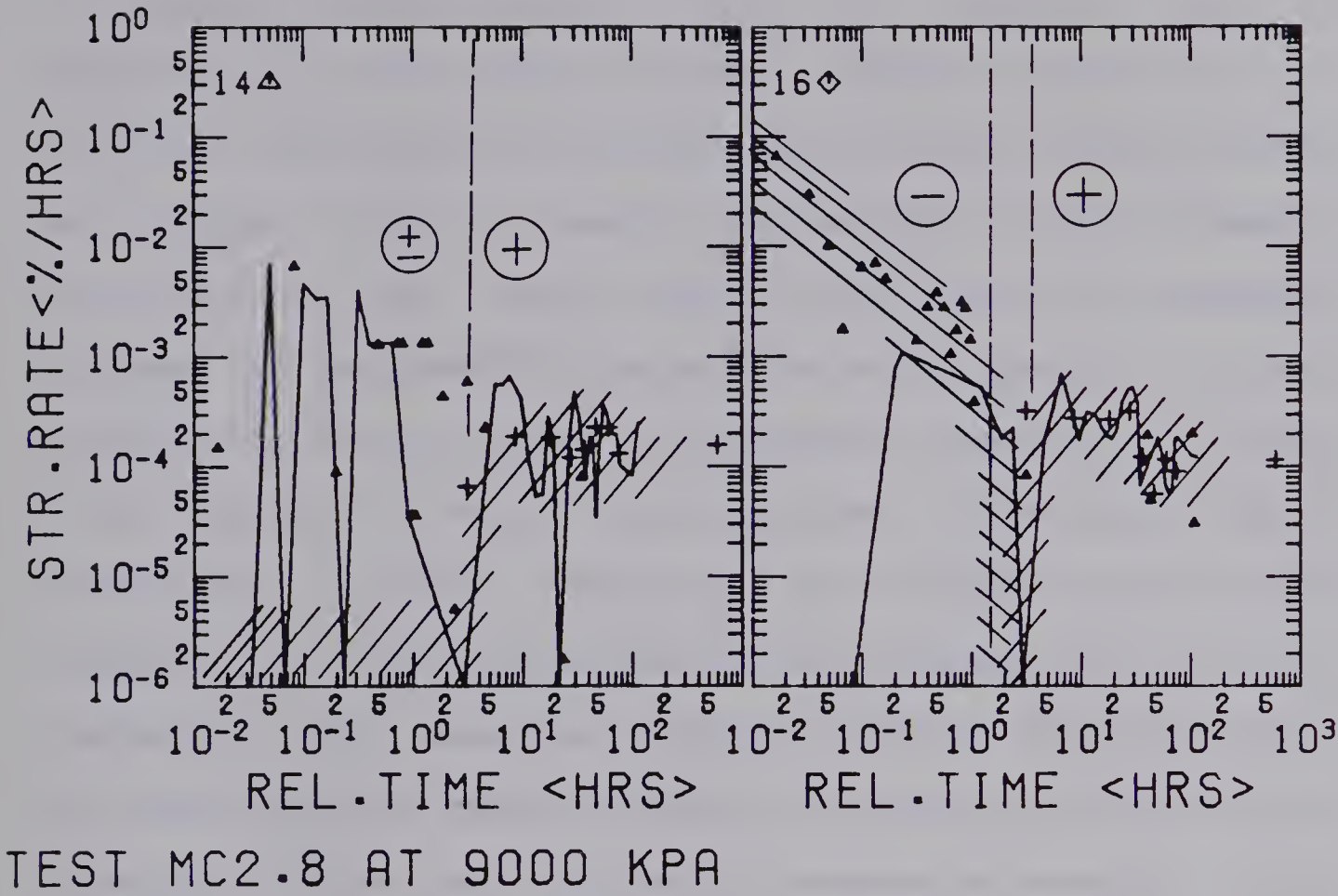


Figure 5.2 Typical Log Strain Rate versus Log Time and Normalized Stress versus Log Time Plot

Stress versus Strain Plot: All records, with the exception of the data recorded during creep tests, are plotted and joined by straight lines. Every thirtieth point is plotted with a symbol. The meaning of this symbol is indicated in the upper right hand corner in a schematic diagram of the sample. The outline of the sample, the joint orientation (two lines from opposite corners), the tunnel (full circle) and the location of the two rows of internal instruments (dashed circles), as well as the approximate location of the instruments whose readings are plotted are indicated. The axes are labeled "Surface Stress Vertical" for the applied field stress in the vertical direction and "Average Strain %" for overall strain or average internal strain or tunnel closure (=tunnel wall deformation divided by tunnel radius).

Strain versus Time Plot: All records are plotted and connected with straight lines. Every thirtieth record is plotted with a symbol whose meaning is indicated in the schematic diagram. In addition, the N-value, the vertical surface stress and TZERO, the time at the beginning of the creep stage, are shown. The time axis is labeled "Rel. Time" to indicate that the time is related to the beginning of the creep stage.

Normalized Stress versus Log Time: Each stress measurement is normalized to the average stress, calculated separately for each stress direction over the whole creep stage. The example shows that it is possible to maintain the

stresses over a period of 180 hours with a variation in stress of less than $\pm 0.5\%$.

Log Strain Rate versus Log Time: The strain rate was calculated in the following manner: The strain rate is the slope of a line calculated by linear regression through three data points and is plotted at the time corresponding to the mid-point. These three points are selected by the following procedure: if the time from the beginning of the creep test is less than one hour, consecutive points are taken; if the time is between one and twenty hours every second point is considered; and if the time is greater than twenty hours every third point is selected. This results in an increased smoothening process as time increases and the recorded strain differences become smaller. If the strain rate is negative it is plotted as a triangle and if it is positive no symbols are plotted but all positive strain rates are connected by a straight line. These points are connected even if there are negative strain rates between positive strain rates (e.g. Figure 5.2, curve 16 between 12 and 60 minutes). If the absolute strain rate is less than $10^{-6}\%/hrs$ it is plotted at $10^{-6}\%/hrs$. Furthermore rates are calculated by linear regression through three points where only every tenth data point is considered. These strain rates are plotted as plusses for positive strain rates and crosses inclined at 45° for negative strain rates. The strain rate is again plotted at the midpoint and is called the trend of the strain rate since it neglects local

variations. This trend is calculated only after 30 readings are taken. Finally, an overall trend is calculated between the thirty-first point (approximately at one hour) and the last point measured to indicate the overall inclination of the strain-time curve after one hour. This point is plotted at 700 hours with a plus or a 45°-cross depending on the sign.

This representation allows plotting of all positive and negative strain rates on one diagram. The trend analysis is a smoothening process which may be useful if the rate fluctuation is too large. The number and the symbol in the upper left corner relates these diagrams to the strain-time plots. Two examples of log strain rate versus log time plots are shown in Figure 5.2 for curves 16 and 14 in Figure 5.1. Curve 16 changes from initial extension to compression with a 2 hour transition zone between 1.5 and 3.5 hours as indicated by the shaded area. A few positive strain rates in the initial zone could be attributed to pressure variations. The trend analysis shows that there is a strain rate minimum at about 40 hours but the overall trend is still positive trending towards lower strain rates at large times. Curve 14 shows a case where a zone of almost zero strain rate is followed by compression as indicated by the shading. Compression is initiated at the same time (at about 3 hours) as in curve 16. Up to this point, the strain rate fluctuates between negative, positive or negligible values of strain rate. This variation is a result of the recording accuracy

and diminishes as soon as the time intervals increase since the ratio of recording error to time interval becomes smaller. As soon as the "true" strain rate is in excess of about $10^{-3}\%/hrs$ or the time interval is greater than about 15 minutes the effects of the recording accuracy become negligible. Figure 5.3 shows artificial data which were generated in the following manner: An error was superimposed on a power function. The absolute value of this error was increased six times by a constant amount and the sign was changed after each increase resulting in the strain-time curve shown in Figure 5.3. After 6 increases this procedure was reinitiated. The time intervals were increased in a manner similar to the changes undertaken during a real test. The corresponding log strain rate versus log time plots are shown in diagram 1, for the power function, and in diagram 2, for the function with superimposed error. A comparison with real data shows that the artificial error is significantly larger than the real recording error.

5.3.6 Preliminary Tests

Several tests on sand-plaster model blocks of various sizes (1 x 1 foot and 2 x 2 feet), with and without tunnel, have been undertaken with the main purpose of gaining experience on the test equipment. One sample was loaded until the tunnel collapsed and similar results as the ones reported by Heuer and Hendron (1969) have been achieved. Some creep testing indicated that a portion of the

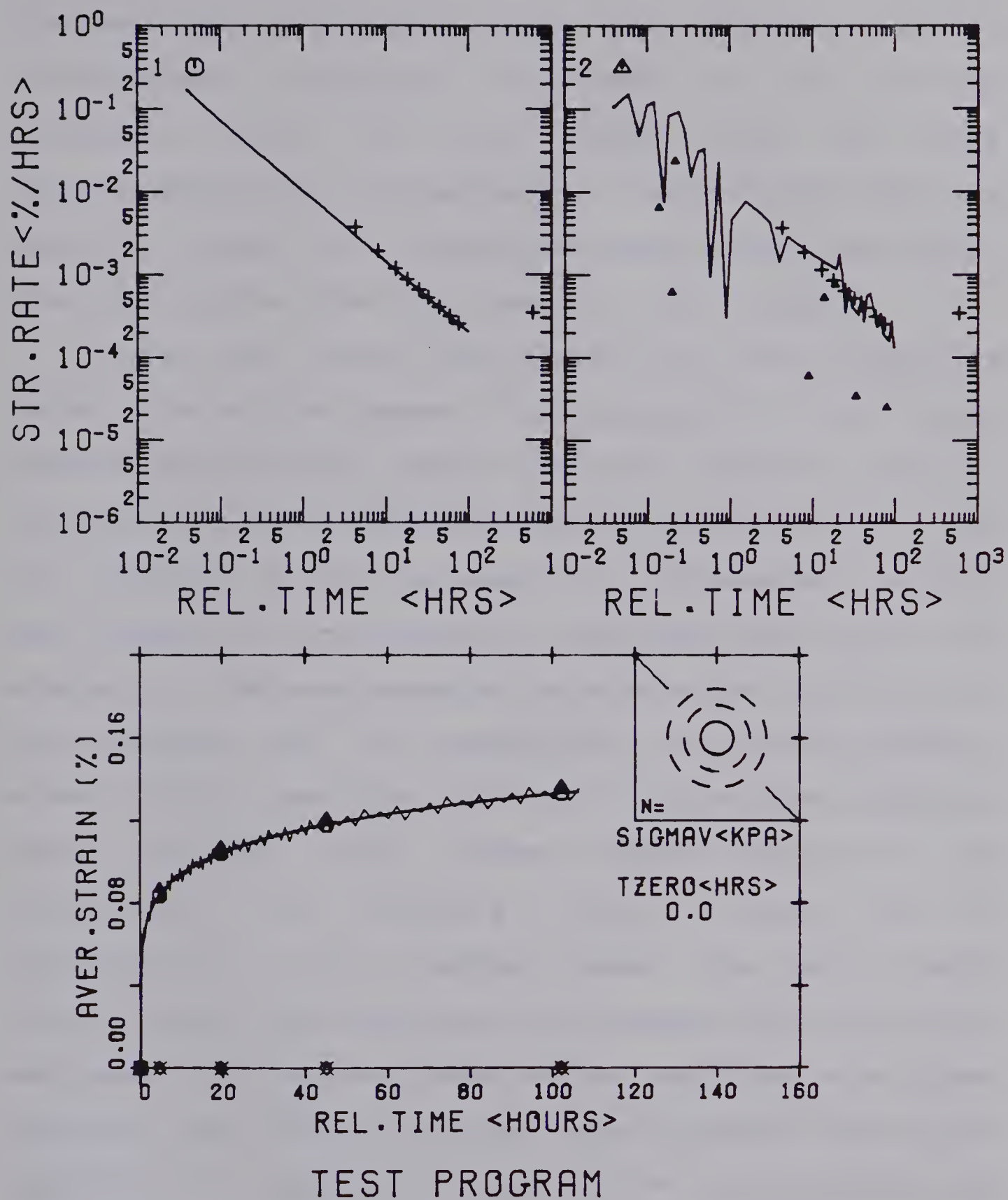


Figure 5.3 Processed Artificial Data and Effect of Recording Error

time-dependent deformations were most likely a result of time-dependent compaction comparable to the behaviour discussed later on test number MC-2 (or MC-4 (Guenot(1979))). No new information, compared with Heuer and Hendron's tests, was gained from these tests. The results have been omitted from this thesis for this reason.

During the first test on coal, MC-1 (MC-1 stands for "Model test on Coal number 1"), the capacity of the testing machine was reached before yielding occurred around the opening. Even under different stress conditions ($N < 1$) it was not possible to fail the tunnel. As a consequence, testing was stopped to strengthen the test frame. The results are similar to the ones reported later on sample MC-2 but much more variable due to inexperience in long-term testing. Plane strain conditions could not be maintained adequately during several creep stages mainly because of the unexpectedly low Poisson's ratio of less than 0.1 perpendicular to the bedding planes. The data is again omitted from this thesis for two reasons: the test will be continued in the near future on the test frame with higher capacity and with an increased tunnel opening. Under these conditions it should be possible to cause yielding and collapse of the tunnel; the amount of recorded data and its interpretation would increase the volume of this thesis without significant contribution to the solution of the problem investigated.

Reproducibility will be shown on Test MC-2 where

repeated loading at various stress ratios has been undertaken.

In summary, the model test facilities developed for the study of the time-dependent rock mass behaviour around underground cavities has the following capabilities. Various sample sizes, presently 60 x 60 x 20 cm with a tunnel diameter of up to 15 cm, can be tested under plane strain or triaxial stress conditions. The maximum field stress of 16 MPa for the present sample geometry is provided by rams of a maximum capacity of 890 kN at 69 MPa oil pressure. This pressure is supplied by hydraulic pumps with a pressure multiplication factor of one hundred. The load can be maintained over several days or weeks with fluctuations of less than $\pm 1.0\%$. The overall straining of the sample, internal average strains from multiple extensometers, and the tunnel closure in various directions can be measured with high accuracy. Creep or closure rates as low as $10^{-5}\%/hr$ have been recorded consistently without major influences due to cycling of the hydraulic pumps or variations in the applied field stress. The electronic data recording and processing system allows frequent reading of large numbers of instruments and rapid data evaluation to assure an optimum testing program. Intended alterations to the testing apparatus will allow application of support pressure by a pressure-meter or a model lining, and drilling under load for improved modeling of the reality.

CHAPTER 6

INTERPRETATION OF MODEL TEST DATA

6.1 Introduction

Many worthwhile solutions and processes of general applicability have been developed in the last decade and the position is reached where - in principal at least - solution of all engineering stress analysis problems with properly described constitutive relationships is possible. (Quote: Zienkiewicz and Valliappan(1969))

While this statement was true in 1969 and still is ten years later, it must be realized that the most critical point in the above statement is the requirement of proper constitutive relationships. In most geotechnical problems it is difficult to determine these relationships, especially if the material to be considered is a non-linear, inhomogeneous, orthotropic, discontinuous medium with time - dependent strength and deformation properties. If model tests are undertaken with such a material and, as is the case in this study, relevant parameters to describe the constitutive relationship have not been determined in an extensive material testing program, it would be irrational to try and analyse model test data with complex material models. In the following chapter the most basic relationships are used to compare the results with theoretical predictions. The purpose of this comparison is to evaluate some of the dominant parameters in order to guide future testing, and to establish a process model to justify reasonable assumptions for more elaborate calculations.

The following interpretation of the pre-yield stages concentrates on linear elasticity for the time-independent constitutive relationship and on a history dependent (linear visco-elasticity) relationship for the time-dependent constitutive law. After yielding is initiated an elasto-plastic or visco-elastic, visco-plastic material model may be used in an initial investigation at small strains and a limit equilibrium approach (Feder(1977) , Feder(1978) , or Rabcewicz(1969)) could be applied at large strains. This latter portion of the study is not described in detail in this thesis but is being undertaken in a companion study by Guenot (1979). The use of finite element models, with joint elements and strain-weakening as well as time-dependent properties, is relegated to future work.

Available theoretical solutions for predicting the behaviour of a circular unlined opening have been applied to the problem under investigation. Since no new theories have been developed all derivations and available equations are summarized in Appendix A6.1.

6.2 Description of Test MC-2

6.2.1 Sample Description

The sample was trimmed in such a manner that the bedding plane was perpendicular to the tunnel axis and the jointing parallel to a diagonal of the sample (45° to the principal stress axis). The dimensions of Sample MC-2 before the test were 61.4 x 61.6 x 20.8 cm (including the Plaster

of Paris layer). The joint pattern was variable across the sample and joint spacing changes between bedding planes. At the top face of the sample the spacing between joints was between 0.3 and 1.6 cm but no major jointing was observed near the intended tunnel location. On one side of the sample two major fractures almost parallel to the side at about 2 to 5 cm depth have been observed. These fractures may have influenced the external displacement measurements at low stress levels. The moisture content of the sample was on average 19% after Test MC-2.9, about 4% lower than the average moisture content in the field. During drilling of the tunnel with a diameter of 12.1 cm the core broke into 4 pieces along bedding planes. The joint spacing was 0.6 to 1.4 cm near the top and much larger or invisible at lower levels. Figure 6.1 shows the crack pattern inside and near the tunnel after the sample was unloaded following Test MC-2.9. Major cracks along the spring lines, roof and floor have been observed. All cracks were open after unloading and it is difficult to determine whether they were created by shear or tension. The longitudinal cracks near the left spring line and the floor showed some indication of shear displacement whereas the roof crack appeared to be a tensile crack. Plate 6.1 shows the total crack pattern on the top face of the sample, the jointing and cracks near the tunnel, and several details inside the tunnel (e.g. tensile and "sheared" cracks).

The location of the internal gauges measuring average

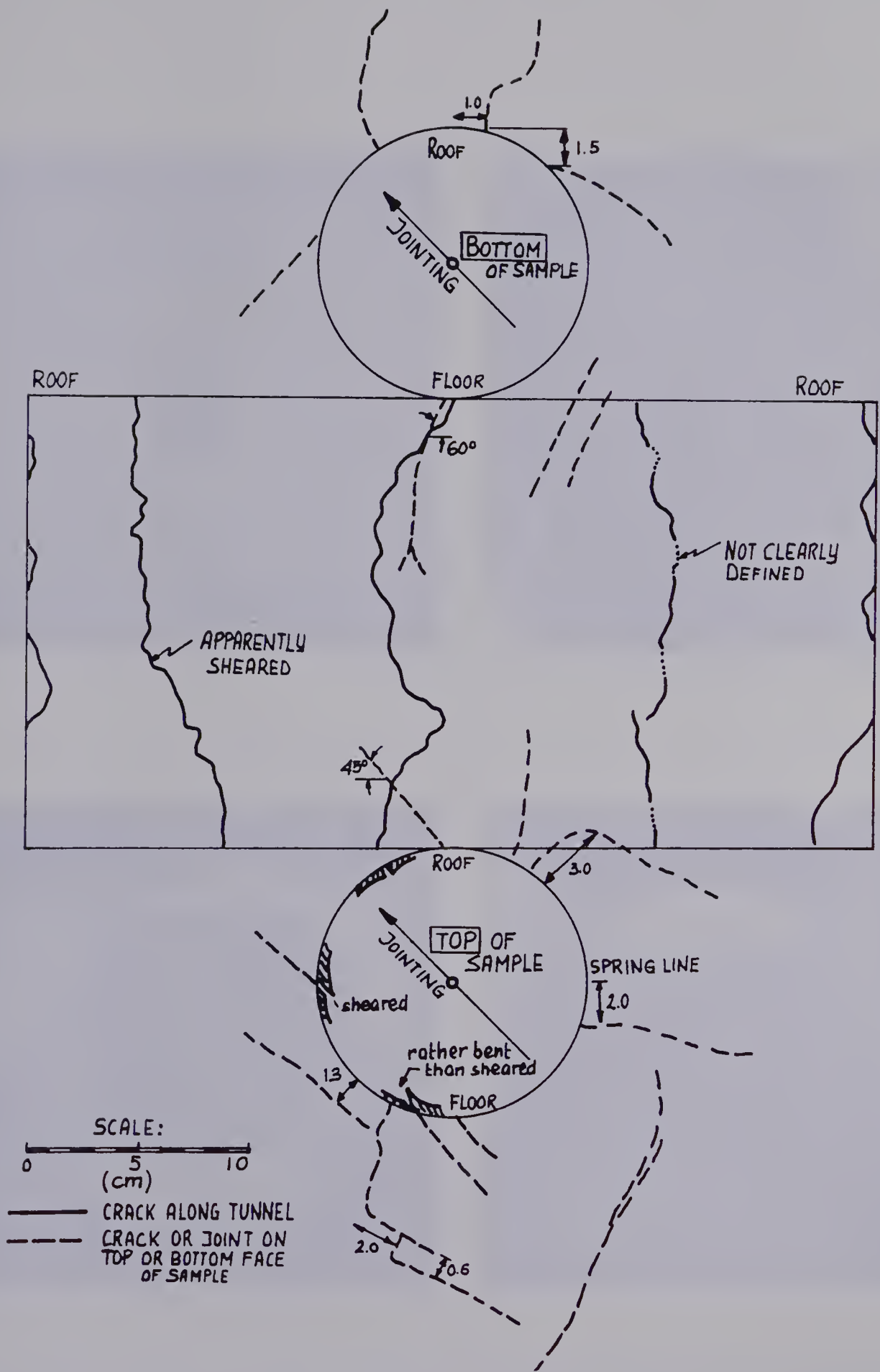


Figure 6.1 Crack Pattern Inside or Near Tunnel after Unloading during Test MC-2.9

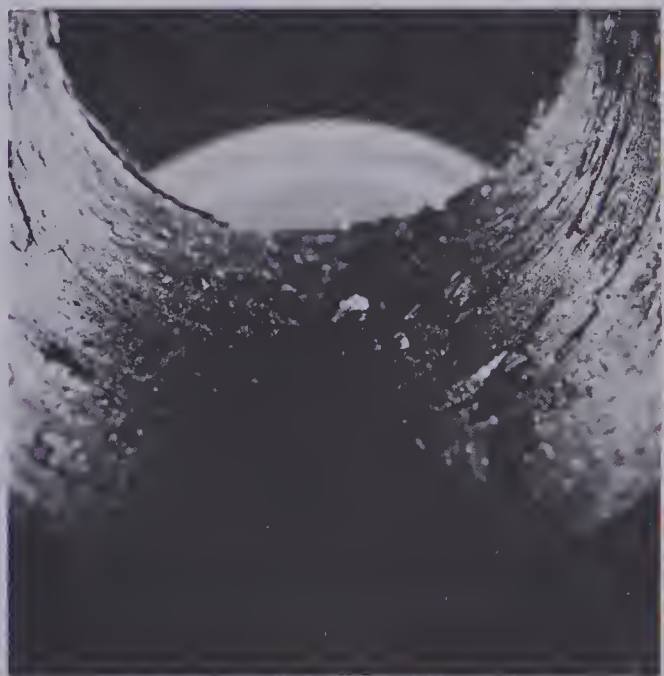


Plate 6.1 Crack Pattern on Top Face of Sample MC-2 and
Details near and inside Tunnel

radial strain are shown (to scale) in Figure 6.12 and numbered according to the diagrams presented later. The row of gauges near the tunnel measures the average strain over a distance of 5 cm between approximately 1.4 to 2.2 times the tunnel radius (a) and corresponds therefore to the strain at about $1.75a$. The second row measures over a distance of 5 cm between 2.2 and $3.1a$, corresponding to the strain at about $2.7a$. Two instruments measure over a distance of 10 cm and this strain corresponds to the strain at about $2.1a$. The external gauges are grouted into the sides of the sample at a depth of 3 cm. The tunnel closure was measured from a stand fixed to the steel plate at the bottom of the sample. The vertical distance between each LVDT is 1.3 cm (the two LVDTs measuring one diameter are therefore 1.3 cm apart) and these LVDTs are rotating counter-clockwise starting from the top (parallel to the jointing) to the bottom (parallel to the major principal stress direction). According to this arrangement, the diameter parallel to the jointing was measured at 14.6 cm, the one perpendicular to the jointing at 9.5 cm, the one parallel to the minimum stress direction at 12.1 cm, and the one parallel to the maximum stress direction at 7.0 cm from the bottom of the sample.

6.2.2 Loading History

The Sample for Test MC-2 was collected and trimmed during winter 1976/1977. It was instrumented during August 1977 and testing at various stress ratios (N) was undertaken

from September 1977 until June 1978. The following is a summary of the complete loading history:

1. MC-2.0: stress ratio $N=1$; block without tunnel loaded to 7 MPa with three creep stages of less than two hours; one reloading cycle;
2. MC-2.1: $N=1$; loading of sample with tunnel to 3 MPa with one reloading cycle; no results reported in this thesis;
3. MC-2.2: $N=1$; same as MC-2.1; testing of internal gauges; no results reported in this thesis;
4. MC-2.3: $N=1$; same as MC-2.1; testing of internal gauges; no results reported in this thesis;
5. MC-2.4: $N=1$; loading to 12 MPa with 5-day creep tests at approximately 3, $5 + (n \times 1)$ to 12, 10 and 0 MPa; load cells overstressed at 10 MPa;
6. MC-2.5: $N=0.5$; loading to 3 MPa with one 5-day creep test at maximum load and one 5-day recovery test; no data reported in this thesis;
7. MC-2.6: $N=0.75$; loading to 14 MPa with 5-day creep tests at approximately 3, $5+(n \times 1)$ to 14, 0 MPa;
8. MC-2.7: $N=0.33$; loading to 10 MPa with 5-day creep tests at 3, $5 + (n \times 1)$ to 10, 0 MPa; unloading was necessary because of increasing sample rotation;
9. MC-2.8: $N=0.33$; loading to 15 MPa with 5-day creep tests at 5, $8 + (n \times 1)$ to 15, 0 MPa;
10. MC-2.9: $N=0.2$; loading to 15 MPa with 5-day creep tests at 5, $8 + (n \times 1)$ to 15 MPa; test had to be terminated due to damage of the sample during uncontrolled

rotation.

The loading or unloading rate between stages was normally between 0.05 and 0.1 MPa/min resulting in a total time of maximum 2.5 hours for rapid loading to the maximum capacity of 15 MPa.

6.2.3 Presentation of Measurements

During this extensive testing period data was collected electronically and stored on magnetic tape. In the order of 200,000 readings have been recorded and plotted in stress-strain, strain-time and log strain rate - log time diagrams. These diagrams have been collected in an internal report (1979) of the Geotechnical Section in the Department of Civil Engineering, University of Alberta. Because of the extent of this report only a limited selection of data is included in this thesis throughout Chapter 6 and in Appendix A6.2. The selected data are typical with a normal range of scatter. This data has been selected to illustrate specific points which will be discussed later.

6.2.3.1 Stress-Strain Relationship

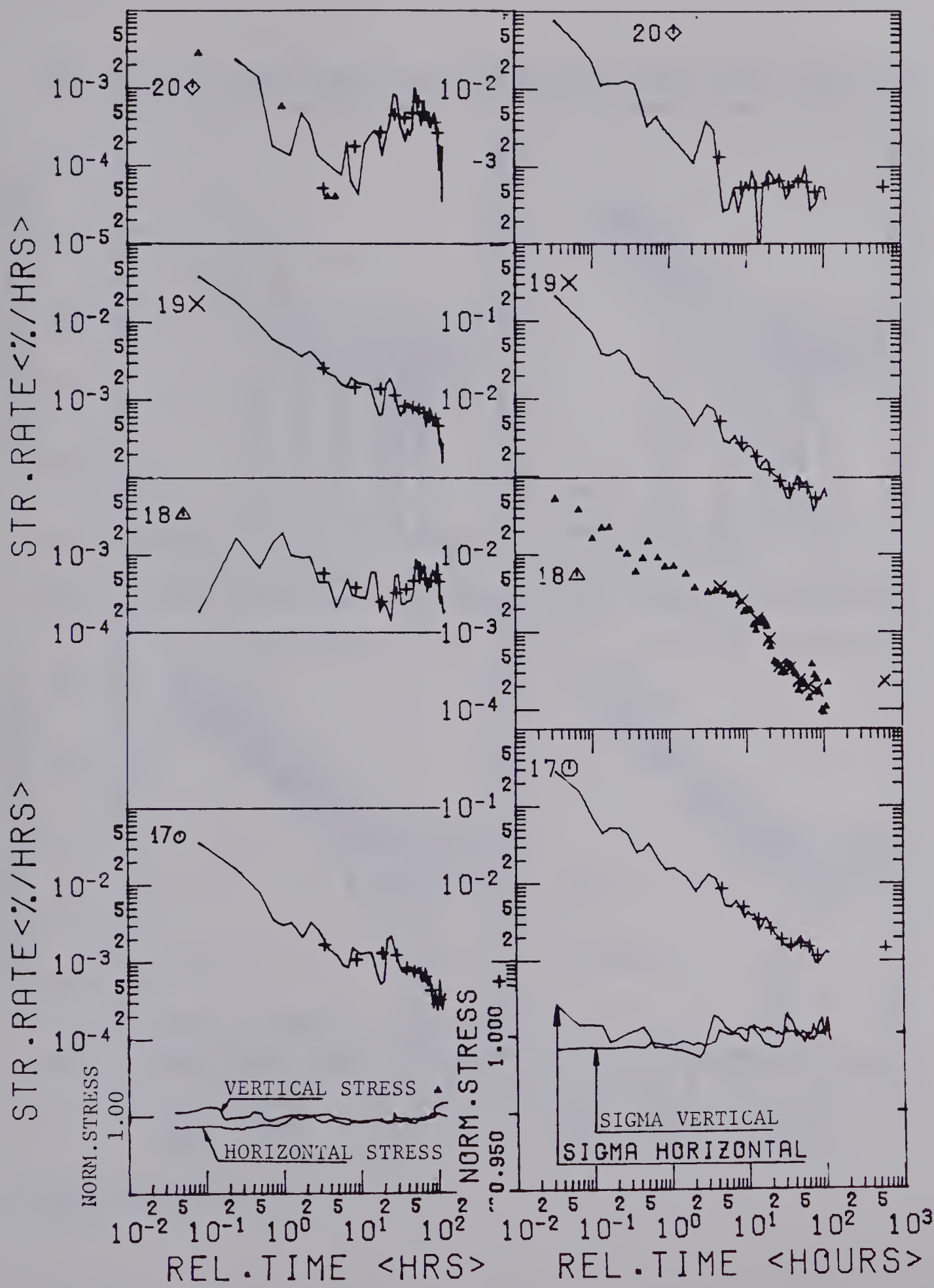
One complete set of stress-strain diagrams is later given, as an example, for Test MC-2.8 ($N=0.33$) in Figure 6.13 for the internal radial extensometers and in Figure 6.14 for the overall strain (triangle and circle, top left diagram), for the tunnel closures (bottom left diagram) the loading head displacement (4 corners, top right diagram) and

the loading history (circle=maximum load, triangle=minimum load and cross=longitudinal load, bottom right diagram). A summary plot of maximum field stress versus overall strain, tunnel closure, and selected radial strain measurements for the other tests MC-2.0, 2.4, 2.6, 2.7 and 2.9 are presented in Appendix A6.2 (Figures A6.1 to A6.5).

6.2.3.2 Strain - Time Relationship

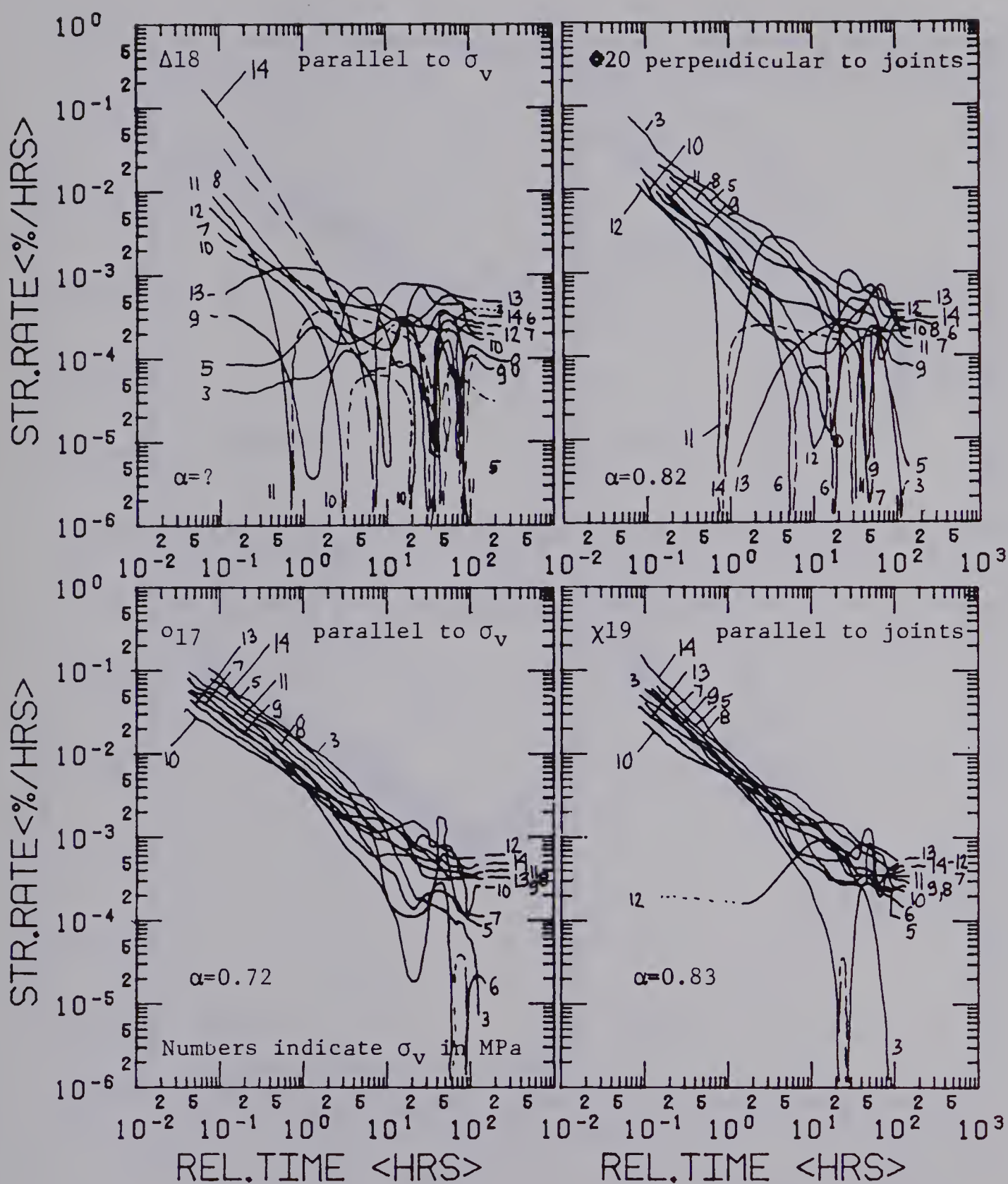
One complete set of strain-time diagrams and the corresponding log strain rate - log time diagrams for Test MC-2.6 at 9 MPa are shown in Appendix A6.2 (Figures A6.6 and A6.13). Corresponding curves are identified by the same number. The stress variation is shown for the same creep stage. A summary plot for one radial extensometer for Test MC-2.4, 2.6 and 2.7 to 2.9 is shown later in Figure 6.17 and a few examples of log strain rate - log time diagrams are given in Figure 6.16. Figures 6.2 to 6.5 summarize the development of the time-dependent tunnel closure during incremental loading of Test MC-2.6 ($N=0.75$) and MC-2.9 ($N=0.2$) (compare with the radial strain summary in Figure 6.17).

Figure 6.2 gives the tunnel closure rates for the stress increment at 13 MPa for the two Tests MC-2.6 and MC-2.9 together with the normalized field stress. The closure is not significantly affected by the load fluctuations, which were less than $\pm 0.1\%$. The most obvious differences between the two sets of data is that extension



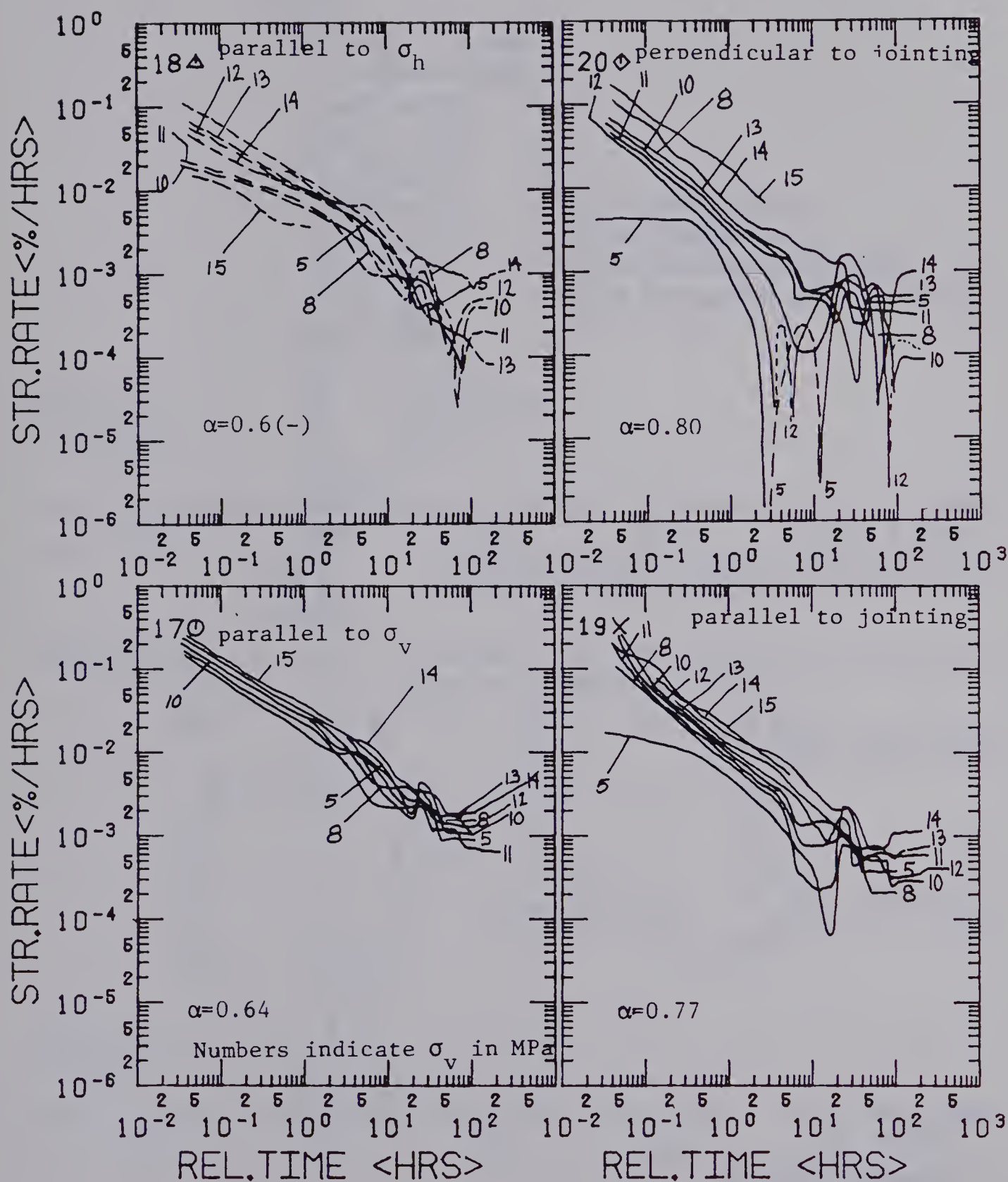
TEST MC-2.6 13000 KPA TEST #MC-2.9

Figure 6.2 Typical Tunnel Closure Rate Diagrams from Tests
MC-2.6 and MC-2.9 at 13 MPa



TEST MC-2.6

Figure 6.3 Summary Sketch of Tunnel Closure Rates for all Increments During Test MC-2.6



TEST MC-2.9

Figure 6.4 Summary Sketch of Tunnel Closure Rates for all Increments During Test MC-2.9

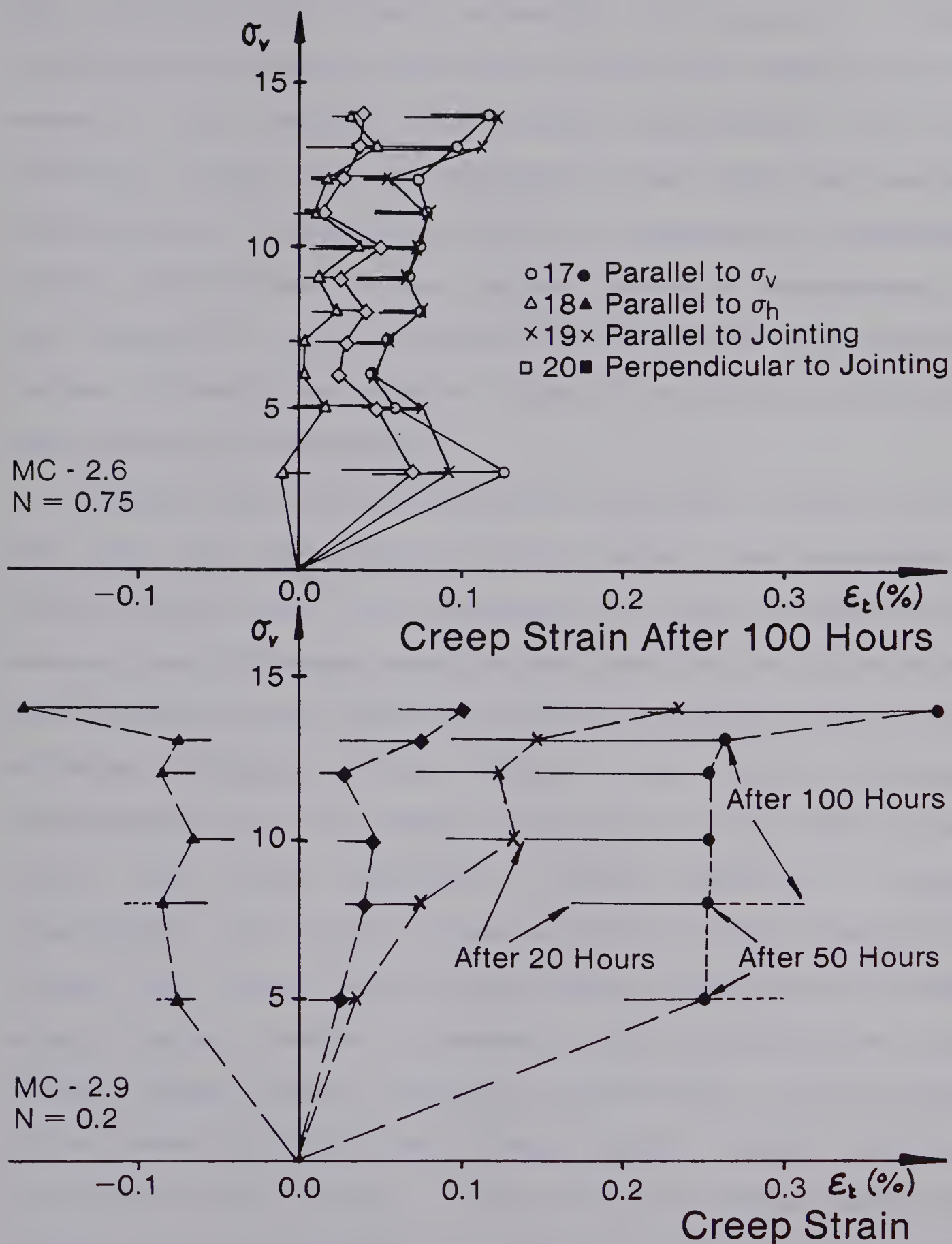


Figure 6.5 Stress versus Creep Strain Diagrams for Tests MC-2.6 and MC-2.9; Strain after 20 Hours and 100 Hours

was observed in the direction of minimum stress (18-triangle) during Test MC-2.9 ($N=0.2$, for explanation of symbols see Chapter 5). Further differences will be discussed later but it should be noted that these curves correspond to different equivalent openings (as discussed later) and different stress fields. (Curve 17 corresponds to the diameter in the direction of the maximum field stress, curves 19 and 20 to diameters parallel and perpendicular to the jointing, respectively).

Figures 6.3 and 6.4 summarize the tunnel closure rates for the two Tests MC-2.6 and 2.9 for all load increments. These curves have been sketched by hand to follow the general trend (through trend points) and are not intended to show details which are given in the internal report or in selected diagrams like Figure 6.2. The following observations of the general character of this data can be made: the rate decreases almost linearly in these logarithmic plots with a slope α of 0.6 to 0.83 (individual values are given inside each plot); a leveling off of the strain rates towards a constant value may be observed for higher stress levels whereas deceleration to very small rates seems apparent for lower stress levels; and all increments fall within a surprisingly narrow band even though load increments vary between 1 and 5 MPa and stress levels increase from 3 to 15 MPa.

From a comparison of the two Figures 6.3 and 6.4 the effect of the stress ratio N can be evaluated. During Test

MC-2.6 the stress ratio N was 0.75 and during Test MC-2.9 this ratio N was 0.2. It can be seen that the average strain rates after 100 hours for the curves 17, 18, 19, 20 are 0.4, ± 0.0 , 0.4, 0.3 times $10^{-3}\%/hr$, and 1.5, -0.4, 0.5, 8.5 times $10^{-3}\%/hr$ for $N=0.75$ and $N=0.2$, respectively; the average strain rates after one hour are 7.0, ± 0.0 , 7.0, 1.8, and 25.0, 8.5, 13.0, 6.0 times $10^{-3}\%/hr$ for the corresponding instruments; and instruments No. 18 and 20 in Test MC-2.6 ($N=0.75$) are strongly affected by load variations since very low creep rates are observed throughout the test. In general, the creep rates are almost one order of magnitude higher in creep tests with $N=0.2$ than in tests with $N=0.75$.

Figure 6.5 summarizes the creep strains accumulated during each creep stage up to 20 hours and up to 100 hours. During Test MC-2.6 this creep strain remains almost constant or increases only slightly up to relatively high stress levels. A higher creep strain was observed during the first creep stage and this is most likely due to initial crack closure and larger initial load increment. The behaviour observed is similar to the response expected from a linear visco-elastic material exposed to an identical loading history. The same holds true for Test MC-2.9 except for the instrument parallel to the jointing (cross) and at stress levels higher than 1.3 MPa. These observations will be discussed in more detail in Section 6.4.

6.3 Interpretation of Data by Linear Elastic Model

The elastic solution for the stress distribution around a circular hole in a flat plate is attributed to Kirsch and the derivation of these equations from an Airy stress function is given in numerous texts (e.g. Obert and Duvall(1967)). These equations for strains and displacements around a tunnel are summarized in Appendix A6.1 and describe the model behaviour (called: "Model") where the field stress is applied to a sample with a preexcavated tunnel. Only radial strains and displacements are given since no measurements have been taken in the tangential direction.

The strains and displacements measured during the excavation of a tunnel in an elastic medium (called: "Reality") can be found by direct superposition of the above solutions and the solutions for a sample without a tunnel (called: "Plate"). While the stress distribution remains the same, the strains and displacements are lower in reality than in the model where the plate is compressed during load application. The corresponding equations for the additional two states - Plate and Reality - are given in Appendix A6.1.

Examination of these equations shows that the strains measured in reality always show extension whereas in the model extension is measured only close to the tunnel and at high values of Poisson's Ratio where the material is almost incompressible. This point will be discussed in more detail in the section on time-dependent strain measurements. The

tunnel closure and the external displacements in general are larger in the model than in reality, again due to the compression of the plate itself.

It is evident that a non-linear behaviour may result from a non-linear material stiffness or a non-linear Poisson's Ratio. These non-linearities will not affect the behaviour of the model tunnel in the same proportion as the tunnel in reality. For example, if only the Bulk Modulus is non-linear, the stress-strain response for a stress ratio $N=1$ will be linear in reality but non-linear in the model. The radial strain for $N=1$ is a function of $1/G$ in reality, where G is the Shear Modulus, and the radial strain for the plate is a function of E/KG , where K is the Bulk Modulus and E the Young's Modulus. For the model therefore, the radial strain must be a function of K , G and E . It should be realized that a change in N -value during a test may cause an apparent non-linearity. During most tests it was not possible to control N with an accuracy higher than $\pm 5\%$.

The most reliable deformation measurements made during the test are the tunnel deformations and the overall straining of the model block. The internal deformations or average radial strains are strongly affected by local material properties and show, as expected, wide variations in results. In addition, many of the instruments produced questionable results and the others may therefore be used only to support general conclusions from the overall behaviour. In later tests (MC-3 and MC-4, Guenot (1979)),

with an improved measuring device, it was found that these internal gauges still showed large variations, but that the average calculated from corresponding gauges was in agreement with the overall measurements. As a consequence, it is preferable to try and interpret the tunnel closure and the external deformations first.

The ratio between the external deformations of a block without a tunnel loaded in plane strain condition ($N=1$) and the same block loaded after drilling of the tunnel ($N=1$) is a function of Poisson's Ratio only (1.04, 1.06, 1.18, 1.29 and 1.48 for Poisson's Ratio equal to 0.0, 0.1, 0.2, 0.25 and 0.3). From Test MC-2.0 and MC-2.4 this ratio was determined to be 1.43 for the horizontal and 1.34 for the vertical direction. The corresponding Poisson's Ratios are 0.29 and 0.24. The Poisson's ratio in the longitudinal direction was determined from load measurements under the assumption of isotropic material properties to be equal to about 0.1. Two factors have to be considered in this determination of Poisson's Ratio. First, the loading rate during Test MC-2.0 was approximately 500 times the rate during Test MC-2.4. This results in a significant overestimation of Poisson's Ratio if the stiffness decreases with decreasing loading rate. From a comparison with tests (MC-2.8 or 2.9) where the strain rate was changed during the test it was found that the measured deformation ratio was at least 1.25 times the ratio for tests with equal loading rate. After this correction Poisson's Ratio must be between

0.1 and 0.2. Secondly, the deformations in Sample MC-2.0 were taken from the reloading curve whereas they had to be taken from the initial loading curve of Test MC-2.4 after drilling of the tunnel. The vibrations during drilling must have caused some loosening of the sample and a slight underestimation of Poisson's Ratio would be expected. Taking both factors into account and comparing with results from a similar analysis by Guenot (1979) it can be assumed that Poisson's Ratio is equal or slightly lower than 0.2 parallel the bedding plane and about 0.1 perpendicular to the bedding plane.

As mentioned earlier the coal shows a non-linear stress-strain relationship. The tangent modulus was determined from several stress-strain curves to give an indication of the sample stiffness. Assuming a Poisson's Ratio of 0.2, this modulus, for a stress range between 5 and 7 MPa, reached a maximum value of 1900 to 2050 MPa during the reloading test on Sample MC-2.0 without a tunnel at a fast loading rate of 6800 MPa/hour. This value was determined from external displacement measurements and must be slightly lower than the short-term modulus. During Test MC-2.4, with slow loading at a rate of about 14 MPa/hour, the tangent modulus between stresses of 6 and 8 MPa was determined from external displacement measurements to be 1500 MPa (at 45° to the joints) and from tunnel closure measurements to be 1300 MPa (at 45° to the joints), 1100 and 1450 MPa (parallel and perpendicular to the joints,

respectively). These latter values must be close to the long-term stiffness since creep had almost terminated at these stress levels. An anisotropy ratio of approximately 1.3 would result from these results but this ratio could not be verified by the internal extensometers and might be exaggerated due to non-symmetric stress redistribution (see later).

In summary, conventional elasticity theory has been used to evaluate the material properties. The extensometers installed did not perform satisfactorily during the loading of the sample without a tunnel. Because of this the material properties, Young's Modulus and Poisson's Ratio, have been estimated from a comparison with the first test with a tunnel. It was found that these parameters were loading rate-dependent and non-linear. The initial closure was extremely variable but the stiffness, as a tangent modulus over a specific stress range, was reasonably consistent. To eliminate the effects of variability in stiffness the test results from further tests were compared in a normalized form. A closure ratio, defined as the ratio of the closure for a given N-value to the closure measured during the test with N equal to unity, has been used. From linear elasticity this ratio can be calculated as a function of N, Poisson's Ratio, and for various diameters. This predicted, linear relationship is shown later in Figure 6.9.A for three orientations, at 45° to each other, and for three cases; for the "Model", for the "Reality", and for the "External

Deformation Gauges". This relationship is independent of the Poisson's Ratio for the case of the Model. The full circles in Figure 6.9.A represent observed tunnel closure ratios and the full squares represent the external deformation ratios. Reasonable agreement with the predicted ratio can be observed at $\theta=45^\circ$. At $\theta=0^\circ$, in the direction of the maximum field stress, increasing deviation is evident and at $\theta=90^\circ$ a non-linear trend with similarly increasing deviation at low N-values can be noticed.

In general, it was observed that the tunnel deformed to an elliptical shape. Three conditions may cause this type of deformation pattern: (a) a principal stress ratio N of less than one; (b) anisotropic (orthotropic) material properties; and (c) non-symmetric stress redistribution. A decrease of the horizontal stress field increases the closure in the vertical direction and decreases or reverses the tunnel wall displacement in the horizontal direction. The same response can be achieved by a lower modulus of elasticity in the direction of maximum closure and a higher modulus in the direction perpendicular to it. The first point has already been considered in Figure 6.9.A and the second point cannot be justified because of the 45° -inclination of the joints. The deviation can therefore not be explained by conventional elasticity theory.

The third condition (c) of non-symmetric stress redistribution has to be discussed in some detail before the test results can be examined. It is based on the working

hypothesis of stress redistribution due to non-linear, stress-dependent creep properties, time-dependent strength, and strain-weakening which has been introduced in Chapter 1.

If a circular opening is excavated in an isotropic, initially elastic material, concentrations of the tangential stresses in areas of reduced radial stress cause rock elements near the tunnel to be loaded to high stress levels relative to their peak strengths. These elements will creep more than elements further away from the tunnel due to low confinement pressure and the fact that most rocks exhibit a strain-rate which depends on the stress level. This process, which has been analysed for an axisymmetric case by da Fontoura (1980), causes tangential stresses to be transferred away from the tunnel. This is schematically illustrated in Figure 6.6.a. Nair et al. (1968) (or Nair and Boresi (1970)) investigated this process, by application of the finite element method, for spherical and egg-shaped openings in a material with non-linear time-dependent properties and Hayashi and Hibino (1968) studied this process around an underground cavity by a finite element analysis based on a stress-dependent creep law. Nair concluded that these "stress relaxations" take place after a short interval of time and significantly influence the stress and displacement field. Due to this stress redistribution the stress concentration near the opening reduces significantly and yielding is initiated only after loading to much higher field stresses than predicted from elasticity.

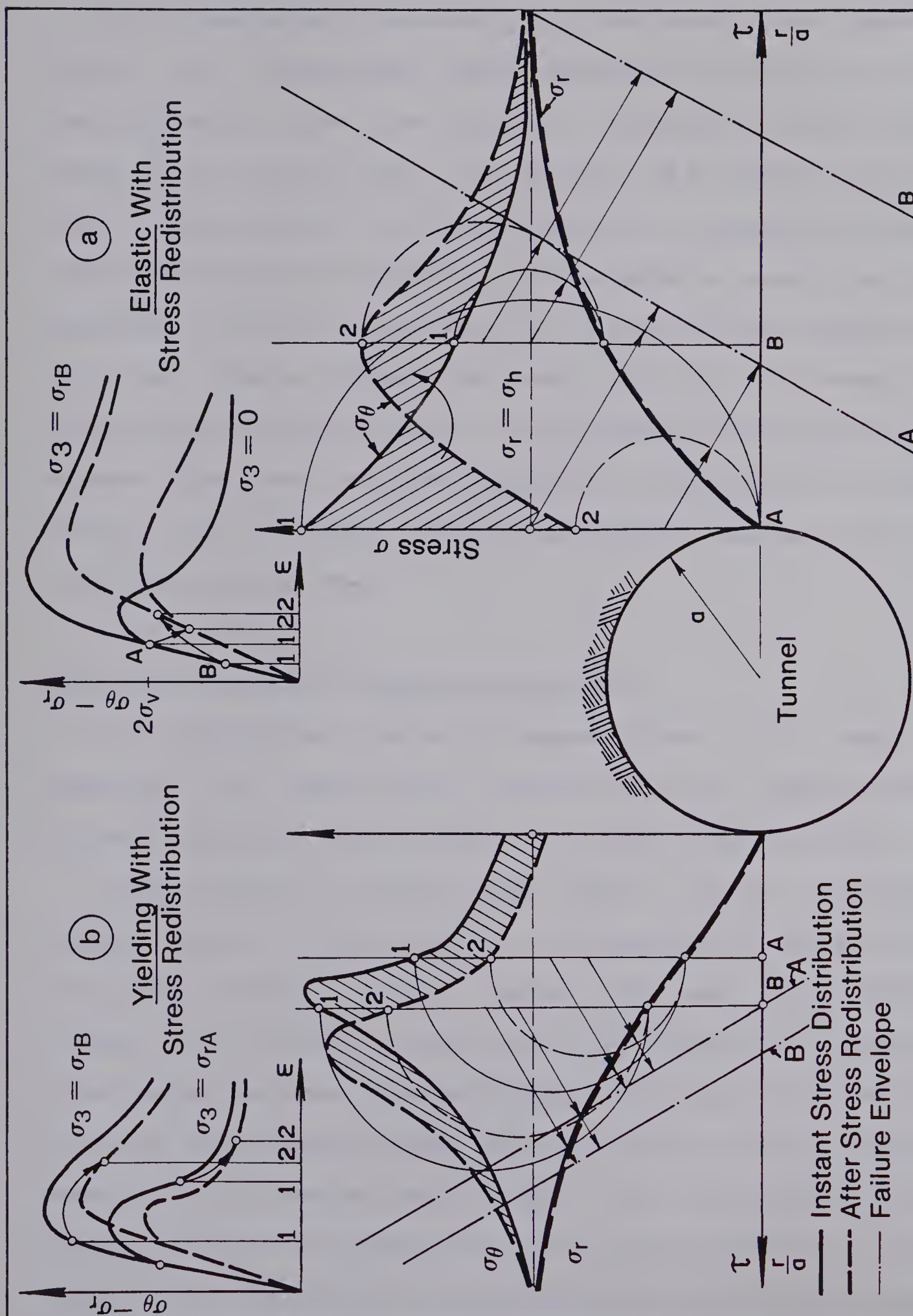


Figure 6.6 Schematic Diagram Illustrating Stress Redistribution around an Opening

The equivalent process for the case where yielding occurs is illustrated schematically in Figure 6.6.b. Visco-plastic flow of elements stressed beyond their capacity (A) and creep of element (B) loaded to stress levels below their yield strength cause comparable stress redistribution and propagation of the plastic zone. The time dependence of this process will be discussed and illustrated later on results from the model test. At this stage the stress-strain relationship is considered only, but it is assumed that the Young's Modulus is a function of loading history and decreases with increasing loading time and decreasing loading rate.

6.3.1 The "Equivalent Opening Approach"

The equivalent opening approach has been used to describe the model test results and to qualitatively evaluate practical implications of stress redistribution.

This approach states that there is an equivalent opening in an linear elastic or visco-elastic medium with the same stiffness which, under the same stress field, deforms in the same manner as the real opening in a medium experiencing stress redistribution. The shape and the size of this fictitious opening is a function of time if stress redistribution occurs with time. This is illustrated in Figure 6.7 for an axisymmetric case and in Figure 6.8 for a case with anisotropic creep properties. After establishing an initial stress field, stress redistribution may occur

either instantaneously or gradually. The stresses are at any time in equilibrium with the field stresses and the sum of these stresses has to be equal to the sum of the stresses around the equivalent opening. It is further assumed that the tunnel wall displacements, for the real and the equivalent opening, are the same and that the trend and shape of the strain pattern is similar. It is understood that this is an approximate model which is to some extent inaccurate. This fictitious opening has a boundary somewhere between the wall of the real opening and the maximum tangential stress. The exact location is affected by many factors such as local yielding, change of the real opening shape (due to instability), and support measures.

The equivalent opening is therefore an opening in a linear elastic medium whose wall displacements correspond at a particular instant to the wall displacement pattern observed in the real opening.

The shape and orientation of such an equivalent opening can be determined from field or model test data if the type of the geometrical shape is selected, e.g. circular or elliptical opening. If the equivalent opening is known the shape of the stress redistribution zone is known too and this can be checked against the local rock structure, the material property distribution, and the stress field. Optimum excavation layouts and support systems can be designed if the shape and the orientation of the equivalent opening is known. This will be discussed in Chapter 7.

The most important point emerging from this approach is that deformations, in excess of deformations predicted from the original opening shape in an elastic medium, can be explained by the shape change of the equivalent opening. For example, if a circular tunnel in an elastic medium experiences axisymmetric stress redistribution to a depth of say 0.5 times the tunnel radius the equivalent opening will be between 1 and 1.5 times the original tunnel radius. Due to the linear relationship between the tunnel wall displacement and the radius of the opening, the tunnel closure could be between 1 and 1.5 times, but most likely in the order of 1.3 to 1.4 times, the predicted elastic closure. If the shape changes, in addition to the stress redistribution due to local creep or yielding, to an elliptical opening, then significantly higher closures of more than double the predicted value would occur. These two cases are now discussed in some detail.

6.3.1.1 Tunnel Closure and External Displacement

Figure 6.7 illustrates stress, strain and displacement patterns around a circular opening without stress redistribution for an axisymmetric case ($N=1$, all properties isotropic). The equivalent opening is a circular tunnel with increased diameter but with an elastic stress field. The corresponding strain and displacement distribution are plotted in the same diagram, and the stress - internal strain diagram with initiation of an equivalent opening at

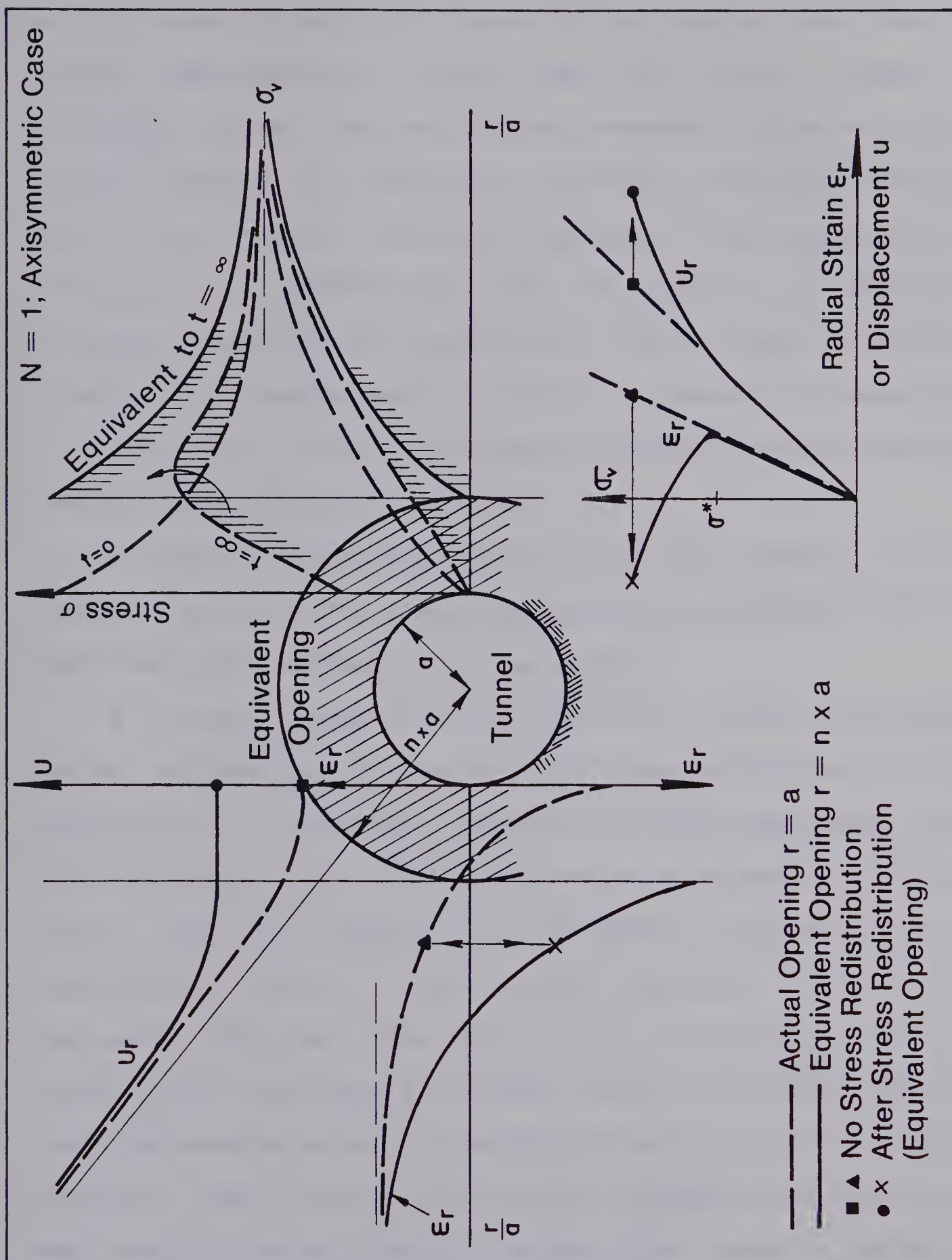


Figure 6.7 Equivalent Opening Approach for an Axisymmetric Case

σ^* is shown below this figure. It has been assumed that no stress redistribution occurs when the field stress is increased to σ^* , but that stress transfer occurs at higher stress levels. An equivalent opening therefore develops above this stress level and the tunnel wall displacements increase at a faster rate. With the transfer of tangential stresses away from the opening the radial strain pattern is altered to a shape similar to the one shown in Figure 6.7. As a result of this, the radial strains decrease and tend towards negative radial strains.

It must be realized that this approach assumes a volume decrease in the zone inside the equivalent opening but this could be easily adjusted if necessary.

A further step in this logic is to assume isotropic, static properties but anisotropic (e.g. orthotropic) creep properties. A schematic diagram of the resulting stress redistribution for an example where an element (I) creeps faster than an element (II) is shown in Figure 6.8 for a hydrostatic stress field ($N=1$). During a fixed time increment stresses drop more rapidly at point (I) than at point (II) resulting in a rapid stress redistribution away from the opening along the horizontal axis and a slow stress transfer along the vertical axis. An equivalent opening of the shape of an ellipse is created. This causes a reduction of the tangential stress concentration at the roof and an increase at the spring line at a distance b , inside the rock mass. As soon as an elliptical, equivalent opening is

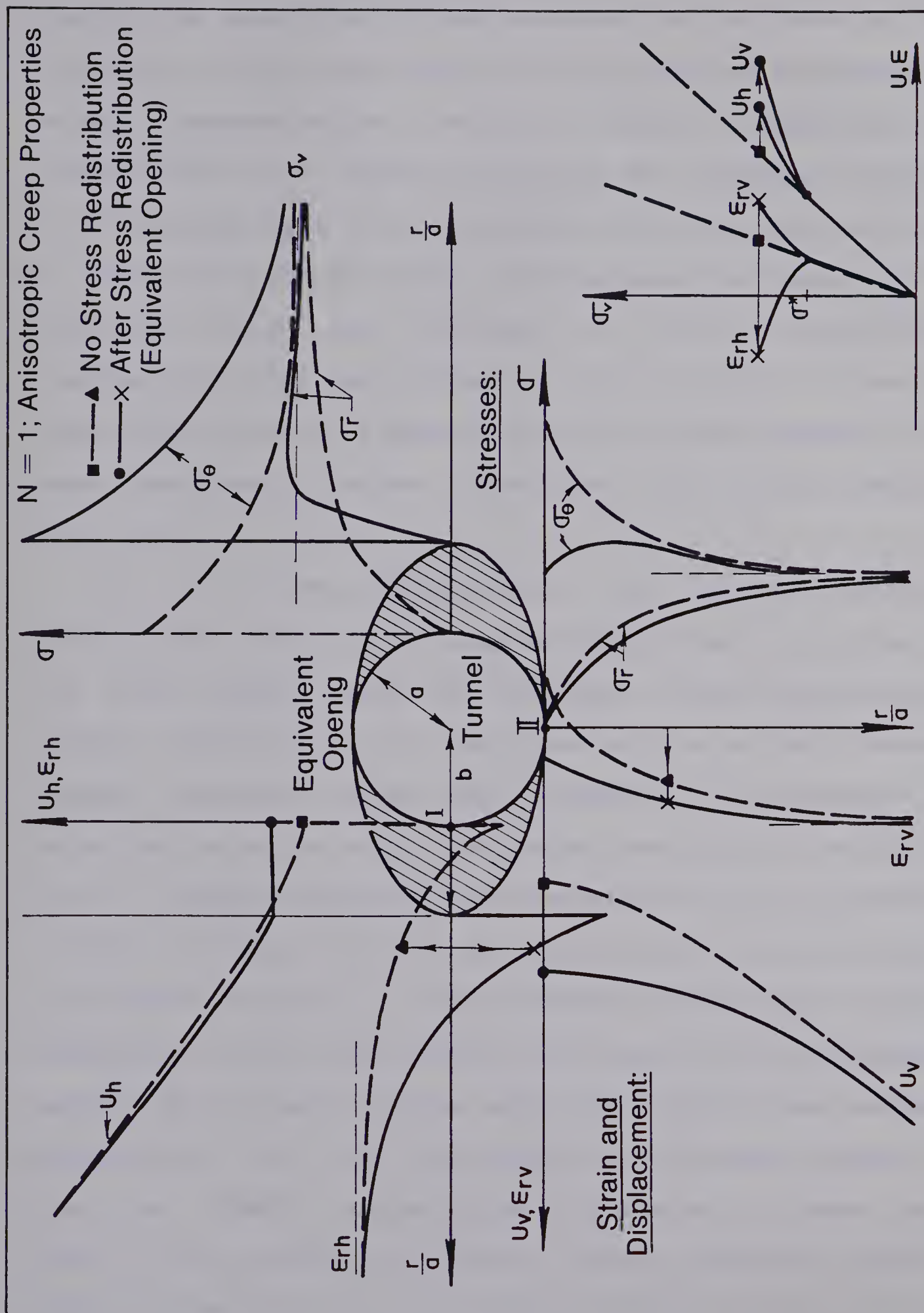


Figure 6.8 Equivalent Opening Approach for a Case, with Non-symmetric Stress Redistribution

created the tangential stress concentration increases in the direction of the major axis of the ellipse and enhances the stress redistribution process. Stable propagation is achieved due to a steady increase of the confining pressure σ_r . The development of the tangential σ_t and radial stresses σ_r around an ellipse as the ratio between the length of the major and minor axis increases is given by Feder(1978, Figures 16 to 18), for ratios $b/a = 1.0, 1.5, 2.0$. It can be seen that the radial stresses exceed the field stresses even under hydrostatic stress conditions ($N=1$) if b/a reaches about 2.0.

As a first approximation it can be assumed, particularly in the case where no fracturing or yielding of the rock occurs, that the overall volume change during stress redistribution is zero since the sum of the stresses remains constant. Under this condition it is possible to determine the shape of the equivalent opening, the ratio b/a for an ellipse, from the measured closure of the initially circular opening. For this purpose a closure ratio has been introduced, similar to the one defined earlier for circular openings, as the ratio between the closure of an equivalent opening in an elastic medium under the applied field stress, measured at $r=a$, and the closure of a circular opening in the same elastic medium under an hydrostatic stress field ($N=1$). The calculated closure ratios (ordinate) together with some test data are summarized in Figure 6.9.A, B and C. Figure A gives, as discussed earlier, the predicted closure

ratio for a circular opening in an isotropic medium as a function of stress ratio N (abscissa), angle θ (orientation of tunnel diameter) and Poisson's Ratio for the "Reality", the "Model" and the "External Displacement" for the model (overall deformation of the model block). For the remaining Figures 6.9.B and C only the case of the "Model" has been considered.

Figure 6.9.B shows the predicted closure ratios for elliptical openings as a function of N , θ , the axis ratio b/a , and Poisson's Ratio (for equations see Appendix A6.1, and for data Appendix A6.2, Tables A6.1, A6.2). The shaded area in this diagram indicates a range of axis ratios b/a which have been predicted from the actual observations on Test MC-2. Dashed lines with arrows show the prediction path.

As mentioned earlier, the full circles in Figure 6.9.A give the closure ratios for the various Tests MC-2.4 to MC-2.9 and the full squares give the corresponding ratios of external displacements. At $N=0.5$ the stiffness was underestimated (due to loading to 3 MPa only) and the point would move, if corrected, in the direction of the arrow near the stars in parantheses. Where two or more squares are shown, the one close to the theoretical line corresponds to a higher loading rate than the one farther away from this line. The arrows therefore indicate the effect of a loading rate decrease and it can be seen, in connection with Figure 6.9.B, that the ratio b/a of the equivalent opening

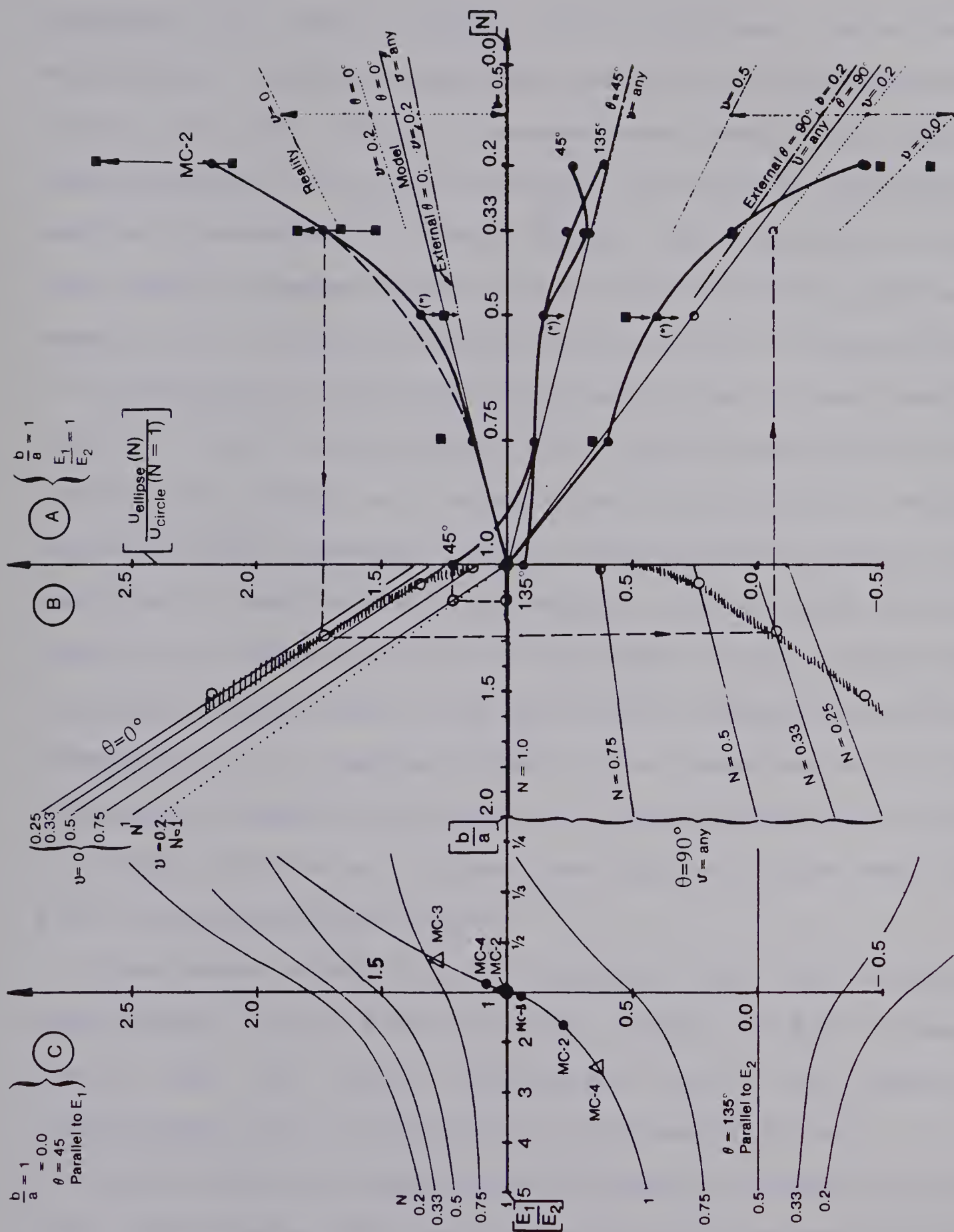


Figure 6.9 Closure Ratio as a Function of (A) Stress Ratio N , (B) Equivalent Opening Shape b/a , and (C) Anisotropy Ratio

increases as the loading rate decreases. From this observation it can be concluded, and this will be supported later by the internal measurements, that the stress redistribution is a function of time and that the equivalent opening increases in size or changes shape with time. From the tunnel closure ratio it follows that the equivalent opening was close to the real opening up to a stress ratio of approximately 0.5. This is misleading due to the loading history. Test MC-2.5 at $N=0.5$ was executed before MC-2.6 at $N=0.75$ and stopped at a stress level of 3.0 MPa. No stress redistribution occurred during these first two tests. The equivalent opening then increased, during Test MC-2.6 ($N=0.75$) to $b/a=1.3$ and to $b/a=1.55$ during Test MC-2.8 ($N=0.33$), which means that the stress redistribution zone propagated to a maximum depth of at least 4.5 cm at the beginning of Test MC-2.9. From the crack pattern shown later in Figure 6.12 it can be seen that b/a was in the order of 2.0 at the end of Test MC-2.9.

The same trend can be observed from the external displacement ratio (full squares, Figure 6.9.A). Figure 6.9.B has not been constructed for the external displacements but it would show a corresponding trend.

The effects of anisotropic deformation properties have been neglected so far. The data points for a stress ratio $N = 1$ (Figure 6.9.A) show that there is more closure parallel to the joints and less closure perpendicular to the joints. To evaluate this effect a third graph (Figure 6.9.C) has

been constructed showing the predicted closure ratio as a function of E_1/E_2 , the stiffness ratio, and N for $b/a = 1$, Poisson's Ratio equal to zero, and directions of loading parallel and perpendicular to the direction of maximum stiffness. The equations have been derived from Sonntag(1958) and are summarized in Appendix A6.1. The ratios for $N = 1$ are drawn in full circles for tests MC-2, 3 and 4 and the resulting stiffness ratios are 1.65, 1.1 and 0.8 for the directions perpendicular and parallel to the jointing, and 1.0, 0.6 and 2.5 in the directions of the principal field stresses (empty triangles). While it appears that Sample MC-2 could have a anisotropy ratio of 1.65 (not proven by internal strain measurements) in the direction expected for the coal, the samples MC-3 and 4 show little anisotropy in the corresponding directions. This is supported by internal strain measurements. The tunnel closure ratio in the principal field stress direction of these tests shows a high anisotropy which is not expected because of the joint orientation at 45° to the tunnel axis. It seems therefore entirely possible that this closure ratio is a result of stress redistribution, or the creation of an elliptical, equivalent opening, due to anisotropic creep properties. The corresponding b/a values lie between 1.1 and 1.2 but with the ellipse oriented parallel to the jointing in Test MC-2 and at 45° to the jointing in Test MC-3 and 4. The explanation of the observed closure by non-symmetric stress redistribution appears, at least for Tests MC-3 and

4, to be more plausible due to the isotropy observed from internal and external strain measurements.

The implication of this observation is that non-symmetric stress redistribution may occur around a circular opening even if the stress field is hydrostatic. Non-axisymmetric and non-linear closure of an opening does not therefore necessarily indicate a non-hydrostatic stress field, non-linear elastic properties or yielding of the rock, but rather a non-axisymmetric stress redistribution. Many interpretations of field observations by elasto-plastic or linear visco-elastic models seem therefore questionable. Furthermore, evaluation of the stability of underground openings on the basis of stress concentrations predicted from elasticity theory may be very conservative in conditions where stress redistribution can be expected. This resulted in the underdesign of the model test frame by at least a factor of two.

6.3.1.2 Internal Radial Strains

Figures 6.7 and 6.8 indicated how the internal radial strains are affected by the development of an equivalent opening. The following discussion of the radial strain pattern around an opening is based on the equivalent opening approach and is only qualitative for two major reasons: (a) the radial strain measurements are strongly affected by local properties and therefore vary over a wide range (e.g. closure of discontinuities seems to dominate at low stress

levels), and (b) the solution for radial strains around an elliptical opening under a biaxial stress field were not readily available, and it was decided that their derivation was not essential at this stage due to the fact that the general strain pattern could be estimated from the stress distribution around an elliptical opening (Feder(1978)).

Figure 6.10 shows schematically the expected stress-strain relationship for a small N -value and three special shapes of openings in a linear elastic material. Corresponding to the instrument locations in Test MC-2, the strains have been plotted for a point at a distance of approximately 1.7 times the tunnel radius. Figure 6.10.a shows for a circular opening ($N \ll 1$) that extension is expected along the horizontal axis and compression at an angle of 45° as well as in the vertical direction. The next figure indicates that the amount of strain in the principal directions is expected to increase if an equivalent opening with a ratio $b/a > 1$ exists. The instruments at 45° to the principal axis may show compression or extension depending on geometry of the opening, Poisson's Ratio, and anisotropy ratio. If it is now assumed that stress redistribution propagates non-symmetrically, due to non-uniform creep or yield, as indicated in Figure 6.10.c, the radial strains are expected to be affected as sketched. In the vertical direction (1,5), a slight increase due to shape and size change of the equivalent opening would develop while the instruments in the direction of the opening expansion would

$N = \text{Small (eg. 0.2)}$
 Material: Linear Elastic

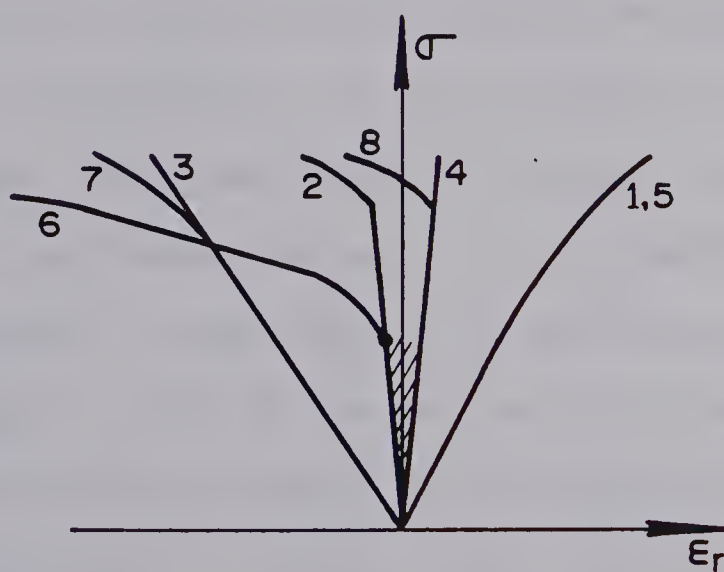
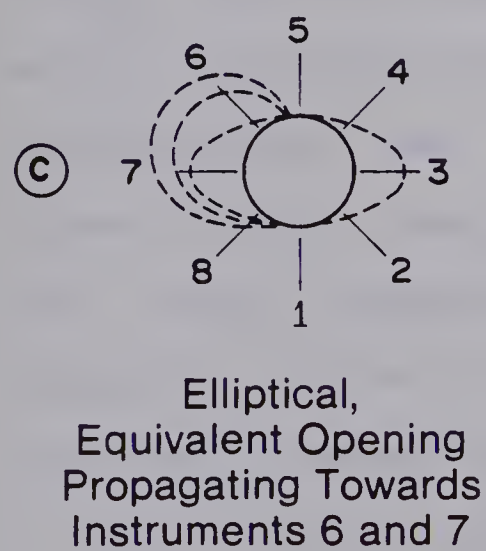
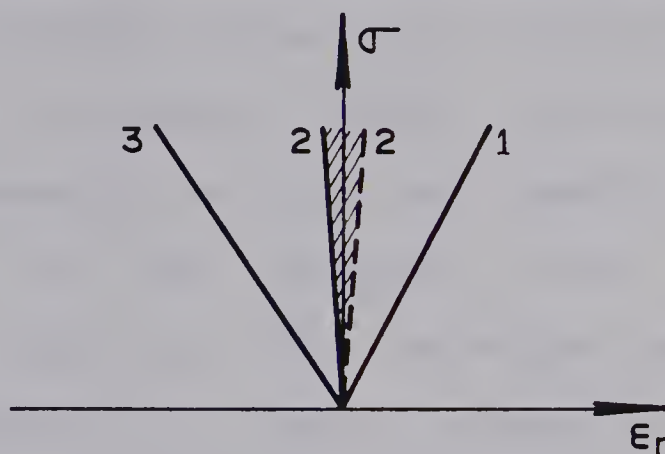
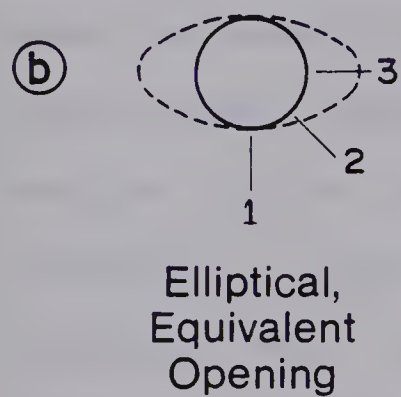
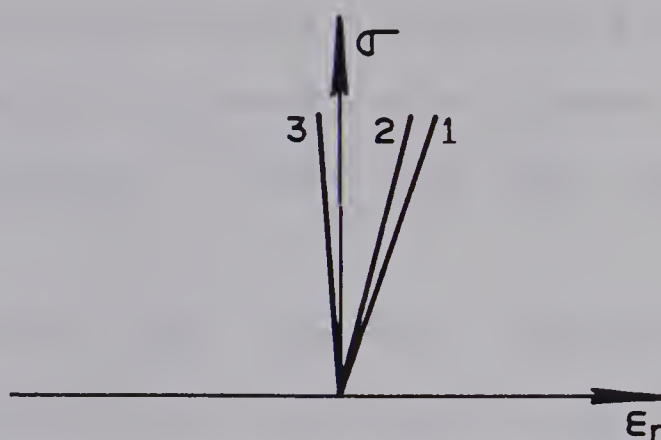
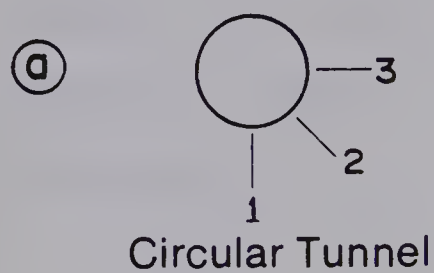


Figure 6.10 Schematic Diagram to Illustrate Radial Strain Development

show increasing extension. The non-linearity introduced in the stress-strain curves will be obvious at different stress levels as the propagation increases with stress, and possibly time, at different rates for the various directions.

Figure 6.11 summarizes the observed stress-strain curves for Test MC-2.9 ($N=0.2$). All instruments show trends which correspond to the predicted stress-strain relationship after some scatter at low stress levels. As mentioned earlier it is not reasonable to try and explain each individual instrument. It was observed that some contradictions, in the light of the equivalent opening approach, exist when explaining radial strains measured during tests at different stress ratios. Nevertheless, the general trend supports the existence of an elliptical stress redistribution zone and the curvature of these curves at higher stress levels indicates the mode of propagation of this stress redistribution zone. The early deviation from linearity of two gauges parallel to the jointing shows a definite propagation towards the upper left corner and with a total strain accumulated of more than 2% it can be expected that some yielding occurred in this region in addition to the stress transfer. Non-linearities in two gauges perpendicular to the jointing and in two horizontal gauges at higher stress levels indicate clearly that the stress redistribution zone propagates, at a lower rate, towards the lower left corner. Since strains do not exceed

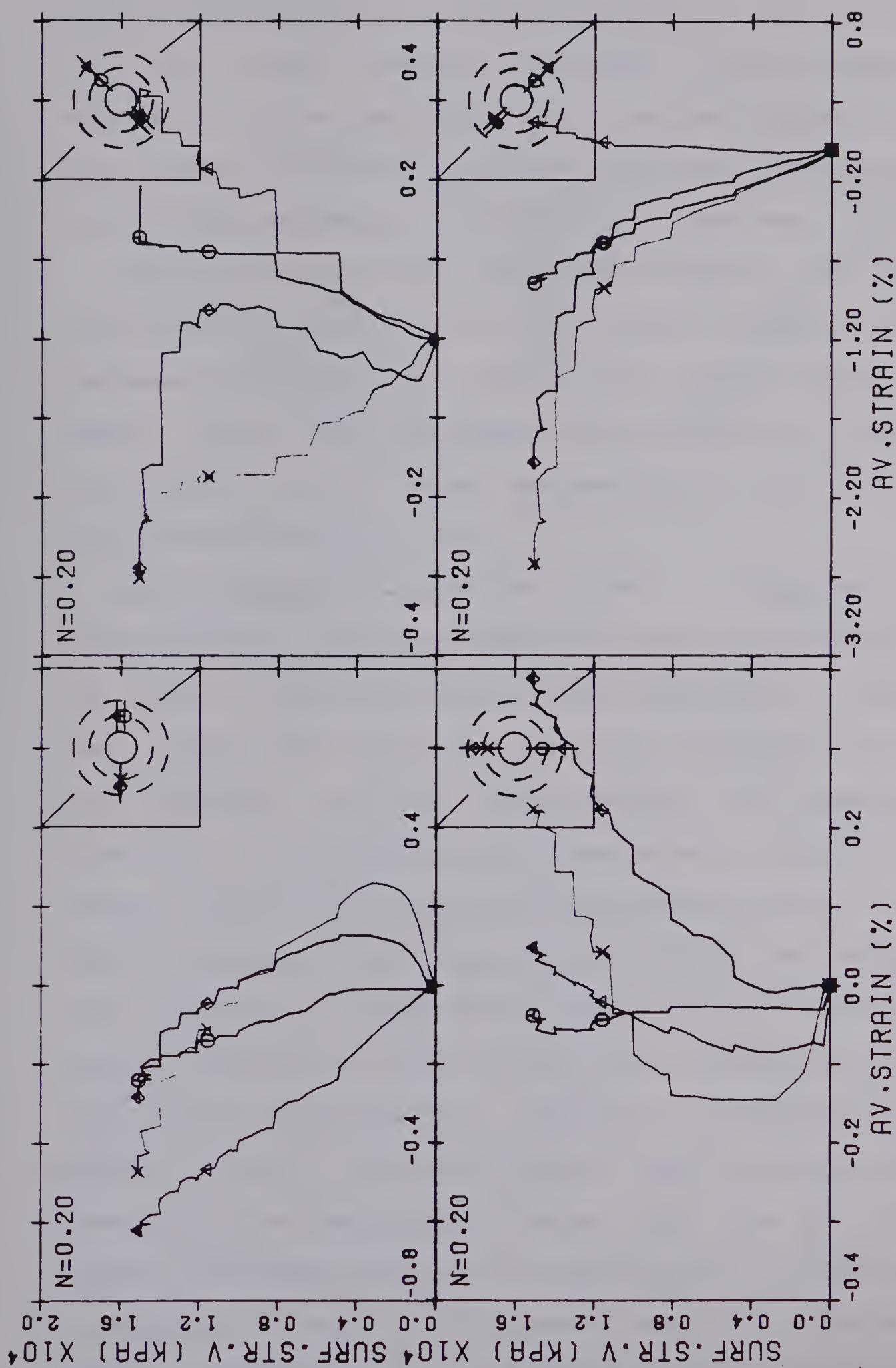


Figure 6.11 Test MC-2.9: Stress versus Radial Strain Measurements at $N=0.2$

TEST #MC-2.9 WITH TUNNEL 1977

0.4% in compression and -0.6% in extension it can be assumed that very little yielding occurred in this region. This suggestion of no yielding could not be verified for Test MC-2 because no unloading curves have been recorded during uncontrolled unloading while the sample rotated.

For comparison, the maximum closure of the tunnel at this point is 6.8% and the minimum closure -1.2%. The instrumentation on the other sides of the tunnel (lower right) support the existence of an elliptical, equivalent opening but do not show propagation of this elliptical stress redistribution zone.

The mechanism considered here is supported by the observed crack pattern. Figure 6.12 shows a picture of the top face of the Sample MC-2 after unloading at the end of Test MC-2.9 ($N = 0.2$). The following information is shown: the location of the instrumentation (to scale); the direction of the jointing; the approximate direction of the maximum (parallel to the joints) and minimum tunnel diameter after unloading (b/a approximately 0.97); the location of the longitudinal cracks in the tunnel (by the dot in a half circle close to the tunnel wall); and a possible outline of the stress redistribution zone. The orientation of the minimum axis of this elliptical zone coincides with the location of the longitudinal cracks which seem to be tensile cracks and support again the hypothesis of the existence of an elliptical stress redistribution zone. The crack pattern, which is essentially an indication of differential straining

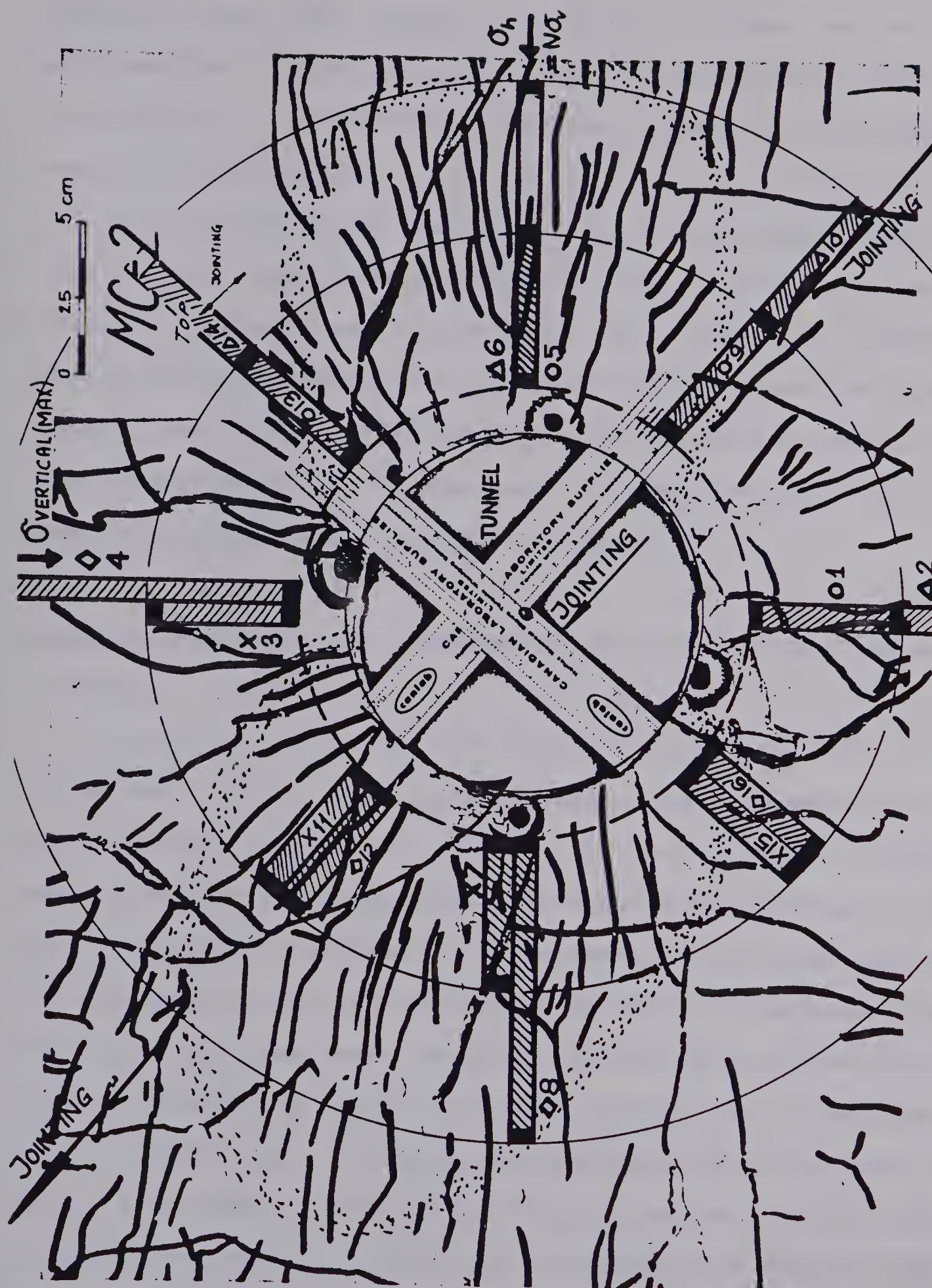


Figure 6.12 Crack Pattern near Tunnel and Location of Internal Sample Instrumentation

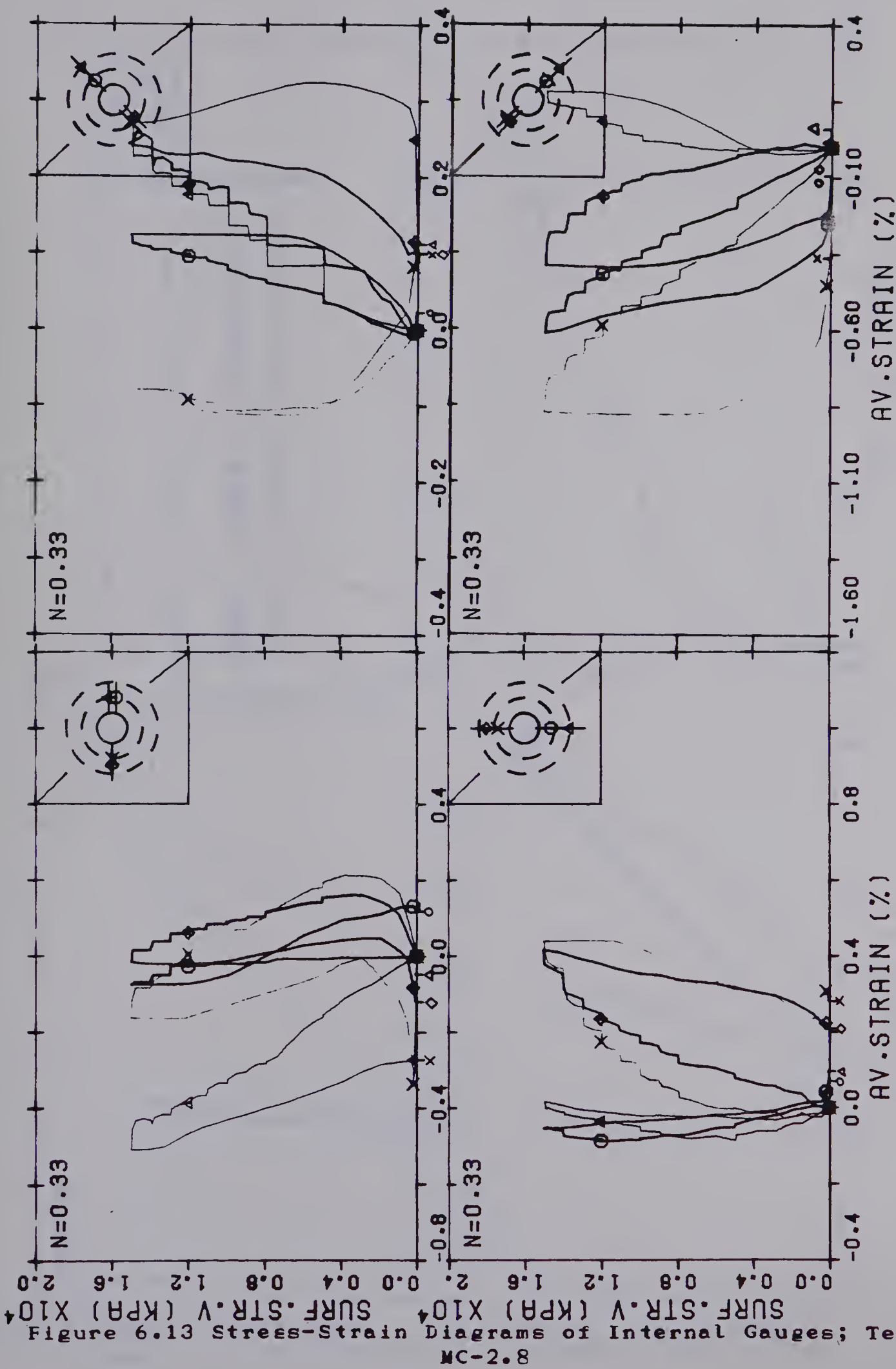
(between coal and plaster of Paris) during unloading, confirms the assumed mechanism. Tensile cracking is visible, as expected, perpendicular to the direction of highest compressive straining.

The time-dependent behaviour will be discussed later in more detail but it becomes obvious, from the stress-strain curves presented in Figure 6.11 and from the process discussed above, that stress redistribution is not the major reason for creep at low stress levels but that it dominates the time-dependent deformations at high stress levels as soon as the equivalent opening is expanded.

6.3.1.3 Extension of "Equivalent Opening Approach" Beyond Yielding

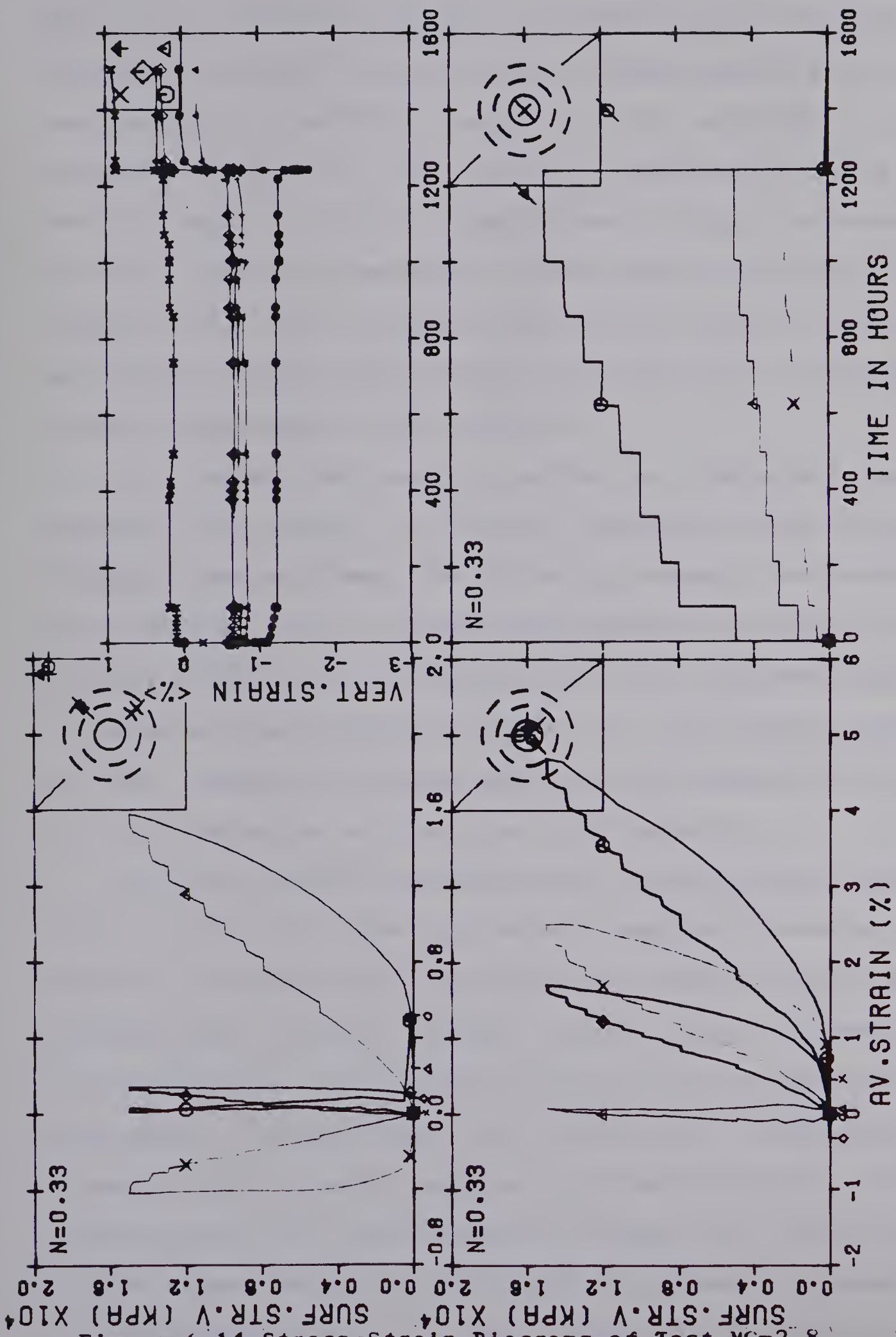
From the previous discussion it follows that non-linearity in the stress-strain or stress-closure relationship may be a result of two factors: stress redistribution and expansion of an equivalent opening due to (a) non-linear, stress-dependent creep and (b) yielding of overstressed rock. It is rather difficult to separate the two factors from the recorded measurements but there is strong indication of very little yielding up to the final test MC-2.9. The following observations are in support of this view. The tunnel wall remained intact during the whole testing program and no cracking was observed before the last unloading. Most of the external displacements and tunnel closures have been recovered. For example, in Test MC-2.8

both principal closure measurements have recovered completely (Figure 6.14) whereas the tunnel diameter perpendicular to the jointing showed about 0.35% extension and the diameter parallel to the jointing showed 0.45% compression after 10 days of recovery. (Recovery had not completely terminated at this time). This observation may be explained, but is not supported analytically in this thesis, by the stress redistribution process due to anisotropic, or non-linear, stress-dependent creep properties. A certain stress pattern which has been created during the loading history of the model test is relieved elastically if the sample is unloaded. The stress patterns created during loading and during unloading are not identical due to the different loading histories, and a residual stress pattern with tensile stresses inside the equivalent opening and compressive stresses near the limit of this equivalent opening remains. These stresses are redistributed slowly during recovery. Because of stress-dependent creep parameters it is impossible to reach the original state of zero stress and the original shape of the opening. This may result in an over-closure in one direction and an under-closure in the other. The existence of such a residual stress field may be the reason for the gradual increase of the equivalent opening between tests ($b/a = 1.0, 1.1, 1.4, 1.75$, see Figure 6.9). This point is further supported by some internal gauges which showed over-recovery (Figure 6.13) whereas others did not recover completely. The proof



TEST #MC-2.8 WITH TUNNEL 1977

Figure 6.13 Stress-Strain Diagrams of Internal Gauges; Test MC-2.8



TEST #MC-2.8 WITH TUNNEL 1977

for this explanation cannot be given here but it should be possible to support it by a finite element analysis with the corresponding material properties. In addition to the evidence given, it can be seen from the two tests with $N=0.33$ that no change in equivalent opening size occurred due to the first loading to 10 MPa during Test MC-2.7 (see Figure 6.9, both closure ratios of Test MC-2.7 and MC-2.8 are equal to 1.7). This would not be expected if yielding or stress redistribution had occurred.

It is not the intent to extend the equivalent opening approach to predict the model behaviour after extensive yielding has occurred. The following comments are therefore speculations based on some qualitative observations during further testing and are included only as a hypothesis and as a proposal for further research; e.g. for further analysis of the results from Test MC-3 and MC-4 (Guenot(1979)) and for the evaluation of data from case histories.

Volume change characteristics constitute one problem which complicates the equivalent opening approach. The effect of dilation may for many rock masses be small, since displacement occurs mainly along shear planes or discontinuities. The overall volume change may therefore be negligible. Nevertheless, the effect of dilation on the closure of the real opening must be incorporated in the determination of the equivalent opening. Any volume change in the stress relieved zone affects the closure measurements and therefore bears on the method used to determine the

shape of the equivalent opening. Other rock properties such as the post-peak slope of the stress-strain relationship do not influence this approach. The stress distribution and therefore the shape and size of the equivalent opening is a direct response to the rock mass deformation characteristics. For example, if a zone of overstressed rock is created, one portion will be at its ultimate resistance while an intermediate zone is weakening. The zone farthest from the tunnel will deform elastically but will undergo stress redistribution. The extent of the equivalent opening will lie between the zone with material at ultimate strength and the zone with maximum tangential stress. The time-dependent strength and fracture process will influence the deformation pattern as soon as a weakening zone exists. In practice, however, this process may be important only in supported tunnels. In unsupported tunnels, as observed in the model tests MC-3 and 4 (Guenot(1979)), rupture due to sudden local instability (spalling or buckling) may dominate the time-dependent failure process of an opening.

6.3.1.4 Implications Resulting from Stress - Strain Observations

Local zones of weakening or rapidly deforming material causes stress redistributions which dominate the time-dependent strain deformation pattern long before yielding is initiated. In practice, this stress redistribution may be affected significantly by the excavation process (full or

partial face, blasting or machine excavation, rate of advance), initial support (rock bolting, anchoring, shotcrete), water infiltration, and other factors. Many generally applied methods of comparing field measurements assume no stress transfer and a constant shape of the equivalent opening. This assumption leads to fundamentally wrong data interpretation because of the neglected effects of a change in the shape of the equivalent opening boundary. The elastic deformations are altered significantly if an opening is changed from a circular to an elliptical shape.

The time-dependent weakening process has not been studied in detail in this test series but it evolves from the observed behaviour in the pre-yield stage that weakening may be an important process, particularly for supported openings. This conclusion supports the view expressed by Nakano(1979) that softening in shale may be a more important factor than swelling or that long-term loading of supports in shales must be attributed to softening and weakening rather than swelling.

6.4 Interpretation of Time - Dependent Data

From the previous discussion it follows that time - dependent processes during the loading of the model tunnel, due to deviatoric and hydrostatic creep of the rock mass, results in time-dependent stress redistribution and the development and propagation of an equivalent opening. This process is controlled by non-linear, stress-dependent and

anisotropic creep properties at stress levels lower than the long-term strength, and by the time-dependent strength, yielding and weakening of the rock mass if the long-term peak strength is exceeded.

The equivalent opening approach may also be applied to predict the time-dependent behaviour and to explain the test results. It is necessary to concentrate on the internal radial strain measurements to evaluate stress redistribution. The tunnel closure or the external displacement measurements are influenced by the overall rock mass response whereas the internal gauges react to local processes. A gradual stress redistribution away from the opening with increasing stress level will influence internal gauges more and more depending on the location of the measuring point.

6.4.1 Interpretation of Time - Dependent Results by Equivalent Opening Approach

Figure 6.15 schematically illustrates the process of propagation of an equivalent opening and shows predicted strain - time curves. For a circular opening under a hydrostatic stress field, elastic extension near the opening changes gradually to compression further away from the opening. Over the measuring distance (AC) it is likely that for the geometry chosen for the test, compression is recorded due to the overall compression of the sample. Under deviatoric stresses, time-dependent extension would be

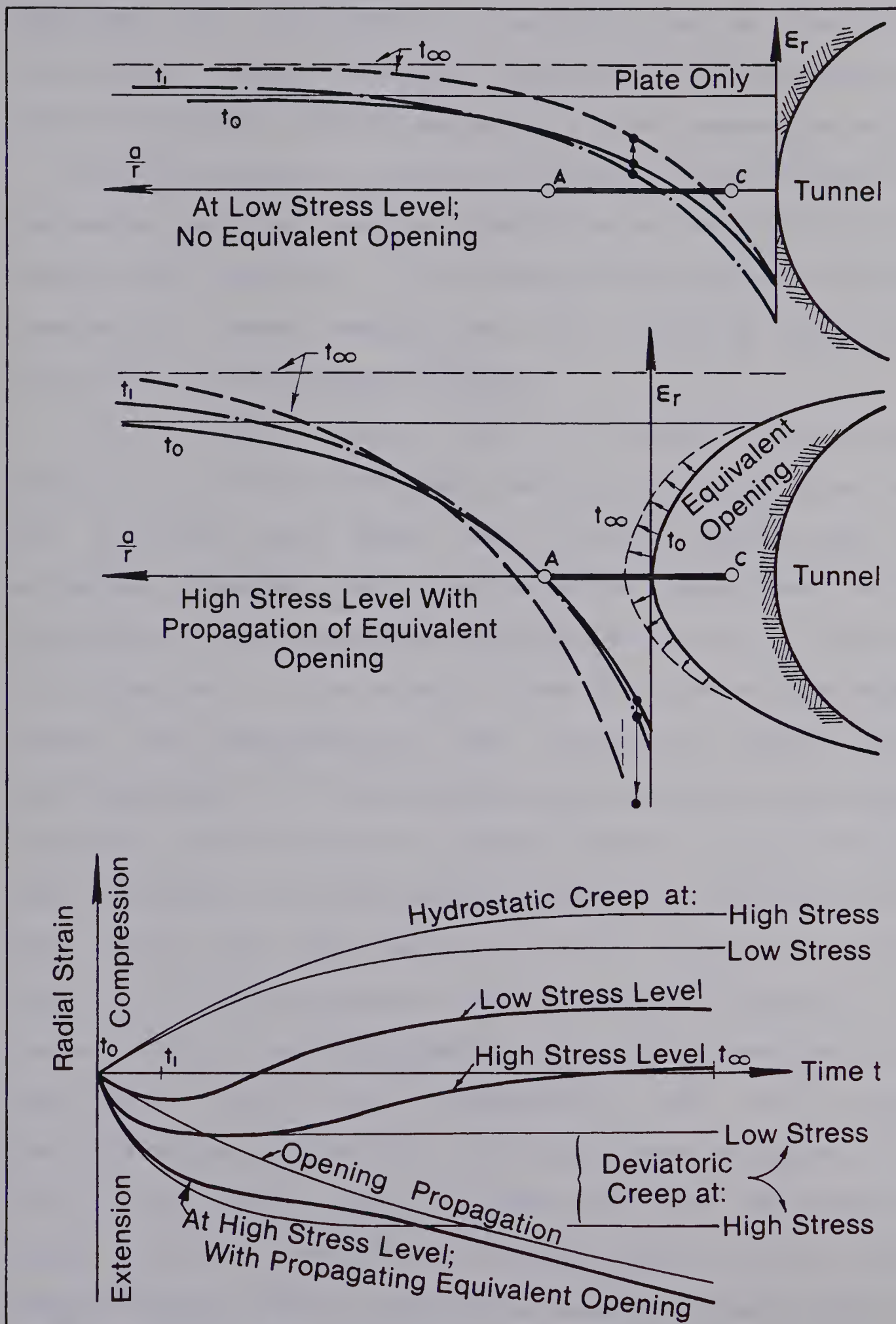


Figure 6.15 Schematic Diagram to Illustrate the Time - Dependent Radial Strain Development

expected but time-dependent compression may be observed if hydrostatic creep dominates immediately after loading or after deviatoric creep terminates. The corresponding strain - time relationship is shown for this low stress level (the extension portion may be missing or be replaced by a low creep rate plateau). It is important to realize that this hydrostatic creep process does not occur in reality, at least not in an axisymmetric case.

At a higher stress level, or after an equivalent opening has been developed, the second drawing shows that the extension zone moves away from the tunnel. Over the measuring distance (AC) the relative importance of the deviatoric creep increases, and less compression is observed as indicated by the strain - time curve for a high stress level. If propagation of the equivalent opening occurs simultaneously at this stress level even more extension is observed. This is shown by another strain - time curve. The same process is illustrated schematically, and supported by real data from Test MC-2.6, in Figure 6.16 in log strain rate - log time diagrams. For the schematic diagram it was assumed that the hydrostatic creep (I, compression), the deviatoric creep (II, extension), and the stress redistribution effects (III, extension) plot as linear lines in a log strain rate versus log time plot. The resultant curve (1) for a test at a low stress level σ_1 and no stress redistribution shows decreasing negative strain rates for the first 20 hours and then positive strain rates. The same

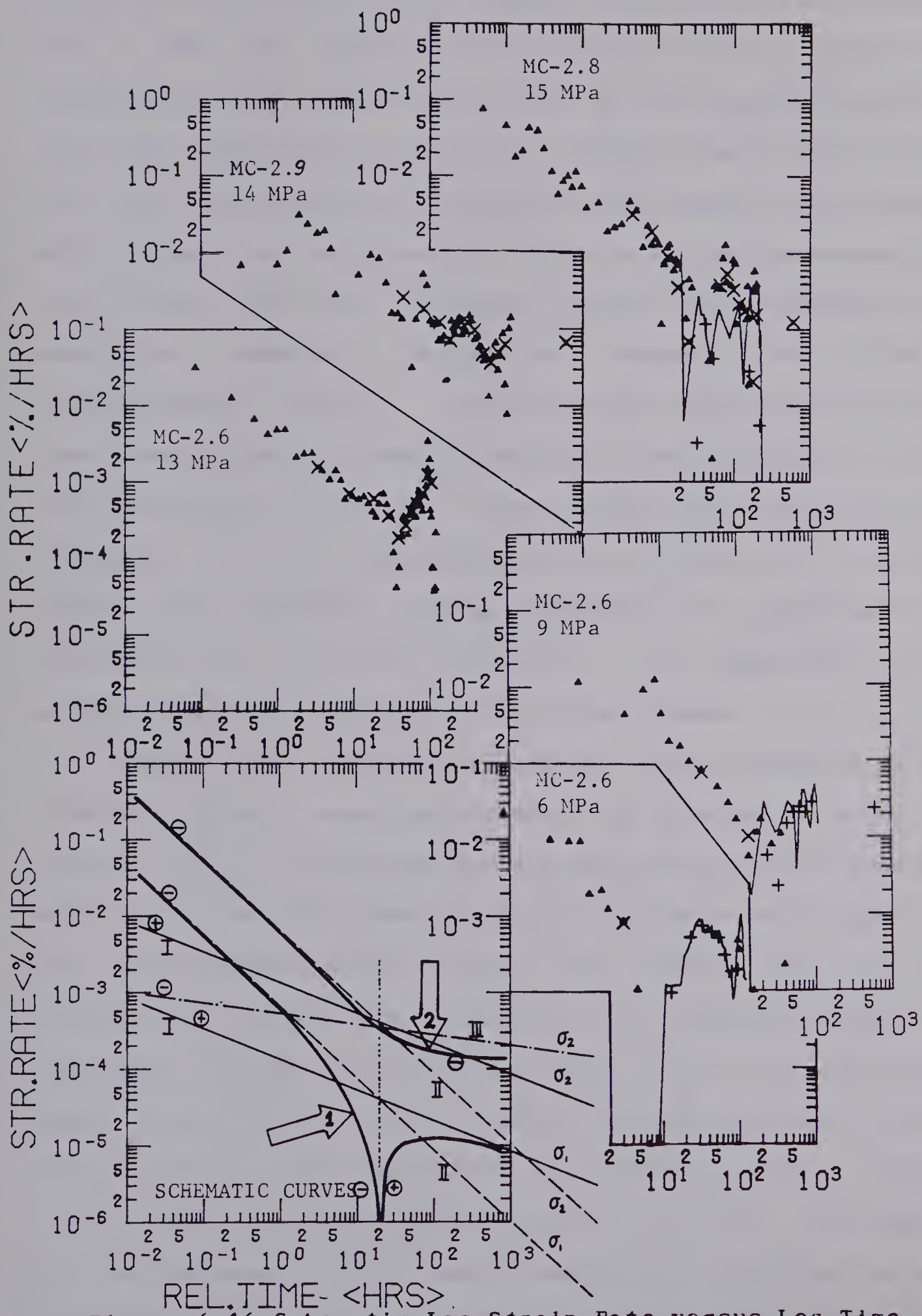


Figure 6.16 Schematic Log Strain Rate versus Log Time
Diagrams in Comparison with Measurements

trend has been observed for example in Test MC-2.6 at 6 MPa and 9 MPa. At higher stress levels stress redistribution influences this behaviour as shown by the schematic curve 2 and test data from Test MC-2.6 at 13 MPa, Test MC-2.9 at 14 MPa and Test MC-2.8 at 15 MPa. At this stage various types and shapes can be observed. After an initial deceleration the strain rate may increase, change sign or behave in a wave-like fashion indicating surges of stress redistribution. Some of these surges can be attributed to load variations but usually indicate local yielding. Stress redistribution occurs at lower stress levels but does not dominate; it is a time-independent or short-term process. During the selected loading history the time-dependent straining is controlled largely by the magnitude of the stress increment relative to the stress level.

Figure 6.17 summarizes typical data recorded by an internal strain measuring device. The location is shown in Figure 6.12. It measures the average radial strain between about 1.4 and 2.35 times the tunnel radius in the direction of the minimum field stress. The ratio b/a for the elliptical, equivalent opening, as discussed earlier, increases during Test MC-2.6 from 1.0 to 1.4 and during Tests MC-2.7 and 2.8 to 1.75. The point of zero radial strain lies, depending mainly on Poisson's Ratio, at least 0.25 times the tunnel radius further away from the tunnel. If the average radial creep strain at the location of the instrument is small, as observed during MC-2.4, it follows

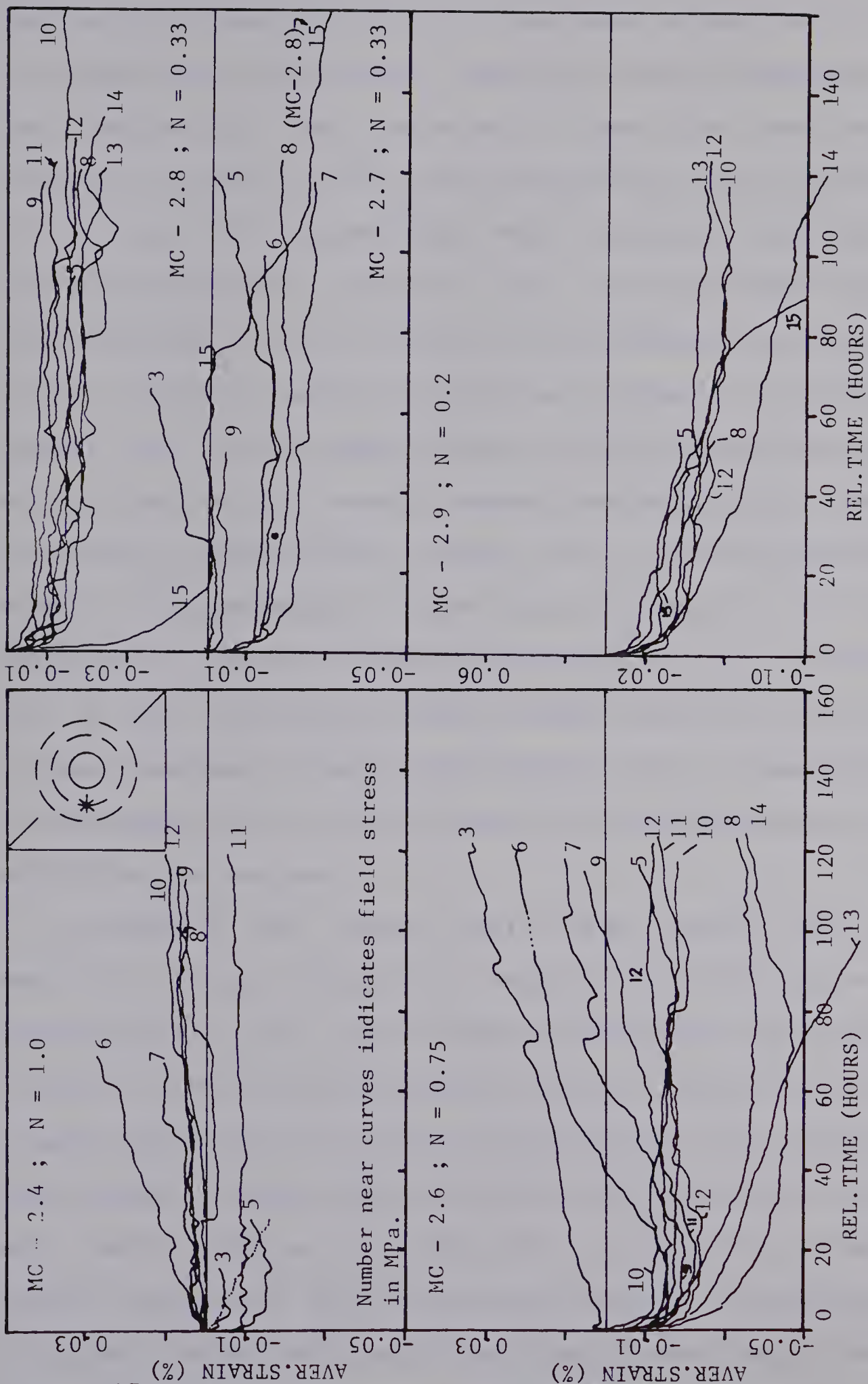


Figure 6.17 Summary of Strain - Time Diagrams from Test MC-2 for one Specific Instrument; N=1, 0.75, 0.33 and 0.2.

TEST #MC - 2.4, 2.6, 2.7, 2.8, 2.9 WITH TUNNEL 1977

that the instrument is close to this zero strain point, that no significant equivalent opening is being developed, and that hydrostatic and deviatoric creep are more or less balanced (at $\sigma_y=3, 5$ and 11 MPa deviatoric creep and at $6, 7$ to 10 and 12 MPa hydrostatic creep dominates slightly). It would therefore be expected that the equivalent opening would propagate and influence this instrument during Test MC-2.6 ($N=0.75$) and at high stress levels in the following tests. This can be observed very clearly from Figure 6.17, $N=0.75$. At stress levels below 8 MPa deviatoric creep is followed by hydrostatic creep; at 8 MPa time-dependent stress redistribution occurs and increases the radial extension but becomes stable after about 70 hours; between 9 and 12 MPa deviatoric creep is more pronounced; at 13 MPa another increased stress redistribution with no deceleration is observed; and at 14 MPa further, but decelerating, stress redistribution occurs.

Throughout the three tests with $N=0.33$ and $N=0.2$ deviatoric creep dominated. This is reasonable since less compression of the coal occurred during repeated reloading and due to the reasons discussed earlier. During Test MC-2.8 a major time-dependent stress redistribution was observed at the maximum stress level of 15 MPa. The equivalent opening must have increased to $b/a=1.75$ at the end of this last loading increment. Test MC-2.8 which had to be discontinued at 10 MPa did not show any significant stress redistribution effect and this was supported by the results from the study

of the equivalent opening size (Figure 6.9) which showed no significant change of the ratio b/a between MC-2.7 and 2.8.

Finally, during Test MC-2.9 ($N=0.2$) (note: double scale) time-dependent stress redistribution was apparent at low stress levels, most likely due to stress redistribution in the tensile stress zone at the tunnel roof. At stresses of 14 and 15 MPa the equivalent opening increased significantly but no collapse of the tunnel occurred. The sample rotated at this stress level and the test had to be discontinued due to damage of one corner.

It is now of interest to go back and review the time - dependent tunnel closure measurements, Figures 6.2 to 6.5. From the equivalent opening approach, it is concluded that tunnel closure is governed entirely by the properties of the rock mass surrounding the equivalent opening and the propagation of the stress redistribution zone. A non - symmetric propagation results in a shape change of the equivalent opening and affects the tunnel closure ratio between diameters in different orientations. This explanation is generally supported by the time-dependent tunnel closure measurements. Figure 6.5 shows nearly constant creep strains up to high stress levels. This would be expected for a linear visco-elastic rock mass under the given loading history if no significant stress redistribution at low stress levels occurs. If the rock mass can be described by a three parameter solid with a number of Kelvin elements in series, resulting in a power-law

relationship between strain rate and time, the tunnel closure should show a power relationship with different parameters depending on stress ratio and angle of tunnel diameter orientation. A change in shape of the equivalent opening would alter these parameters and, if this change is time-dependent, it should affect the linearity of the log closure rate - log time plot. No such non-linear trend can be observed from the summary sketches, Figures 6.3 and 6.4, even though internal gauges clearly indicate stress redistribution with time (see Figure 6.17). Nevertheless, individual curves show some non-linearities; curves 18 and 20 (MC-2.6), and 20 (MC-2.9) in Figure 6.2. None of these deviations support clearly the development observed from internal gauges. This does not contradict the equivalent opening approach because of the strong support by the measured stress-tunnel closure relationship but it confirms the earlier statement that tunnel closure is dominated by the overall rock mass response to stress redistribution. Stress transfer in one zone may result in tunnel closure in another direction depending on the shape change of the equivalent opening.

6.4.2 Interpretation of Data by Linear Visco - Elasticity

In this section, a linear visco-elastic material model is used to describe the observed creep behaviour at low stress levels. It must be realized that this model represents the material properties only to a limited extent

and may have to be replaced by a non-linear model for better interpretation of the data. Nevertheless, this simple model will help to explain the difference between the time-dependent behaviour of the model tunnel and a tunnel in reality, particularly the effects of hydrostatic creep or consolidation. Furthermore, it will be possible to illustrate the effect of a non-linear Bulk Modulus on the model behaviour.

No attempt was made to determine the rheological parameters for the selected models by curve fitting model test or laboratory test data. It is possible to determine these parameters by comparison of creep and recovery data, but this is not necessary for the purpose described above. Parameters for the calculations were estimated from test results presented by Kidybinski (1966) and Morlier (1964) and selected in such a way that calculated creep rates and retardation times compared with observations from the model tests. Linear visco-elasticity was chosen for three reasons: many authors describe the time-dependent properties of coal by a Burger Model, some with a number of Kelvin elements (Terry(1956)) in series and some with bi-linear properties (Kidybinski(1966)); the results from repeated relaxation tests reported in Chapter 2 support the selection of a linear visco-elastic model; the chosen loading history can be modeled by linear superposition and it is possible to compare the behaviour at different stress levels without unnecessary complications.

The stress field predicted from linear visco - elasticity does not change with time under the boundary conditions of the model test. The effects of stress redistribution can therefore not be described by this material model but the equivalent opening approach may be applied if the opening does not change size or shape with time (no time-dependent stress redistribution). The behaviour during time-dependent stress redistribution could be simulated by considering an equivalent opening in a linear-elastic medium with time-dependent shape parameters. This has not been undertaken in this thesis but this process model describes conceptually the observations made during the model tests. For example, creep (extension) rates and total creep strains decrease after the tangential stress maximum has passed by an instrument. This may be observed from Figure 6.17 from results collected during tests after Test MC-2.6. As discussed earlier it can be assumed that the stress redistribution zone affects the instrument mainly during Test MC-2.6. Much less stress redistribution can be observed in later tests except during further extension of the equivalent opening in Test MC-2.8 at 15 MPa and Test MC-2.9 at 14 and 15 MPa.

The procedure to derive of the visco-elastic solutions for radial strains and tunnel closure from known elastic solutions by application of the Laplace Transformation is described in Appendix A6.1. The diagrams discussed later represent specific solutions calculated and plotted by

computer. The results are presented in similar diagrams as the test data and have been calculated for a unit load increment of 1 MPa. The response due to higher increments can be determined by linear superposition.

For comparison, the radial strains at the tunnel wall in reality (REAL) are given together with the radial strain at a distance (a) from the centre of a plate without tunnel (PLATE), the displacement at the tunnel wall ($U(A)$) and the sample boundary ($U(4a)$), and the radial strains (at $R=1.0A$, $1.25A$, $1.5A$, $2.0A$ and $3.0A$, see Figure 6.19). A 3-parameter solid (Kelvin element in series with a Hooke spring) has been selected to investigate the deviatoric creep effect. During this analysis the hydrostatic component was assumed to be linear elastic (spring element). In the second part both deviatoric and hydrostatic material properties have been represented by 3-parameter solids with different rheological parameters. The individual parameters selected will be discussed later.

6.4.2.1 Effect of Time - Independent, Non - Linear Modulus of Compressibility

The Bulk Modulus K (or $1/K$, the modulus of compressibility) varies as a function of stress, in many porous or fissured materials like coal. It increases from an initial minimum towards a maximum which is equal to the Bulk Modulus of the intact material. It may be assumed therefore that K increases during a model test as the field stress

increases. The corresponding radial strain distribution for stress increments at various K -values is shown in a schematic diagram in Figure 6.18 and two stress-strain curves for the radial strain near the opening and at depth are sketched in the same figure. A comparison of these curves with real data presented in Figure 6.11 (top left diagram) shows that the coal sample possesses a low Bulk Modulus at stress levels below approximately 4 MPa and gradually approaches a maximum above this stress level. The opposite behaviour observed in the same figure but in the bottom left diagram is a result of the stress ratio $N=0.2$.

For an incompressible material the strain pattern in reality corresponds to the strain pattern in the model. For a lower Bulk Modulus radial strains increase (become positive) and tunnel closure increases accordingly. The latter may be up to two times the closure of the equivalent case ($N=1$) in reality. The strains and displacements for a stress ratio of unity are independent of K in reality but depend strongly on K in the model. This applies as well to time-dependent strains and tunnel wall displacements.

The effects of compressibility on the time-dependent behaviour is illustrated by Figure 6.19. The rheological model selected to calculate these curves was composed of a Kelvin Model with a spring stiffness $E_{12}=6000$ MPa and a coefficient of viscosity $N_{12}=20000$ MPa-Hr (both values are one order of magnitude lower than the ones given by Kidybinski(1966) or Morlier(1964) and have been selected to

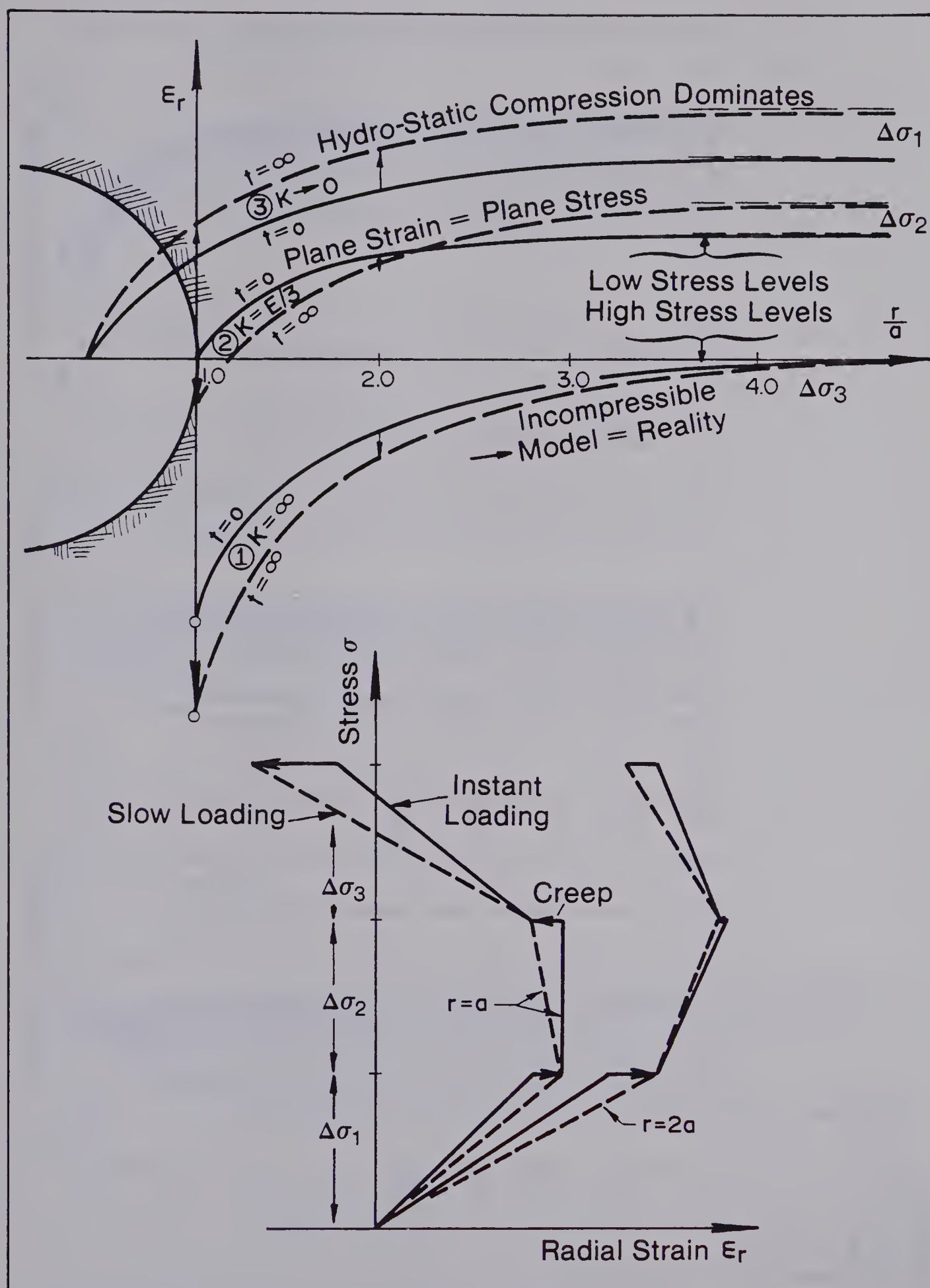
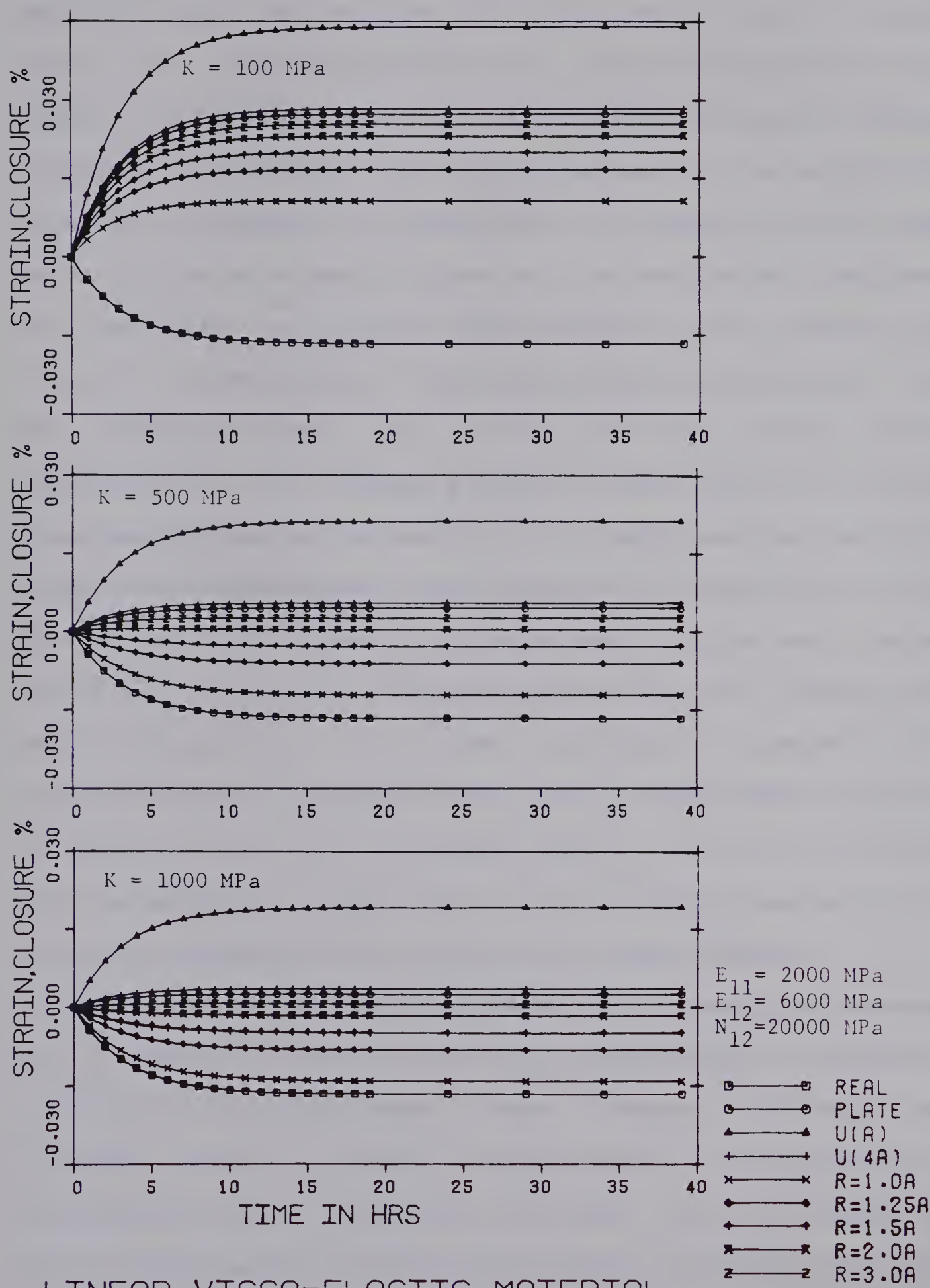


Figure 6.18 Schematic Diagram to Illustrate Effect of Non-linear Bulk Modulus



LINEAR VISCO-ELASTIC MATERIAL

Figure 6.19 Time-Dependent Behaviour of a Linear Visco-Elastic Material; Bulk Modulus K=1000,500,100 MPa

maintain the retardation time but reduce the total creep strain to values comparable with actual observations). The spring in series with the Kelvin Element had an assumed stiffness $E_{11}=2000$ MPa (corresponding to a short-term material stiffness of $E_0=2400$ MPa for Poisson's Ratio equal to 0.2. This is slightly lower than determined by Kidybinski or Morlier). As a first approximation it was assumed, and this is reasonable for the time intervals considered, that the viscous element in series with the spring can be neglected in the Burger's Model. A unit load of 1 MPa has been applied instantaneously to this model and the resulting strains and displacements were plotted as a function of time for three Bulk Moduli $K = 1000, 500, 100$ MPa and a stress ratio N of unity. For a linear elastic material (above 4 MPa field stress) and the given rheological parameters the K -value would be expected to be close to 1000 MPa. A smaller K means a smaller Poisson's Ratio (for K near 500 MPa, Poisson's Ratio is about zero if E is assumed constant) or a negative Poisson's Ratio if K is less than 500 MPa.

It can be seen that extension creep should be observed to a depth of $1.5a$ except if the material is extremely compressible. Furthermore, these diagrams show that creep strains should decrease continuously in extension or compression with increasing distance from the tunnel and that displacements should continuously increase. This does not correspond to observations from some of the extensometers which showed a reversal of creep rate after

about 20 hours.

It may also be seen from these figures that the radial creep strains at the tunnel wall are independent of K in reality (REAL) and increases with decreasing K in the model test due to compression of the plate without tunnel (PLATE). This comparison can also be made in future figures and will not be repeated each time.

From this discussion it follows that:

1. the compressibility has to be considered if model test results are compared with or applied to real field conditions;
2. compressibility may dominate both the stress-strain and strain-time relationship observed in the model;
3. the time-independent effect would be expected to dominate mainly at low stress levels; and
4. if K is time-independent the observed strain rate reversals cannot be explained from linear visco - elasticity.

Because of this last point it was decided to study the influence of time-dependent compaction (hydrostatic creep).

6.4.2.2 Effect of Hydrostatic Creep

Time-dependent compaction, consolidation or hydrostatic creep, would be expected to dominate at stress levels in excess of the instant crack closure range but below stress levels where deviatoric creep dominates. In addition, it is reasonable to assume that both parts, the deviatoric and the

hydrostatic creep components, possess different rheological parameters which could explain the observed reversals in strain rate. The observation of a general trend towards radial compression after a certain time led to the following selection of rheological parameters. The deviatoric creep was simulated by a 3-parameter solid with $E_{11}=4000$ MPa (Spring) and $E_{12}=8000$ MPa, $N_{12}=50000$ MPa-Hr (Kelvin element), and the hydrostatic creep was represented by a 3-parameter solid with $E_{21}=4000$ MPa (Spring) and $E_{22}=12000$ MPa, $N_{22}=600000$ MPa-Hr (Kelvin element). These parameters result in a strain-time relationship where the deviatoric portion has a short retardation time and the hydrostatic part has a long retardation time. They have been selected to produce strain rates, strain reversal times, and stress-strain relationships comparable to the model test results. Two stress ratios $N=1$ and $1/3$ have been analysed, for the latter case in three directions θ , parallel and perpendicular to the principal field stress and at 45° to it. The results are shown for a load increment of 1 MPa and a stress ratio of unity in Figure 6.20 in strain-time and in log strain rate versus log time diagrams. Figures 6.21 and 6.22 give the corresponding curves for a stress ratio of one third and for orientation angles θ of 0° , 45° and 90° . The following Figure 6.23 summarizes strain rate plots for both cases and for all locations. These curves have been copied by hand and are therefore not as accurate as the other curves.

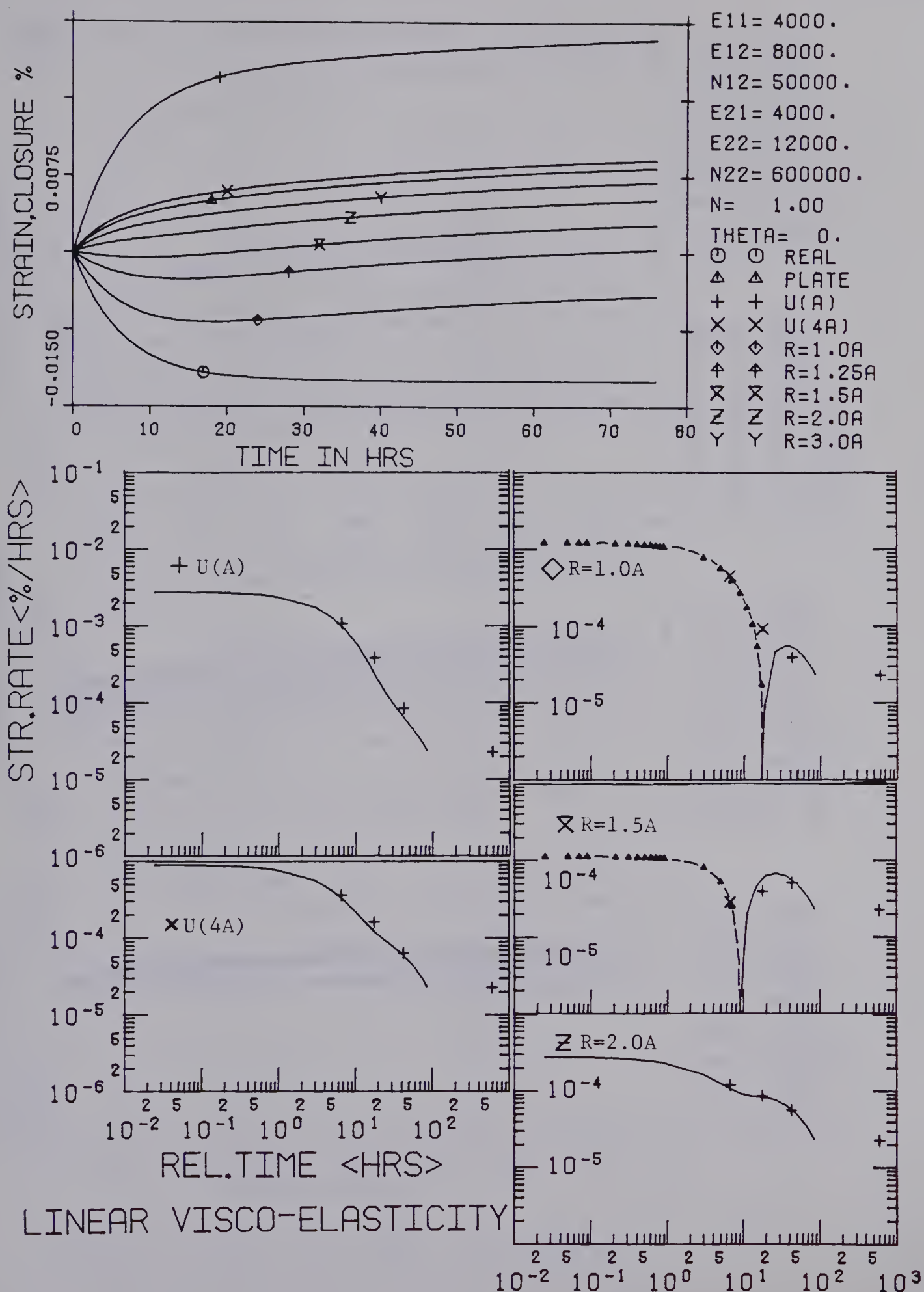
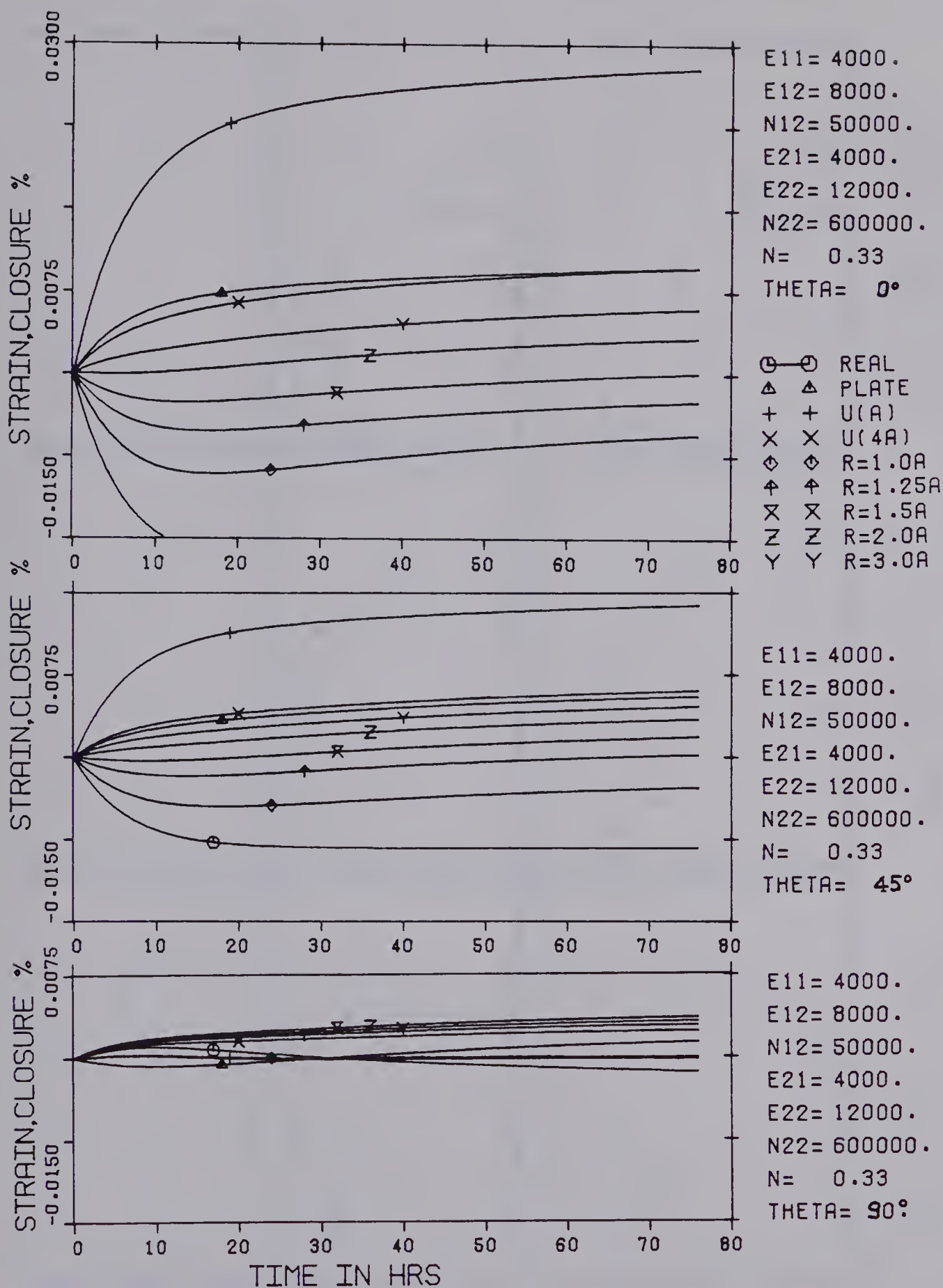


Figure 6.20 Linear Visco-Elasticity with Deviatoric and Hydrostatic Creep; $N=1$.



LINEAR VISCO-ELASTIC MATERIAL

Figure 6.21 Strain-Time Diagrams: Linear Visco-Elasticity with Deviatoric and Hydrostatic Creep; $N=1/3$.

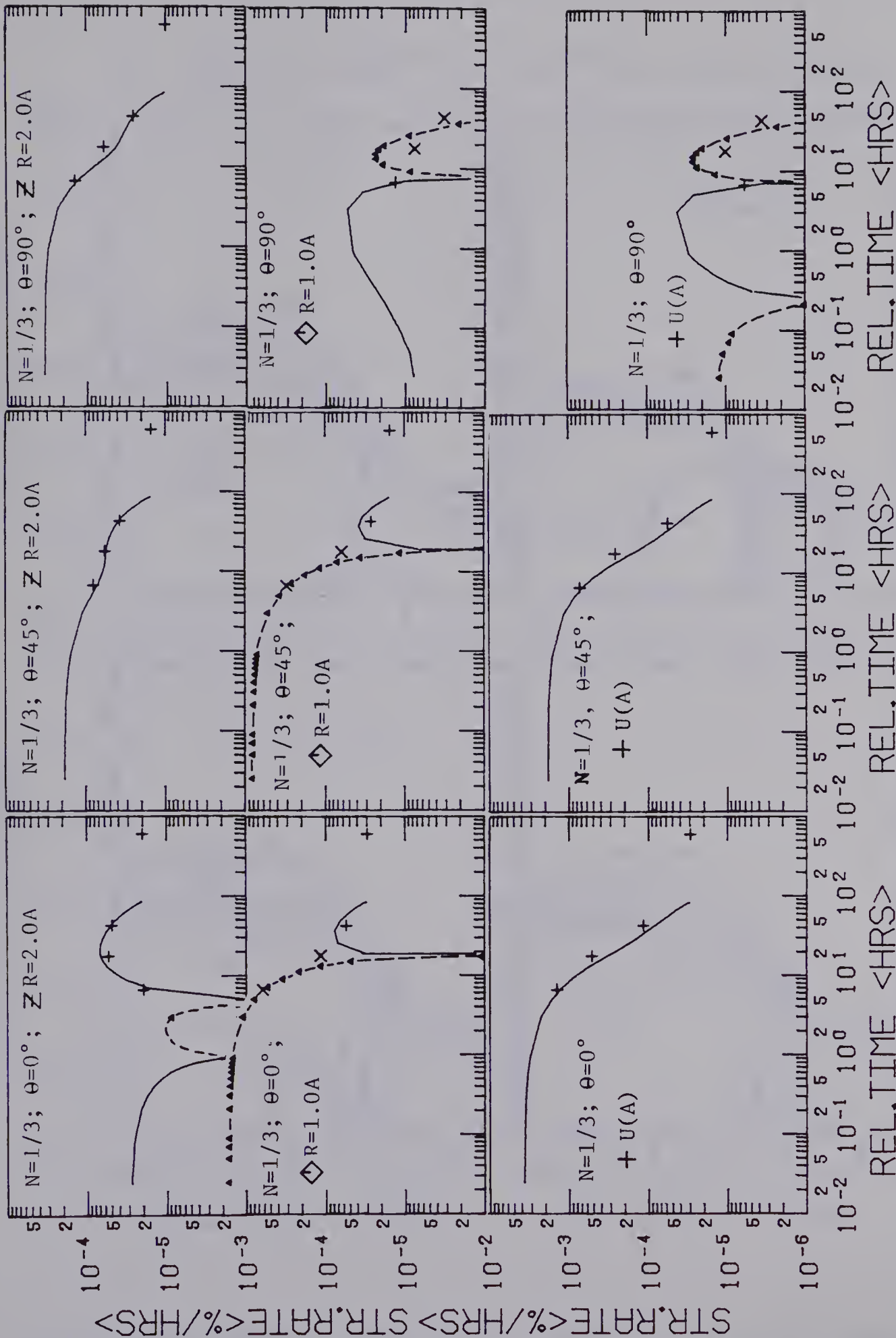


Figure 6.22 Log Strain Rate - Log Time Diagrams: Linear Visco-Elasticity with Deviatoric and Hydrostatic Creep; $N=1/3$.

LINEAR VISCO-ELASTICITY

P....Plate; R....Reality; 3.0...3.0A

a....U(A); 4a...U(4A); 1.0...1.0A; 1.5...1.5A; 2.0...2.0A;

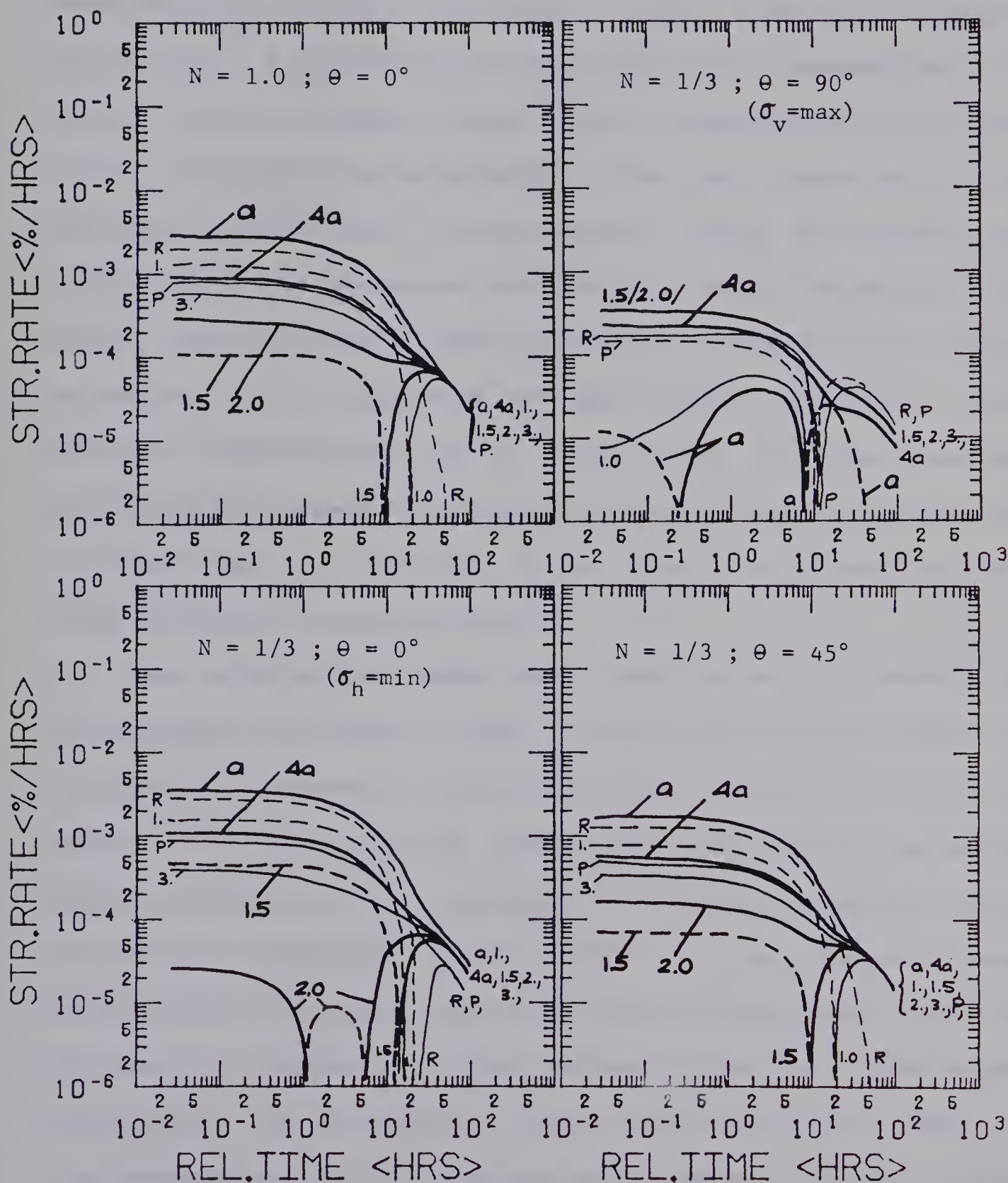


Figure 6.23 Summary Plots in Log Strain Rate - Log Time Diagrams: Linear Visco-Elasticity with Hydrostatic and Deviatoric Creep, $N=1$, $N=1/3$.

A comparison of figures of test data, presented earlier or in Appendix A6.2, shows that this simple linear visco-elastic model predicts the observed behaviour accurately. A variation of the individual parameters would result in a change of the relative importance of the two creep components or retardation times and almost any of the observed strain-time relationships could be modeled. The first row of instruments measures the radial strain between $R=1.5$ and $2.0 A$ and shows, according to Figure 6.20, slight extension or a no-creep plateau which gradually tends towards compression. If an equivalent opening has been developed the expected behaviour would be close to the curve corresponding to $R=1.25A$, which shows more extension and a clear reversal of strain rate.

The similarity with real test data is even more pronounced in Figure 6.22. It must be realized that the originally horizontal log strain rate - log time curve is a result of the selected model of two single 3-parameter solids. Linking of a series of Kelvin elements with a retardation spectrum would result in an almost linear relationship in Figure 6.22 for both the deviatoric and the hydrostatic component. The dotted lines in this figure correspond to extension rates and the full lines to compression rates. For a stress ratio equal to unity initial extension close to the tunnel changes to compression between 8 and 50 hours depending on instrument location. All instruments tend towards the same compression rate which is

completely controlled by the hydrostatic creep parameters. Examination of the typical data set given in Appendix A6.2 for Test MC-2.6 ($N=0.75$, not unity) supports these theoretical curves. The same is true for the results shown in the remaining three diagrams for a stress ratio of $1/3$. A few interesting observations are worth describing in more detail. The predicted behaviour at an angle θ of 45° is very similar to the results from $N=1$. Actual data showed significant deviations from this prediction and has been attributed to stress redistribution effects or the development of an equivalent opening. For $\theta=90^\circ$ (minimum stress direction) the tunnel closure rates $\dot{u}(a)$ are very low and change from extension to compression and back to extension. This was actually observed in some creep tests and can not be explained by load fluctuations. A similar behaviour, but with opposite signs, has been predicted for the instrument at $R=2.0A$ and $\theta=0^\circ$ (maximum stress direction). Again, such behaviour was observed during testing and can not be explained otherwise.

In summary, the model of linear visco-elastic creep under deviatoric and hydrostatic stress conditions predicts observed model test results extremely well. The parameters selected for this prediction are close to values reported in the literature. A modification of the rheological model would be necessary to improve the prediction for the time intervals of less than one hour and more than about 100 hours.

6.4.3 Conclusion

Stress redistribution occurs around an opening as a result of non-linear, stress-dependent creep, non-isotropic creep properties and/or yielding, strength loss and strain-weakening. Collapse is initiated by rupture due to strength loss or local instability. The time-dependent process observed in the model test may be explained considering a non-linear Bulk Modulus at low stress levels, hydrostatic and deviatoric creep at intermediate stress levels, and time-dependent propagation of an equivalent opening at higher stress levels. This time-dependent propagation is a result of non-linear stress-dependent creep properties, local creep, and local or global yielding due to time-dependent strength loss. The time-dependent rupture process has not been investigated.

The implications are that:

1. time-dependent compressibility must be considered when applying the results from model test to field conditions;
2. time-dependent compressibility may play an important role in reality if the stress ratio is not unity and if this compressibility is not isotropic; and
3. non-isotropic creep properties and the principle of an equivalent opening due to time-dependent stress redistribution must be considered in the interpretation of field observations.

These three points will be discussed in Chapter 7. 336

CHAPTER 7

CONCLUSIONS, IMPLICATIONS AND RECOMMENDATIONS

7.1 Time-Dependent Properties of Rock Masses

Detailed conclusions related to time-dependent properties of rock and rock masses resulting from laboratory testing and the development of a phenomenological model are given at the ends of Chapters 3 and 4. Only a few of the most important points are repeated here and discussed in the light of their implications or as a justification for further research.

A schematic stress - strain curve for brittle rock has been developed on the basis of results from multiple-stage repeated relaxation tests on coal. It has been concluded that the stress - strain - time relationship is a response to the rock structure at a particular instant and its evolution as time, strain or stress increases. Strain - weakening rock can be stressed within a stable zone, where time-dependent deformation terminates within an engineering time scale, and within an unstable zone where the rate of deformation depends on the stress level relative to the current available strength; the current available strength is the maximum strength which can be reached if the rock is loaded instantaneously. The rock structure which develops, and therefore the current available strength mobilized, depends on the stress history and the accumulated strain. The stress history is controlled by three, important

parameters: the loading history, the development of the confinement pressure, and the stiffness of the loading system. A particular rock possesses a structure-dependent peak strength, strain to failure, ultimate resistance and extent of the unstable zone within which time-dependent fracture processes occur. The same rock or rock mass may develop different structures in situ and respond accordingly. Many authors have investigated the response of rock to a certain loading history at various stages of the rock structure evolution but more effort should be directed towards the study of the development of different fracture modes, and the related time-dependent and time-independent behaviour. The results presented in Chapter 3 describe only one fracture mode, the development of a shear plane through a discontinuous joint system (coal) at low confining pressure. It has been concluded that such a material, representing a brittle rock mass under a low stress field, can be described as an elastic or visco-elastic, strain-weakening, visco-plastic material. Further research should concentrate on the investigation of the time-dependent behaviour of rock during the development and evolution of different fracture modes for various rock types under different conditions. It is essential for practical applications to understand this evolution rather than the response at a particular instant.

A phenomenological model of rock with time-dependent properties, supported qualitatively by results from various

testing methods reported in the literature, has been developed. It illustrates clearly how the rock structure controls the time-dependent behaviour of rock. Both a time-dependent and a time-independent resistance of a rock can be mobilized or exhausted depending on the stress history, the state of stress, and other factors like rock alteration. This phenomenological model has to be extended to a numerical model and expanded to include other essential parameters. It should eventually be implemented by finite element analyses to allow investigation of structures in rock experiencing time-dependent fracture.

7.2 Underground Openings in Rock Masses with Time-Dependent Properties

7.2.1 Model Testing

Practical conclusions and implications are discussed in Section 7.2.2. In the following a few comments on the model testing itself will be presented.

The model studies undertaken for this research project are unconventional in the sense that it is not the intent to simulate a specific prototype but rather a particular process. Difficulties normally encountered during model testing are significantly increased as soon as time-dependent processes are involved. Similitude relationships can only be established if severe assumptions about the material creep law are made (e.g. linear visco-elasticity). This very important problem of similitude has

not been investigated and is relegated to further research. It is assumed that the observed processes (e.g. stress redistribution) exist in reality but it is understood that the time-scale and even the relative importance of individual processes may differ. It is recommended that this problem of time-scale be investigated by a study of existing data from case histories rather than from dimensionless analysis or similitude considerations.

The non-linear and time-dependent compressibility of the model material has complicated the interpretation of the time-dependent measurements considerably. This is particularly important because the rock mass compressibility does not influence the deformation behaviour in reality in the same manner as in the model. In reality, under a hydrostatic stress field and with isotropic material properties, displacements are a function of the shear modulus only and independent of the compressibility or Bulk Modulus. The stress path is therefore very important and it is recommended that the possibility of drilling the tunnel under applied field stress or loading with simultaneous application of an internal (tunnel support) pressure be investigated. Nevertheless, the total straining of the rock is the same in both reality and the model, and it can be assumed that the fracture mode itself is not affected significantly by the compressibility. On the other hand, it is likely that the time-scale and the amount of stress redistribution is exaggerated due to the compressibility.

The model test system is developed to a stage where it produces reliable data. The sample instrumentation performs well but it is important to record the location of the instruments accurately and to minimize the distance between the anchor points of the extensometers. The instruments should be positioned as close as possible to the tunnel if the influence of the tunnel is to be observed and further away from the tunnel if the time-dependent failure process is to be investigated. More testing should be undertaken on the sample without a tunnel to establish the creep properties of the coal, the loading and unloading moduli for fast and slow loading, the anisotropy ratio, and the heterogeneity of the sample (stiffness distribution).

It is now essential to develop numerical tools which allow the investigation of many of the questions that have arisen. Numerical methods have to be adopted mainly because of the apparent importance of anisotropic and non-homogeneous rock mass properties. More strength and creep testing of coal at high confining pressures may be needed to determine the material properties more accurately.

Because of the problem of material compressibility it seems advisable to concentrate, during further model tests, on the study of the time-dependent failure process rather than on the pre-failure behaviour. A flexible tunnel support system might have to be developed and installed in the tunnel to increase the value of the tunnel closure measurements recorded during the failure process. During

this phase of the test spring-loaded LVDT-pointers may penetrate into the broken material and render the measurements useless.

7.2.2 Application to Underground Openings

The time-dependent stress redistribution and failure process around an underground opening can be separated into four phases:

- I) Development of an initial stress state (elastic or elasto-plastic);
- II) Stress redistribution to zones of high confinement;
- III) Progressive yielding and rupture (if stress level higher than long-term yield stress);
- IV) Development of stable equilibrium or protective zone (German: Schutzhuelle).

The mechanisms involved in each phase and particularly the relative importance of these processes are not clearly understood. Opinions still diverge considerably especially in connection with the time-dependent development of these phases. Yielding and the expansion of a plastic zone are generally accepted as the major factors causing stress redistribution. This fact is reflected in design methods based on elasto-plastic, dilatant and strain-weakening material models. The results of this investigation do not support the relative importance of the progressive yielding process. This is true, even though global yielding has not been reached in the test, since theoretical calculations

with reasonable material properties predict significant yield zones at the maximum stress level. It has been concluded that other processes causing comparable stress redistribution patterns may be equally relevant. Furthermore, it follows from the conclusions in Chapter 3 that the stress-history must be considered in the evaluation of the plastic zone since the stress-strain relationship of a certain rock mass may be significantly affected by the stress-history.

The results of Test MC-2 describe mainly the developments within Phase I, II and IV. Phase III is non-existent, because of the load level, or its importance is minor. The relevance of Phase III will be investigated in more detail in the future on the basis of the data reported by Guenot(1979) but some of the observations made during his tests are reflected in the conclusions presented here.

The loading in steps, as applied to the model, differs from reality, but it simulates the actual conditions during tunnel advance reasonably well. In reality, the initial stress field changes from the initial state of stress through a three dimensional to an axisymmetric stress field (for $N=1$) as the face of the tunnel passes a particular chainage. The radial stress, or the equivalent support pressure (Lombardi(1971)), corresponding to the initial field stress is gradually decreased from a maximum ahead of the face to zero at some distance behind the face. The stress pattern which develops at this point during the

tunnel advance is comparable to the stress pattern which develops during step loading of the model block. The tangential stress reaches a maximum at the tunnel face and a plastic zone develops if the tunnel is advanced further or the stress is increased in the model test. The deformation patterns are significantly different as a result of the stress history. The deformations in the model are increased because of the compression due to application of the field stresses. The differences can be corrected by considering the deformations observed during the compression of the sample without a tunnel. The observations made during the model test can therefore be related directly to describe the behaviour of a real tunnel during face advance. The similitude in time or the relative time scale has not yet been established. It appears that it is more appropriate to determine this time scale from field observations rather than from similitude considerations.

It has been found that stress redistribution due to differential creep, non-linear, stress-dependent creep properties or local yielding of stiff and weak zones may be much more important than generally accepted. Tunnel closure has been explained to be a result of stress redistribution but the interpretation that yielding is the dominant cause for stress redistribution may be misleading. This has been illustrated in a convincing manner by Guenot (1979). During Test MC-2, tangential stress concentrations in excess of 30 MPa should have existed according to elasticity theory and a

plastic zone of several centimeters should have been created according to an elasto-plastic material model. No such yield zone has been observed and this can only be explained by stress redistribution to zones of higher confinement. In addition, local yielding in zones of high stiffness, not necessarily at the tunnel wall, may have occurred as indicated by the internal gauges.

During later testing (Guenot(1979)) again no clear evidence of global yielding has been observed. Collapse was initiated in these tests, after stress redistribution, due to local instabilities or rupture of rock in areas of weakness. The behaviour in Phase III was observed in these tests. Stable equilibrium (Phase IV) was reached after propagation of the fracture zone terminated, possibly due to size effects and a general change in post-peak behaviour due to increasing confining pressure (more ductile). As a result of these observations it has been concluded that Phase I, II and IV are most important and that Phase III may not exist even if displacements in excess of the ones predicted from elasticity occur, or if low tangential stresses are measured near an opening. Phase III might be initiated by local instabilities but it dominates the behaviour in general only near collapse of the opening. A flow chart in Figure 7.1 summarizes processes and controlling properties, and shows the influence of parameters affecting individual phases. It can be seen that most factors which are under the control of the designer influence the stress redistribution or

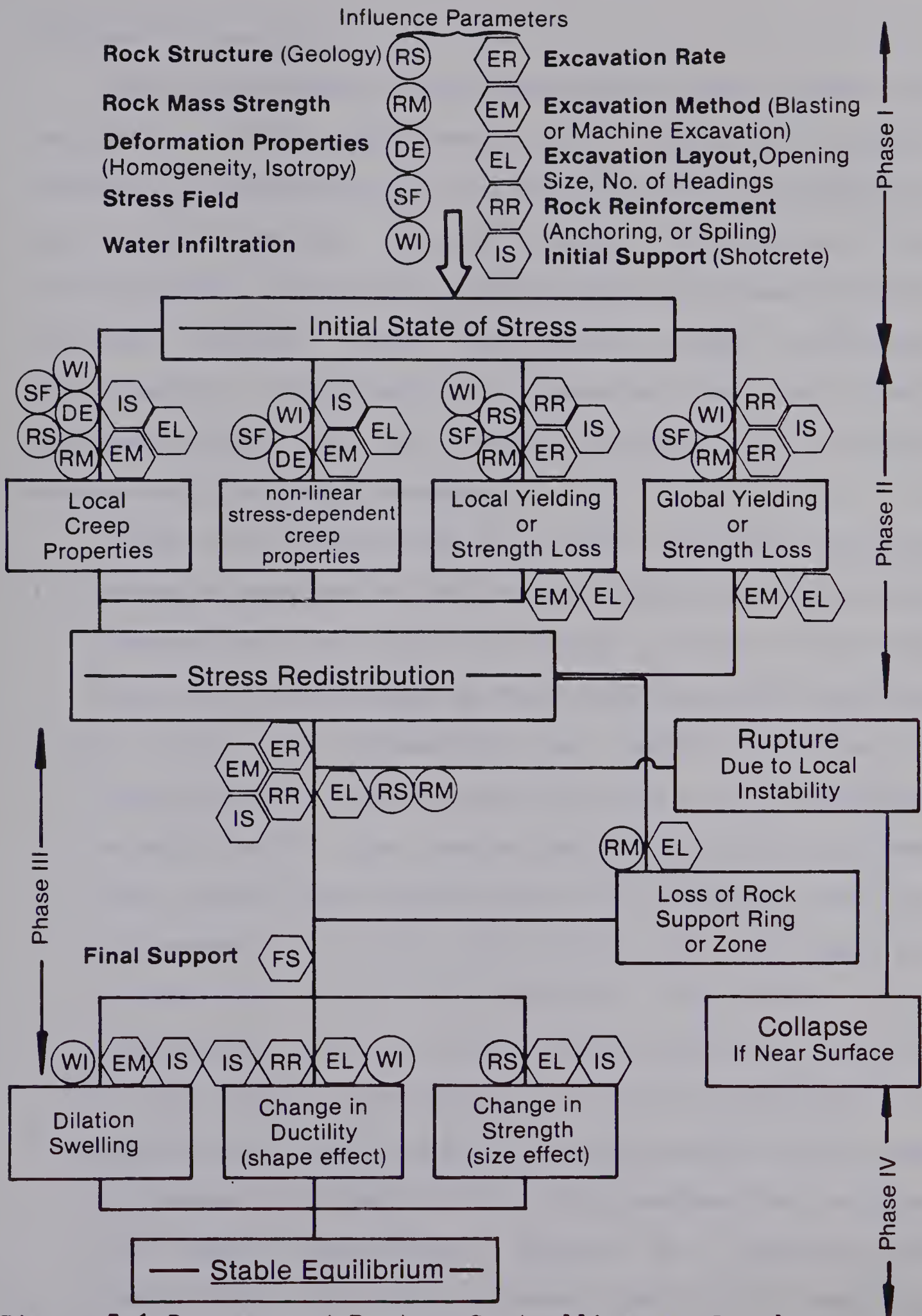


Figure 7.1 Process and Factors Controlling the Development of a Stable Equilibrium Condition around an Opening in a Rock Mass with Time - Dependent Properties

eliminate Phase III.

The implications of these observations are, if directly applied to field conditions, quite significant. Present methods of interpretation of tunnel closure measurements, e.g. by ground reaction curves determined from elasto-plastic materials models under the assumption of a constant opening shape, are under certain conditions questionable. Furthermore, it appears also that field instrumentation is not always designed in a manner compatible with these processes.

Three major conclusions of practical importance follow:

1. Stress redistribution may be dominated by time-dependent deformation properties rather than yielding or strength loss. The general shape of the resulting stress pattern, of both the tangential and radial stresses, is comparable to the one predicted from an elasto-plastic material model and general conclusions which had been drawn from these models may in principle still be applicable. On the other hand, the non-symmetric distribution of time-dependent properties, e.g. compressible fault or shear zones, and their influence on the stress redistribution has to be investigated in more detail. The equivalent opening approach can be used to predict the shape of the stress redistribution zones and these predictions should be compared with observations of field stresses and local rock mass features. The concept of the ground reaction curve

should be reviewed in this light since non-linearities can be attributed to stress redistribution rather than yielding.

2. Excavation layout, tunnel orientation, rate of excavation, and support system are very important factors which control the process of stress redistribution. The first three have often been neglected in the design of tunnels. The aim of a tunnel design should be to keep the size of the equivalent opening minimal, to maintain it at an optimum shape, and to control the stress history. For example, it is better to excavate the top heading first, then the middle (left and right) and bottom headings, e.g. Arlberg Tunnel (Pacher and Seeber(1978) or others in the same publication), than to excavate two parallel adits and then expand them to a full opening (e.g. St.Gotthard, Lombardi(1974)). In the first case (Figure 7.2), the equivalent opening increases whenever the real opening is expanded but a portion of the real, and therefore the equivalent, opening is already supported or at least reinforced. In the second case, the equivalent opening is almost equal to the final equivalent opening as soon as the two adits are excavated. Only a minor portion of this equivalent opening can be supported easily, without anchoring areas which will have to be excavated later. The related deformations causing straining of the rock mass will be much larger in the second case. This might

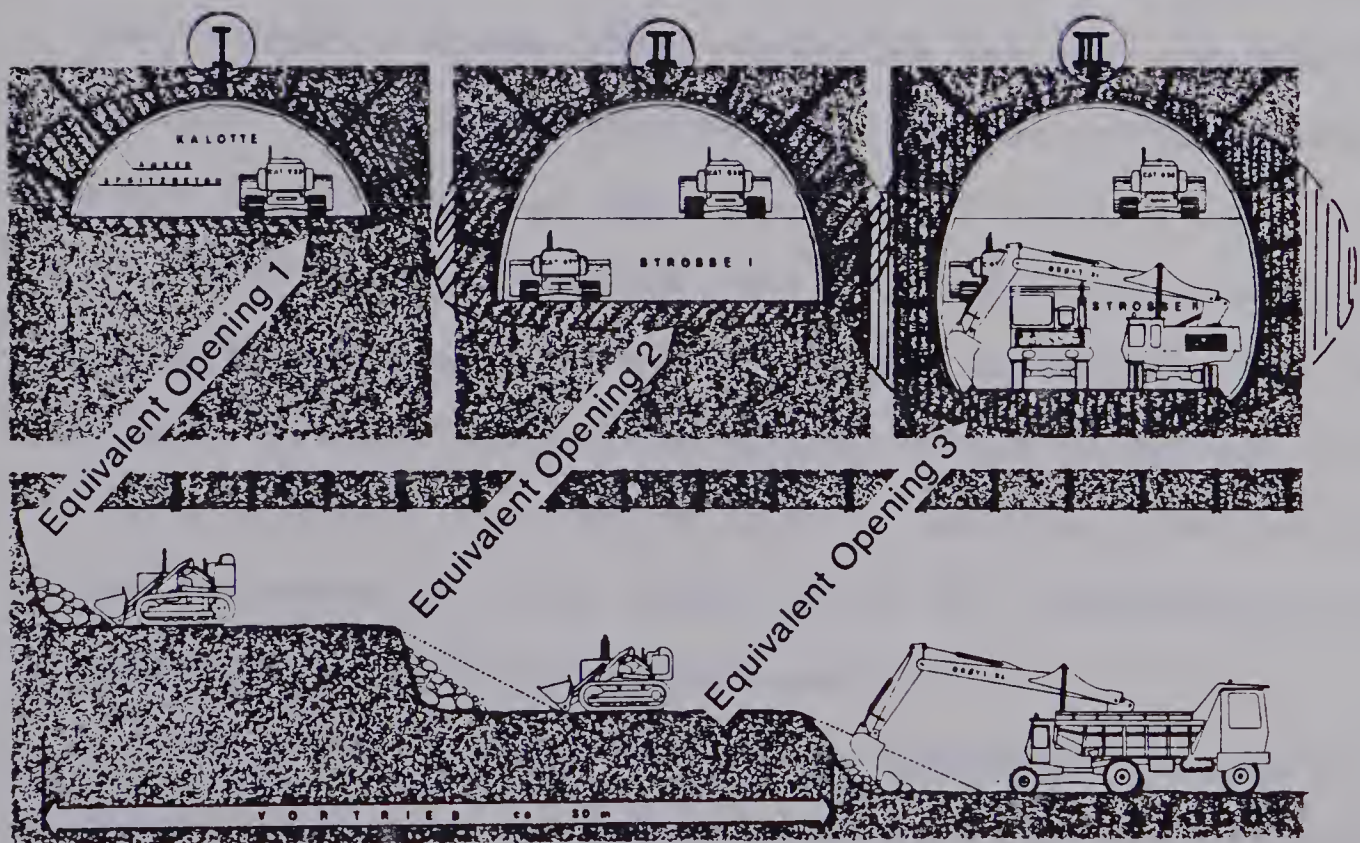
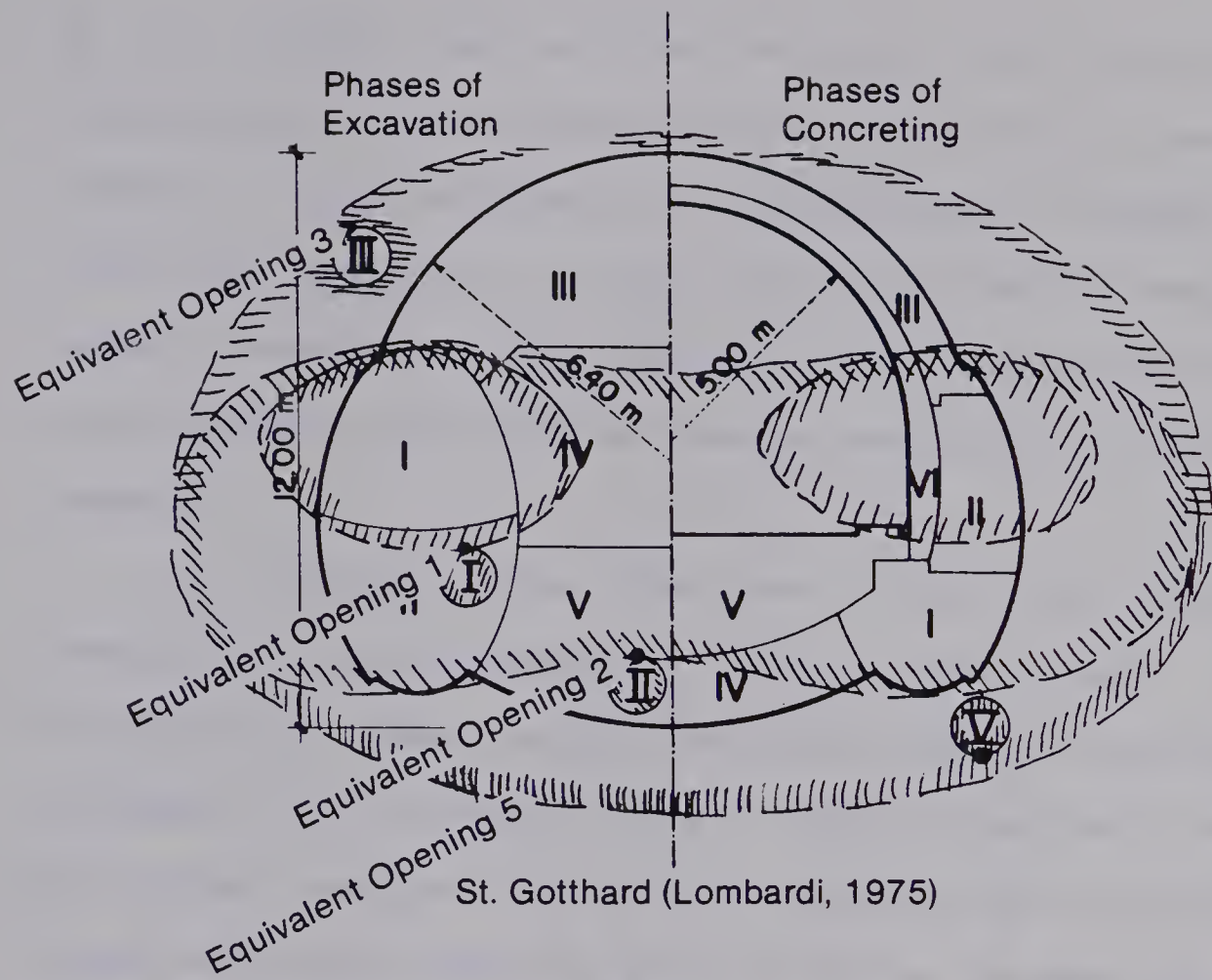


Figure 7.2 Development of the Equivalent Opening during two Excavation Layouts

be at least one of the reasons for the extreme difficulties encountered at St.Gotthard and it may also explain the significant differences between the behaviour observed during the excavation of the small safety tunnel near the location of the major tunnel and the problems encountered during excavation of the main tunnel.

It follows from the same logic that tunnels advanced simultaneously will experience more difficulties than during delayed advance. The support provided by the first, already lined tunnel will reduce the size of the equivalent opening. But at the same time, more load would be expected to be transferred onto the support of the first tunnel in the case of delayed advance due to changing size of the equivalent opening after the support has been installed.

The excavation rate may influence the type of instability experienced if it is comparable to the stress redistribution rate, e.g. a rock burst may only occur if the excavation rate is high relative to the stress redistribution rate. This is supported by an extensive literature on rock bursts.

The excavation procedure (blasting or machine excavation) does not only reduce the rock mass strength but it may also change its creep properties by prefabricating the rock. Anisotropic property distribution may result as a function of the excavation

method and affect the shape and size of the equivalent opening.

Support systems (anchoring, shotcrete, steel ribs and lagging, etc.) further influence the stress redistribution and change the shape and extent of the equivalent opening by increasing the rock mass strength, by preventing local yielding and instability, and by changing the creep properties due to reinforcement and confinement.

Both water infiltration and water pressure may influence the creep properties and the strength parameters causing stress redistribution and time - dependent overstressing of the rock.

It is important to point out that the equivalent opening approach (as presented here) does not consider gravitational forces and that their effect on tunnel stability has to be considered separately.

3. The type of monitoring program must be directed towards two possible problems: (a) the observation of the overall rock mass response and performance of the opening, and (b) the stability of the cavity. In the first case, closure measurements are adequate and allow extrapolation for the design of the final lining. In the second case, multiple extensometers (or, less practically stress measurements) are best suited to detect local yielding and possible zones of instability. Only a combination of the two methods allows delineation

of the actual mechanism involved in the development of the stress redistribution zone. This is in agreement with current practice in Austria where the time of installation of the final lining is determined by limiting the closure rate (e.g. Tauern Tunnel 6 mm/month or approximately $1 \times 10^{-4}\%$ /hr, Arlberg Tunnel 10 mm/month or approximately $1.5 \times 10^{-4}\%$ /hr (Pacher and Seeber(1978))). Extensometer readings have been used for the same purpose but not directly for the evaluation of the real deformation process. It is recommended that results from field measurements be studied in the light of the conclusions presented in this thesis.

It appears to be essential for the evaluation of the limit equilibrium state and the time-dependent transition stages of a tunnel to consider the stress-history since the post-failure behaviour of many rock masses is affected by the stress-history. The extent and the shape of the plastic zone as well as the type of instability occurring in such a material may be stress-history-dependent.

The implications of these conclusions on design criteria can be summarized in three statements. Firstly, the initial tunnel support should limit and control the stress redistribution or the development of the equivalent opening. It should be flexible and it should mainly improve the rock mass properties in the critical areas. Secondly, the initial support must prevent local yielding or instabilities and,

under extremely high stress conditions, stop major instabilities like wedge failures. Thirdly, the final lining must be designed to stop stress redistribution by increasing the confinement and therefore reducing rock mass deformations.

It is recommended that these conclusions be verified by further model testing, but even more important, by an evaluation of closure measurements, observations from extensometers, and anchor load records. Detailed studies of case histories are necessary to support and prove some of these conclusions. Simple numerical models applied to the concept of the equivalent opening will be most useful during the initial stages of this investigation.

The objective of this research project has been to investigate the time-dependent fracture process around an underground opening. The results presented in this thesis indicate that this process may not be as dominant as expected or alternatively may be significant only near the rupture point. This would imply that the time-dependent fracture process occurs only locally. Further testing and a detailed analysis of the data collected by Guenot (1979) will clarify this point.

References

- Afanasev, B.F. and Pushkarev, V.I., 1976. "A simplified method of determining the long-term strengths of rocks", Soviet Mining Sciences, Vol.12, pp.219-221. , 57
- Afanasev, B.G. and Abramov, B.K., 1975. "Determining the long-term shear strength of contacts between rocks", Soviet Mining Sciences, Vol.11, pp.588-591. , 57
- Ballivy, G., Ladanyi, B. and Gill, D.E., 1976. "Effect of water saturation history on the strength of low-porosity rocks", Soil Specimen Preparation for Laboratory Testing, ASTM STP 599, pp.4-20., 68
- Barton, N., 1974. "Rock slope performance as revealed by a physical joint model", Third Congress of the International Society of Rock Mechanics, Denver, Vol.2B, pp.765-773. , 95
- Bieniawski, Z.T., 1967. "Mechanism of brittle fracture of rock", International Journal of Rock Mechanics and Mining Sciences, Vol.4, pp.395-430., 165
- Bieniawski, Z.T., 1970. "Time - dependent behaviour of fractured rock," Rock Mechanics, Vol.2, No.3, pp.123-137., 53
- Brace, W.F. and Martin, R.J., 1968. "A test of the law of effective stress for crystalline rocks of Low Porosity", International Journal of Rock Mechanics and Mining Sciences, Vol.5, pp.615-626., 181
- Broadbent, C.D. and Ko, K.C., 1972. "Rheologic aspects of rock slope failure", Thirteenth Symposium on Rock Mechanics, Illinois, pp.573-593., 174
- Cogan, J., 1978. "An approach to creep behaviour in failed rocks", 19th U.S. Rock Mechanics Symposium, Stateline, Nevada, Vol.1, pp.400-407., 161
- Cohen, S.C., 1978. "The visco-elastic stiffness model of seismicity", Journal of Geophysical Research, Vol.83, No.B11, pp.5425-5431., 174, 206
- Colback, P.S.B. and Wild, B.L., 1965. "The influence of moisture content on the compressive strength of rocks", Proceedings of the Third Canadian Rock Mechanics Symposium, Toronto, pp.65-83., 68
- da Fontoura, S., 1980. Ph.D. Thesis (to be published), Department of Civil Engineering, University of Alberta., 55, 138
- Daemen, J.J.K., 1975. "Tunnel Support Loading Caused by Rock Failure", Ph.D. thesis in Civil Engineering, University of Minnesota., 6
- Denkhaus, H.G., 1958. "Ueber die Bedeutung einiger Eigenschaften des Gesteins fuer das Problem der Gebirgsschlaege in Gruben grosser Tiefe", Internationale Gebirgsdrucktagung, Leipzig, Akademie-Verlag Berlin., 50
- Egger, P., 1973. "Einfluss des Post-Failure-Verhaltens von Fels auf den Tunnel Ausbau", Veroeffentlichungen des

- Institutes fuer Bodenmechanik und Felsmechanik,
Universitaet Fridericiana Karlsruhe, Heft 57,
pp.1-83., 6
- Evans, I. and Pomeroy, C.D., 1966. "The Strength, Fracture
and Workability of Coal", Pergamon Press., 61
- Feder, G., 1977. "Versuchsergebnisse und analytische
Ansätze zum Scherbruchmechanismus im Bereich
tiefliegender Tunnel", Rock Mechanics, Supplementum
6, pp.71-102., 266
- Feder, G., 1978. "Bergbau und Tunnelbau - Anregungen und
Ergänzungen", Rock Mechanics, Supplementum 7,
pp.103-127., 266
- Findley, W.N., Lai, J.S., Onaran, K., 1976. "Creep and
Relaxation of Nonlinear Viscoelastic Materials",
North - Holland Publishing Company, 364pp., 354
- Finnie, I., 1960. "Stress analysis in the presence of
creep", Applied Mechanics Reviews, Vol.13, No.10,
pp.705-712., 84, 98
- Guenot, A., 1979. "Investigation of Tunnel Stability by
Model Tests", M.Sc.Thesis, Department of Civil
Engineering, University of Alberta., 35
- Hacquebard, P.A., 1951. "The correlation, by petrographic
analyses, of No.5 seam in the St.Rose and Chimney
Corner Coalfields, Inverness Country, Cape Breton
Island, Nova Scotia", Geological Survey of Canada,
Bull.19, 33pp., 17
- Hardy, H.R.Jr. and Chugh, Y.P., 1959. "Time-dependent
deformations and failure of geological materials",
Quarterly Colorado School of Mines, Vol.54,
pp.135-175., 50, 98
- Hayashi, M. and Hibino, S., 1968. "Progressive relaxation
of rock masses during excavation of an underground
cavity", Proceedings of the International Symposium
on Rock Mechanics, Madrid, Spain, pp.343-349., 286
- Heuer, R.E. and Hendron, A.J., 1971. "Geomechanical model
study of the behaviour of underground openings in
rock subjected to static loads", U.S. Corps of
Engineers Report N-69-1, Report 2, Contract No.
DACA39-67-C-0009 , 222
- Hoefer, K.H., 1958. "Die Gesetzmaessigkeiten des Kriechens
der Salzgesteine und deren allgemeine Bedeutung fuer
den Bergbau", International Gebirgsdrucktagung,
Leipzig, Akademie-Verlag, Berlin., 49
- Hudson, J.A. and Brown, E.T., 1973. "Studying time -
dependent effects in failed rock", Fourteenth
Symposium on Rock Mechanics, Pennsylvania State
University, ASCE, pp.25-34., 59, 172, 186
- Hungr, O., 1977. "Personal Communication"., 137
- John, M., 1974. "Time-dependence of fracture process of
rock materials", Third Congress of the International
Society of Rock Mechanics, Denver, Colorado, Vol.2A,
pp.330-335., 205
- John, M., 1976. "Geotechnical measurements in the Arlberg
- Tunnel and their consequences on construction",

- (in German), Rock Mechanics, Supplementum 5, pp.157-177., 1
- Kaiser, P.K. and Morgenstern, N.R., 1979. "Time-dependent deformation of jointed rock near failure", Proceedings of the Fourth International Congress on Rock Mechanics, Montreux, Switzerland, Vol.1, pp.195-202., 61
- Kenney, T.C., 1978. "Influence of water on the compressibility of rock - fill materials", Thirty-first Canadian Geotechnical Conference, pp.3.3.1-3.3.13., 68
- Kidybinski, A., 1966. "Rheological models of Upper Silesian Carboniferous rocks", International Journal of Rock Mechanics and Mining Sciences, Vol.3, pp.279-306., 61, 91
- Ko, H.Y. and Gerstle, K.H., 1977. "Creep of coal", Personal Communication, to be published in "Creep and time-dependent strain", monograph published by Journal of Strain Analysis, 12pp., 61
- Kovari, K., 1977. "Micromechanics models of progressive failure in rock and rock - like materials", International Symposium on Geomechanics of Structurally Complex Formations, Capri (Italy), Vol.1, pp.307-316., 173
- Krahn, J. and Morgenstern, N.R., 1979. "The ultimate frictional resistance of rock discontinuities", International Journal of Rock Mechanics and Mining Science, Vol.16, pp.127-133., 27
- Krahn, J., 1974. "Rock Slope Stability," Ph.D. Thesis, Department of Civil Engineering, University of Alberta., 20
- Kranz, R., L., 1979. "Crack growth and development during creep of Barre granite", International Journal of Rock Mechanics and Mining Sciences, Vol.16, No.1, pp.23-36., 193
- Kranz, R.L. and Scholz, C.H., 1977. "Critical dilatant volume of rocks at the onset of tertiary creep", Journal of Geophysical Research, Vol.82, No.30, pp.4893-4898., 60, 135
- Krokosky, E.M. and Husak, A., 1968. "Strength characteristics of basalt rock in ultra-high vacuum", Journal of Geophysical Research, Vol.73, No.6, pp.2237-2247., 68
- Lajtai, E.Z., 1969. "Shear strength of weakness planes in rocks," International Journal of Rock Mechanics and Mining Sciences, Vol.6, pp.499-515., 28
- Lama, R.D., 1974. "Concept on the creep of jointed rocks and the status of research project A-7", Jahresbericht SFB-77, Institut fuer Boden- und Felsmechanik, Universitaet Karlsruhe, pp.105-134., 199
- Lombardi, G., 1971. "Zur Bemessung der Tunnelauskleidung mit Beruecksichtigung des Bauvorganges", Schweizerische Bauzeitung, Jahrgang 89, Heft 32,

- pp.793-801., 344
- Lombardi, G., 1974. "Felsmechanische Probleme am Gotthard", Rock Mechanics, Supplementum 3, pp.113-130., 349
- Mandel, J., (1963) "Tests on reduced scale models in soil and rock mechanics, a study of the conditions of similitude", International Journal of Rock Mechanics and Mining Science, Vol.1, pp.31-42., 222
- Morgenstern, N.R. and Noonan, D.K.J., 1974. "Fractured coal subjected to direct shear", Proceedings of the Third Congress of the International Society of Rock Mechanics, Denver, Colorado, Vol.2A, pp.282-287., 18
- Morlier, P., 1964. "Etude expérimentale de la déformation des roches", Revue de l'Institut Français du Pétrole, Octobre, Pt.2, p.1187., 61, 91
- Mueller-Salzburg, L. and Goetz, H.P., 1973. "In-Situ Measurement in jointed rock masses as a means to study their failure behaviour", Veröffentlichung III. Internationale Tagung ueber den Bruch, Teil 10, pp.(IX-423)-1-7., 46, 55
- Mueller-Salzburg, L., Sauer, G. and Vardar, M., 1978. "Dreidimensionale Spannungsumlagerungsprozesse im Bereiche der Ortsbrust", Rock Mechanics, Supplementum 7, pp.67-85., 218
- Muir Wood, A., M., 1979. "Ground behaviour and support of mining and tunnelling", Tunnels and Tunnelling, Vol.11, No.4/5, pp.43-48/ 47-51., 5
- Nadai, A., 1952. "Ueber den Spannungszustand und die von ihm hervorgerufenen Verformungen der aeussern Kugelschale der Erde", Transactions of the American Geophysics Union, Vol.33, No.2., 50
- Nair, K. and Boresi, A.P., 1970. "Stress Analysis for time-dependent problems in rock mechanics", Proceedings of the International Society for Rock Mechanics, Beograd, Vol.2, paper 4-21., 286
- Nair, K., Sandhu, R.S. and Wilson, E.L., 1968. "Time-dependent analysis of underground cavities under an arbitrary initial stress field", Tenth Symposium on Rock Mechanics, Texas, Chapter 27, pp.699-730., 286
- Nakano, R., 1979. "Geotechnical properties of mudstone of Neogene Tertiary in Japan with special reference to the mechanism of squeezing swelling rock pressure in tunneling", International Symposium on Soil Mechanics, Mexico, Vol.1, pp.75-92., 312
- Noonan, D.K.J., 1972. "Fractured Rock Subjected to Direct Shear", M.Sc.Thesis, Department of Civil Engineering, University of Alberta, Edmonton., 16
- Obert, L. and Duvall, W.I., 1967. "Rock Mechanics and the Design of Structures in Rock", John Wiley and Sons, New York, 650pp., 280
- Pacher, F. and Seeber, G., 1978. "Spezielle Probleme bei der Durchörterung des Arlbergs aus der Sicht der Gutachter", Oesterreichische Ingenieur Zeitschrift,

- Vol.21, No.11, pp.402-407., 349, 353
- Patching, T.H., 1965. "Variations in permeability of coal", Proceedings of the Rock Mechanics Symposium, Toronto, pp.185-199., 32
- Patching, T.H., 1970. "The retention and release of gas in coal - review", Transactions of the Canadian Institute of Mining and Metallurgy, Vol.73, pp.328-334., 67
- Pearson, G.R., 1959. "Coal reserves for strip mining, Wabamun Lake District Alberta", Research Council of Alberta, Geology Division, Preliminary Report 59-1, 37pp., 14
- Peng, S.S. and Podnieks, E.R., 1972. "Relaxation and the behaviour of failed rock", International Journal of Rock Mechanics and Mining Sciences, Vol.9, No.6, pp.699-712., 59, 178
- Peng, S.S., 1973. "Time-dependent aspects of rock behavior as measured by a servo-controlled hydraulic testing machine", International Journal of Rock Mechanics and Mining Sciences, Vol.10, No.3, pp.235-246., 178, 186, 187
- Pomeroy, C.D., 1956. "Creep in coal at room temperature", Nature, Vol.178, pp.279-280., 61
- Posch, H., 1978. "Die Bewaeltigung des Verkehrshindernisses Arlberg", Oesterreichische Ingenieur - Zeitschrift, Jahrgang 21, No.11, pp.356-373., 1
- Price, N.J., 1969. "Laws of rock behaviour in the earth's crust", The Eleventh Rock Mechanics Symposium, Berkeley, California, pp.3-23., 164, 174
- Pushkarev, V.I. and Afanesev, B.G., 1973. "A rapid method of determining the long-term strength of weak rocks", Soviet Mining Science, Vol.9, pp.558-560.,
- Rabcewicz, L.v., 1969. "Stabilities of tunnels under rock load", Water Power, No.5/6/7, pp.225-229/ 266-273/ 297-301., 266
- Reik, G. and Zacas, M., 1978. "Strength and deformation characteristics of jointed media in true triaxial compression", International Journal of Rock Mechanics and Mining Sciences, Vol.15, No.6, pp.295-303., 217
- Ruesch, H., 1960. "Research toward a general flexural theory for structural concrete", Proceedings of the American Concrete Institute, Vol.57, pp.1-28., 178
- Rutter, E.H., 1972. "The effect of strain-rate changes on the strength and ductility of Solenhofen Limestone at low temperatures and confining pressures", International Journal of Rock Mechanics and Mining Sciences, Vol.9, pp.183-189., 57, 181
- Salustowicz, A., 1958. "Neue Anschauungen ueber den Spannungs- und Formaenderungszustand im Gebirge in der Nachbarschaft bergmaennischer Hohlräume", Internationale Gebirgsdruck Tagung Leipzig, Akademik Verlag Berlin., 50
- Singh, D.P. and Bamford, W.E., 1971. "The prediction and

- measurement of the long-term strength of rock", Proceedings of the First Australia-New Zealand Conference on Geomechanics, Melbourne, Vol.1, pp.37-44., 55
- Singh, D.P., 1975. "A study of creep of rocks", International Journal of Rock Mechanics and Mining Sciences, Vol.12, pp.271-275., 195
- Sonntag, G., 1958. "Einfluss der Anisotropie auf die Beanspruchung des Gebirges in der Umgebung von Stollen", Der Bauingenieur, Vol.33, no.8/9, pp.288-294/ 344-351., 298
- Standfield, E. and Lang, W.A., 1944. "Coals of Alberta, their occurrence, analysis and utilization", Research Council of Alberta, Report 35, 174 pp., 17
- Talobre, M.T., 1957. "La Mécanique des Roches", Dunod, Paris., 50
- Teeni, M. and Staples, G.E., 1969. "Stress phase interaction models", in: "Structure, Solid Mechanics and Engineering Design", Southampton, Vol.1, pp.469-486., 46
- Terry, N.B., 1956. "The elastic properties of coal", British National Coal Board, Mining Research Establishment Report 2080, Part 6., 61, 139, 194
- Van Eeckhout, E.M., 1976., "The mechanisms of strength reduction due to moisture in coal mine shales", International Journal of Rock Mechanics and Mining Sciences, Vol.13, pp.61-67., 68
- Walsh, J.B., Leyde, E.E., White, A.J.A. and Carragher, B.L., 1977. "Stope closure studies at West Driefontein Gold Mine", International Journal of Rock Mechanics and Mining Sciences, Vol.14, pp.277-281., 52
- Walsh, J.B., 1977. "Energy changes due to mining", International Journal of Rock Mechanics and Mining Sciences, Vol.14, pp.25-33., 52
- Wawersik, W.R. and Fairhurst, C., 1970. "A study of brittle rock fracture in laboratory compression experiments", International Journal of Rock Mechanics and Mining Sciences, Vol.7, pp.561-575., 58
- Wawersik, W.R., 1973. "Time-dependent rock behaviour in uniaxial compression", Proceedings of the Fourteenth Symposium on Rock Mechanics, Pennsylvania, pp.85-106., 57
- Zienkiewicz, O.C. and Valliappan, S., 1969. "Analysis of real structures for creep, plasticity and other complex constitutive laws", in: "Structure, Solid Mechanics and Engineering Design", Vol.1, pp.27-48., 265
- Zienkiewicz, O.C., Humpheson, C. and Lewis, R.W., 1975. "Associated and non-associated visco-plasticity and plasticity in soil mechanics", Géotechnique, Vol.25, No.4, pp.671-689., 162

APPENDIX A5
WORKING DRAWINGS OF MODEL TEST APPARATUS

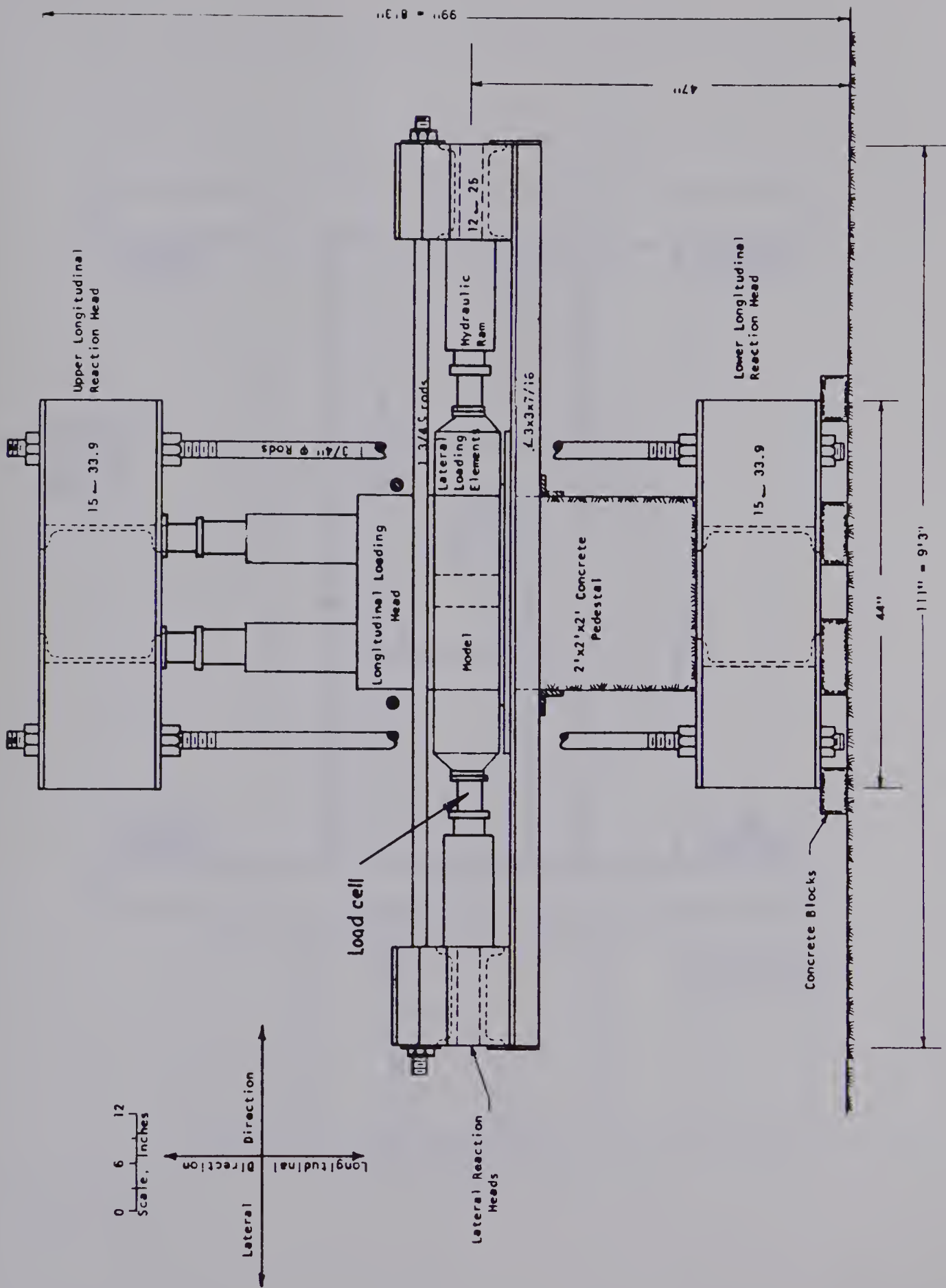


Figure A5.1 Test Frame, Side View

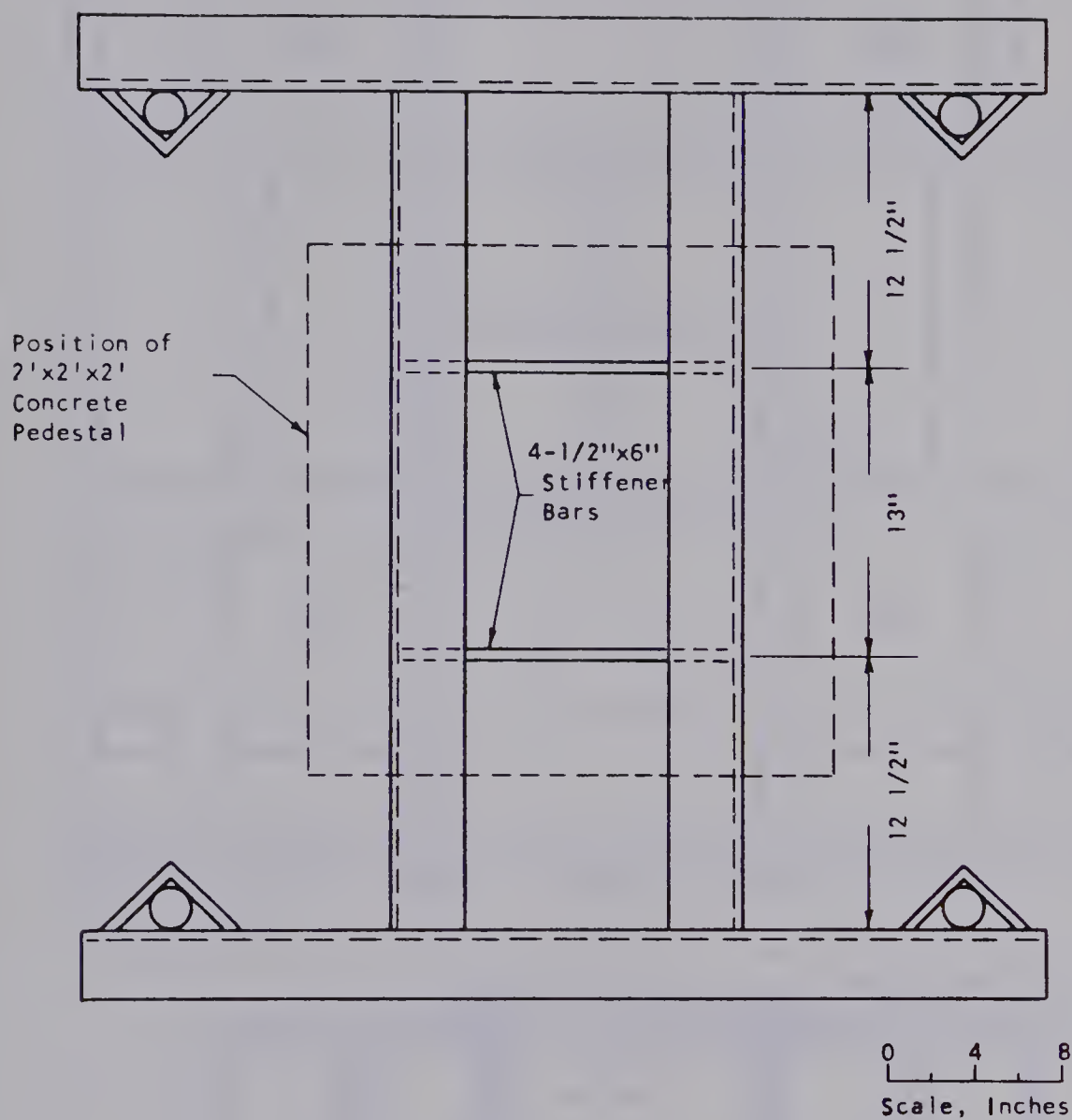


Figure A5.2 Bottom Reaction Head

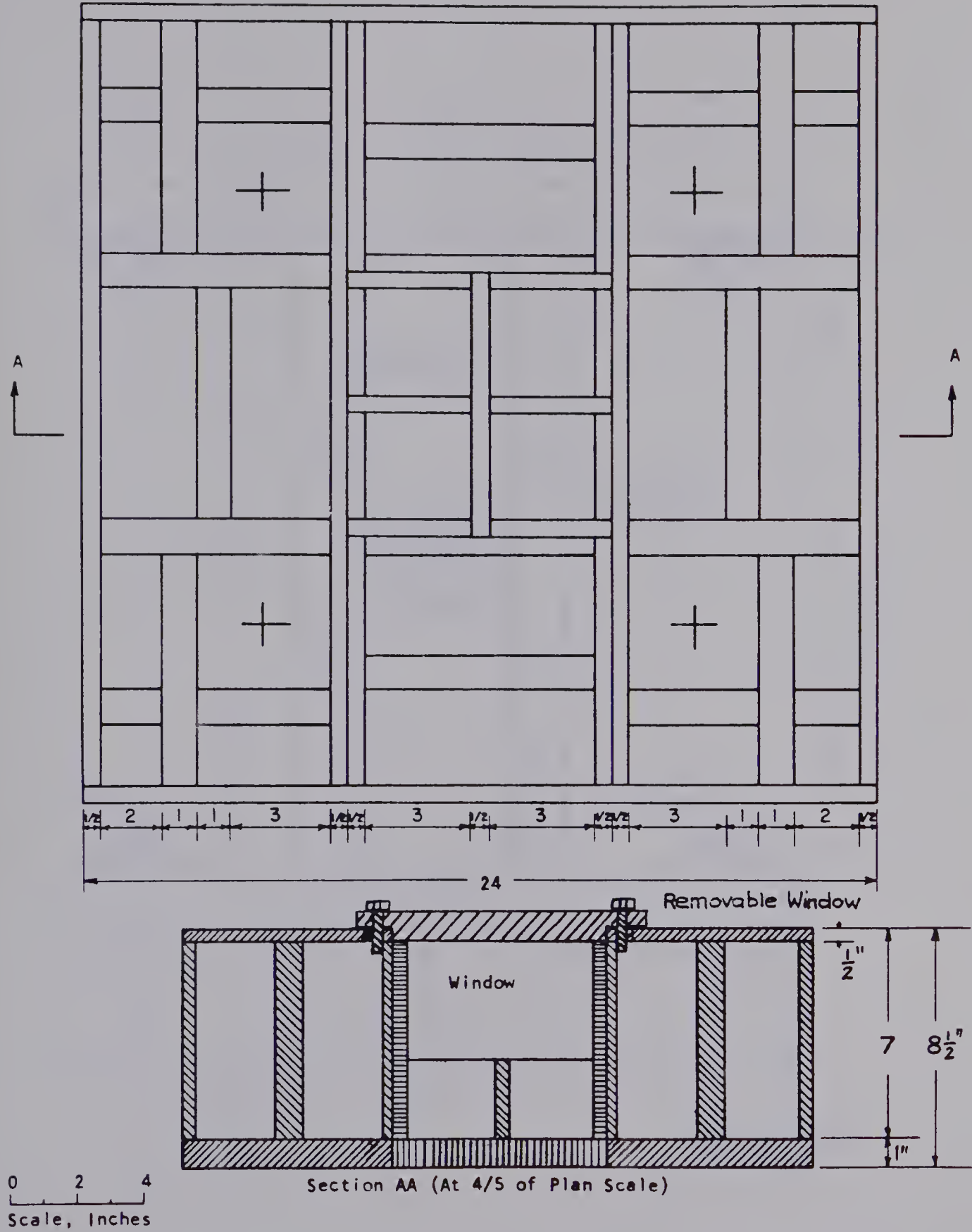


Figure A5.3 Loading Head

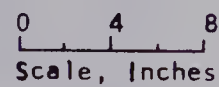


Figure A5.4 Top Reaction Head

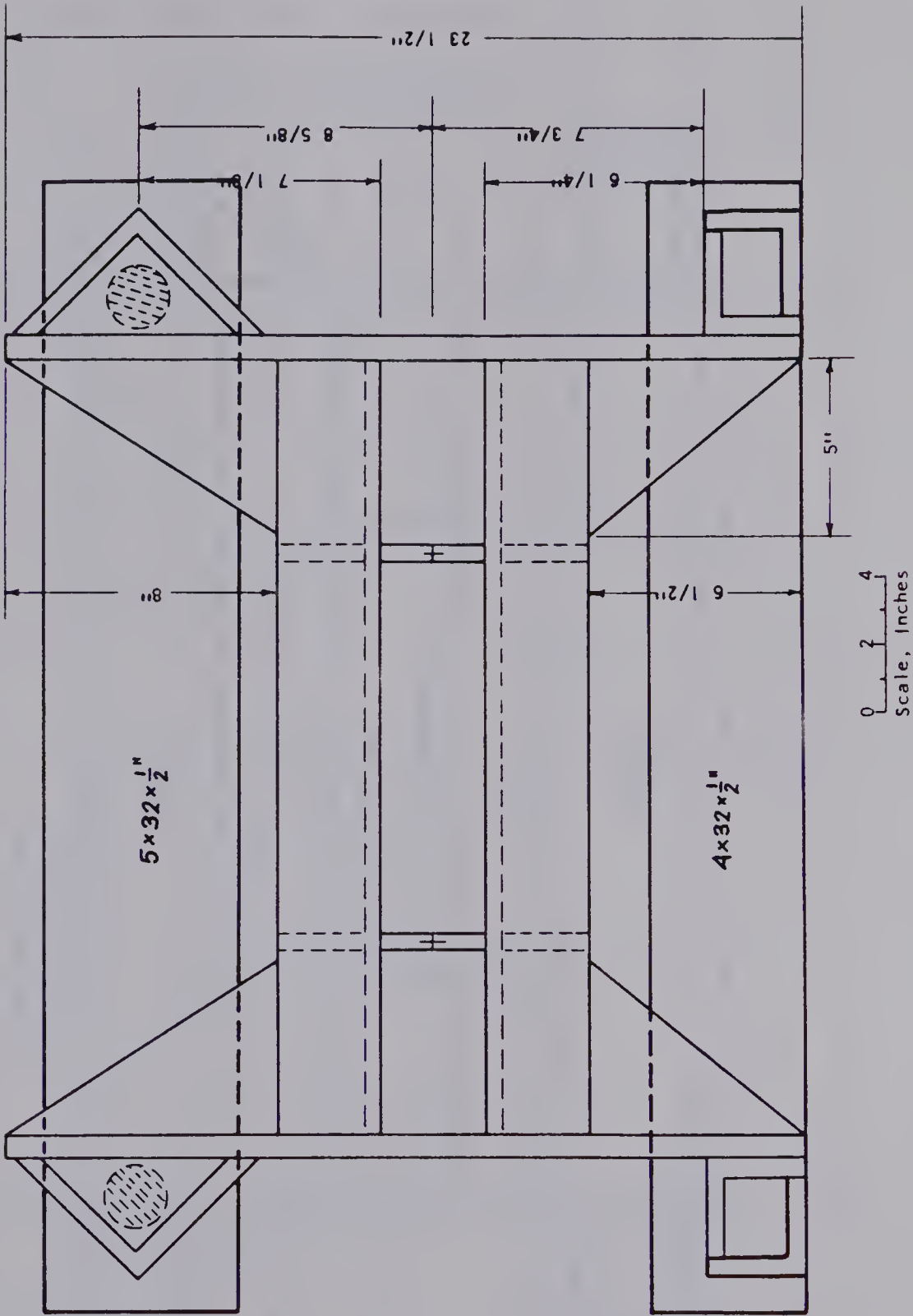


Figure A5.5 Lateral Reaction Head 1

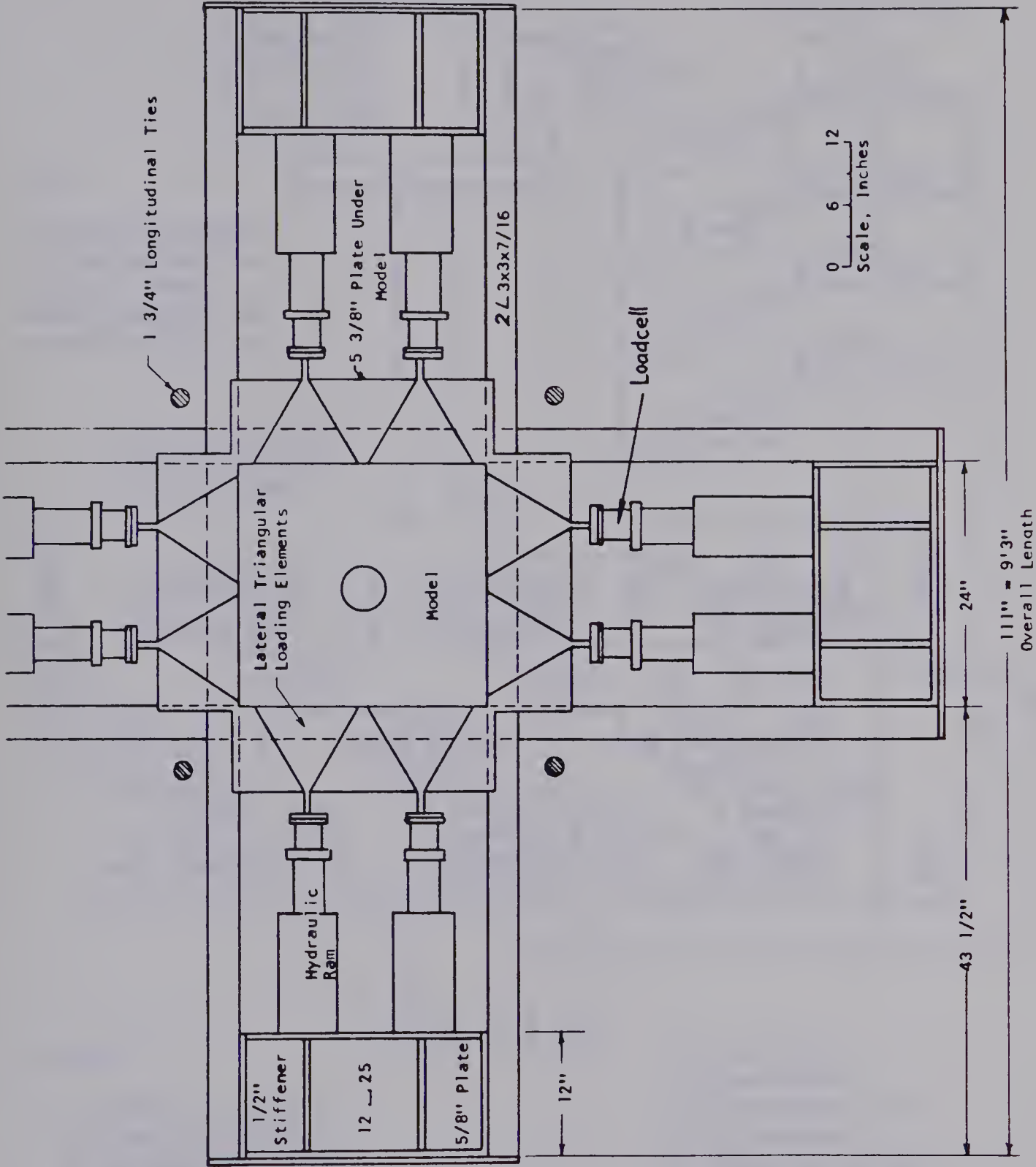
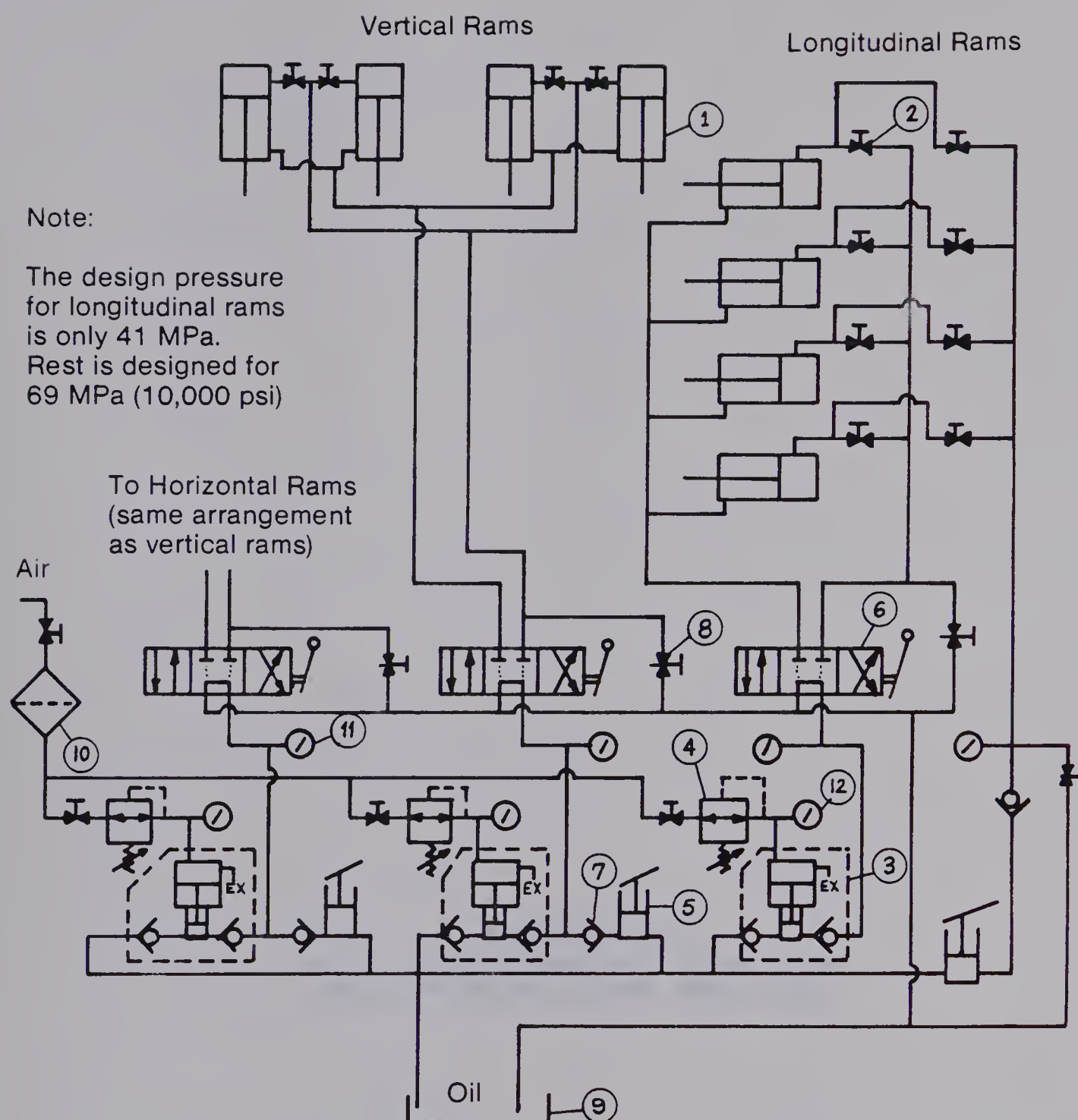


Figure A5.7 Assembly of Lateral Loading Elements



Legend:

- | | |
|--------------------------|----------------------------|
| 1. Double acting ram | 6. 3-way valve |
| 2. Valve (10,000 psi) | 7. Check valve |
| 3. Pump (air-oil; 1:100) | 8. Fine needle valve |
| 4. Air Regulator | 9. Oil reservoir |
| 5. Hand pump | 10. Water trap, air filter |
| | 11. Oil pressure gauge |
| | 12. Air pressure gauge |

Figure A5.8 Schematic of Hydraulic System

APPENDIX A6
A6.1 DERIVATIONS AND EQUATIONS
A6.2 SELECTED MODEL TEST DATA

APPENDIX A6

A6.1 DERIVATIONS AND EQUATIONS

A6.1.1 Linear Elasticity

a) Behaviour of a Tunnel in an Elastic Medium in Plane Strain Conditions:

PLATE: refers to the behaviour of a sample without a tunnel;

MODEL: refers to the behaviour of a sample with tunnel; and

REALITY: refers to the behaviour of a tunnel excavated in a prestressed material.

For a linear elastic medium the MODEL behaviour can be determined by superposition of the PLATE and REALITY behaviour.

Compression is positive;

Volumetric strain: $\epsilon_{vol} = \epsilon_r + \epsilon_\theta$;

Stresses, Strains, and Displacements:

- in radial direction: σ_r, ϵ_r, u
- in tangential direction: $\sigma_\theta, \epsilon_\theta, v$;

Field stresses:

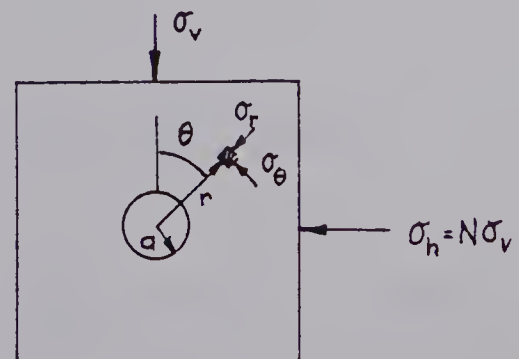
- | | | |
|----------------|--------------|--|
| - vertical | σ_v | } stress ratio $N = \frac{\sigma_h}{\sigma_v}$ |
| - horizontal | σ_h | |
| - longitudinal | σ_l ; | |

ν . . . Poisson's Ratio;

G . . . Shear Modulus;

K . . . Bulk Modulus;

E . . . Young's Modulus.



- Stress Distribution (MODEL and REALITY)(Obert and Duvall, 1967)

$$\sigma_r = \frac{\sigma_v}{2} \left[(1 + N) \left(1 - \frac{a^2}{r^2}\right) + (1 - N) \left(1 + 3\frac{a^4}{r^4} + 4\frac{a^2}{r^2}\right) \cos 2\theta \right] \quad (\text{A6.1})$$

$$\sigma_\theta = \frac{\sigma_v}{2} \left[(1 + N) \left(1 + \frac{a^2}{r^2}\right) - (1 - N) \left(1 + 3\frac{a^4}{r^4}\right) \cos 2\theta \right] \quad (\text{A6.2})$$

$$\tau_{r\theta} = -\frac{\sigma_v}{2} (1 - N) \left(1 - 3\frac{a^4}{r^4} + 2\frac{a^2}{r^2}\right) \sin 2\theta \quad (\text{A6.3})$$

Note: Stresses are independent of material properties.

MODEL:

- Radial Strain Distribution (MODEL)

$$\begin{aligned} \epsilon_r = & \frac{\sigma_v(1 - \nu^2)}{2E} \left[(1 + N) \left(1 - \frac{a^2}{r^2}\right) + (1 - N) \left(1 - \frac{3a^4}{r^4} - 4\frac{a^2}{r^2}\right) \cos 2\theta \right] \\ & - \frac{\sigma_v\nu(1 + \nu)}{2E} \left[(1 + N) \left(1 + \frac{a^2}{r^2}\right) - (1 - N) \left(1 + \frac{3a^4}{r^4}\right) \cos 2\theta \right] \end{aligned} \quad (\text{A6.4})$$

- Radial Displacement (MODEL)

$$\begin{aligned} u = & \frac{\sigma_v(1 - \nu^2)}{2E} \left[(1 + N) \left(r + \frac{a^2}{r}\right) + (1 - N) \left(r - \frac{a^4}{r^3} + 4\frac{a^2}{r}\right) \cos 2\theta \right] \\ & - \frac{\sigma_v\nu(1 + \nu)}{2E} \left[(1 + N) \left(r - \frac{a^2}{r}\right) - (1 - N) \left(r - \frac{a^4}{r^3}\right) \cos 2\theta \right] \end{aligned} \quad (\text{A6.5})$$

at $r = a$:

$$u_a = \frac{\sigma_v(1 - \nu^2)}{E} a[(1 + N) + 2(1 - N) \cos 2\theta] \quad (\text{A6.6})$$

or in general for the axisymmetric case of a circular tunnel:

$$\epsilon_r = \frac{\partial u}{\partial r} ; \quad \epsilon_\theta = \frac{u}{r} .$$

PLATE:

- Radial Strain Distribution (PLATE)

$$\epsilon_r = \frac{\sigma_v(1 + \nu)}{2E} [(1 - 2\nu)(1 + N) + (1 - N) \cos 2\theta] \quad (\text{A 6.7})$$

and for $N = 1$: $\epsilon_r = \frac{\sigma_v E}{6KG}$

- Radial Displacement (PLATE) (Berry, 1967)

$$u = \frac{\sigma_v(1 + \nu)}{2E} r[(1 - 2\nu)(1 + N) + (1 - N) \cos 2\theta] \quad (\text{A6.8})$$

and by subtracting the two sets of equations from each other:

REALITY:

- Radial Strain Distribution (REALITY)

$$\epsilon_r = \frac{-\sigma_v(1 + \nu)}{2E} [(1 + N)(\frac{a^2}{r^2}) + (1 - N)(\cos 2\theta) \{4\frac{a^2}{r^2} - 3\frac{a^4}{r^4} - \nu(-2 - 6\frac{a^4}{r^4} + 4\frac{a^2}{r^2})\}] \quad (\text{A6.9})$$

and for $N = 1$: $\epsilon_r = \frac{-\sigma_v}{2G} \left(\frac{a^2}{r^2}\right)$

- Radial Displacement (REALITY)

$$u = \frac{\sigma_v(1 + \nu)}{2E} \left[(1 + N) \left(\frac{a^2}{r}\right) + (1 - N)(\cos 2\theta) \left\{ 4\frac{a^2}{r} - \frac{a^4}{r^3} - \nu(2r - 2\frac{a^4}{r^3} + 4\frac{a^2}{r}) \right\} \right]$$

(A6.10)

and at $r = a$: (Berry, 1967)

$$u_a = \frac{\sigma_v(1 + \nu)}{2E} [(1 + N) + (1 - N)(\cos 2\theta)(3 - 4\nu)]$$

b) Closure Ratio for Circular and Elliptical Openings:

The following is based on the equation and the graphs given by Feder (1978). The Closure Ratio (CR) is defined as the ratio between the closure of an elliptical (or circular) opening, with an axis ratio b/a , subjected to a particular stress field (N), and the closure of a circular opening, subjected to a stress field with a stress ratio N of unity. The closure of the ellipse in the direction of the long axis b has been calculated as if it was measured at a distance $r = b$ from the tunnel axis. It is therefore assumed that the material between the equivalent opening and the real opening does experience a volume decrease. (Short axis of ellipse = tunnel radius a ; long axis of ellipse = b ; $b/a = 1 \rightarrow$ circle;

$b/a > 1 \rightarrow$ ellipse in direction of b ;

el ... ellipse;

ci ... circle;

$F_r \dots$ constants given by Feder (1978, Figure 23).

$$F_\eta \dots \left. \begin{array}{l} \\ \\ \end{array} \right\} u = \frac{N\sigma_v a}{E} [F_r(1 - \nu^2) + F_\eta \nu(1 + \nu)]$$

$$CR = \frac{u(N)_{\text{ellipse}}}{u(N=1)_{\text{circle}}} = \frac{u(N)_{\text{el, REALITY}} + u(N)_{\text{PLATE, } r=b}}{u(N=1)_{\text{ci, REALITY}} + u(N=1)_{\text{PLATE, } r=a}}$$

$$= \frac{N[F_{r,\text{el}}(1 - \nu^2) + F_{\eta,\text{el}}\nu(1 + \nu)] + C(N,b)}{N[F_{r,\text{ci}}(1 - \nu^2) + F_{\eta,\text{ci}}\nu(1 + \nu)] + C(N=1, b=a)} \quad (\text{A6.11})$$

where:

$$C(N,b) = \frac{b}{2a}(1 + \nu)[(1 + N)(1 - 2\nu) + (1 - N) \cos 2\theta]$$

This equation (A6.11) has been used to calculate Figure 6.9.B.

c) Circular Tunnel in an Orthotropic Medium:

From Sonntag (1958, eqn. 1.33, 1.34) the following tunnel wall displacement ($r = a$) has been derived:

(E_1 parallel to σ_v and E_2 parallel to σ_h)

MODEL:

$$\left. \begin{array}{l} u_v = \sigma_v a \left[\frac{1}{E_1} + \frac{(1 - N)}{\sqrt{E_1 E_2}} \right]; \\ u_h = \sigma_v a \left[\frac{N}{E_2} - \frac{(1 - N)}{\sqrt{E_1 E_2}} \right]; \end{array} \right\} \quad (\text{A6.12})$$

PLATE:

$$u_v = \frac{\sigma_v a}{E_1} ; \quad u_h = \frac{N\sigma_v a}{E_2} ; \quad (A6.13)$$

REALITY:

$$u_v = \sigma_v a \frac{(1 - N)}{\sqrt{E_1 E_2}} ; \quad u_h = -\sigma_v a \frac{(1 - N)}{\sqrt{E_1 E_2}} \quad (A6.14)$$

A6.1.2 Linear Visco-Elasticity

The correspondence principle has been used to calculate the time-dependent tunnel closure and the radial strains for a linear visco-elastic material. The elastic behaviour under hydrostatic pressure and the visco-elastic behaviour under distortion (Case I), as well as case (II) with visco-elastic behaviour under both hydrostatic and deviatoric stress, has been analysed. The stresses are independent of material properties and therefore independent of time. This follows from the correspondence principle.

The equivalent to a Young's modulus in terms of the time operators is (Findley, et al., 1976):

$$E_v(t) = \frac{3\bar{Q}_1\bar{Q}_2}{\bar{P}_2\bar{Q}_1 + 2\bar{P}_1\bar{Q}_2} \quad \begin{matrix} \text{(Relaxation Modulus)} \\ E_v(t) = \sigma(t)/\epsilon(t) \end{matrix} \quad (A6.15)$$

and the equivalent of Poisson's ratio is

$$\nu_v(t) = \frac{\bar{P}_1\bar{Q}_2 - \bar{P}_2\bar{Q}_1}{\bar{P}_2\bar{Q}_1 + 2\bar{P}_1\bar{Q}_2} \quad (A6.16)$$

The transformed time operators are tabulated for various material models in Findley, et al. (1976) or Fluegge (1967).

For the two cases considered here they are:

I) distortional 1: Hooke + Kelvin(3-parameter solid)

(E_{11}, E_{12}, N_{12})

Hydrostatic 2: elastic (E_{21})

$$\left. \begin{aligned} P_1(s) &= 1 + p_1 s & Q_1(s) &= q_0 + q_1 s \\ P_2(s) &= 1 & Q_2(s) &= 3K \end{aligned} \right\} \quad (A6.17)$$

where: K = Bulk Modulus;

$$p_1 = N_{12}/(E_{11} + E_{12});$$

$$q_0 = E_{11}E_{12}/(E_{11} + E_{12});$$

$$q_1 = E_{11}N_{12}/(E_{11} + E_{12}).$$

II) distortional 1: Hooke + Kelvin (3-parameter solid)

(E_{11}, E_{12}, N_{12})

hydrostatic 2: Hooke + Kelvin(3-parameter solid)

(E_{21}, E_{22}, N_{22})

$$\left. \begin{aligned} P_1(s) &= 1 + p_1 s & Q_1(s) &= q_0 + q_1 s \\ P_2(s) &= 1 + r_1 s & Q_2(s) &= v_0 + v_1 s \end{aligned} \right\} \quad (A6.18)$$

where: $r_1 = N_{22}/(E_{21} + E_{22})$

$$v_0 = E_{21}E_{22}/(E_{21} + E_{22})$$

$$v_1 = E_{21}N_{22}/(E_{21} + E_{22}).$$

The time-dependent closures or strains can be found by transformation of the known elastic solution, e.g. the tunnel wall displacement $u(r = a)$ for a hydrostatic stress field $N = 1$ is in reality (from A6.10):

$$u = \frac{(1 + \nu)}{E} \sigma_v a; \quad f = \frac{1 + \nu}{E} \rightarrow u = f \sigma_v a \quad (\text{A6.19})$$

After Laplace transformation and substituting the transformed equivalents for E and ν (A6.15, A6.16):

$$u(s) = \frac{P_1}{Q_1} \sigma_v a; \quad f(s) = \frac{P_1}{Q_1} \quad (\text{A6.20})$$

(Note: tunnel closure in reality is independent of hydrostatic behaviour).

For a suddenly applied field stress σ_v the transformed stress is $\sigma_v(s) = \sigma_v/s$. Inserting this, and equations A6.17, for case I gives:

$$u(s) = \frac{1 + p_1 s}{q_0 + q_1 s} \frac{1}{s} \sigma_v a = \frac{f(s)}{s} \sigma_v a \quad (\text{A6.21})$$

After the inverse Laplace transformation, employing mathematical tables or partial fraction expansion (Findley, et al., 1976, A4); the displacement as a function of time is:

$$u(t) = \frac{1}{q_0} \left[1 - \underbrace{\left(1 - \frac{p_1 q_0}{q_1} \right) e^{-\alpha t}}_{f(t)} \right] \sigma_v a; \quad \alpha = \frac{q_0}{q_1} \quad (\text{A6.22})$$

$$\rightarrow u(t) = f(t) \sigma_v a.$$

In short form: $u = f\sigma_v a \rightarrow$

$$u(s) = \frac{f(s)}{s} \sigma_v a \rightarrow$$

$$u(t) = f(t) \sigma_v a.$$

Examination of equations A6.4 to A6.10 shows that various f -functions have to be transformed.

$$f_1 = \frac{(1 + v)}{E} ; \quad f_1(s) = \frac{P_1}{Q_1} ; \quad \text{for "REALITY".}$$

$$f_2 = \frac{(1 + v)(1 - 2v)}{E} ; \quad f_2(s) = \frac{3P_1P_2}{P_2Q_1 + 2P_1Q_2} ; \quad \text{for "PLATE".}$$

$$f_3 = \frac{(1 - v^2)}{E} ; \quad f_3(s) = \frac{P_1 (2P_2Q_1 + P_1Q_2)}{Q_1 (P_2Q_1 + 2P_1Q_2)} ; \quad \text{for "MODEL".}$$

$$f_4 = \frac{v(1 + v)}{E} ; \quad f_4(s) = \frac{P_1 (P_1Q_2 - P_2Q_1)}{Q_1 (P_2Q_1 + 2P_1Q_2)} ; \quad \text{for "MODEL" and "REALITY".}$$

(A6.23)

The time functions after inverse transformation are:

CASE I

$$f_1(t) = \frac{1}{q_0} \left[1 - \left(1 - \frac{p_1 q_0}{q_1} \right) e^{-\alpha t} \right]; \quad \alpha = \frac{q_0}{q_1}$$

(A6.24)

$$f_2(t) = \frac{3}{A} \left[\frac{1}{\beta} - \left(\frac{1}{\beta} - p_1 \right) e^{-\beta t} \right]; \quad A = q_1 + 6Kp_1$$

$$\beta = \frac{q_0 + 6K}{q_1 + 6Kp_1}$$

$$f_3(t) = \frac{1}{q_1 A} [B + C e^{-\alpha t} + D e^{-\beta t}]; \quad B = \frac{a}{\alpha \beta} \quad (\text{A6.24})$$

$$C = \frac{a}{\alpha(\alpha - \beta)} + \frac{b}{(\beta - \alpha)} + \frac{c\alpha}{(\alpha - \beta)}$$

$$D = \frac{a}{\beta(\beta - \alpha)} + \frac{b}{(\alpha - \beta)} + \frac{c\beta}{(\beta - \alpha)}$$

$$a = 2q_0 + 3K; \quad b = 2q_1 + 3Kp_1 + 2p_1q_0 + 3Kp_1;$$

$$c = 2p_1q_1 + 3Kp_1^2.$$

$f_4(t)$ was not used.

CASE II

$f_1(t)$ same as for case I;

The other functions are of the following general form:

$$f(t) = C_0 [C_1 + C_2 e^{-s_0 t} + C_3 e^{-s_1 t}] \quad (\text{A6.25})$$

with complicated constants C_0 , C_1 , C_2 , and C_3 .

A small computer program has been written to calculate the individual constants, the displacements and strains. It is not reproduced in this thesis since it is a straightforward application of the principles discussed above. For example, the tunnel wall displacement in the model test, as a function of time, follows from equation A6.6:

$$u_a(t) = f_3(t) \sigma_v \cdot a[(1 + N) + 2(1 - N) \cos 2\theta].$$

A6.2.1 Tables of Measured and Predicted Closure Ratios:

The data presented in Figure 6.9.A and the predicted values are presented in the following two tables:

TABLE A6.1: Displacement u and Displacement Ratio u/u_0 of External Gauges for Tests MC-2.0 to MC-2.9 (u = displacement at 10 MPa minus crack closure displacement).

	MC 2.0 (NO TUNNEL)	MC 2.4	MC 2.6	MC 2.5	MC 2.7	MC 2.8	MC 2.9
N	1.0	1.0	0.75	0.5	0.33	0.33	0.2
ϵ ($\frac{\text{kPa}}{\text{hr}}$)	6760	~14	6.4	6800	9.4	30[7.5]	56[8.5]
σ (MPa)	0 - 7 Reloading	0 - 10	0 - 14.5	0 - 3.5 * ₁	0 - 10	0 - 15	0 - 15
$\theta = 0^\circ$	$u_0 =$				non-linear stiffening	non-linear softening	non-linear softening
u	0.38%	0.51%	0.65%	0.65%	0.85%	0.78[0.93]%	1.07[1.35]%
$\frac{u}{u_0}$ {		1.34 * ₂ (1.18)	1.27 (1.10)	1.27 (1.19)	1.67 (1.25)	1.53[1.82] (1.25)	2.1[2.65] (1.31)
$\theta = 90^\circ$	$u_0 =$						
u	0.35%	0.50%	0.31%	0.26%	0.04%	0.02%	-0.25[-0.35]%
$\frac{u}{u_0}$ {		1.43 * ₂ (1.18)	0.62 (0.65)	0.52 (0.31)	0.08 (0.08)	0.04 (0.08)	-0.5[-0.7] % (-0.11)

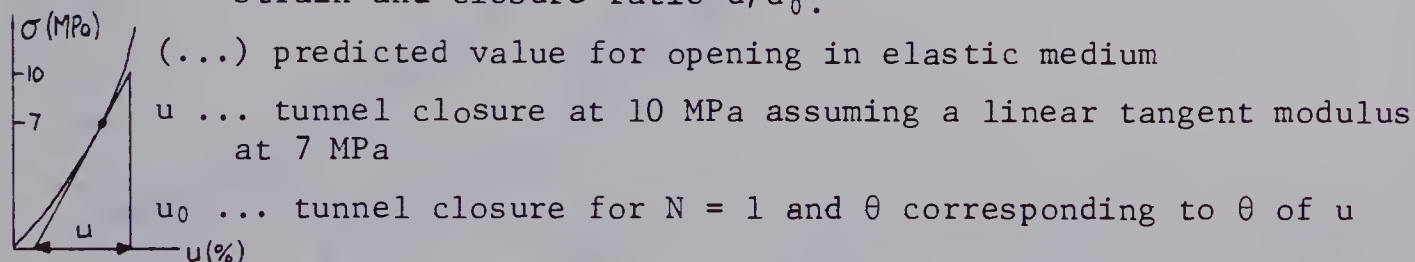
Note:

- for prediction () assumed $r = 5a$, $\nu = 0.2$, linear elasticity.
- value in [] corresponds to lower strain rate
- *₁ may be over estimated since measured over low stress range (<3.5MPa)
- *₂ difference may be due to strain rate change between MC-2.0 and MC-2.4
- for further explanation see Figure A6.2.

Table A6.2: Tunnel Closure u and Closure Ratio u/u_0 for Tests MC-2.4 to MC-2.9 (u = closure at 10 MPa minus effect of crack closure)

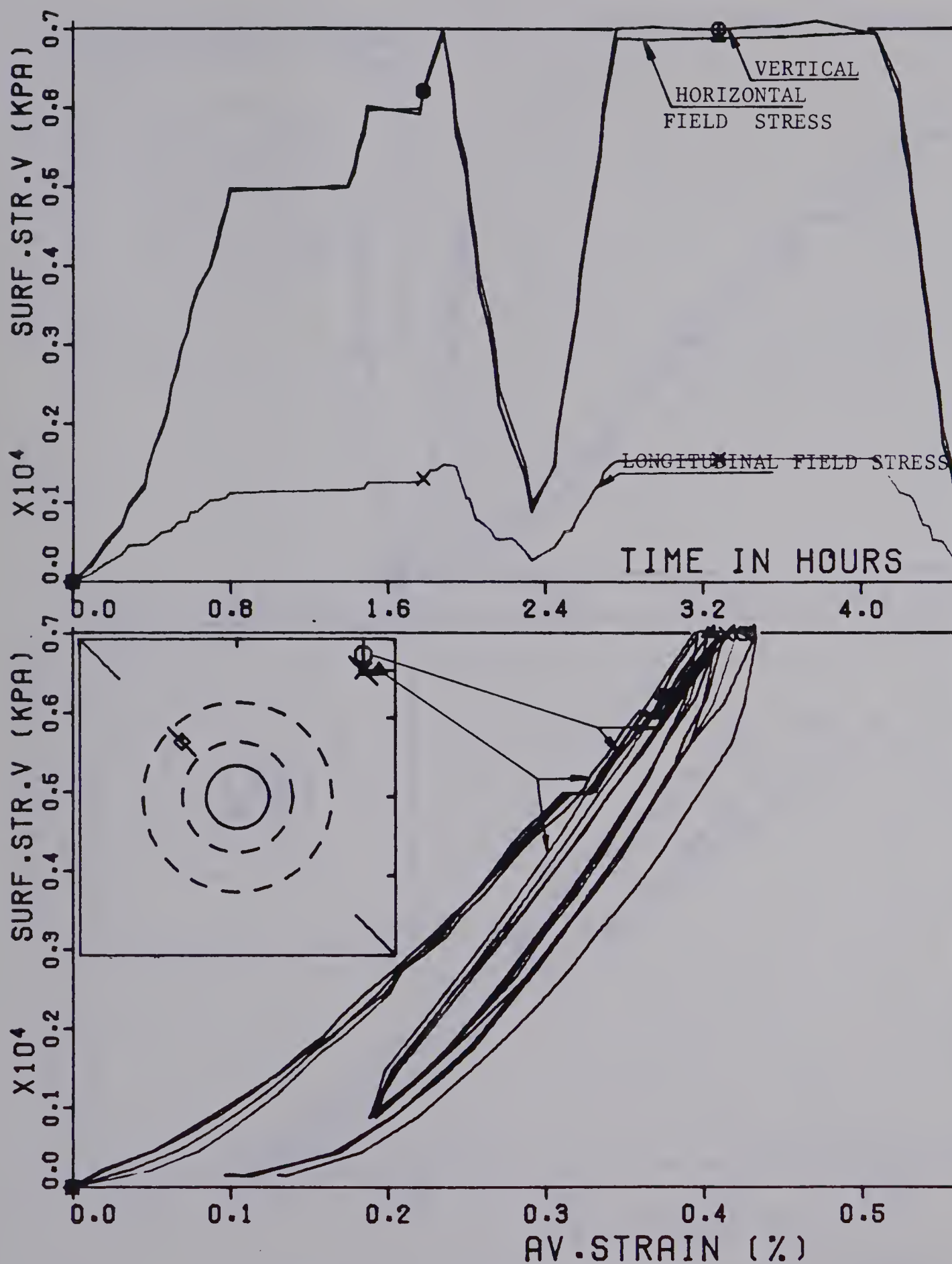
	MC 2.4	MC 2.6	MC 2.5	MC 2.7	MC 2.8	MC 2.9
$N = \sigma_h/\sigma_v$	1.0	0.75	0.5	0.33	0.33	0.2
$\sigma_v(\text{max}), \text{MPa}$	7	14	3(*)	10	15	15
$\theta = 0^\circ$ (vertical)	$\left\{ \begin{array}{l} u \\ \frac{u}{u_0} \end{array} \right\}$ 1.4% 1.0 (1.0)	$\left\{ \begin{array}{l} u \\ \frac{u}{u_0} \end{array} \right\}$ 1.6% 1.14 (1.13)	$\left\{ \begin{array}{l} u \\ \frac{u}{u_0} \end{array} \right\}$ 1.88% 1.34 (1.25)	$\left\{ \begin{array}{l} u \\ \frac{u}{u_0} \end{array} \right\}$ 2.44% 1.74 (1.33)	$\left\{ \begin{array}{l} u \\ \frac{u}{u_0} \end{array} \right\}$ 2.44% 1.74 (1.33)	$\left\{ \begin{array}{l} u \\ \frac{u}{u_0} \end{array} \right\}$ 3.05% 2.18 (1.4)
$\theta = 45^\circ$ (parallel to jointing)	$\left\{ \begin{array}{l} u \\ \frac{u}{u_0} \end{array} \right\}$ 1.7% 1.21 (1.0)	$\left\{ \begin{array}{l} u \\ \frac{u}{u_0} \end{array} \right\}$ 1.49% 0.88 (0.88)	$\left\{ \begin{array}{l} u \\ \frac{u}{u_0} \end{array} \right\}$ 1.47% 0.86 (0.75)	$\left\{ \begin{array}{l} u \\ \frac{u}{u_0} \end{array} \right\}$ 1.15% 0.68 (0.66)	$\left\{ \begin{array}{l} u \\ \frac{u}{u_0} \end{array} \right\}$ 1.1% 0.65 (0.66)	$\left\{ \begin{array}{l} u \\ \frac{u}{u_0} \end{array} \right\}$ 1.25% 0.74 (0.6)
$\theta = 135^\circ$ (perpendicular to jointing)	$\left\{ \begin{array}{l} u \\ \frac{u}{u_0} \end{array} \right\}$ 1.32% 0.94 (1.0)	$\left\{ \begin{array}{l} u \\ \frac{u}{u_0} \end{array} \right\}$ 1.16% 0.88 (0.88)	$\left\{ \begin{array}{l} u \\ \frac{u}{u_0} \end{array} \right\}$ 1.14% 0.86 (0.75)	$\left\{ \begin{array}{l} u \\ \frac{u}{u_0} \end{array} \right\}$ 1.01% 0.77 (0.66)	$\left\{ \begin{array}{l} u \\ \frac{u}{u_0} \end{array} \right\}$ 0.87% 0.66 (0.66)	$\left\{ \begin{array}{l} u \\ \frac{u}{u_0} \end{array} \right\}$ 0.8% 0.61 (0.6)
$\theta = 90^\circ$ (horizontal)	$\left\{ \begin{array}{l} u \\ \frac{u}{u_0} \end{array} \right\}$ 1.44% 1.03 (1.0)	$\left\{ \begin{array}{l} u \\ \frac{u}{u_0} \end{array} \right\}$ 0.85% 0.59 (0.63)	$\left\{ \begin{array}{l} u \\ \frac{u}{u_0} \end{array} \right\}$ 0.58% 0.40 (0.25)	$\left\{ \begin{array}{l} u \\ \frac{u}{u_0} \end{array} \right\}$ 0.14% 0.1 (0.0)	$\left\{ \begin{array}{l} u \\ \frac{u}{u_0} \end{array} \right\}$ 0.14% 0.1 (0.0)	$\left\{ \begin{array}{l} u \\ \frac{u}{u_0} \end{array} \right\}$ -0.6% -0.42 (-0.2)

Note: (*) extrapolation to 10 MPa might result in overestimation of strain and closure ratio u/u_0 .



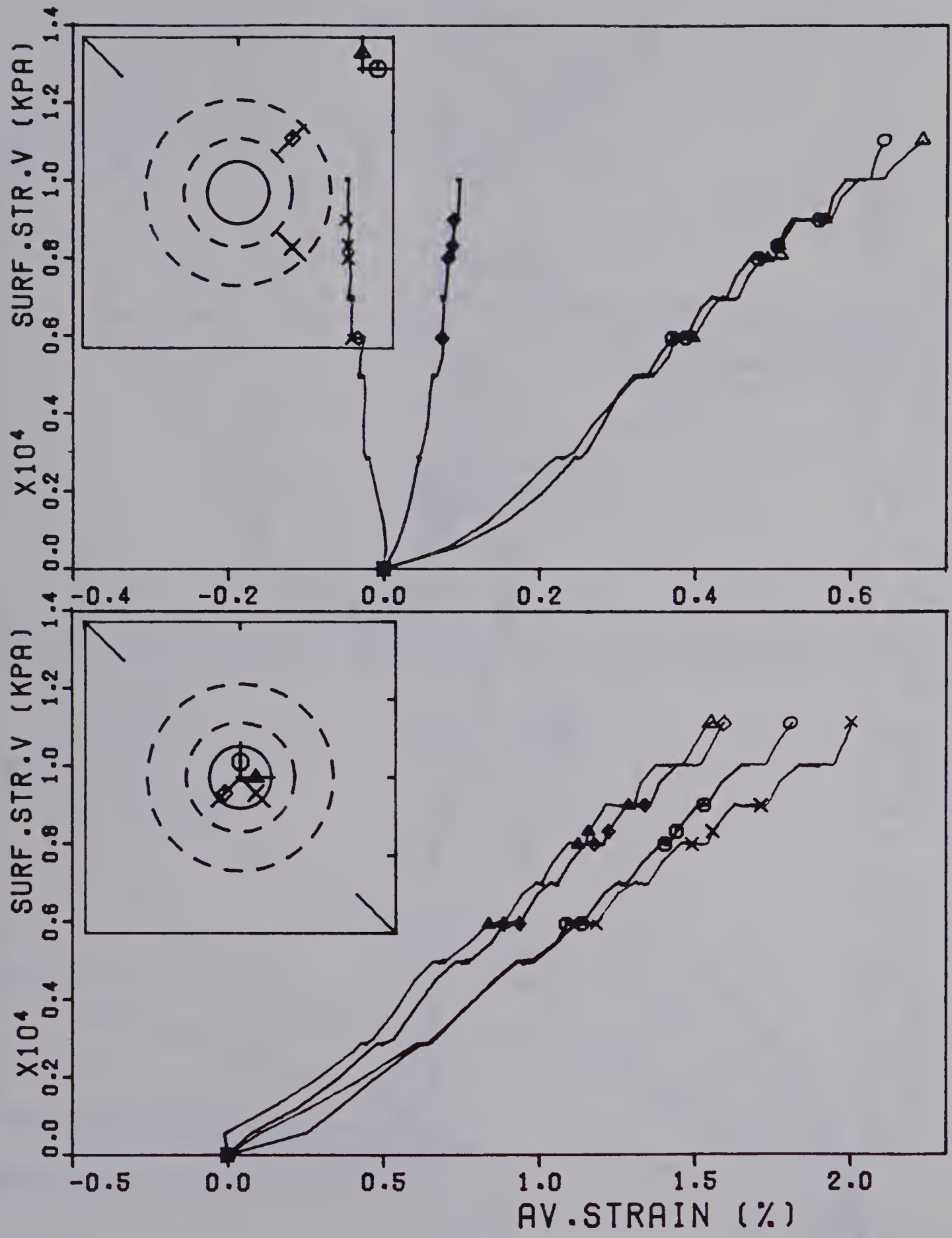
A6.2.2 Collection of Diagrams:

The following thirteen figures include additional data which have not been presented in the core of this thesis.



TEST MC-2.0 WITHOUT TUNNEL 1977

Figure A6.1 Stress-Strain Diagram: Test MC-2.0; no record of internal gauges due to technical problems



TEST #MC-2.4 WITH TUNNEL 1977

Figure A6.2 Stress-Strain Diagram: Test MC-2.4; no record of internal gauges due to technical problems.

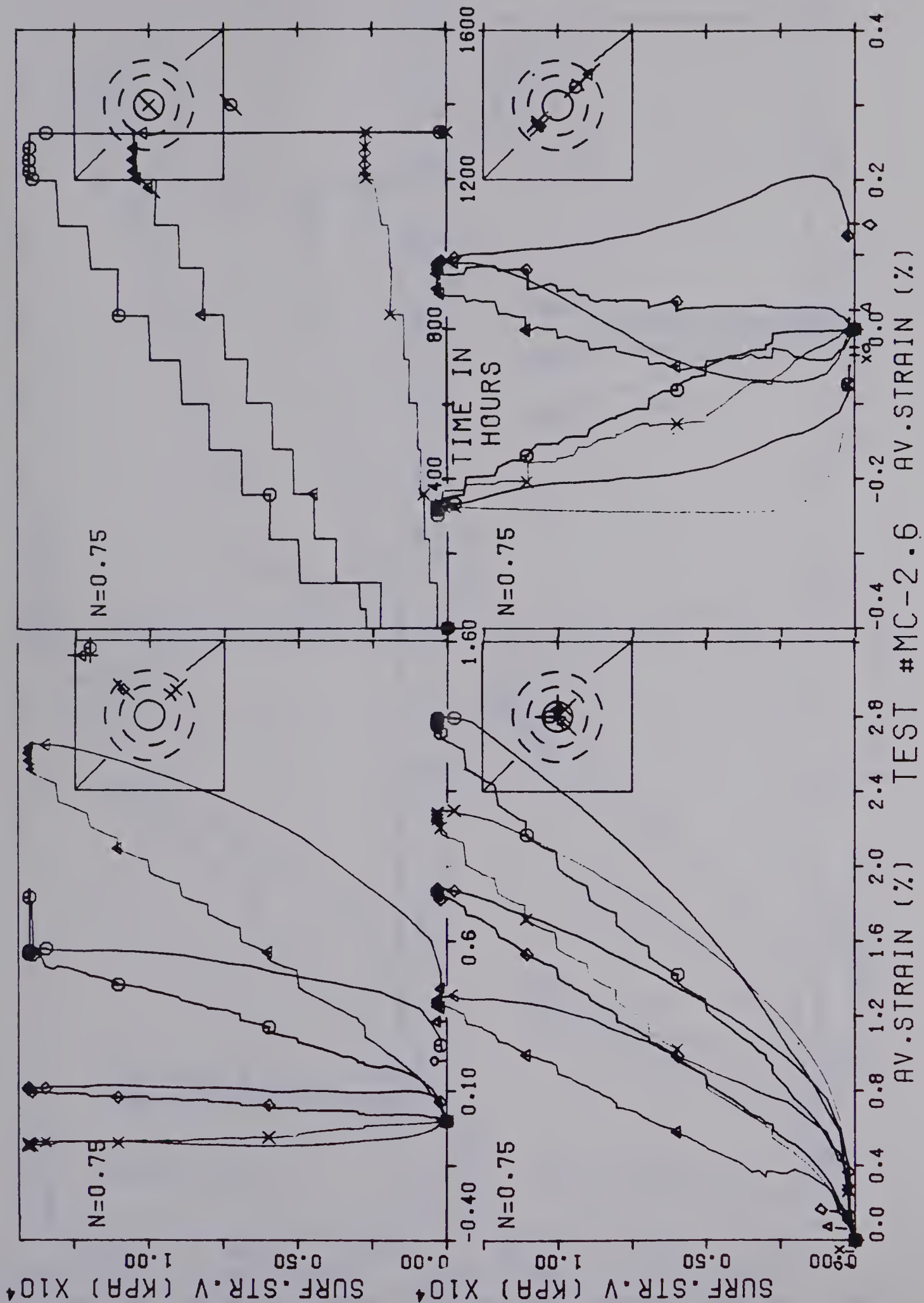


Figure A6.3 Stress-Strain Diagram and Loading History: Test MC-2.6.

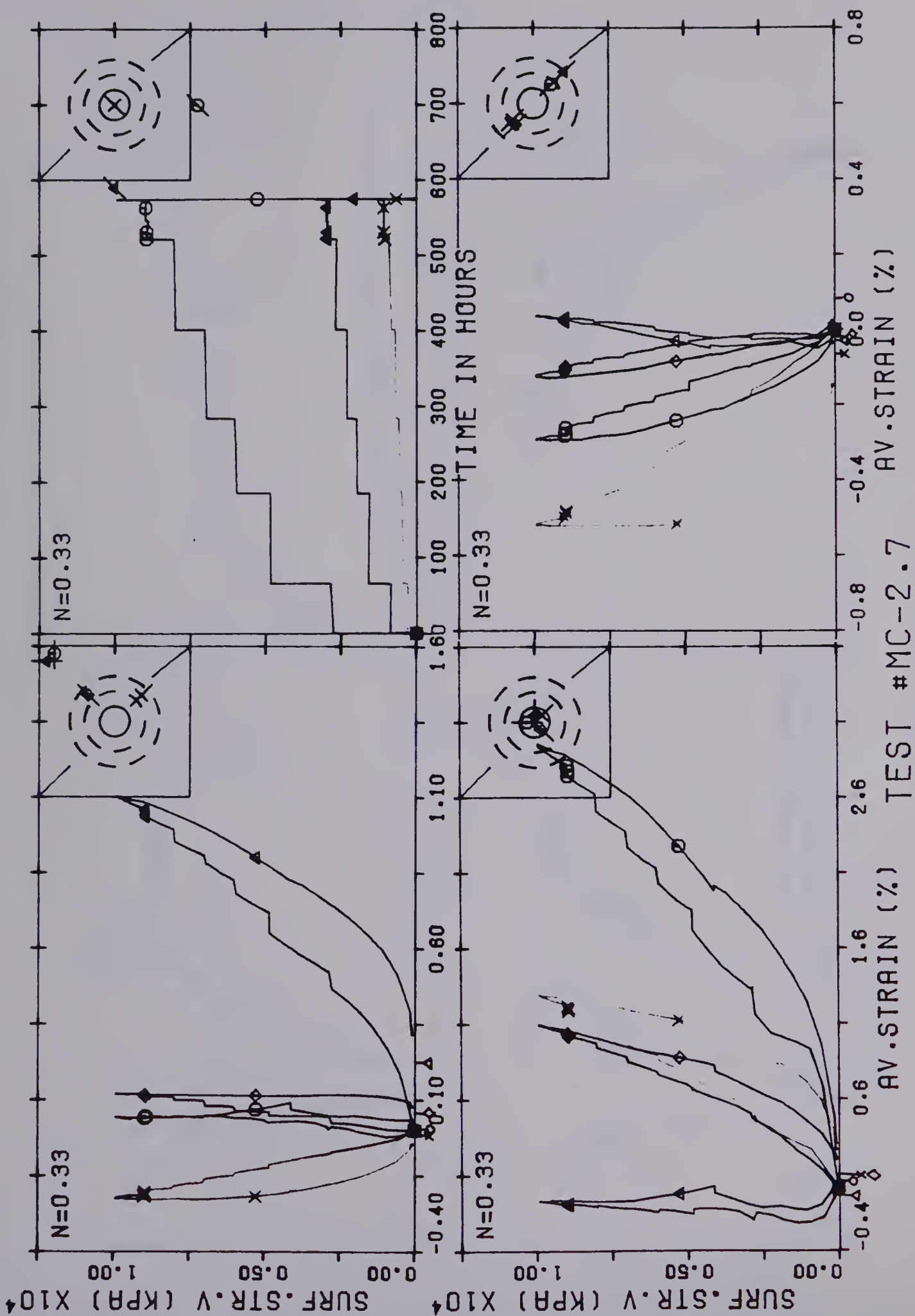
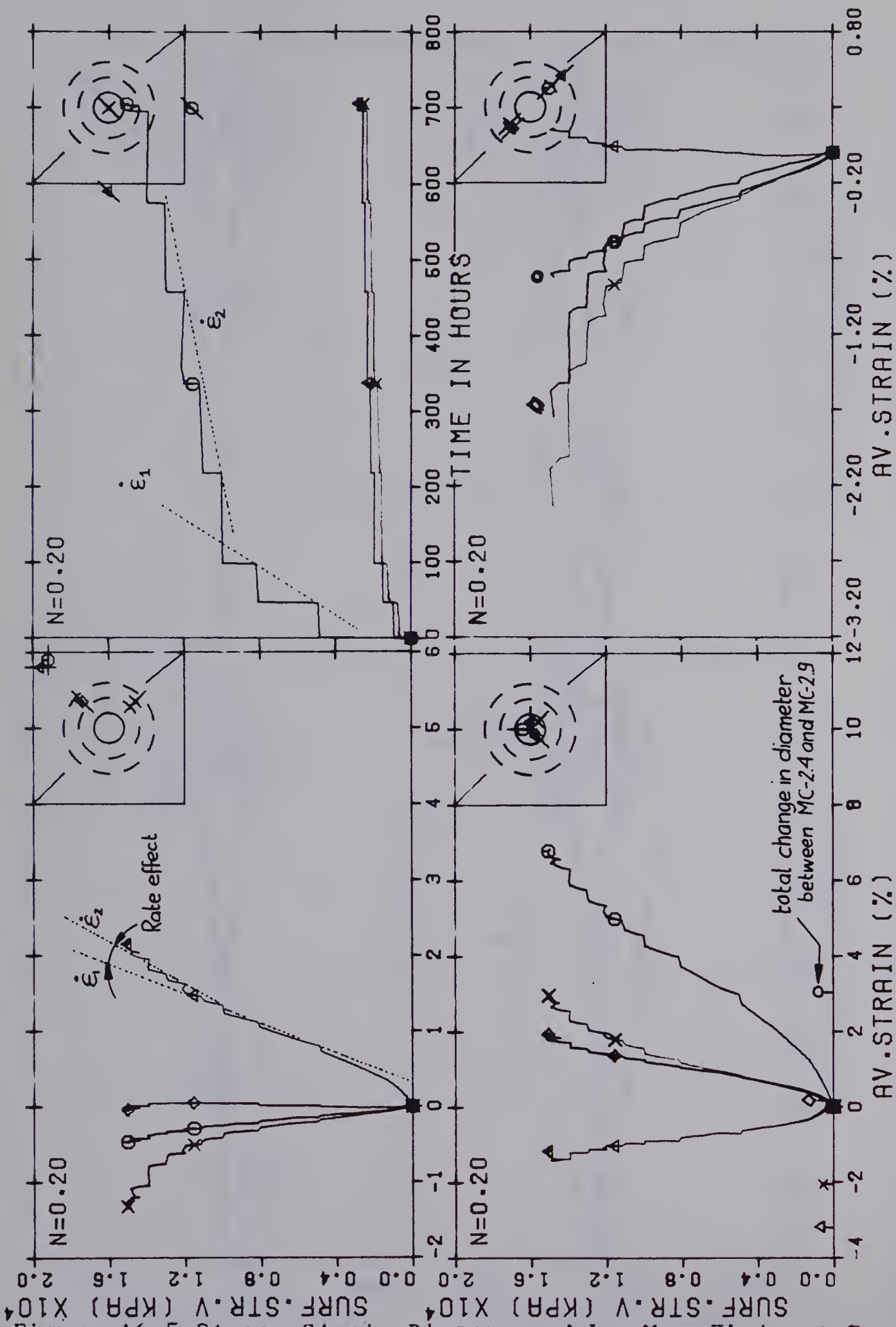


Figure A6.4 Stress-Strain Diagram and Loading History: Test MC-2.7.



TEST #MC-2.9

Figure A6.5 Stress-Strain Diagram and Loading History: Test MC-2.9.

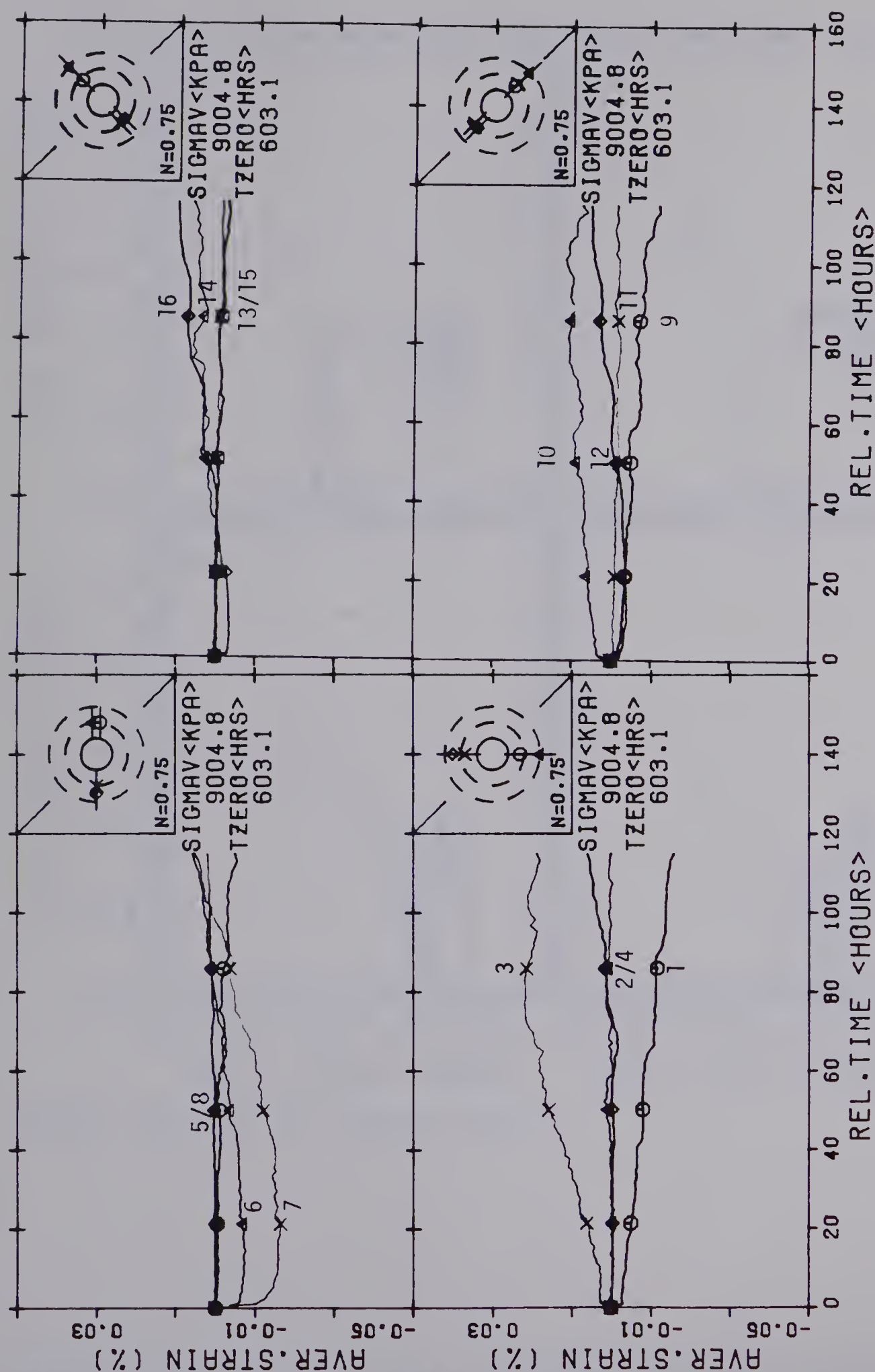
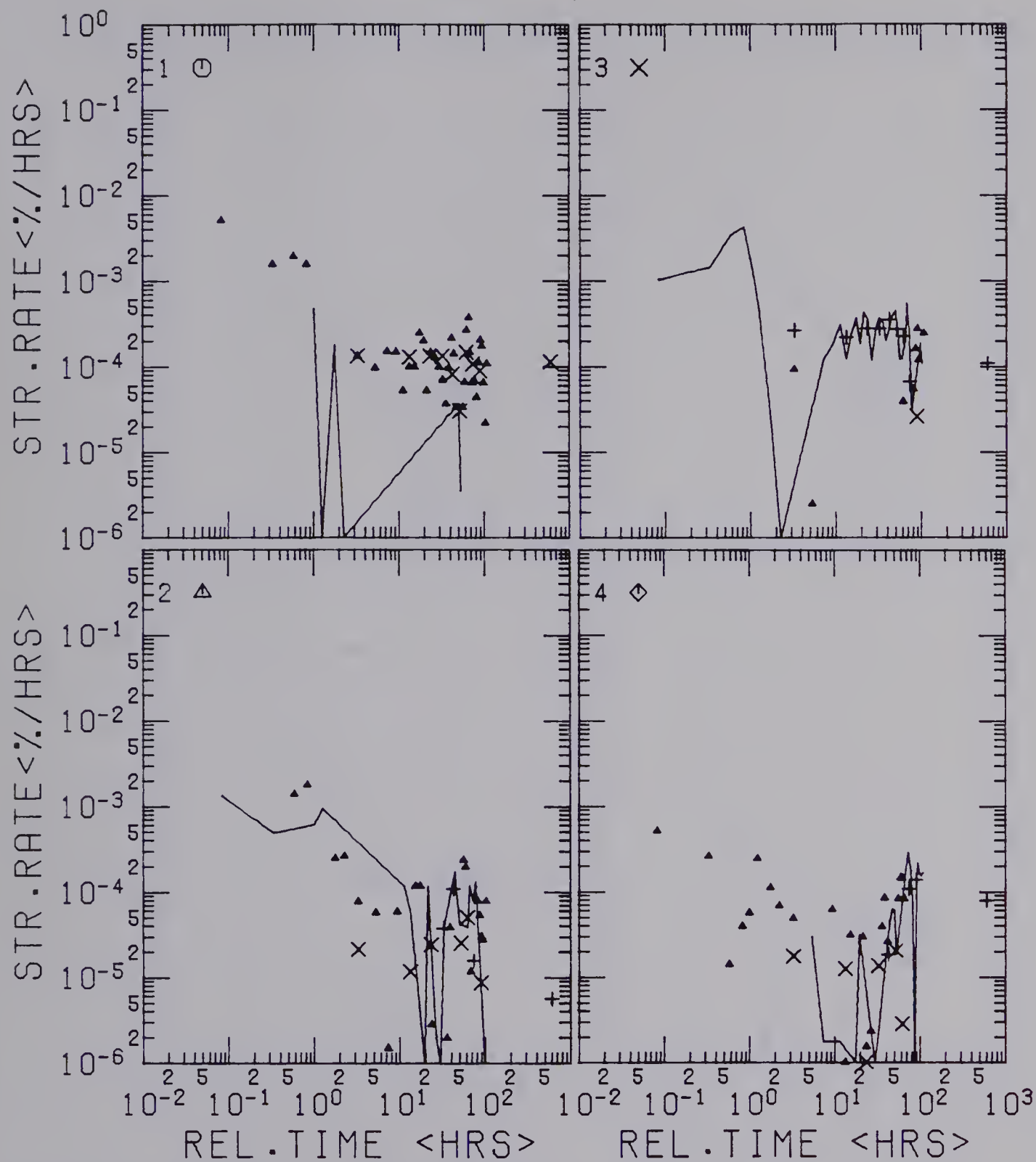


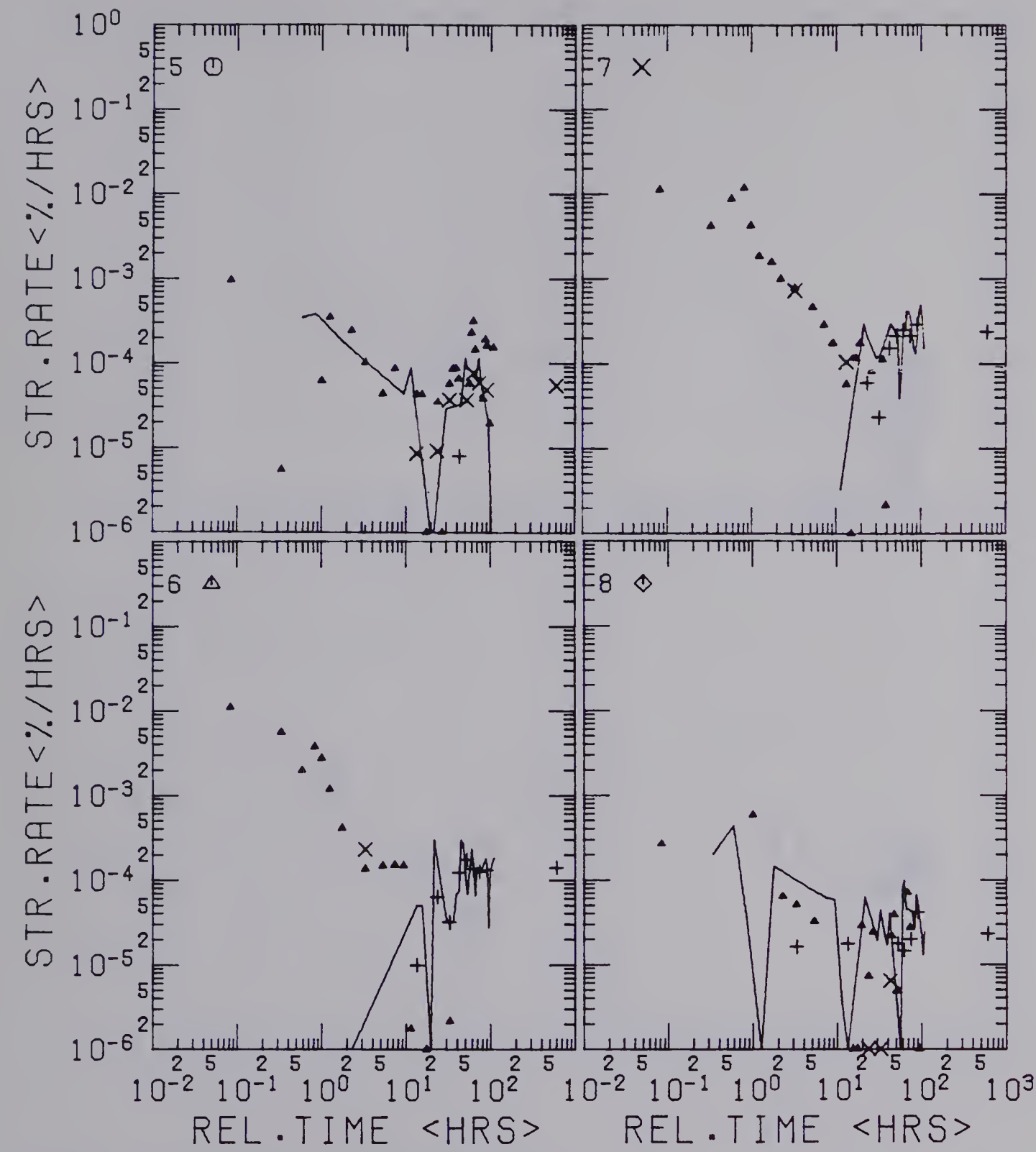
Figure A6.6 Strain-Time Diagram: Test MC-2.6, Gauges 1 to 16

TEST #MC-2.6 WITH TUNNEL 1977



TEST MC2.6 AT 9000 KPA

Figure A6.7 Log Strain Rate - Log Time Diagram: Test MC-2.6, Gauges 1 to 4



TEST MC2.6 AT 9000 KPA

Figure A6.8 Log Strain Rate - Log Time Diagram: Test MC-2.6, Gauges 5 to 8

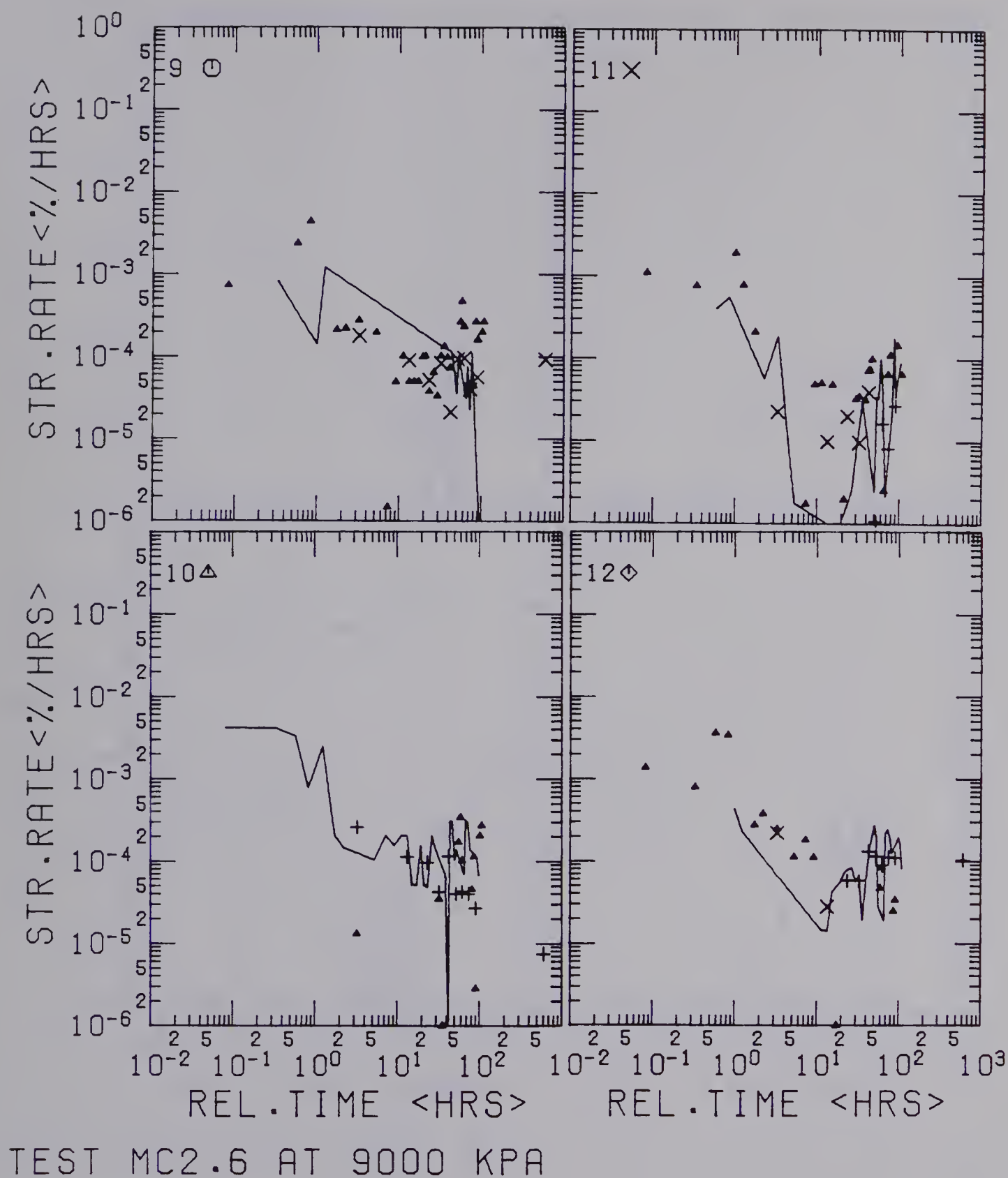


Figure A6.9 Log Strain Rate - Log Time Diagram: Test MC-2.6, Gauges 9 to 12

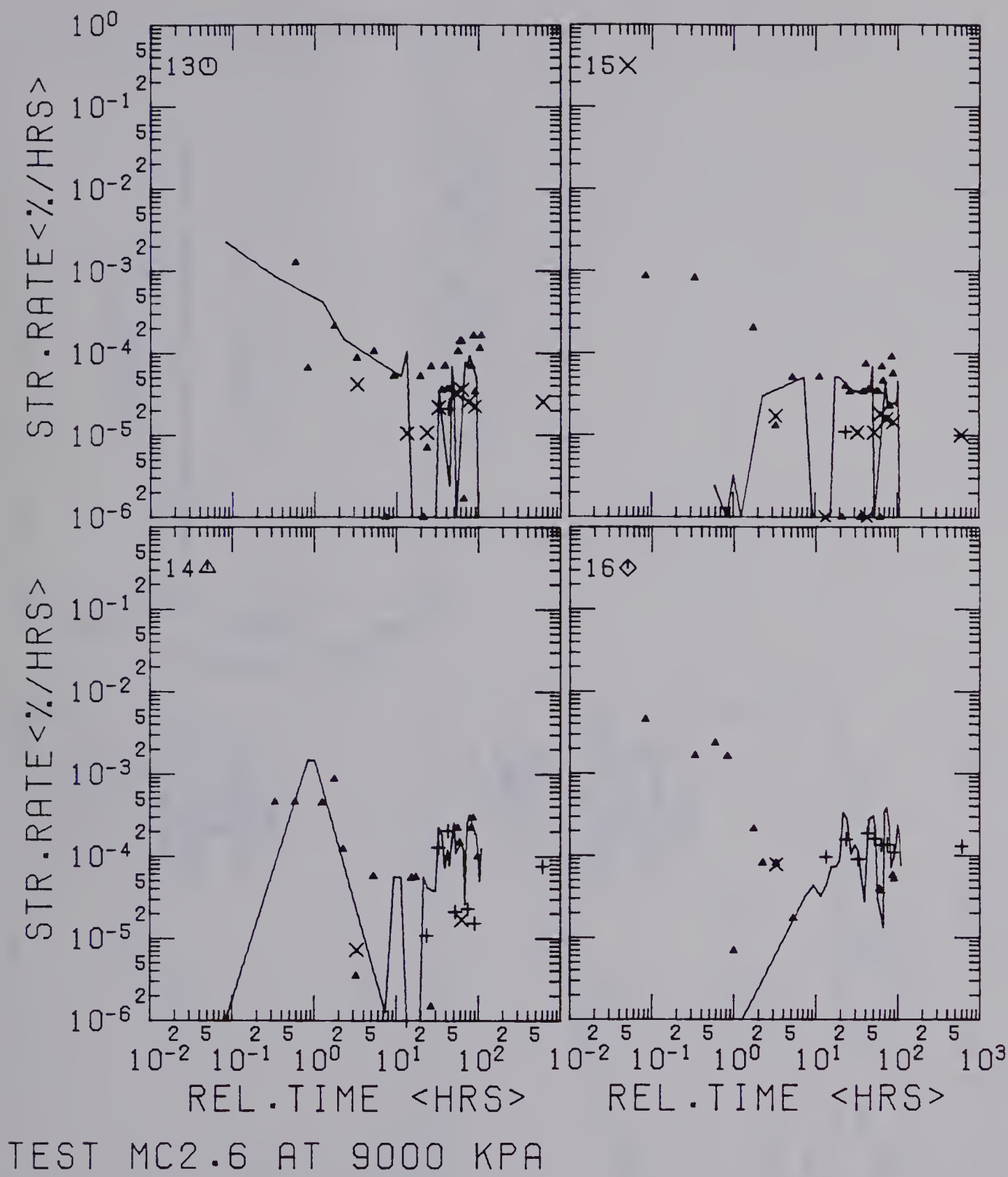


Figure A6.10 Log Strain Rate - Log Time Diagram: Test MC-2.6, Gauges 13 to 16

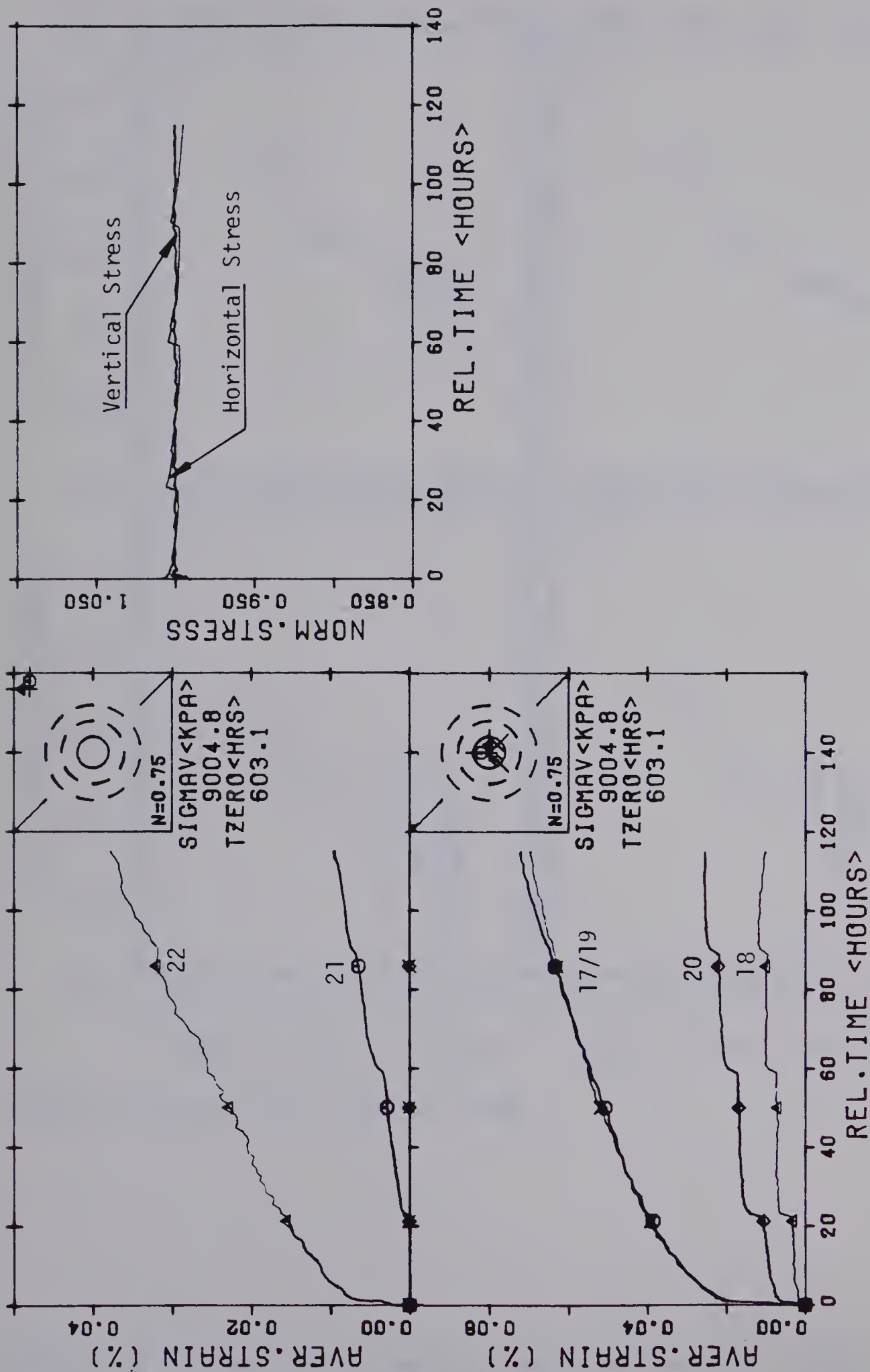


Figure A6.11 Strain-Time and Normalized Stress - Time
Diagram: Test MC-2.6, Gauges 17 to 22

TEST #MC-2.6 WITH TUNNEL 1977

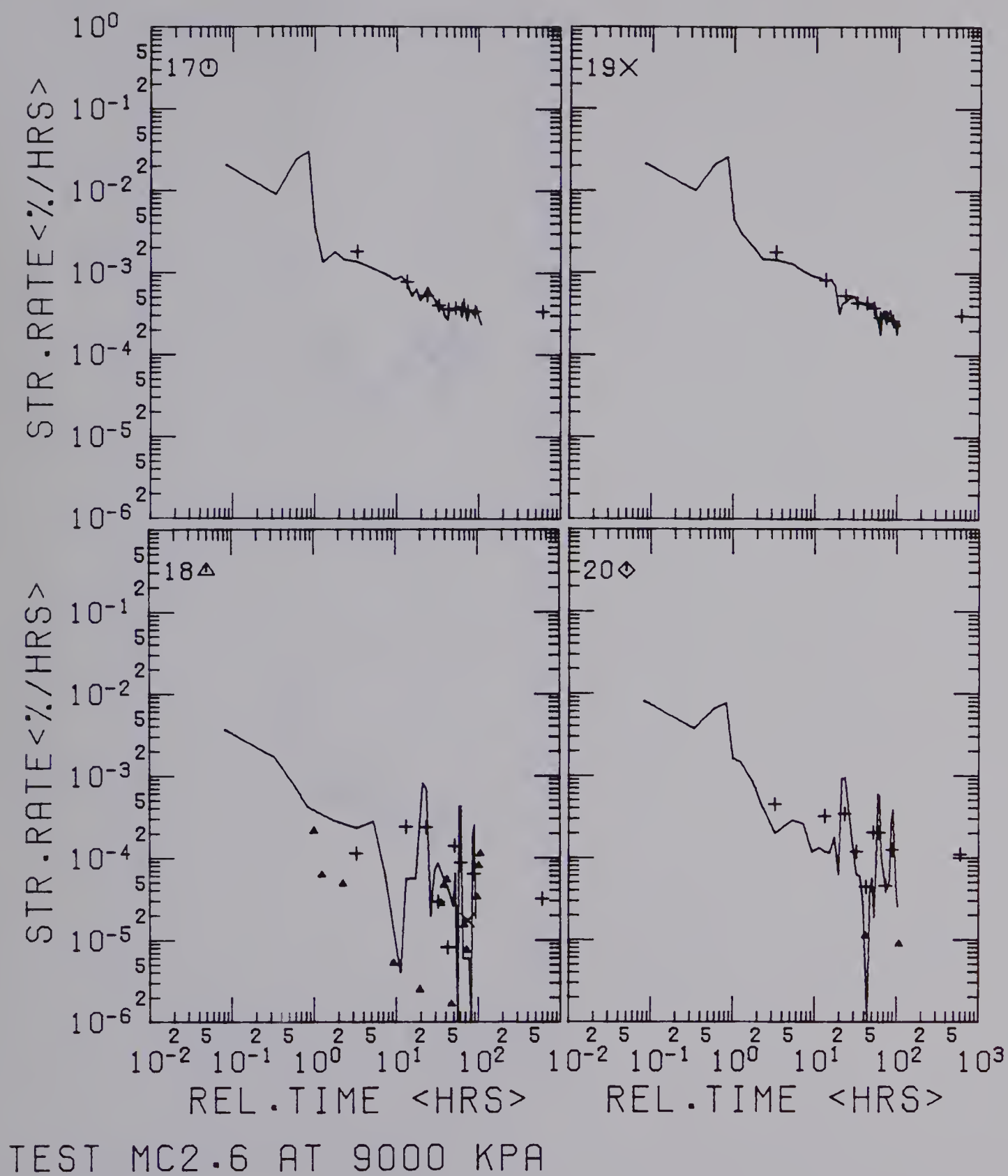
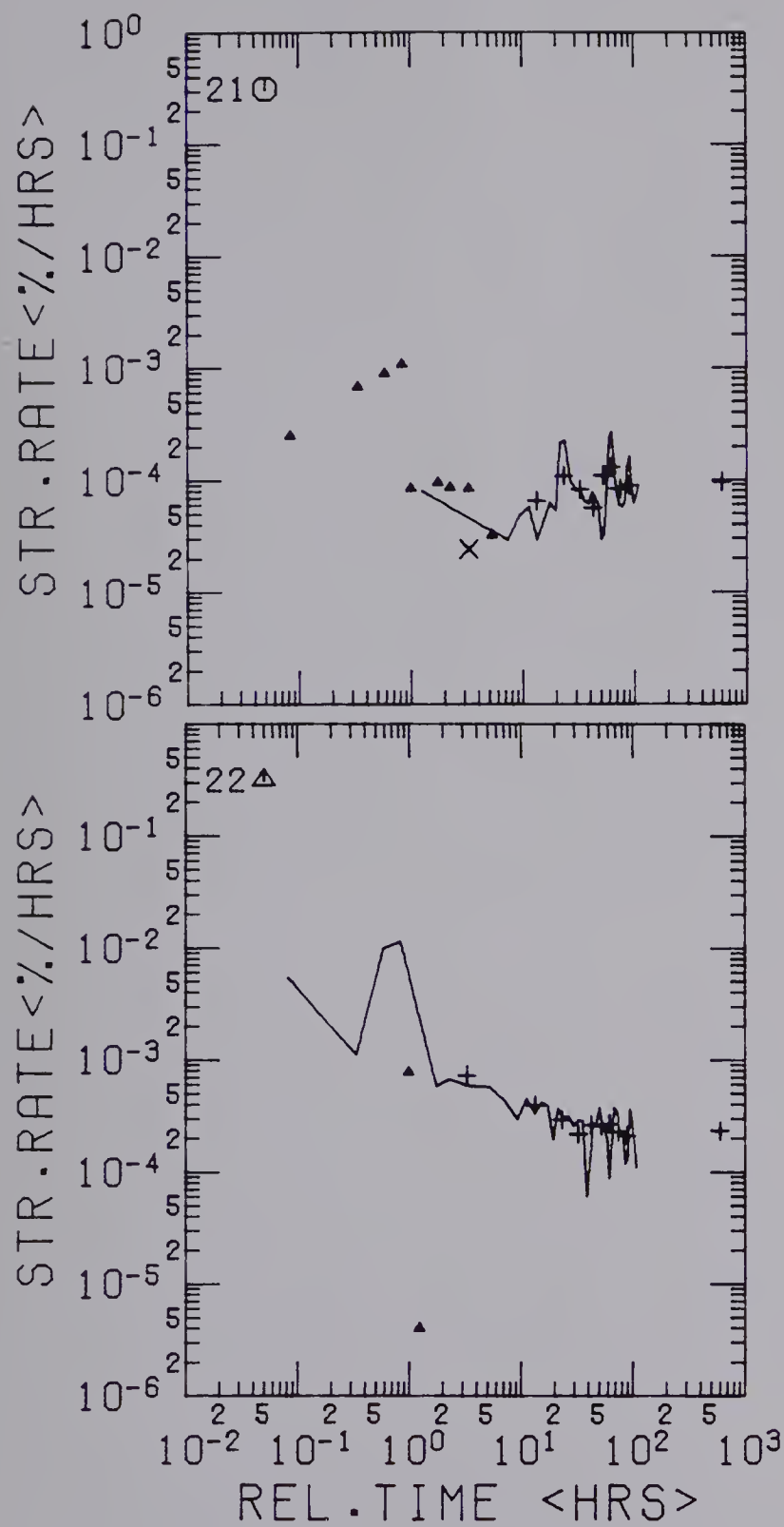


Figure A6.12 Log Strain Rate - Log Time Diagram: Test MC-2.6, Gauges 17 to 20



TEST MC2.6 AT 9000 KPA

Figure A6.13 Log Strain Rate - Log Time Diagram: Test MC-2.6, Gauges 21 to 22

B30261